Journal of Diabetes Research

The Role of Oxidative Stress in the Development of Diabetes Mellitus and its Complications

Lead Guest Editor: Julia M. dos Santos
Guest Editors: Shikha Tewari and Roberta H. Mendes

The Role of Oxidative Stress in the Development of Diabetes Mellitus and its Complications

Journal of Diabetes Research

The Role of Oxidative Stress in the Development of Diabetes Mellitus and its Complications

Lead Guest Editor: Julia M. dos Santos
Guest Editors: Shikha Tewari and Roberta H. Mendes

Editorial Board

Contents

Hindawi
Journal of Diabetes Research
Volume 2019, Article ID 4189813, 3 pages
https://doi.org/10.1155/2019/4189813

Editorial

The Role of Oxidative Stress in the Development of Diabetes Mellitus and Its Complications

Julia M. Dos Santos,[1,2] **Shikha Tewari**,[3] **and Roberta H. Mendes**[4]

[1]*School of Education, Health and Human Performance, Fairmont State University, West Virginia, USA*
[2]*Henry Ford College, Dearborn, Michigan, USA*
[3]*Department of Pathology, King George Medical University, Lucknow, India*
[4]*UCD School of Agriculture and Food Science Institute of Food and Health, University College Dublin, Belfield, Dublin 4, Ireland*

Correspondence should be addressed to Julia M. Dos Santos; jmsantos@detroitrandd.com

Received 11 April 2019; Accepted 11 April 2019; Published 5 May 2019

The thematic issue addresses the role of oxidative stress in the development of diabetes and its related complications. Diabetes is a growing pandemic of the 21st century that has reached 1 in every 11 people worldwide [1]. Changes in lifestyle such as unhealthy diet and physical inactivity are strongly associated with the growing prevalence of this disease [2, 3]. Chronic hyperglycemia, the common outcome of all diabetes types, may negatively influence the structure and function of many organ systems, particularly the cardiovascular, nervous, and renal systems [4, 5]. These diabetic complications are associated with increased rate of morbidity and mortality [1, 5]. The role of oxidative stress has been an important piece of the puzzle for the understanding of the complex mechanism by which diabetes and its complications are developed. In this context, numerous research groups have focused on the characterization of the reactive oxygen species (ROS) source, its triggered pathway, scavenging and antioxidant substances in diabetes [6–9]. The multifaceted effects of oxidative damage in diabetes have been well addressed in the current issue and it provides a bigger picture of complication in a single platform. Therefore, this special issue includes 8 research articles focusing on the role of oxidative stress and antioxidant defense on the development of diabetes and its associated diseases. The guest editors are pleased to present a compendium of these cutting-edge original research and review articles as follows.

In the research article "Astragalus membranaceus and Panax notoginseng, the Novel Renoprotective Compound, Synergistically Protect against Podocyte Injury in Streptozotocin-Induced Diabetic Rats," ever since the diabetic complications have been understood and oxidative injury has been established as a cause, many compounds/-plant extracts that attenuate oxidative damage and cell death have been researched upon. Adding to this field, one article in this issue showed the renoprotective role of treatment with Astragalus membranaceus (AG) and Panax notoginseng (NG). Treatment significantly reduced albuminuria and improved renal histopathology and podocyte foot process effacement in STZ-induced diabetic rats. AG and NG synergistically attenuated the structural and functional abnormalities in the kidney, and in the future, it may provide treatment combination for diabetic nephropathy and other kidney diseases.

The research article "Myocardial Ischemia and Diabetes Mellitus: Role of Oxidative Stress in the Connection between Cardiac Metabolism and Coronary Blood Flow" discusses the physiological and pathophysiological role of oxidative stress in myocardial metabolism and coronary blood flow (CBF), with particular attention to patients with diabetes mellitus. Ischemic heart disease (IHD) being one major current health risk to diabetic patients, the review summarizes the role of oxidative stress in coronary microvascular dysfunction and development of IHD. Oxidative stress further generates ROS, AGEs, and oxidized LDL causing coronary microvascular dysfunction. Therein inflammatory pathway is triggered and ion channel function is altered. The review suggests that

balancing the oxidative stress and restoring the ion channel function may be exploited as therapeutic target in the treatment of IHD.

In the research article "Effect of Baoshenfang Formula on Podocyte Injury via Inhibiting the NOX-4/ROS/p38 Pathway in Diabetic Nephropathy," it is stated that more and more studies demonstrated that diabetic nephropathy is the leading cause of end-stage of renal diseases [10]. Previous study has demonstrated that increased ROS plays a key role in podocyte injury in diabetic nephropathy (DN) [11, 12]. NOX-4, as an important number of nicotinamide adenine dinucleotide phosphate (NADPH) oxidase, is the major source of ROS production in podocyte. This study evaluated the effects of Baoshenfang (BSF: Chinese herbal formula) on podocyte injury *in vivo* and *in vitro* and explored the possible involvement of the nicotinamide adenine dinucleotide phosphate-oxidase-4/reactive oxygen species- (NOX-4/ROS-) activated p38 pathway. The BSF shows therapeutic potential in attenuating oxidative stress and apoptosis in podocytes in DN.

In the research article "Evidence in Practice of Tissue Healing with Latex Biomembrane: Integrative Review," wound healing is a perfectly coordinated cascade of cellular, molecular, and biochemical events which interact in tissue reconstitution. Chronic diseases such as pressure ulcers (PU) and diabetes mellitus (DM) are considered risk factors for wound healing. Latex biomembrane (LBM), a biocompatible material, derived from latex of rubber tree (*Hevea brasiliensis*) appears to create tendencies as an angiogenic inducing tissue healing agent and as biomaterial, resulting from its structural qualities and its low cost when compared to conventional treatments. Therefore, the authors aim to summarize the results, methods, and scientific findings that certify or recommend the use of LBM as a new technique to be applied effectively in the treatment of wounds.

In the research article "Glucagon-Like Peptide-1 Receptor Agonist Protects Dorsal Root Ganglion Neurons against Oxidative Insult," diabetic polyneuropathy (PDN) is one of the most prevalent complications in diabetes. In the article from this issue, exendin-4, a glucagon-like peptide 1 receptor agonist (GLP-1RA), was shown beneficial against oxidative stress insults by activating superoxide dismutase in dorsal root ganglion neuron cell. Therefore, the authors suggest that GLP-1RA attenuates PDN by protecting insults on dorsal root ganglion neuron cell.

In the research article "Effects of High-Fat Diet on eHSP72 and Extra-to-Intracellular HSP70 Levels in Mice Submitted to Exercise under Exposure to Fine Particulate Matter," tha authors suggest that in type 2 diabetes, eHSP70 has been negatively correlated with iHSP70 in skeletal muscles and that leds to impaired glucose uptake. The elevated levels of eHSP70 are associated with insulin resistance in elderly population [13]. In this issue, we discuss an interesting finding correlating two major global health issues of obesity and air pollution (fine particulate matter PM2.5), with reference to diabetes, demonstrating that HFD impaired exercise performance and weakened the standard heat shock response to exercise. This is a concerning fact that regular exercise abrogates oxidative stress and modulates many pathways improving insulin resistance and glucose uptake in skeletal muscle [3], but the growing worldwide pollution may weaken the response.

In the research article "A New Way for Beta Cell Neogenesis: Transdifferentiation from Alpha Cells Induced by Glucagon-Like Peptide 1," it is stated that current treatment modalities for diabetes include drug therapy or pancreatic islet transplantation which has its own limitations [14]. One study in the current issue highlights the use of glucagon-like peptide 1 (GLP1), a gut-derived hormone secreted by the intestine as a prospective target for type 2 diabetes therapy. It is interesting to discuss how it ameliorates hyperglycemia in diabetic models, inducing regeneration of beta cells by the endogenous neogenesis in a rat model. This study elaborates cellular and molecular mechanisms that regulate adult pancreatic differentiation in the management of diabetes.

In the research article "Advanced Glycation End Products Increase MDM2 Expression via Transcription Factor KLF5," the authors state that increase in the level of AGEs has been associated with diabetic complications for a long time; however, their role in the overexpression of MDM2 and colon cancer development is an exciting finding by one of the papers in the current issue. The research highlights the activation of oncogenic pathway through activation of MDM causing Rb and p53 degradation, which may stimulate cell proliferation and metastasis. The concept of initiation of tumorigenesis or epithelial mesenchymal transition, in diabetics, via P53, AKT/mTOR, RAS signaling or Wnt signaling is a recent an open platform to explore.

The editors anticipate this special issue to be of tremendous interest to the medical and scientific community. We hope researchers benefit in this issue to continuously make further progress in the understanding of the role of oxidative stress in the development of diabetes and its complications.

Conflicts of Interest

The authors declare that they have no conflict of interest.

Acknowledgments

The editors would like to thank the authors for submitting their insightful research for publication and the reviewers for their important input and critiques to improve the manuscripts.

Julia M. Dos Santos
Shikha Tewari
Roberta H. Mendes

References

[1] World Health Organization, "Diabetes report," 2016, https://www.who.int/news-room/fact-sheets/detail/diabetes.

[2] R. al Ali, F. Mzayek, S. Rastam et al., "Forecasting future prevalence of type 2 diabetes mellitus in Syria," *BMC Public Health*, vol. 13, no. 1, p. 507, 2013.

[3] J. M. Dos Santos, M. L. Moreli, S. Tewari, and S. A. Benite-Ribeiro, "The effect of exercise on skeletal muscle glucose uptake in type 2 diabetes: an epigenetic perspective," *Metabolism*, vol. 64, no. 12, pp. 1619–1628, 2015.

[4] J. M. Santos, S. B. Ribeiro, A. R. Gaya, H. J. Appell, and J. A. Duarte, "Skeletal muscle pathways of contraction-enhanced glucose uptake," *International Journal of Sports Medicine*, vol. 29, no. 10, pp. 785–794, 2008.

[5] A. M. Alshehri, "Metabolic syndrome and cardiovascular risk," *Journal of Family & Community Medicine*, vol. 17, no. 2, pp. 73–78, 2010.

[6] J. M. Dos Santos, D. S. de Oliveira, M. L. Moreli, and S. A. Benite-Ribeiro, "The role of mitochondrial DNA damage at skeletal muscle oxidative stress on the development of type 2 diabetes," *Molecular and Cellular Biochemistry*, vol. 449, no. 1-2, pp. 251–255, 2018.

[7] J. M. Santos, G. Mohammad, Q. Zhong, and R. A. Kowluru, "Diabetic retinopathy, superoxide damage and antioxidants," *Current Pharmaceutical Biotechnology*, vol. 12, no. 3, pp. 352–361, 2011.

[8] A. G. Miranda-Díaz, L. Pazarín-Villaseñor, F. G. Yanowsky-Escatell, and J. Andrade-Sierra, "Oxidative stress in diabetic nephropathy with early chronic kidney disease," *Journal of Diabetes Research*, vol. 2016, Article ID 7047238, 7 pages, 2016.

[9] D. Zephy and J. Ahmad, "Type 2 diabetes mellitus: role of melatonin and oxidative stress," *Diabetes & Metabolic Syndrome: Clinical Research & Reviews*, vol. 9, no. 2, pp. 127–131, 2015.

[10] J. Ahmad, "Management of diabetic nephropathy: recent progress and future perspective," *Diabetes & Metabolic Syndrome: Clinical Research & Reviews*, vol. 9, no. 4, pp. 343–358, 2015.

[11] A. Piwkowska, D. Rogacka, I. Audzeyenka, M. Jankowski, and S. Angielski, "High glucose concentration affects the oxidant-antioxidant balance in cultured mouse podocytes," *Journal of Cellular Biochemistry*, vol. 112, no. 6, pp. 1661–1672, 2011.

[12] K. Susztak, A. C. Raff, M. Schiffer, and E. P. Bottinger, "Glucose-induced reactive oxygen species cause apoptosis of podocytes and podocyte depletion at the onset of diabetic nephropathy," *Diabetes*, vol. 55, no. 1, pp. 225–233, 2006.

[13] M. Krause, K. Keane, J. Rodrigues-Krause et al., "Elevated levels of extracellular heat-shock protein 72 (eHSP72) are positively correlated with insulin resistance in vivo and cause pancreatic β-cell dysfunction and death in vitro," *Clinical Science*, vol. 126, no. 10, pp. 739–752, 2014.

[14] X. Y. Miao, Z. Y. Gu, P. Liu et al., "The human glucagon-like peptide-1 analogue liraglutide regulates pancreatic beta-cell proliferation and apoptosis via an AMPK/mTOR/P70S6K signaling pathway," *Peptides*, vol. 39, pp. 71–79, 2013.

Hindawi
Journal of Diabetes Research
Volume 2019, Article ID 1602892, 14 pages
https://doi.org/10.1155/2019/1602892

Research Article

Astragalus membranaceus and Panax notoginseng, the Novel Renoprotective Compound, Synergistically Protect against Podocyte Injury in Streptozotocin-Induced Diabetic Rats

Ruonan Zhai,[1] **Guihua Jian**,[1] **Teng Chen**,[2] **Ling Xie**,[3] **Rui Xue**,[1] **Chongting Gao**,[1] **Niansong Wang**,[1] **Youhua Xu**,[4] **and Dingkun Gui**[1]

[1]*Department of Nephrology, Shanghai Jiao Tong University Affiliated Sixth People's Hospital, Shanghai 200233, China*
[2]*Shanghai University of Traditional Chinese Medicine, Shanghai 201203, China*
[3]*Shanghai Ocean University, Shanghai 201306, China*
[4]*Faculty of Chinese Medicine, State Key Laboratory of Quality Research in Chinese Medicine, Macau University of Science and Technology, Taipa, Macao 999078, China*

Correspondence should be addressed to Niansong Wang; wangniansong2012@163.com, Youhua Xu; yhxu@must.edu.mo, and Dingkun Gui; dingkungui@alu.fudan.edu.cn

Received 22 December 2018; Accepted 6 March 2019; Published 16 April 2019

Guest Editor: Shikha Tewari

This study was aimed at investigating the synergistical protective effects of Astragalus membranaceus (AG) and Panax notoginseng (NG) on podocyte injury in diabetic rats. Diabetes was induced in rats by a single intraperitoneal injection of streptozotocin at 55 mg/kg. Diabetic rats were then orally administrated with losartan, AG, NG, and AG plus NG (2 : 1) for 12 weeks. Albuminuria, biochemical markers, renal histopathology, and podocyte number per glomerulus were measured. Podocyte apoptosis was determined by triple immunofluorescence labeling including TUNEL assay, WT1, and DAPI. Renal expression of nephrin, α-dystroglycan, Bax, Bcl-xl, and Nox4 was evaluated by immunohistochemistry, western blot, and RT-PCR. AG plus NG ameliorated albuminuria, renal histopathology, and podocyte foot process effacement to a greater degree than did AG or NG alone. The number of podocytes per glomerulus, as well as renal expression of nephrin, α-dystroglycan, and Bcl-xl, was decreased, while podocyte apoptosis, as well as renal expression of Bax and Nox4, was increased in diabetic rats. All of these abnormalities were partially restored by AG plus NG to a greater degree than did AG or NG alone. In conclusion, AG and NG synergistically ameliorated diabetic podocyte injury partly through upregulation of nephrin, α-dystroglycan, and Bcl-xl, as well as downregulation of Bax and Nox4. These findings might provide a novel treatment combination for DN.

1. Introduction

Diabetic nephrology (DN) is one of the most frequent complications of diabetes, and end-stage renal disease (ESRD) in almost 50% of patients was attributed to diabetes in developed countries [1]. Diabetes has also become the leading cause of chronic kidney disease in urban Chinese patients since 2011 [2]. Current therapeutic approaches for DN have been limited to drugs acting on glycemic and blood pressure control; however, there is no effective treatment to delay or prevent the progression of DN [3, 4]. Thus, there is an urgent need for the development of novel approaches for treatment of DN. Podocytes are highly specialized, terminally differentiated epithelial cells, which are important for maintaining glomerular permselectivity [5]. Recent studies indicated that podocyte detachment promoted kidney disease in type 2 DN [6]. Podocytes may encounter foot process effacement and podocyte loss in diabetic conditions [7]. Podocyte loss is the strongest predictor of progression of DN [8]. Taken together, podocyte injury played a critical role in the initiation and progression of DN [9]. Increasing amount of data suggested a beneficial role of Traditional Chinese Medicine (TCM) in DN because of its multiple actions and integral regulation [10]. Astragalus membranaceus (AG), one of the

most commonly used Chinese herbs, has been widely used as an immune stimulant and antioxidant [11]. It has been reported that Astragalus membranaceus injection reduced albuminuria in DN patients [12]. Our previous study indicated that Astragaloside IV, one of the active components of AG, prevented podocyte apoptosis *in vivo* and *in vitro* [13]. Panax notoginseng (NG) has long been prescribed for prevention and treatment of cardiovascular diseases in China and other Asian countries [14]. Our previous study demonstrated that Notoginsenoside R1, one of the active components of NG, ameliorated podocyte adhesion *in vivo* and *in vitro* [15]. However, the combined effects of AG and NG on DN have not been investigated yet. Therefore, the present study was aimed at examining the combined effects of AG and NG on podocyte injury in diabetic rats and then providing a novel treatment combination for DN.

2. Materials and Methods

2.1. Drugs and Reagents. Losartan was purchased from Merck Sharp & Dohme Limited (Merck Sharp & Dohme, Australia). AG granule was purchased from Sichuan Baili Pharmaceutical Co. Ltd. (Sichuan, China). NG granule was purchased from China Resources Sanjiu Medical & Pharmaceutical Co. Ltd. (Shenzhen, China). Streptozotocin (STZ) was purchased from Sigma-Aldrich Company (Sigma-Aldrich, USA). Mouse monoclonal anti-Wilms tumor (WT1) (ab212951), rabbit monoclonal anti-Bax (ab32503), rabbit monoclonal anti-Bcl-xl (ab32370), rabbit monoclonal anti-nephrin (ab216341), rabbit monoclonal anti-Nox4 (ab133303), goat anti-rabbit IgG (ab6721), and monoclonal anti-β-actin antibodies (ab8226) were purchased from Abcam Biotechnology (Abcam, England). A rabbit polyclonal anti-α-dystroglycan (abs125549a) antibody was purchased from Absin Biochemical Company (Absin, Shanghai, China). The FastQuant RT Kit (with gDNase) was purchased from Tiangen Biochemical Technology Co. Ltd. (Beijing, China). ChamQ Universal SYBR qPCR Master Mix was purchased from Vazyme Biotech Co. Ltd. (Nanjing, China).

2.2. Animal Study. The animal protocols were approved by the Animal Ethics Committee of Shanghai Jiao Tong University Affiliated Sixth People's Hospital (Animal Welfare Ethics acceptance number: DWLL2018-0334 and Animal Experiment Registration number: DWSY2018-014), Shanghai, China. All the procedures were performed in accordance with the *Guide for the Care and Use of Laboratory Animals* published by the National Institutes of Health. Eight-week-old healthy male Sprague-Dawley rats, weighing between 200 and 250 g, were housed at a clean-grade laboratory animal room in the Animal Laboratory Center of Shanghai Sixth People's Hospital. Rats were housed in an air-conditioned room at 23 ± 1°C on a 12 : 12 h light-dark cycle. All animals were given free access to standard rat chow and water. Diabetes was induced by a single intraperitoneal injection of streptozotocin (STZ, 55 mg/kg), freshly dissolved in citrate buffer (0.1 mol/L). Seventy-two hours after injection of STZ, the blood glucose level was measured from the tail vein. Rats with a blood glucose level over 16.7 mmol/L were considered to be diabetic [16] and selected for the subsequent experiments. Diabetic rats were then randomly divided into 5 groups ($n = 6$/each group), which were treated with saline, losartan ($0.01\ g{\cdot}kg^{-1}{\cdot}d^{-1}$), AG ($0.8\ g{\cdot}kg^{-1}{\cdot}d^{-1}$), NG ($0.4\ g{\cdot}kg^{-1}{\cdot}d^{-1}$), and AG ($0.8\ g{\cdot}kg^{-1}{\cdot}d^{-1}$) plus NG ($0.4\ g{\cdot}kg^{-1}{\cdot}d^{-1}$), respectively. Normal Sprague-Dawley rats were also treated with saline. After being treated for 3 and 12 weeks, 24 h urine was collected with individual metabolic cages. At the end of 12 weeks of treatment, all the rats were sacrificed and blood samples and kidneys were harvested.

2.3. Urinary Albumin and Biochemical Markers. After being harvested, the urine samples were centrifuged at 2000 rpm for 10 minutes and the supernatants of urine were measured for the albumin creatinine ratio (ACR) by an automatic biochemistry analyzer (Hitachi Model 7600-120E, Japan). Blood samples were taken from the abdominal aorta, and EDTA was used for anticoagulation; after being harvested, blood samples were centrifuged at 2000 rpm for 10 minutes and the supernatants of blood were measured for serum creatinine and alanine aminotransferase (ALT) by an automatic biochemistry analyzer (Hitachi Model 7600-120E, Japan).

2.4. Light Microscopy. Hematoxylin and eosin (H&E) staining and periodic acid-Schiff (PAS) staining were performed on paraffin sections. Slides were dried for 30 minutes at 65°C and then were deparaffinized and rehydrated through dimethylbenzene(I), dimethylbenzene(II), 100% ethanol(I), 100% ethanol(II), 95% ethanol, 90% ethanol, 80% ethanol, and deionized water, 10 minutes for each step. The sections were then subjected to H&E staining and PAS staining and observed under a light microscope (Leica, Germany).

2.5. Transmission Electron Microscopy. The renal cortices were prefixed with 2% glutaraldehyde for 2 hours at 4°C and washed with phosphate-buffered saline (PBS) for three times and then were postfixed with 1% osmic acid for 2 hours at 4°C. After step-by-step dehydration with ethyl alcohol, renal cortices were embedded in epoxy resin. Ultrathin sections were prepared with an ultramicrotome (LKB Company, Sweden), stained with uranyl acetate and lead citrate, and were then examined with a Philip electron microscope (Philip CM-120, Netherlands). The number of podocyte foot processes per μm of GBM was calculated using a curvimeter. Three glomeruli were randomly selected from each rat, and 10 electron micrographs were taken in each glomerulus.

2.6. Western Blot Analysis. The renal cortex was lysed in radioimmunoprecipitation assay (RIPA) lysis buffer with phenylmethanesulfonyl fluoride (PMSF), loading buffer, and phosphatase on ice, and protein concentration was determined by the bicinchoninic acid protein assay kit (Biosharp, China). Proteins from renal cortex lysates were denatured in boiling water for 10 minutes, loaded to 10% SDS-polyacrylamide gel electrophoresis (SDS-PAGE), and transferred onto nitrocellulose membranes. The membranes were blocked for 1 hour with 5% bovine serum albumin (BSA) in Tris-buffer saline containing 0.1% Tween 20 (TBST) at room temperature. The membrane was incubated overnight at 4°C with a primary antibody, then washed with

TBST for five times and incubated with horseradish peroxidase-conjugated secondary antibodies (Beyotime, China) at room temperature for 1 hour and developed with an enhanced chemiluminescence agent. The membranes were placed on the ChemiDoc Touch Imaging System (Bio-Rad Laboratories, USA) to image a protein band, and ImageJ (Adobe Corp., USA) was used to determine band intensity. Protein expression was quantified as the ratio of a specific band to β-actin.

2.7. Immunohistochemistry. Immunohistochemistry was performed on paraffin sections. After being deparaffinized and rehydrated, antigens were retrieved by boiling in citrate buffer. Slides were blocked with 0.3% H_2O_2 for 15 minutes and 5% BSA (Meilunbio, China) for 1 hour. The primary antibody was incubated overnight at 4°C. After being washed with TBST for three times, slides were incubated with peroxidase-conjugated secondary antibodies (Beyotime, China) for 1 hour at room temperature. Images were recorded with a microscope (Leica, Germany). Image analysis was performed using the ImageJ software (Adobe Corp., USA). For quantitative determination of podocyte numbers, the WT1-positive cells were counted in three randomly chosen glomeruli. Other protein expressions were quantified as the ratio of the positive area to the control group.

2.8. Immunofluorescence. Podocyte apoptosis was determined by triple immunofluorescence labeling including terminal deoxynucleotidyl transferase-mediated dUTP nick-end labeling (TUNEL) assay, WT1, and 4′,6-diamidino-2-phenylindole (DAPI). The apoptotic cells were determined with the In Situ Cell Death Detection Kit (POD) (Roche, Switzerland) on paraffin-embedded kidney sections. The TUNEL assay was performed according to the manufacturer's instructions. The triple-positive cells, WT1 (red), TUNEL (green), and DAPI (blue), were identified as the apoptotic podocytes. The fluorescent images were examined under a fluorescence microscope (Leica, Germany). The sections were evaluated independently by two blinded investigators.

2.9. Quantitative Real-Time Reverse Transcription Polymerase Chain Reaction (RT-PCR). Total RNA was isolated from the kidney with TRIzol (Invitrogen, USA), and reverse transcription was performed to generate a cDNA template. The relative mRNA levels were determined via fluorogenic quantitative PCR, and β-actin was served as an internal reference gene. Specific primers for the use of SYBR Green are as follows: nephrin: 5′-AGAGACT GGGAGA AGAAGAG-3′ (forward) and 5′-AGCAAATCGGACGA CAAG-3′ (reverse); Nox4: 5′-CAGTCAAACAGATGGG ATACAGA-3′ (forward) and 5′-ATAGAACTGGGTC CACAGCAGA-3′ (reverse); and Bax: 5′-GTGGTTGCCCT CTTCTACTTTG-3′ (forward) and 5′-CACAAAGATGG TCACTGTCTGC-3′ (reverse). The PCR parameters were as follows: 95°C for 30 s followed by 40 cycles of denaturation at 95°C for 10 s and annealing at 60°C for 30 s. The relative mRNA levels were normalized to those of β-actin.

2.10. Statistical Analysis. SPSS 23.0 software was adopted to perform statistical analysis. All data were presented as mean ± standard deviation (SD). One-way analysis of variance (ANOVA) followed by Fisher's least significant difference (LSD) post hoc test was applied for multiple comparisons. P value < 0.05 was considered statistically significant. GraphPad Prism v5 was used for the histograms.

3. Results

3.1. Effects of AG and NG on Physical and Biochemical Parameters in Diabetic Rats. Compared with normal control rats, diabetic rats developed severe albuminuria, at 3 weeks (Figure 1(a)) and 12 weeks (Figure 1(b)) after STZ injection. However, treatment with losartan, AG, NG, and AG plus NG significantly reduced the urinary albumin/creatinine ratio (ACR). Remarkably, AG plus NG reduced ACR to a greater degree than did AG or NG alone at 3 weeks (Figure 1(a)) and 12 weeks (Figure 1(b)) after STZ injection. Blood glucose (Figure 1(c)) was much higher in diabetic rats than in normal control rats. No significant differences in the level of serum creatinine (Figure 1(d)) and ALT (Figure 1(e)) were observed between each group, which indicated that AG, NG, and AG plus NG did not cause apparent toxicity to the liver and kidney. Moreover, diabetic rats showed a higher kidney weight per body weight ratio than normal control rats. However, AG plus NG, rather than AG or NG alone, decreased the kidney weight per body weight ratio in diabetic rats (Figure 1(f)). These results demonstrated that AG and NG synergistically attenuated albuminuria in diabetic rats.

3.2. Effects of AG and NG on Renal Histopathology and Podocyte Foot Process Effacement in Diabetic Rats. Twelve weeks after diabetes induction, diabetic rats were characterized with mesangial expansion compared with nondiabetic rats (Figures 2(a) and 2(c)). However, treatment with losartan, AG, NG, and AG plus NG ameliorated mesangial expansion in diabetic rats. Quantitative analysis also revealed a significant improvement in mesangial expansion from the kidneys of rats treated with AG and NG (Figures 2(b) and 2(d)). Transmission electron microscopy images showed apparent podocyte foot process effacement in diabetic rats (Figure 2(e)). However, treatment with losartan, AG, NG, and AG plus NG markedly increased the number of podocyte foot processes per μm of GBM (Figure 2(f)). The effects of AG plus NG on renal histopathology and podocyte foot process effacement were better than those of AG or NG alone. The above results indicated that AG and NG synergistically attenuated renal histopathology and podocyte foot process effacement in diabetic rats.

3.3. Effects of AG and NG Treatment on Podocyte Number and mRNA and Protein Levels of Nephrin and α-Dystroglycan in STZ-Induced Diabetic Rats. To assess podocyte number per glomerulus, the renal tissue sections were immune stained with WT1. The number of podocytes per glomerulus was determined by counting the number of WT1-positive nuclei per glomerulus. At 12 weeks after STZ injection, diabetic rats showed a severe reduction in podocyte

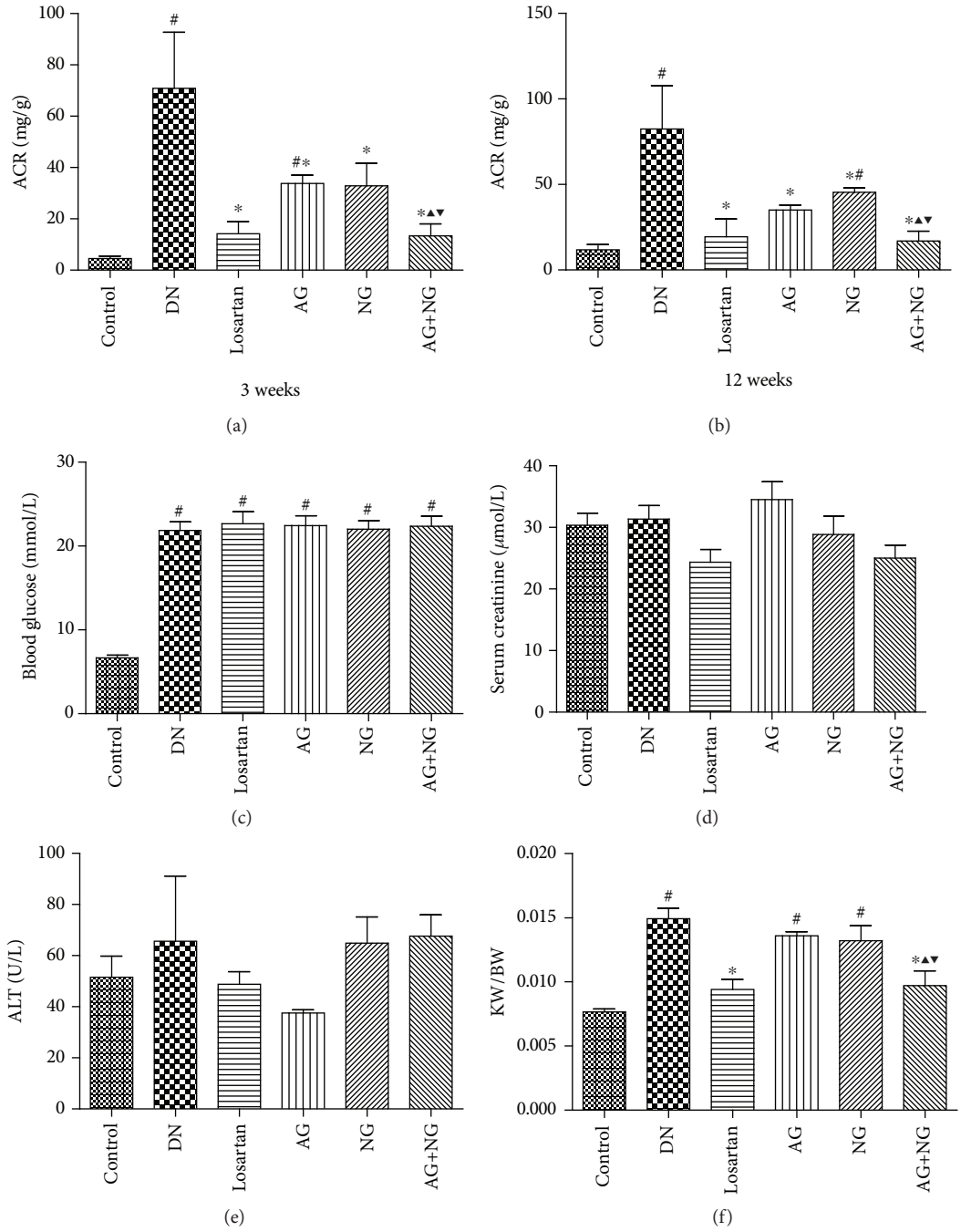

Figure 1: Effects of AG and NG on physical and biochemical parameters in diabetic rats. ACR in diabetic rats after treatment with AG and NG for 3 weeks (a) and 12 weeks (b). Blood glucose (c) after STZ injection. Serum creatinine (d), ALT (e), and KW/BW (f) after treatment with AG and NG for 12 weeks. ACR: albuminuria/creatinine ratio; ALT: alanine aminotransferase; KW/BW: kidney weight per body weight ratio; control: normal control rats; DN: STZ-induced diabetic rats; losartan: DN rats treated with losartan; AG: DN rats treated with Astragalus membranaceus; NG: DN rats treated with Panax notoginseng; AG+NG: DN rats treated with Astragalus membranaceus plus Panax notoginseng. Results were expressed as the mean ± SD ($n = 6$). $^{\#}P < 0.05$ vs. control group, $^{*}P < 0.05$ vs. DN group, $^{\blacktriangle}P < 0.05$ vs. AG group, $^{\blacktriangledown}P < 0.05$ vs. NG group.

number per glomerulus when compared with the normal control rats (Figure 3(a)). However, daily treatment with losartan, AG, NG, and AG plus NG for 12 weeks had a substantial normalizing effect on podocyte density in diabetic rats (Figure 3(b)). Importantly, AG plus NG increased podocyte number per glomerulus to a greater degree than did AG or NG alone. We further investigated the effects of AG and NG on nephrin and α-dystroglycan expression in diabetic rats. As shown by immunohistochemical staining (Figure 3(a)) and western blot (Figure 4(a)), the expression of nephrin and α-dystroglycan was reduced in the renal tissue from STZ-induced diabetic rats when compared with the normal control

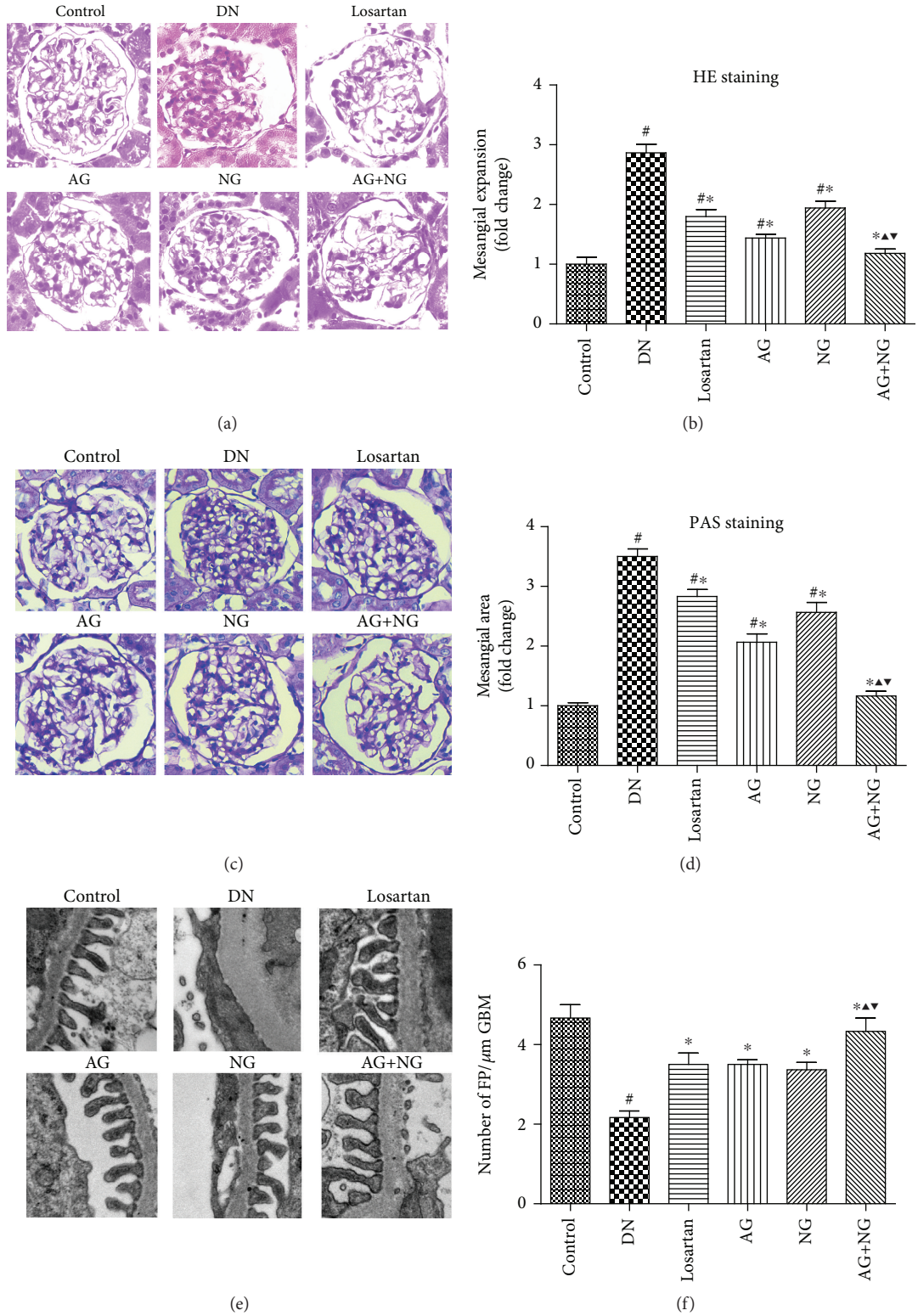

Figure 2: Effects of AG and NG on renal histopathology and podocyte foot process effacement in diabetic rats. Representative hematoxylin and eosin (H&E, kidney histology (×400)) staining (a) and periodic acid-Schiff (PAS, kidney histology (×400)) staining (c) of kidney sections. Representative ultrastructure photos of glomerular podocytes taken by transmission electron microscopy (TEM) (×13500) (e). Semiquantitative analysis of mesangial expansion (b), mesangial area (d), and podocyte foot process density (f). FP: foot process; GBM: glomerular basement membrane; control: normal control rats; DN: STZ-induced diabetic rats; losartan: DN rats treated with losartan; AG: DN rats treated with Astragalus membranaceus; NG: DN rats treated with Panax notoginseng; AG+NG: DN rats treated with Astragalus membranaceus plus Panax notoginseng. Results were expressed as the mean ± SD. $^{\#}P < 0.05$ vs. control group, $^{*}P < 0.05$ vs. DN group, $^{\blacktriangle}P < 0.05$ vs. AG group, $^{\blacktriangledown}P < 0.05$ vs. NG group.

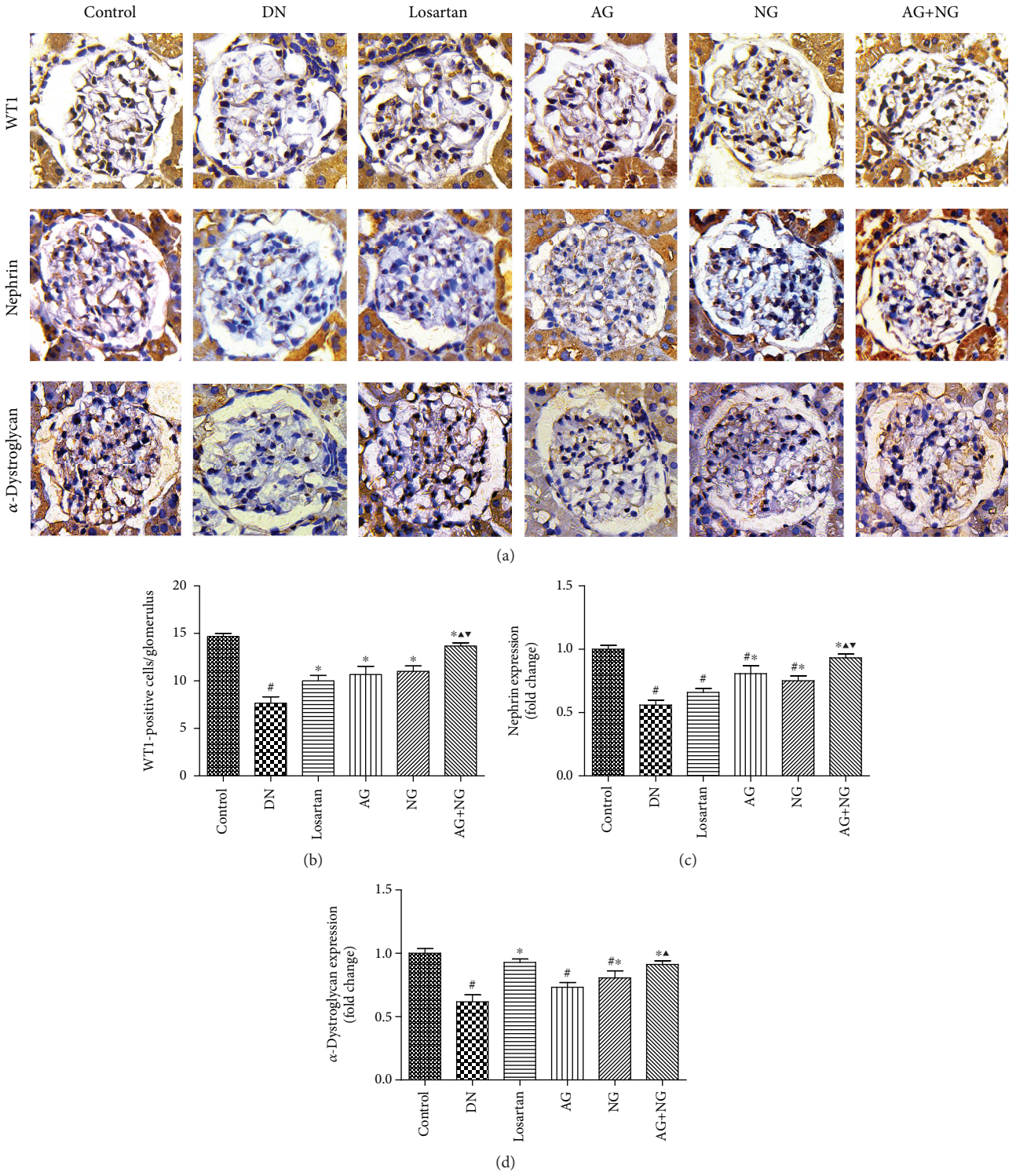

Figure 3: Effects of AG and NG on the expression of WT1, nephrin, and α-dystroglycan detected by immunohistochemical staining. Representative photomicrographs of immunostaining for WT1, nephrin, and α-dystroglycan (a) in the glomeruli of kidney sections. Quantitative analyses of changes in the number of podocytes per glomerular volume (b). The number of podocytes per glomerulus was determined by counting the number of WT1-expressing nuclei per glomerulus. Semiquantitative analyses of immunostaining for nephrin (c) and α-dystroglycan (d) per glomerulus. Control: normal control rats; DN: STZ-induced diabetic rats; losartan: DN rats treated with losartan; AG: DN rats treated with Astragalus membranaceus; NG: DN rats treated with Panax notoginseng; AG+NG: DN rats treated with Astragalus membranaceus plus Panax notoginseng. Results were expressed as the mean ± SD. $^{\#}P < 0.05$ vs. control group, $^{*}P < 0.05$ vs. DN group, $^{\blacktriangle}P < 0.05$ vs. AG group, $^{\blacktriangledown}P < 0.05$ vs. NG group.

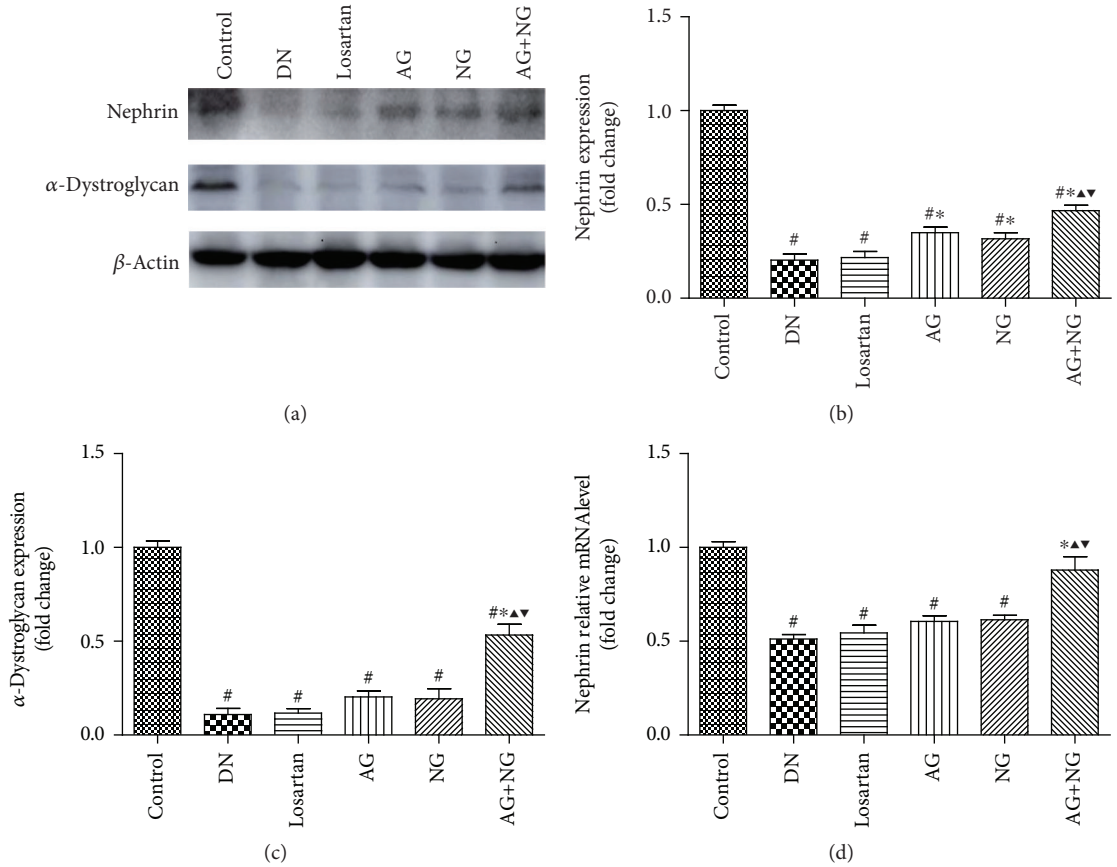

Figure 4: Effects of AG and NG on the levels of nephrin and α-dystroglycan detected by western blot and RT-PCR. Representative western blots for nephrin and α-dystroglycan (a) in the glomeruli of kidney sections. Semiquantitative analyses of western blot for nephrin (b) and α-dystroglycan (c). Glomerular relative mRNA level of nephrin (d). Control: normal control rats; DN: STZ-induced diabetic rats; losartan: DN rats treated with losartan; AG: DN rats treated with Astragalus membranaceus; NG: DN rats treated with Panax notoginseng; AG+NG: DN rats treated with Astragalus membranaceus plus Panax notoginseng. Results were expressed as the mean ± SD. $^{\#}P < 0.05$ vs. control group, $^{*}P < 0.05$ vs. DN group, $^{\blacktriangle}P < 0.05$ vs. AG group, $^{\blacktriangledown}P < 0.05$ vs. NG group.

rats. However, AG plus NG treatment increased the expression of nephrin and α-dystroglycan in diabetic rats. Quantitative analysis also showed a significant increase in the expression of nephrin (Figures 3(c) and 4(b)) and α-dystroglycan (Figures 3(d) and 4(c)) from the kidneys of rats treated with AG plus NG. We also studied the effect of AG and NG on the mRNA level of nephrin, and the renal mRNA level of nephrin was reduced in diabetic rats. However, AG plus NG treatment increased the renal mRNA level of nephrin (Figure 4(d)). The above results indicated that AG plus NG synergistically attenuated podocyte loss and restored the mRNA and protein level of nephrin, as well as the expression of α-dystroglycan in diabetic rats.

3.4. Effects of AG and NG on Podocyte Apoptosis and mRNA and Protein Levels of Bax and Bcl-xl in STZ-Induced Diabetic Rats. Podocyte apoptosis was significantly increased in diabetic rats when compared with normal control rats. However, treatment with losartan, AG, NG, and AG plus NG for 12 weeks attenuated podocyte apoptosis in diabetic rats (Figure 5). To reveal the mechanisms underlying the effects of AG plus NG on podocyte apoptosis, the mRNA and protein levels of Bax and Bcl-xl were examined. The Bax expression was elevated, and the Bcl-xl expression was reduced in diabetic rats, as shown by immunohistochemical staining (Figure 6(a)) and western blot (Figure 6(e)). However, treatment with losartan and AG plus NG for 12 weeks restored the Bax and Bcl-xl expression in diabetic rats. Quantitative analysis also showed a significant decrease in Bax expression (Figures 6(b) and 6(f)) and an increase in Bcl-xl expression (Figures 6(c) and 6(g)) from the kidneys of rats treated with AG plus NG. As shown by the RT-PCR study, the mRNA level of Bax was increased in diabetic rats (Figure 6(d)). However, treatment with losartan and AG plus NG for 12 weeks restored the mRNA level of Bax in diabetic rats. The above results demonstrated that AG plus NG synergistically attenuated podocyte apoptosis and restored the balance of Bax and Bcl-xl expression.

3.5. Effects of AG and NG on mRNA and Protein Levels of Nox4 in STZ-Induced Diabetic Rats. Compared with the normal control rats, the protein expression and mRNA level of Nox4 were significantly increased in diabetic rats, as shown by immunohistochemical staining (Figure 7(a)), western blot

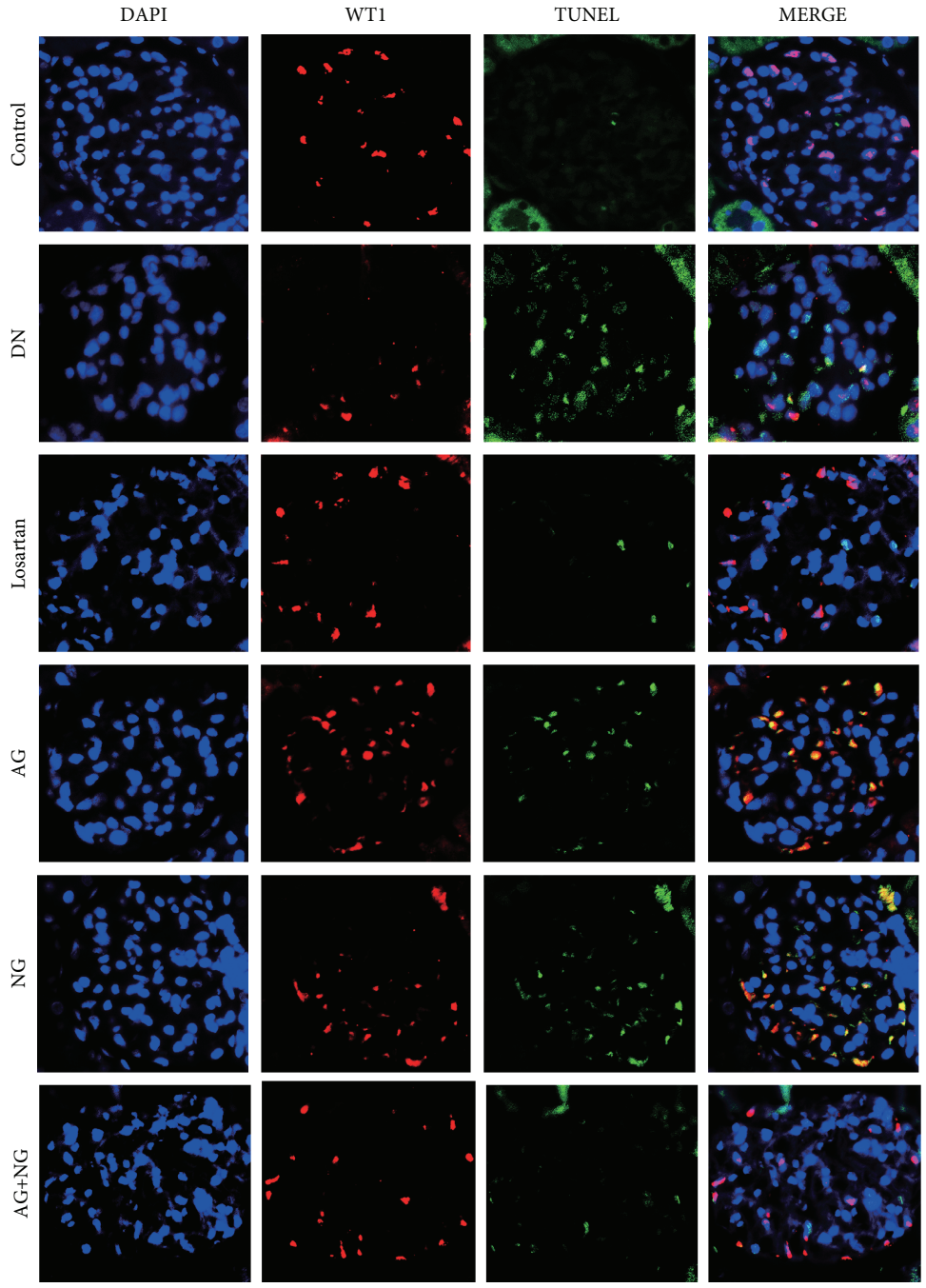

Figure 5: Effects of AG and NG on podocyte apoptosis in diabetic rats. The triple-positive cells, WT1 (red), TUNEL (green), and DAPI (blue), were identified as the apoptotic podocytes. Control: normal control rats; DN: STZ-induced diabetic rats; losartan: DN rats treated with losartan; AG: DN rats treated with Astragalus membranaceus; NG: DN rats treated with Panax notoginseng; AG+NG: DN rats treated with Astragalus membranaceus plus Panax notoginseng.

(Figure 7(c)), and RT-PCR (Figure 7(e)). However, treatment with losartan, AG, NG, and AG plus NG for 12 weeks significantly reduced the protein expression and mRNA level of Nox4 in the kidney cortex (Figures 7(b), 7(d), and 7(e)). Remarkably, AG plus NG reduced Nox4 expression and mRNA level to a greater degree than did AG or NG alone. The above results indicated that AG plus NG synergistically reduced Nox4 mRNA and protein levels in diabetic rats.

4. Discussion

In the present study, we firstly reported that AG plus NG synergistically ameliorated podocyte injury in STZ-induced diabetic rats. Our conclusion was supported by the following findings. (i) AG plus NG attenuated albuminuria, renal histopathology, and podocyte foot process effacement to a greater degree than did AG or NG alone. (ii) AG plus NG increased

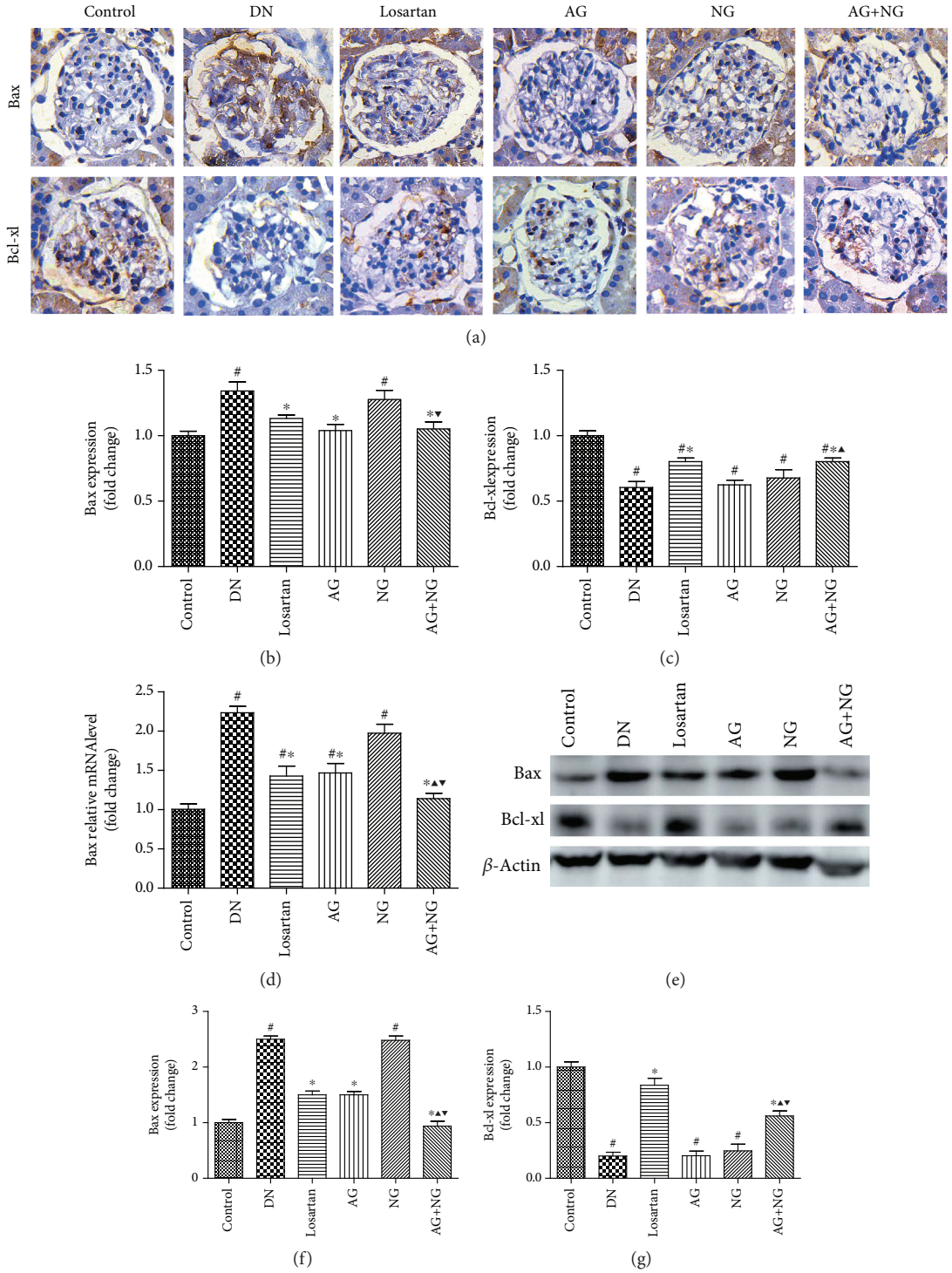

FIGURE 6: Effects of AG and NG on the expression of Bax and Bcl-xl in diabetic rats. Representative photomicrographs of immunostaining (a) and western blots (e) for Bax and Bcl-xl in the glomeruli of kidney sections. Semiquantitative analyses of immunostaining for Bax (b) and Bcl-xl (c). Glomerular relative mRNA levels of Bax (d). Semiquantitative analyses of western blots for Bax (f) and Bcl-xl (g). Control: normal control rats; DN: STZ-induced diabetic rats; losartan: DN rats treated with losartan; AG: DN rats treated with Astragalus membranaceus; NG: DN rats treated with Panax notoginseng; AG+NG: DN rats treated with Astragalus membranaceus plus Panax notoginseng. Results were expressed as the mean ± SD. $^{\#}P < 0.05$ vs. control group, $^{*}P < 0.05$ vs. DN group, $^{\blacktriangle}P < 0.05$ vs. AG group, $^{\blacktriangledown}P < 0.05$ vs. NG group.

podocyte number and decreased apoptotic podocytes to a greater degree than did AG or NG alone. (iii) AG plus NG increased renal expression of nephrin, α-dystroglycan, and Bcl-xl, while it decreased renal expression of Nox4 to a greater degree than did AG or NG alone. These results clearly demonstrated that the combination of AG and NG synergistically attenuated podocyte injury and subsequent podocyte loss (Figure 8). AG, commonly known as Huangqi, is famous

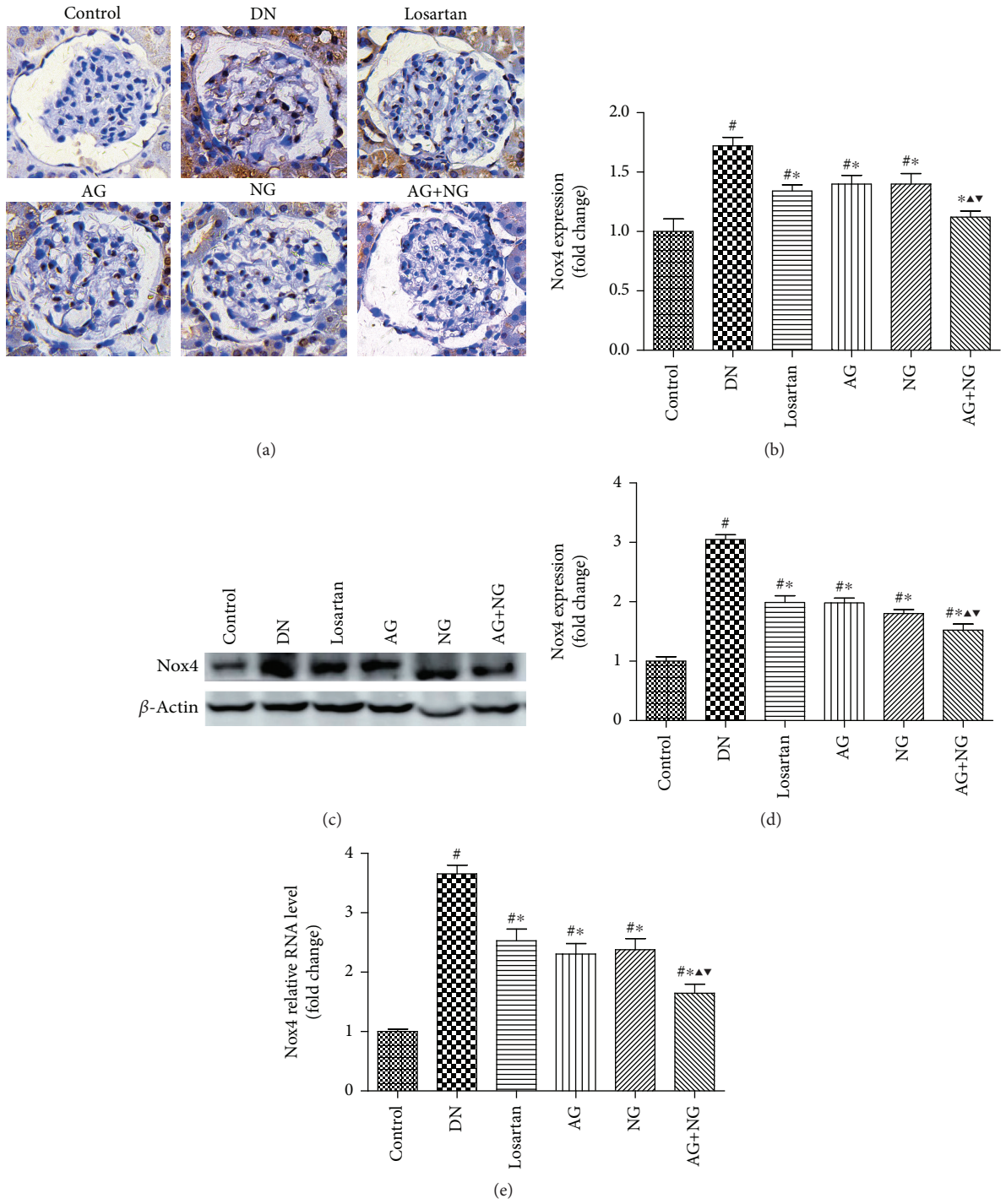

Figure 7: Effects of AG and NG on NADPH oxidase 4 (Nox4) in diabetic rats. Representative photomicrographs of immunostaining (a) and western blots (c) for Nox4 in the glomeruli of kidney sections. Semiquantitative analyses of immunostaining (b) and western blots (d) for Nox4. Glomerular relative mRNA levels of Nox4 (e). Control: normal control rats; DN: STZ-induced diabetic rats; losartan: DN rats treated with losartan; AG: DN rats treated with Astragalus membranaceus; NG: DN rats treated with Panax notoginseng; AG+NG: DN rats treated with Astragalus membranaceus plus Panax notoginseng. Results were expressed as the mean ± SD. $^{\#}P < 0.05$ vs. control group, $^{*}P < 0.05$ vs. DN group, $^{\blacktriangle}P < 0.05$ vs. AG group, $^{\blacktriangledown}P < 0.05$ vs. NG group.

for tonifying qi (Yiqi). NG, commonly known as Sanqi, is famous for invigorating blood (Huoxue). A meta-analysis indicated that the Yiqi Yangyin Huoxue method is beneficial to DN patients in reducing microalbuminuria [17]. In the present study, treatment with losartan, AG, NG, and AG plus NG for 12 weeks significantly reduced albuminuria and improved renal histopathology and podocyte foot process effacement in STZ-induced diabetic rats. The effect of AG or NG on decreasing albuminuria was worse than that of losartan; however, the effect of AG plus NG on decreasing

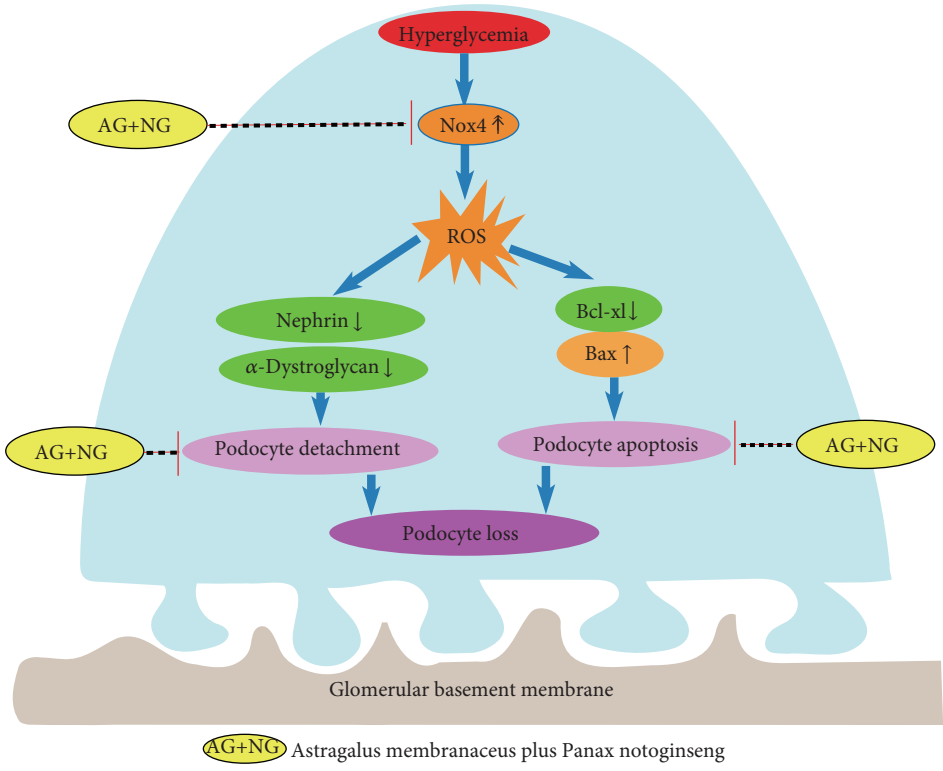

Figure 8: Graphic representation of the potential protection mechanism of AG plus NG on podocyte injury in diabetic rats.

albuminuria was similar to that of losartan. These results clearly demonstrated that AG and NG synergistically attenuated the structural and functional abnormalities in diabetic rats. These findings provide a novel treatment combination for DN and other kidney diseases affecting podocytes.

Podocyte injury plays a critical role in the progression of DN. It has been reported that the number of podocytes is decreased in the glomeruli of diabetic patients [18] and diabetic animal models [19]. The reduction in podocyte density is the strongest predictor of progressive DN [20]. Podocyte depletion may lead to glomerular sclerosis and progressively renal dysfunction [21]. Studies have shown that the number of podocytes is the most powerful predictor of renal prognosis in type 2 DM patients [22]. WT1 is expressed throughout life in the podocyte nucleus and used as a specific marker for podocytes [23, 24]. Thus, we used WT1 immunohistochemistry staining for podocyte nuclei and measured the podocyte number per glomerulus. In this study, diabetic rats showed a significant reduction in podocyte number per glomerulus. However, daily treatment with losartan, AG, NG, and AG plus NG for 12 weeks had a substantial normalizing effect on podocyte density in diabetic rats, and the effect of AG plus NG was better than those of losartan, AG, and NG. These results indicated that AG plus NG ameliorated podocyte loss in diabetic rats. The main cause underlying podocyte loss has been considered to be detachment and apoptosis [25, 26]. Detached viable podocytes have been found in the urine of DN patients [27], suggesting that impaired podocyte adhesion to the glomerular basement membrane (GBM) may be a pivotal step in the development of DN. Nephrin is the central component of podocyte slit diaphragm [28]. Nephrin functions as a signaling scaffold, influencing signal transduction pathways which control podocyte adhesion, shape, and survival [29]. α-Dystroglycan is localized to basal cell membrane domains of the podocyte and stabilizes podocytes on the GBM [30]. Splitting of dystroglycan-matrix interaction leads to podocyte flattening and disorder of GBM [31]. In this study, diabetic rats showed reduced expression of nephrin and α-dystroglycan in the renal cortex. However, treatment with AG plus NG upregulated the expression of nephrin and α-dystroglycan in diabetic rats, and the effects of AG plus NG were better than those of losartan, AG, and NG. These results indicated that AG plus NG ameliorated podocyte detachment partly by increasing the expression of nephrin and α-dystroglycan in diabetic rats.

We also investigated the effects of AG plus NG on podocyte apoptosis and the underlying mechanisms. Podocyte apoptosis was accurately detected by triple immunofluorescence labeling including TUNEL assay, WT1, and DAPI. We found that diabetic rats showed more apoptotic podocytes, which was consistent with previous research results [32, 33]. Treatment with losartan, AG, NG, and AG plus NG ameliorated podocyte apoptosis in diabetic rats. We then examined the expression of Bax and Bcl-xl expression in diabetic rats to further explore the antiapoptotic effects of AG plus NG. Apoptosis is triggered by either an intrinsic pathway or an extrinsic pathway; the intrinsic apoptotic pathway is controlled by the family of B-cell lymphoma-2 proteins [34]. Bax is activated by stress stimulus, then accumulates on mitochondria and increases the permeability of the mitochondrial outer membrane, resulting in the release of cytochrome C, which in turn promotes the apoptotic process

[35]. Bcl-xl acts as an inhibitor of Bax by preventing Bax accumulation to mitochondria and thus prevents the apoptotic process [36]. In this study, diabetic rats showed increased expression of Bax and reduced expression of Bcl-xl in kidneys. However, treatment with losartan and AG plus NG reduced Bax expression and increased Bcl-xl expression, and the effect of AG plus NG was better than that of losartan on Bax expression and was equal with that of losartan on Bcl-xl expression. These results indicated that AG plus NG inhibited podocyte apoptosis partly through restoring the balance of Bax and Bcl-xl expression in diabetic rats.

Finally, we examined the effects of AG plus NG on oxidative stress in diabetic rats. NADPH oxidases are one of the major causes of reactive oxygen species (ROS), which is a key event influencing the pathogenesis of DN [37]. During the progression of DN, ROS is an important second messenger of apoptosis and inflammation-related signaling pathways [38]. Exposure to ROS leads to deglycosylation of α-dystroglycan and subsequent podocyte detachment [39]. Glucose-induced ROS also cause podocyte apoptosis and podocyte depletion at the onset of diabetic nephropathy [20, 40]. It was reported that Astragaloside IV inhibited oxidative stress in renal proximal tubular cells [41] and Panax notoginseng saponins protected the kidney from diabetes by activating antioxidant proteins in rats [42]. Nox4 is one of the isoforms of NADPH oxidases and is highly expressed in renal tissues [43]. Nox4-derived ROS participate in the pathological process of DN by reducing glucose tolerance, increasing the production of proteinuria, and promoting renal fibrosis [44]. Nox4 expression was upregulated in diabetic mice and genetic depletion or pharmacologic inhibition of Nox4 provided renoprotection in long-term DN [45, 46], while specific induction of Nox4 expression in podocytes can lead to typical pathological changes of DN in rats' kidneys [47]. In this study, the kidney of diabetic rats showed elevated expression of Nox4 compared with the kidney of nondiabetic rats. While treatment with losartan, AG, NG, and AG plus NG for 12 weeks significantly reduced Nox4 expression in diabetic rats, the effect of AG plus NG was better than those of losartan, AG, and NG. These results indicated that AG plus NG protected against podocyte injury partly by inhibiting oxidative stress in diabetic rats.

We also examined the serum creatinine and ALT levels and blood glucose in rats, and AG plus NG exhibited no effects on the levels of serum creatinine and ALT, indicating that AG plus NG did not cause apparent toxicity to the kidney and liver. Diabetic rats were randomly divided into four groups, namely, diabetic rats (DN) and diabetic rats treated with AG, NG, and AG plus NG. Figure 1(c) shows the level of blood glucose at baseline and at the period when AG, NG, and AG plus NG treatment was not started. Therefore, there was no significant difference in the level of blood glucose among these three groups.

According to the package inserts, the doses of AG and NG in human being was 8 $g \cdot d^{-1}$ [48] and 4 $g \cdot d^{-1}$ [49], respectively. According to the FDA guidance [50], the doses of AG and NG in rats were 0.76 $g \cdot kg^{-1} \cdot d^{-1}$ and 0.38 $g \cdot kg^{-1} \cdot d^{-1}$, respectively, equivalent to the doses used in human, so the doses we adopted in this study were 0.8 $g \cdot kg^{-1} \cdot d^{-1}$ and 0.4 $g \cdot kg^{-1} \cdot d^{-1}$, respectively.

There are limitations in this study. First, we only performed *in vivo* studies and the effects of AG and NG on podocytes cultured in high glucose condition need to be further investigated. Second, we cannot be sure that the results from the rodent model can be translated to human. Therefore, the effects of AG and NG in a clinical setting need to be further investigated.

5. Conclusions

Taken together, AG and NG, the novel renoprotective compound, synergistically ameliorated diabetic podocyte injury partly through upregulation of nephrin, α-dystroglycan, and Bcl-xl, as well as downregulation of Bax and inhibition of oxidative stress. These findings might provide a novel treatment combination for DN.

Data Availability

The data that support the findings of this study are available from the corresponding authors upon reasonable request.

Conflicts of Interest

The authors declare that they have no competing interests.

Acknowledgments

This research was funded by grants from the National Nature Science Foundation of China (81774052 and 81573738), Pudong New Area Science and Technology Commission (PKJ2015-Y10) and Integrated Chinese and Western Medicine Program of Shanghai Comprehensive Hospital (ZHYY-ZXYJHZX-201607 and ZHYY-ZXYJHZX-2-01). This work was also supported by the Shanghai Pujiang Program (17PJD031) and three-year action plan for Shanghai further accelerating the development of traditional Chinese medicine (ZY(2018-2020)-CCCX-4007).

References

[1] J. J. Neumiller, R. Z. Alicic, and K. R. Tuttle, "Therapeutic considerations for antihyperglycemic agents in diabetic kidney disease," *Journal of the American Society of Nephrology*, vol. 28, no. 8, pp. 2263–2274, 2017.

[2] L. Zhang, J. Long, W. Jiang et al., "Trends in chronic kidney disease in China," *The New England Journal of Medicine*, vol. 375, no. 9, pp. 905-906, 2016.

[3] V. Lacava, V. Pellicanò, C. Ferrajolo et al., "Novel avenues for treating diabetic nephropathy: new investigational drugs," *Expert Opinion on Investigational Drugs*, vol. 26, no. 4, pp. 445–462, 2017.

[4] S. A. Johnson and R. F. Spurney, "Twenty years after ACEIs and ARBs: emerging treatment strategies for diabetic nephropathy," *American Journal of Physiology-Renal Physiology*, vol. 309, no. 10, pp. F807–F820, 2015.

[5] P. Mundel and W. Kriz, "Structure and function of podocytes: an update," *Anatomy and Embryology*, vol. 192, no. 5, pp. 385–397, 1995.

[6] E. J. Weil, K. V. Lemley, C. C. Mason et al., "Podocyte detachment and reduced glomerular capillary endothelial fenestration promote kidney disease in type 2 diabetic nephropathy," *Kidney International*, vol. 82, no. 9, pp. 1010–1017, 2012.

[7] J. J. Li, S. J. Kwak, D. S. Jung et al., "Podocyte biology in diabetic nephropathy," *Kidney International*, vol. 72, pp. S36–S42, 2007.

[8] M. E. Pagtalunan, P. L. Miller, S. Jumping-Eagle et al., "Podocyte loss and progressive glomerular injury in type II diabetes," *The Journal of Clinical Investigation*, vol. 99, no. 2, pp. 342–348, 1997.

[9] G. Wolf, S. Chen, and F. N. Ziyadeh, "From the periphery of the glomerular capillary wall toward the center of disease: podocyte injury comes of age in diabetic nephropathy," *Diabetes*, vol. 54, no. 6, pp. 1626–1634, 2005.

[10] R. Xue, D. Gui, L. Zheng, R. Zhai, F. Wang, and N. Wang, "Mechanistic insight and management of diabetic nephropathy: recent progress and future perspective," *Journal of Diabetes Research*, vol. 2017, Article ID 1839809, 7 pages, 2017.

[11] J. Fu, Z. Wang, L. Huang et al., "Review of the botanical characteristics, phytochemistry, and pharmacology of Astragalus membranaceus (Huangqi)," *Phytotherapy Research*, vol. 28, no. 9, pp. 1275–1283, 2014.

[12] Z. J. Bi, "Application of Astragalus injection on 68 patients with diabetic nephropathy," *Chinese Journal of Integrative Medicine on Cardio–Cerebro Vascular Disease*, vol. 6, no. 1, pp. 114-115, 2008.

[13] D. Gui, Y. Guo, F. Wang et al., "Astragaloside IV, a novel antioxidant, prevents glucose-induced podocyte apoptosis in vitro and in vivo," *PLoS One*, vol. 7, no. 6, article e39824, 2012.

[14] T. Wang, R. Guo, G. Zhou et al., "Traditional uses, botany, phytochemistry, pharmacology and toxicology of *Panax notoginseng* (Burk.) F.H. Chen: a review," *Journal of Ethnopharmacology*, vol. 188, pp. 234–258, 2016.

[15] D. Gui, L. Wei, G. Jian, Y. Guo, J. Yang, and N. Wang, "Notoginsenoside R1 ameliorates podocyte adhesion under diabetic condition through $\alpha_3\beta_1$ integrin upregulation in vitro and in vivo," *Cellular Physiology and Biochemistry*, vol. 34, no. 6, pp. 1849–1862, 2014.

[16] L. J. Coppey, J. S. Gellett, E. P. Davidson, J. A. Dunlap, D. D. Lund, and M. A. Yorek, "Effect of antioxidant treatment of streptozotocin-induced diabetic rats on endoneurial blood flow, motor nerve conduction velocity, and vascular reactivity of epineurial arterioles of the sciatic nerve," *Diabetes*, vol. 50, no. 8, pp. 1927–1937, 2001.

[17] J. Y. Ou, D. Huang, Y. S. Wu et al., "A meta-analysis of randomized controlled trials of Yiqi Yangyin Huoxue method in treating diabetic nephropathy," *Evidence-based Complementary and Alternative Medicine*, vol. 2016, Article ID 3257603, 12 pages, 2016.

[18] M. W. Steffes, D. Schmidt, R. McCrery, J. M. Basgen, and International Diabetic Nephropathy Study Group, "Glomerular cell number in normal subjects and in type 1 diabetic patients," *Kidney International*, vol. 59, no. 6, pp. 2104–2113, 2001.

[19] M.-L. Gross, A. El-Shakmak, A. Szábó et al., "ACE-inhibitors but not endothelin receptor blockers prevent podocyte loss in early diabetic nephropathy," *Diabetologia*, vol. 46, no. 6, pp. 856–868, 2003.

[20] K. Susztak, A. C. Raff, M. Schiffer, and E. P. Bottinger, "Glucose-induced reactive oxygen species cause apoptosis of podocytes and podocyte depletion at the onset of diabetic nephropathy," *Diabetes*, vol. 55, no. 1, pp. 225–233, 2006.

[21] R. C. Wiggins, "The spectrum of podocytopathies: a unifying view of glomerular diseases," *Kidney International*, vol. 71, no. 12, pp. 1205–1214, 2007.

[22] T. W. Meyer, P. H. Bennett, and R. G. Nelson, "Podocyte number predicts long-term urinary albumin excretion in Pima Indians with type II diabetes and microalbuminuria," *Diabetologia*, vol. 42, no. 11, pp. 1341–1344, 1999.

[23] P. Mundel, J. Reiser, and W. Kriz, "Induction of differentiation in cultured rat and human podocytes," *Journal of the American Society of Nephrology*, vol. 8, no. 5, pp. 697–705, 1997.

[24] A. Moktefi, S.-y. Zhang, P. Vachin et al., "Repression of CMIP transcription by WT1 is relevant to podocyte health," *Kidney International*, vol. 90, no. 6, pp. 1298–1311, 2016.

[25] S. J. Shankland, "The podocyte's response to injury: role in proteinuria and glomerulosclerosis," *Kidney International*, vol. 69, no. 12, pp. 2131–2147, 2006.

[26] P. Anil Kumar, G. I. Welsh, M. A. Saleem, and R. K. Menon, "Molecular and cellular events mediating glomerular podocyte dysfunction and depletion in diabetes mellitus," *Frontiers in Endocrinology*, vol. 5, p. 151, 2014.

[27] A. T. Petermann, J. Pippin, R. Krofft et al., "Viable podocytes detach in experimental diabetic nephropathy: potential mechanism underlying glomerulosclerosis," *Nephron Experimental Nephrology*, vol. 98, no. 4, pp. e114–e123, 2004.

[28] K. Tryggvason, "Unraveling the mechanisms of glomerular ultrafiltration: nephrin, a key component of the slit diaphragm," *Journal of the American Society of Nephrology*, vol. 10, no. 11, pp. 2440–2445, 1999.

[29] C. E. Martin and N. Jones, "Nephrin signaling in the podocyte: an updated view of signal regulation at the slit diaphragm and beyond," *Frontiers in Endocrinology*, vol. 9, p. 302, 2018.

[30] N. Sachs and A. Sonnenberg, "Cell–matrix adhesion of podocytes in physiology and disease," *Nature Reviews Nephrology*, vol. 9, no. 4, pp. 200–210, 2013.

[31] K. Kojima, A. Davidovits, H. Poczewski et al., "Podocyte flattening and disorder of glomerular basement membrane are associated with splitting of dystroglycan-matrix interaction," *Journal of the American Society of Nephrology*, vol. 15, no. 8, pp. 2079–2089, 2004.

[32] Y. Kim, J. H. Lim, M. Y. Kim et al., "The adiponectin receptor agonist AdipoRon ameliorates diabetic nephropathy in a model of type 2 diabetes," *Journal of the American Society of Nephrology*, vol. 29, no. 4, pp. 1108–1127, 2018.

[33] F. Zhong, H. Chen, Y. Xie et al., "Protein S protects against podocyte injury in diabetic nephropathy," *Journal of the American Society of Nephrology*, vol. 29, no. 5, pp. 1397–1410, 2018.

[34] I. Burlaka, L. M. Nilsson, L. Scott et al., "Prevention of apoptosis averts glomerular tubular disconnection and podocyte loss in proteinuric kidney disease," *Kidney International*, vol. 90, no. 1, pp. 135–148, 2016.

[35] F. Edlich, S. Banerjee, M. Suzuki et al., "Bcl-x_L retrotranslocates Bax from the mitochondria into the cytosol," *Cell*, vol. 145, no. 1, pp. 104–116, 2011.

[36] G. Kroemer, L. Galluzzi, and C. Brenner, "Mitochondrial membrane permeabilization in cell death," *Physiological Reviews*, vol. 87, no. 1, pp. 99–163, 2007.

[37] P. Swärd and B. Rippe, "Acute and sustained actions of hyperglycaemia on endothelial and glomerular barrier permeability," *Acta Physiologica*, vol. 204, no. 3, pp. 294–307, 2012.

[38] D. Giugliano, A. Ceriello, and G. Paolisso, "Oxidative stress and diabetic vascular complications," *Diabetes Care*, vol. 19, no. 3, pp. 257–267, 1996.

[39] N. P. J. Vogtländer, W. P. M. Tamboer, M. A. H. Bakker, K. P. Campbell, J. van der Vlag, and J. H. M. Berden, "Reactive oxygen species deglycosilate glomerular α-dystroglycan," *Kidney International*, vol. 69, no. 9, pp. 1526–1534, 2006.

[40] A. P. G. Dingeldein, Š. Pokorná, M. Lidman et al., "Apoptotic Bax at oxidatively stressed mitochondrial membranes: lipid dynamics and permeabilization," *Biophysical Journal*, vol. 112, no. 10, pp. 2147–2158, 2017.

[41] W. Qi, J. Niu, Q. Qin, Z. Qiao, and Y. Gu, "Astragaloside IV attenuates glycated albumin-induced epithelial-to-mesenchymal transition by inhibiting oxidative stress in renal proximal tubular cells," *Cell Stress and Chaperones*, vol. 19, no. 1, pp. 105–114, 2014.

[42] Y.-g. Du, L.-p. Wang, J.-w. Qian, K.-n. Zhang, and K.-f. Chai, "*Panax notoginseng* saponins protect kidney from diabetes by up-regulating silent information regulator 1 and activating antioxidant proteins in rats," *Chinese Journal of Integrative Medicine*, vol. 22, no. 12, pp. 910–917, 2016.

[43] A. Shiose, J. Kuroda, K. Tsuruya et al., "A novel superoxide-producing NAD(P)H oxidase in kidney," *Journal of Biological Chemistry*, vol. 276, no. 2, pp. 1417–1423, 2001.

[44] M. Sedeek, G. Callera, A. Montezano et al., "Critical role of Nox4-based NADPH oxidase in glucose-induced oxidative stress in the kidney: implications in type 2 diabetic nephropathy," *American Journal of Physiology-Renal Physiology*, vol. 299, no. 6, pp. F1348–F1358, 2010.

[45] J. C. Jha, S. P. Gray, D. Barit et al., "Genetic targeting or pharmacologic inhibition of NADPH oxidase Nox4 provides renoprotection in long-term diabetic nephropathy," *Journal of the American Society of Nephrology*, vol. 25, no. 6, pp. 1237–1254, 2014.

[46] T. Etoh, T. Inoguchi, M. Kakimoto et al., "Increased expression of NAD(P)H oxidase subunits, NOX4 and p22phox, in the kidney of streptozotocin-induced diabetic rats and its reversibility by interventive insulin treatment," *Diabetologia*, vol. 46, no. 10, pp. 1428–1437, 2003.

[47] Y.-H. You, T. Quach, R. Saito, J. Pham, and K. Sharma, "Metabolomics reveals a key role for fumarate in mediating the effects of NADPH oxidase 4 in diabetic kidney disease," *Journal of the American Society of Nephrology*, vol. 27, no. 2, pp. 466–481, 2016.

[48] B. Chang, W. Chen, Y. Zhang, Y. Bi, L. Liu, and J. Zhang, "Clinical effects of Tripterygium glycosides combined with Astragalus granules in the treatment for diabetic nephropathy," *Chinese Traditional Patent Medicine*, vol. 36, no. 9, pp. 1827–1830, 2014.

[49] Q. Wang, "Effects of yinke luo plus Panax notoginseng and Astragalus granules on treating diabetic nephropathy," *Journal of Emergency in Traditional Chinese Medicine*, vol. 16, no. 3, pp. 294–296, 2007.

[50] Department of Health and Human Services Food and Drug Administration Center for Drug Evaluation and Research (CDER), *Estimating the Maximum Safe Starting Dose in Initial Clinical Trials for Therapeutics in Adult Healthy Volunteers*, U.S. Food & Drug administration, Rockville, 2005.

Hindawi
Journal of Diabetes Research
Volume 2019, Article ID 2981705, 16 pages
https://doi.org/10.1155/2019/2981705

Research Article

Effect of Baoshenfang Formula on Podocyte Injury via Inhibiting the NOX-4/ROS/p38 Pathway in Diabetic Nephropathy

Fang-qiang Cui,[1,2] Long Tang,[1,2] Yan-bin Gao,[2,3] Yue-fen Wang,[1] Yuan Meng,[1] Cun Shen,[1] Zi-long Shen,[1] Zhi-qiang Liu,[1] Wen-jing Zhao,[1,2] and Wei Jing Liu[4]

[1]*Department of Nephrology, Beijing Hospital of Traditional Chinese Medicine, Capital Medical University, 23 Meishuguanhou Street, Dongcheng District, Beijing 100010, China*
[2]*Beijing Key Lab of TCM Collateral Disease Theory Research, No. 10, Youanmenwai, Xitoutiao, Fengtai District, Beijing 100069, China*
[3]*School of Traditional Chinese Medicine, Capital Medical University, No. 10, Youanmenwai, Xitoutiao, Fengtai District, Beijing 100069, China*
[4]*Key Laboratory of Chinese Internal Medicine of Ministry of Education and Beijing, Dongzhimen Hospital Affiliated to Beijing University of Chinese Medicine, Beijing 100700, China*

Correspondence should be addressed to Wen-jing Zhao; wenjingz@263.net and Wei Jing Liu; liuweijing-1977@hotmail.com

Received 18 October 2018; Revised 29 December 2018; Accepted 15 January 2019; Published 16 April 2019

Guest Editor: Julia M. dos Santos

Diabetic nephropathy (DN) is a serious kidney-related complication of type 1 and type 2 diabetes. The Chinese herbal formula Baoshenfang (BSF) shows therapeutic potential in attenuating oxidative stress and apoptosis in podocytes in DN. This study evaluated the effects of BSF on podocyte injury *in vivo* and *in vitro* and explored the possible involvement of the nicotinamide adenine dinucleotide phosphate-oxidase-4/reactive oxygen species- (NOX-4/ROS-) activated p38 pathway. In the identified compounds by mass spectrometry, some active constituents of BSF were reported to show antioxidative activity. In addition, we found that BSF significantly decreased 24-hour urinary protein, serum creatinine, and blood urea nitrogen in DN patients. BSF treatment increased the nephrin expression, alleviated oxidative cellular damage, and inhibited Bcl-2 family-associated podocyte apoptosis in high-glucose cultured podocytes and/or in diabetic rats. More importantly, BSF also decreased phospho-p38, while high glucose-mediated apoptosis was blocked by p38 mitogen-activated protein kinase inhibitor in cultured podocytes, indicating that the antiapoptotic effect of BSF is p38 pathway-dependent. High glucose-induced upexpression of NOX-4 was normalized by BSF, and NOX-4 siRNAs inhibited the phosphorylation of p38, suggesting that the activated p38 pathway is at least partially mediated by NOX-4. In conclusion, BSF can decrease proteinuria and protect podocytes from injury in DN, in part through inhibiting the NOX-4/ROS/p38 pathway.

1. Introduction

More and more studies have demonstrated that DN is the leading cause of the end stage of renal diseases [1]. Microalbuminuria is the typical clinical symptom of the early stage of DN. Meanwhile, microalbuminuria can induce renal dysfunction and lead to the rapid progression of DN [2]. Thus, decreasing urinary protein excretion has been an important therapeutic strategy for DN [3]. The compound formula of traditional Chinese medicine (TCM) has been widely used for the treatment of DN in China. However, the mechanism underlying a therapeutic effect has been unclear.

Podocyte injury is the key cause of proteinuria in DN [4, 5]. However, the molecular mechanism of podocyte injury in DN remains unclear. The previous study has demonstrated that increased ROS plays a key role in podocyte injury in DN [6, 7]. NOX-4, as an important number of nicotinamide adenine dinucleotide phosphate (NADPH) oxidase, is the major source of ROS production in podocyte [7]. Moreover, ROS can induce p38 phosphorylation to activate the p38 pathway, which is an important pathomechanism of

podocyte injury in DN. Therefore, the NOX-4/ROS/p38 pathway has been the research focus in recent years [8, 9].

Baoshenfang (BSF), a kind of TCM compound, consists of a group of herbal medicines including Astragalus membranaceus, Salvia miltiorrhiza bunge, Fructus ligustri lucidi, leeches, and scorpions. BSF has been widely used in treating DN in our clinical practice. We found that BSF can significantly reduce proteinuria and delay progression of DN. More importantly, Astragaloside IV, a major active component of BSF, exhibits its antioxidant properties and antiapoptotic effects on podocytes in the treatment of DN in the previous study. However, the effect of BSF on podocyte injury, oxidative stress, and p38 pathway in DN has not been explored.

2. Methods

2.1. Clinical Trial. This trial has been approved by the Ethics Committee of Beijing traditional Chinese medicine Hospital (Approval NO16ZY06). The study is a randomized, controlled, and single-blind trial. Total 79 participants were collected for our trial. All participants should conform to the diagnostic criteria of diabetic kidney disease (DKD). Participants were randomly divided into control group and BSF group. Participants of two groups were given to basic therapy of DKD. Moreover, participants of the BSF group received BSF therapy. The intervention lasted for 12 weeks. The levels of HbA1c, serum lipid, serum creatinine, blood urea nitrogen, and 24 h urinary protein were detected at 0 and 12 weeks of intervention.

2.2. Animals. Our study was performed in accordance with the National Institutes of Health Guide. Sprague-Dawley (SD) male rats weighing 440 g to 460 g each were purchased from the Chinese Academy of Medical Sciences (Beijing, China). In order to induce diabetic rats, the rats were intraperitoneally injected streptozotocin (STZ, 60 mg/kg, Sigma, St. Louis, MO, USA) dissolved in 0.1 M citrate buffer (pH 4.5). The rats of the normal control (NC) group were intraperitoneally injected an equal volume of vehicle. The serum glucose was measured at 48 h after the injection of STZ. The rats of serum glucose ≥ 16.7 mmol/L were considered as diabetic rats. Our study consisted of three groups: normal control group (NC group), diabetes mellitus group (DM group), and Baoshenfang group (BSF group). Each group had 12 rats. In the BSF group, the rats were treated with BSF solution (BSF superfine powder, 0.75 g/kg/d, gavage). In the DM and NC groups, the rats were treated with an equal volume of vehicle (normal saline, gavage). All rats of three groups were treated for 12 weeks. At the end of 0, 4, 8, and 12 weeks, serum glucose and urinary albumin excretion (UAE) were measured. After that, the rats were killed and the renal cortex was collected for study purposes.

2.3. High-Performance Liquid Chromatography-Electrospray Ionization/Mass Spectrometer (HPLC-ESI/MSn) Analysis. A Shimadzu UHPLC system (Kyoto, Japan) equipped with a LC-30AD solvent delivery system, a SIL-30AC autosampler, a CTO-30A column oven, a DGU-20A3 degasser, and a CBM-20A controller was used for HPLC-ESI/MSn analysis. The compounds were separated by a Waters ACQUITY UPLC HSS T3 (2.1 × 100 mm, 1.8 μm) at 35°C. The flow rate of the mobile phase was 0.4 ml/min under a gradient program. The mobile phase consisted of 0.05% formic acid in water (A) and acetonitrile (B). The gradient system was 0-1 min, 2% B; 1–40 min, 2–50% B; 40–53 min, 50–95% B; 53–56 min, 95% B; 56-56.1 min, 95-2% B; and 56.1-60 min, 2% B. To monitor the peak intensity, the diode-array detector was set at 254 nm. The TripleTOF™ 5600+ system with a Duo Spray source (SCIEX, Foster City, CA, USA) was used for acquiring the mass spectra in negative and positive ESI mode. For TOF-MS and TOF-MS/MS analysis, the spectra covered the range from m/z 50 to 1,250 Da and 50-1250 Da. The data were analyzed by PeakView Software™ 2.2 (SCIEX, Foster City, CA, USA).

2.4. Preparation of Rat Serum-Containing Drug. Twenty healthy SD rats were randomly divided into the BSF group and control group. The rats of the BSF group were gavaged with BSF solution at a dose of 2 g/ml twice per day for three days. Rats of the NC group were gavaged with an equal amount of vehicle (normal saline) as normal control. Then, all rats were sacrificed and the serum was collected and isolated. The isolated serum was then removed in water bath for 30 min at 56°C. The serum was finally restored in the freezer at -70°C for further study.

2.5. Cell Culture and Treatment. The conditionally immortalized mouse podocyte line, which was obtained from the national platform of experimental cell resources for Sci-Tech, was used in our experiment. DMEM/low-glucose (HyClone) medium supplemented with 10% fetal bovine serum (Excell) was applied for cultured podocyte. In order to induce cell proliferation, the podocyte was cultured in medium with IFN-γ (PeproTech, Rocky Hill, New Jersey, USA) at 33°C. In order to induce cell differentiation, the podocyte was cultured in medium without IFN-γ at 37°C. The cultured podocyte was treated with normal rat serum for 24 h before the following study. The cultured podocyte was divided into five groups: NC group, HG group, SiNOX-4 group, p38 pathway inhibition group, and BSF group. The podocyte of the NC group was treated with DMEM containing 5.5 mmol/L glucose + 24.5 mmol/L mannitol. The podocyte of other groups was treated with DMEM containing 5.5 mmol/L glucose + 24.5 mmol/L glucose. The serum containing BSF was added to the medium of cultured podocyte in the BSF group. NOX-4 siRNA was transfected as described below. SB203580 (Santa Cruz, CA, USA) was added to the medium of the cultured podocyte for p38 pathway inhibition. After being treated for 72 h, the podocyte was collected for study purposes.

2.6. siRNA Transfection. NOX-4 siRNA was purchased from Santa Cruz Biotechnology (Santa Cruz, CA, USA). NOX-4 siRNA was transfected by the Lipofectamine 2000 transfection reagent (Invitrogen) according to the manufacturer's protocol. NOX-4 protein level was assayed by western blot

for the confirmation of transfection. The transfection lasted for 48 h, and the podocyte was collected for experiments.

2.7. Western Blot Analysis. The renal cortex and collected podocyte were lysed using a lysis buffer on ice for 30 min. Protein was extracted from lysed tissues. The extracted protein was added to 10% SDS-PAGE and separated through electrophoresis. Protein was then transferred from SDS-PAGE to polyvinylidene difluoride membranes. After that, the membrane was moved to 5% nonfat dry milk in PBS + 0.05% Tween 20 and the blocked process was lasted for 1 h. The primary antibodies were then added to membranes and incubated at 4°C overnight. The membranes was washed by PBS and incubated with peroxidase secondary antibody for 1 h at room temperature. Antibodies and dilutions included the following: anti-nephrin antibody (Abcam, UK, Ab136894, 1 : 2000), anti-NOX-4 antibody (Abcam, UK, Ab109225, 1 : 1000), anti-p38 antibody (Abcam, UK, Ab31828, 1 : 1000), anti-p38 (phospho Y182) antibody (Abcam, UK, Ab47363, 1 : 1000), anti-Bax antibody (Abcam, UK, Ab7977, 1 : 500), anti-Bcl-2 antibody (Abcam, UK, Ab7973, 1 : 1000), and anti-GAPDH antibody (Proteintech, Chicago, IL, USA, 10494-1-AP, 1 : 1000). The blots were visualized with LumiGLO reagent and peroxide, followed by exposure to X-ray film. Western blot analyses were performed at least in triplicate.

2.8. Capillary Electrophoresis Immunoquantification. For quantitative capillary isoelectric immunoassay, the simple western immunoblots were performed on a Wes instrument (ProteinSimple) using the Size Separation Master Kit with Split Buffer (12–230 kDa) according to the manufacturer's standard instruction; 3 μL of protein was run on the WES system using the following antibodies: anti-p38 antibody (Abcam, Cambridge, MA, USA), anti-p38 (phospho Y182) antibody (Abcam), and anti-GAPDH antibody (Proteintech, Chicago, IL, USA). All other reagents (antibody diluent, secondary antibodies) were from ProteinSimple. The Compass software (ProteinSimple version 3.1.8) was used to program the Wes instrument and for the quantification of the western Immunoblots. Output data was displayed from the software-calculated average of nine exposures (1–512 s). Run conditions were as recommended by the manufacturer. Peak areas were determined using Compass software and normalized to anti-GAPDH.

2.9. Real-Time RT-PCR. The TRIzol reagent (Invitrogen, Carlsbad, CA, USA) was added to the renal cortex and cultured podocyte, and total RNA was isolated from the renal cortex and cultured podocyte. After that, the superscript RT kit (Invitrogen) was used to reverse-transcribe from RNA into cDNAs. The level of RNA was calculated by the $2^{-\triangle\triangle Ct}$method. The sequences of primers are the following: mouse nephrin: forward primer, CCCAACACTGG AAGAGGTGT-3, reverse primer, CTGGTCGTAGATTCCC CTTG; mouse Nox-4: forward primer, CAGAGACATCC AATCATTCCAGTG, reverse primer, CTGGATGTTCA CAAAGTCAGGTCT; mouse Bax: forward primer, CAGG GTTTCATCCAGGATCGAGCAGG, reverse primer, CGGG GGG-AGTCCGTGTCCACGTCAG; mouse Bcl-2: forward primer: CCAGCG-TGTGTGTGCAAGTGTAAAT, reverse primer, ATGTCAATCCG-TAGGAATCCCAACC; rat nephrin: forward primer, GCAAAGACTGGAAGAGGTGT, reverse primer, CTGGCCG-TAGATTCCCAGTG. RT-PCR analyses were performed at least in triplicate.

2.10. Immunofluorescence. When cells were grown to 80% confluences, 4% paraformaldehyde was added to cells for 30 min. After being blocked by 2.5% normal serum, the podocyte was incubated with anti-p38 (phospho Y182) antibody (Abcam) at 4°C overnight. After washing by PBS, cells were incubated with Alexa Fluor® 594 donkey anti-rabbit IgG (Invitrogen) at room temperature for 2 h. The podocyte was then counterstained by DAPI for 5 min. Cells were observed under a confocal microscope (Leica TCS SP5 MP, Leica, Heidelberg, Germany).

2.11. Flow Cytometry Analysis. To collect podocytes, cells of three groups were centrifugated at 2000 rpm for 5 min. The collected cells were then washed twice with PBS and resuspended with binding buffer. After that, Annexin V-FITC and PI were added and the podocytes were collected after 15 min. The data of apoptotic cells was analyzed using FACScan. Flow cytometry analyses of different groups were performed at least in triplicate.

2.12. Determination of ROS. ROS detection kit (Beyotime, Haimen, China) was used for ROS measurement according to the manufacturer's protocol in our study. The podocyte was cultured in a 24-well plate and treated with a different cultured medium, and then the podocyte was incubated with 10 μM DCFH-DA for 20 min at 37°C. The fluorescence intensity was observed and recorded by a fluorescent microscope.

2.13. Caspase-3 Activity. Caspase-3 kit (Beyotime, Haimen, China) was used for caspase-3 activity detection. Podocyte was cultured in a 6-well plate. The podocyte was treated with a different cultured medium for 24 h. After that, the podocyte was collected and lysed with a lysis buffer on ice. The reaction buffer (80 μL) and caspase-3 substrate (10 μL) were added to the cell lysate (10 μL). The optical density (OD) was assayed by a spectrophotometer at 405 nm.

2.14. Statistical Analysis. Data were presented as mean ± S.E .M., counts, or percentage. Statistical analyses were performed by one-way ANOVA followed by the Bonferroni multiple comparison test (for comparison of more than 2 groups) or Student's t-test (for comparison of 2 groups) unless otherwise stated. $P < 0.05$ was considered statistically significant.

3. Results

3.1. Characteristics of Pure Compounds in BSF. Liquid chromatography-mass spectrometry (LC-MS) has been a common way of substance analysis of TCM in recent years. In our study, substance analysis for BSF was performed in both negative and positive ESI modes. The MS spectrum of the negative base peak and positive base peak is displayed

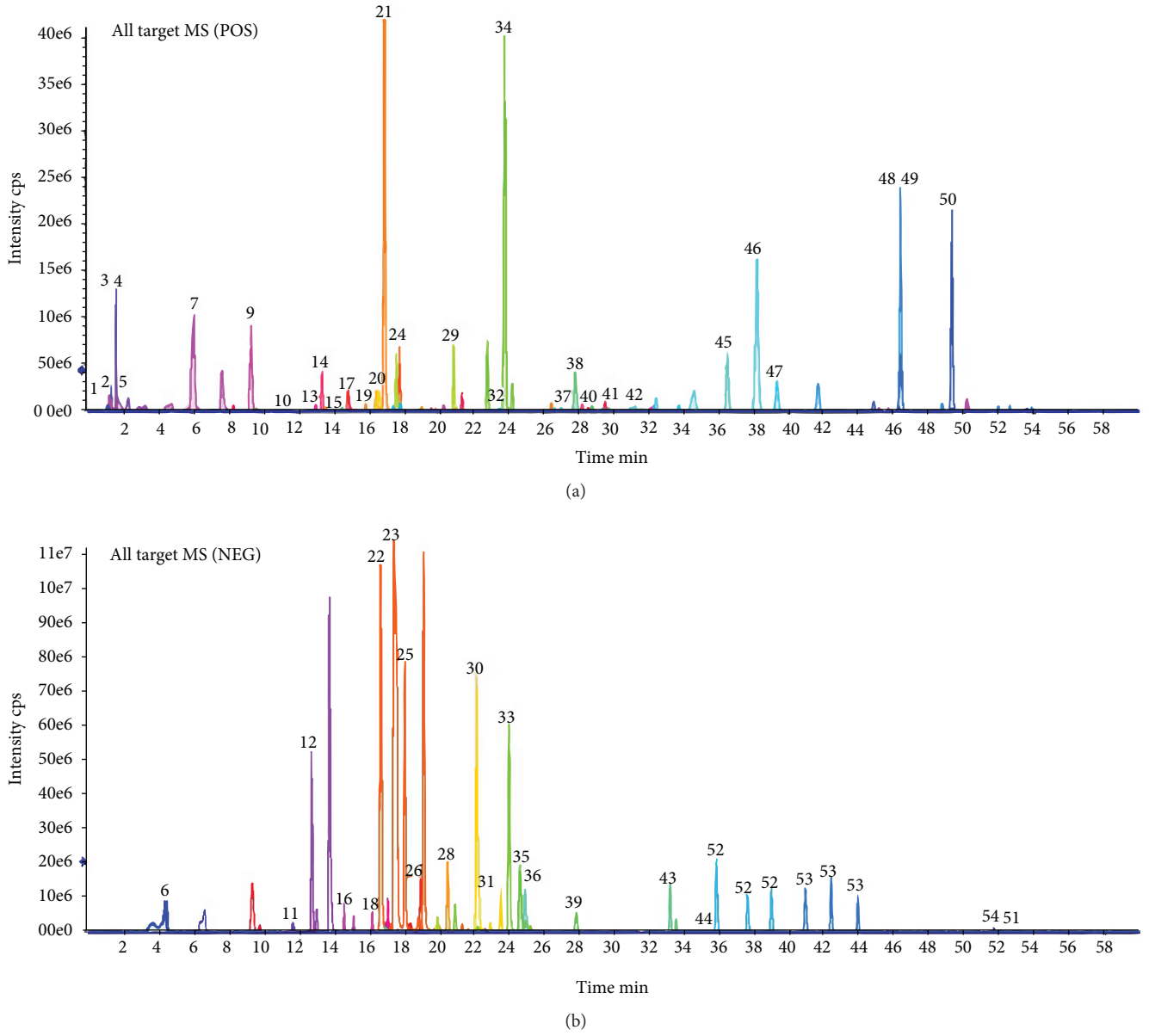

Figure 1: Ion chromatograms of BSF analyzed by high-performance liquid chromatography-electrospray ionization/mass spectrometry (HPLC-ESI/MS*n*) analysis. (a) Positive base peak MS spectrum. (b) Negative base peak mass spectrometry (MS) spectrum.

in Figure 1. There were 54 kinds of substances of BSF identified by MS. The identified compound is displayed in Table 1, including flavones, coumarins, phenylethanoid glycosides, phenolic acids, saponins, and organic acids. More importantly, many substances such as quercetin (number 36), salvianolic acid B (number 30), luteolin (number 35), and astragaloside IV (number 43) might offer the biological activity of antioxidative stress. Therefore, BSF's antioxidative activity and the associated mechanism were studied in our research.

3.2. BSF Decreased 24 h Urinary Protein and Improved Renal Function in Patients with DKD. In our clinical trial, 79 participants of DKD patients were collected for our research. All participants were randomly divided into control group and BSF group. The age, sex, serum albumin, blood urea nitrogen, and 24 h urinary protein were not significantly different before treatment between control group and BSF groups. After intervention for 12 weeks, the 24 h urinary protein of BSF group was significantly decreased compared with the control group. Meanwhile, the levels of serum creatinine and blood urea nitrogen in the BSF group were lower than those in the control group (Table 2).

3.3. BSF Ameliorated Proteinuria and Improved Renal Function in Diabetic Rats. Next, urinary albumin excretion, serum creatinine, and blood urea nitrogen were measured in different rodent groups. Our results showed that urinary albumin excretion of the DM group was significantly increased at 4 weeks and gradually further enhanced at 8

Table 1: Chemical components of BSF identified by HPLC-ESI/MS*n*.

No.	Retention time	Formula	Adduct/charge	Experimental mass	Identification
1	1.18	C4H9NO3	[M + H]+	120.0655	Threonine
2	1.39	C7H13NO2	[M + H]+	144.1019	Stachydrine
3	1.63	C5H5N5	[M + H]+	136.0618	Adenine
4	1.65	C5H4N4O	[M + H]+	137.0458	6-Hydroxypurine
5	1.77	C6H13NO2	[M + H]+	132.1019	Leucine
6	4.44	C7H6O5	[M-H]-	169.0142	Gallic acid
7	6.04	C6H6O3	[M + H]+	127.039	5-Hydroxymethylfurfural
8	6.65	C9H10O5	[M-H]-	197.0455	Danshensu
9	9.35	C14H20O7.NH3	[M + H]+	318.1547	Salidroside
10	11.22	C17H24O9.NH3	[M + H]+	390.1759	Syringin
11	11.7	C9H6O4	[M-H]-	177.0193	Esculetin
12	12.78	C17H26O10.HCOOH	[M-H]-	435.1508	Loganin
13	13.03	C21H20O9	[M + H]+	417.118	Puerarin
14	13.39	C16H22O9	[M + H]+	359.1337	Sweroside
15	13.97	C10H8O5	[M + H]+	209.0444	Fraxetin
16	14.61	C35H46O20	[M-H]-	785.251	Echinacoside
17	14.88	C23H28O11.NH3	[M + H]+	498.197	Paeoniflorin
18	16.22	C36H48O20	[M-H]-	799.2666	
19	16.49	C10H8O4	[M + H]+	193.0495	Isoscopoletin
20	16.61	C10H10O4	[M + H]+	195.0652	Ferulic acid
21	16.96	C22H22O10	[M + H]+	447.1286	Calycosin-7-o-glucoside
22	17.11	C34H44O19	[M-H]-	755.2404	Forsythoside B
23	17.32	C21H20O12	[M-H]-	463.0882	Isoquercitrin
24	17.82	C21H20O11	[M + H]+	449.1078	Homoorientin (isoorientin)
25	18.38	C7H6O3	[M-H]-	137.0244	Salicylic acid
26	18.98	C20H18O10	[M-H]-	417.0827	Salvianolic acid D
27	19.16	C29H36O15	[M-H]-	623.1981	
28	20.52	C18H16O8	[M-H]-	359.0772	Rosmarinic acid
29	20.89	C21H18O12	[M + H]+	463.0871	Scutellarin
30	22.17	C36H30O16	[M-H]-	717.1461	Salvianolic acid B
31	22.24	C21H18O11	[M-H]-	445.0776	Baicalin
32	23.49	C15H12O4	[M + H]+	257.0808	Isoliquiritigenin
33	24.02	C26H22O10	[M-H]-	493.114	Salvianolic acid A
34	24.23	C27H34O11	[M + NH4]+	552.2439	Arctiin
35	24.64	C15H10O6	[M-H]-	285.0405	Luteolin
36	24.66	C15H10O7	[M-H]-	301.0354	Quercetin
37	27.4	C15H12O5	[M + H]+	273.0757	Naringenin
38	27.7	C30H32O12.NH3	[M + H]+	602.2232	Benzoylpaeoniflorin
39	27.85	C15H10O5	[M-H]-	269.0455	Apigenin
40	28.79	C16H12O6	[M + H]+	301.0707	Diosmetin
41	29.73	C15H10O5	[M + H]+	271.0601	Baicalein
42	31	C15H12O4	[M + H]+	257.0808	Liquiritigenin
43	33.2	C41H68O14	[M + FA-H]-	829.4591	Astragaloside IV
44	35.37	C16H12O5	[M-H]-	283.0612	Wogonin
45	36.5	C21H22O8	[M + H]+	403.1387	Nobiletin
46	38.17	C15H20O3	[M + H]+	249.1485	Parthenolide
47	39.32	C20H20O7	[M + H]+	373.1282	Tangeretin
48	46.36	C19H20O3	[M + H]+	297.1485	Cryptotanshinone

Table 1: Continued.

No.	Retention time	Formula	Adduct/charge	Experimental mass	Identification
49	46.37	C18H12O3	[M + H]+	277.0859	Tanshinone I
50	49.29	C19H18O3	[M + H]+	295.1329	Tanshinone IIA
51	52.72	C18H32O2	[M-H]-	279.233	Linoleic acid
52	35.8/37.6/38.98	C43H70O15.HCOOH	[M-H]-	871.4697	Astragaloside II
53	40.9/42.4/43.9	C45H72O16.HCOOH	[M-H]-	913.4802	Astragaloside I
54	51.7/52.1/56.8/57.4	C30H48O3	[M-H]-	455.3531	Oleanolic acid

Table 2: Effect of BSF on biochemical indexes of DKD.

Groups	Control	BSF	*P* value
Sample size	39	40	—
Female sex (%)[a]	20 (51.3%)	18 (45.0%)	>0.05
Age (years)[b]	62.95 ± 7.24	63.35 ± 8.02	>0.05
HbA1c (%)[b] (week 0)	7.81 ± 1.67	7.96 ± 1.40	>0.05
HbA1c (%)[b] (week 12)	6.47 ± 1.92	6.46 ± 0.74	>0.05
Total cholesterol (mmol/l)[b] (week 0)	6.04 ± 1.45	5.87 ± 1.14	>0.05
Total cholesterol (mmol/l)[b] (week 12)	4.59 ± 0.90	4.44 ± 0.87	>0.05
Triglyceride (mmol/l)[b] (week 0)	2.31 ± 0.89	2.29 ± 0.93	>0.05
Triglyceride (mmol/l)[b] (week 12)	1.64 ± 0.45	1.54 ± 0.38	>0.05
Serum albumin (g/l)b (week 0)	28.6 ± 1.4	28.3 ± 1.7	>0.05
Serum albumin (g/l)[b] (week 12)	33.2 ± 2.7	38.0 ± 2.4	<0.05
Serum creatinine (μmol/l)[b] (week 0)	121.6 ± 10.1	124.6 ± 13.0	>0.05
Serum creatinine (μmol/l)[b] (week 12)	115.6 ± 10.1	94.9 ± 13.0	<0.05
Blood urea nitrogen (mmol/l)[b] (week 0)	7.5 ± 0.4	7.6 ± 0.7	>0.05
Blood urea nitrogen (mmol/l)[b] (week 12)	6.7 ± 0.5	5.6 ± 0.3	<0.05
24 h urinary protein (g)[b] (week 0)	3.4 ± 1.9	3.48 ± 2.1	>0.05
24 h urinary protein (g)[b] (week 12)	3.18 ± 1.94	2.55 ± 1.67	<0.05

[a]The data are expressed as counts (%), and the *P* value for the between-group difference is calculated from the Wilcoxon rank sum test. [b]The data are expressed as the mean ± S.E.M., and the *P* value for the two group comparisons is calculated using an independent-sample *t*-test.

and 12 weeks compared with the NC group. Urinary albumin excretion of the BSF group was significantly decreased compared with the DM group at 4, 8, and 12 weeks. Moreover, serum creatinine and blood urea nitrogen were significantly increased in the DM group compared with the NC group at 12 weeks. However, the levels of serum creatinine and blood urea nitrogen were significantly decreased in the BSF group compared with the DM group (Figure 2).

3.4. BSF Increased the Nephrin Expression in High Glucose Cultured Podocyte and Diabetic Rats. Nephrin is a signature molecule of podocyte, and decreased nephrin expression is a hallmark of podocyte injury. Therefore, nephrin expression of different groups was subsequently studied. Nephrin protein and mRNA expressions were quantified by WB and RT-PCR, respectively. We found that either protein or mRNA level of nephrin was significantly decreased in the DM group compared with the NC group. Interestingly, the expression of nephrin protein or mRNA was significantly increased in the BSF group compared with the DM group (Figures 3(a), 3(c), and 3(d)). And similar results were obtained in an *in vitro* study (Figures 3(b), 3(e), and 3(f)).

3.5. BSF Decreased Cellular Apoptosis in Diabetic Rats and High Glucose Cultured Podocytes. Subsequently, early and late apoptosis was subsequently evaluated by flow cytometry after coupled staining with FITC Annexin V in cultured podocytes. Either early or late podocyte apoptosis was higher in the high glucose group than in normal control. Such alteration was significantly inhibited by the serum with BSF (Figures 4(a) and 4(b)). Similarly, hyperglycemia induced an increase in cellular apoptosis in glomerulus, which was reduced by BSF treatment (Figure 4(c)).

3.6. BSF Inhibited NOX-4-Mediated Oxidative Stress in High Glucose Cultured Podocyte. NOX-4, the main NADPH oxidase isoform contributing to the increased oxidative stress, was evaluated in vitro. We found that NOX-4 protein or mRNA level was indeed increased in high glucose-treated podocytes, but suppressed by BSF (Figures 5(a)–5(c)). In addition, high glucose induced a marked enhancement of

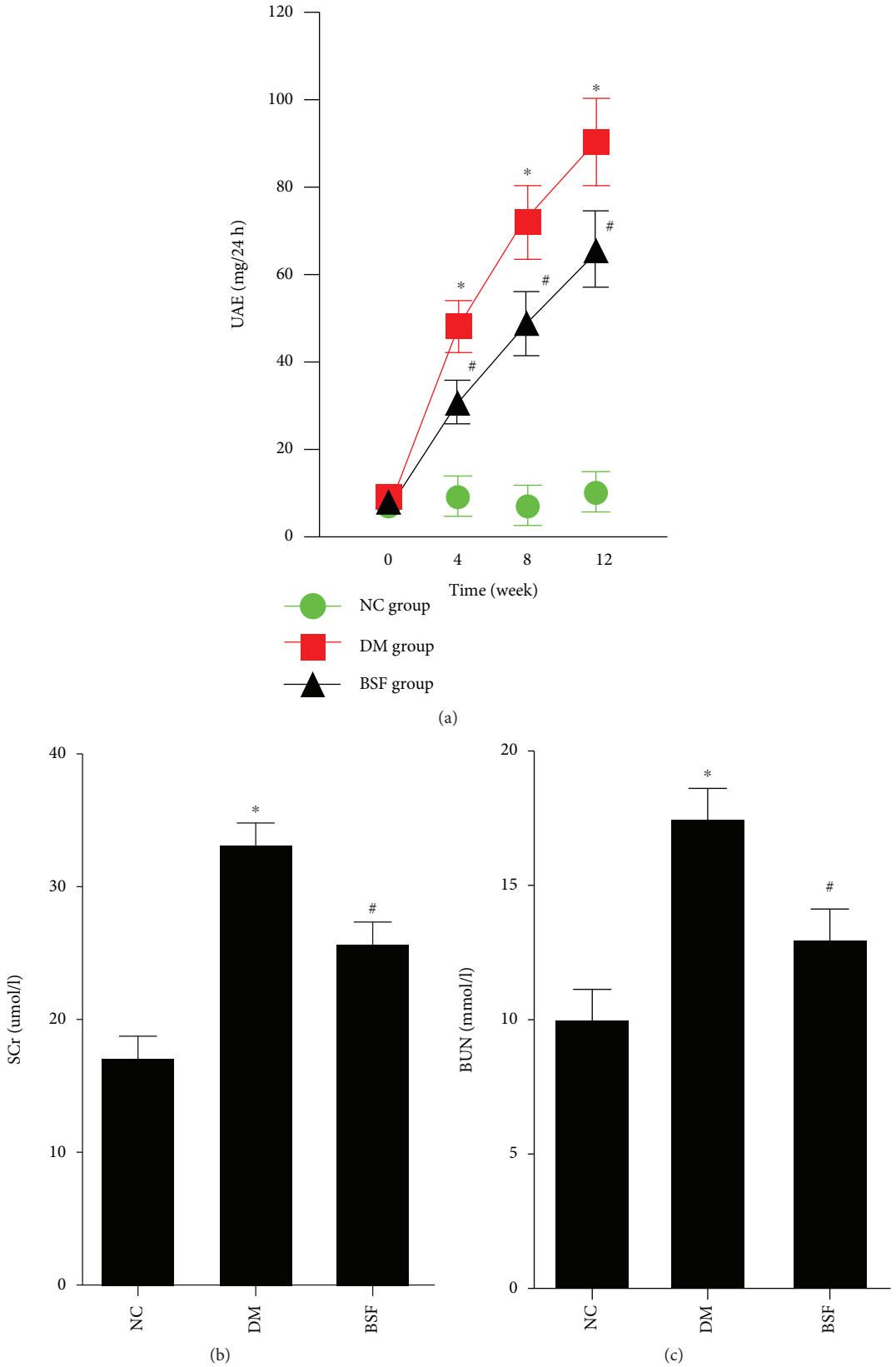

Figure 2: Effect of BSF on urinary albumin excretion (UAE), serum creatinine (SCr), and blood urea nitrogen (BUN) in diabetic rats. The levels of UAE (a), SCr (b), and BUN (c) in different groups. All the indicators were increased in DM rats, but lowered by BSF treatment. $^{*}P < 0.05$ versus normal control (NC), $^{\#}P < 0.05$ versus DM.

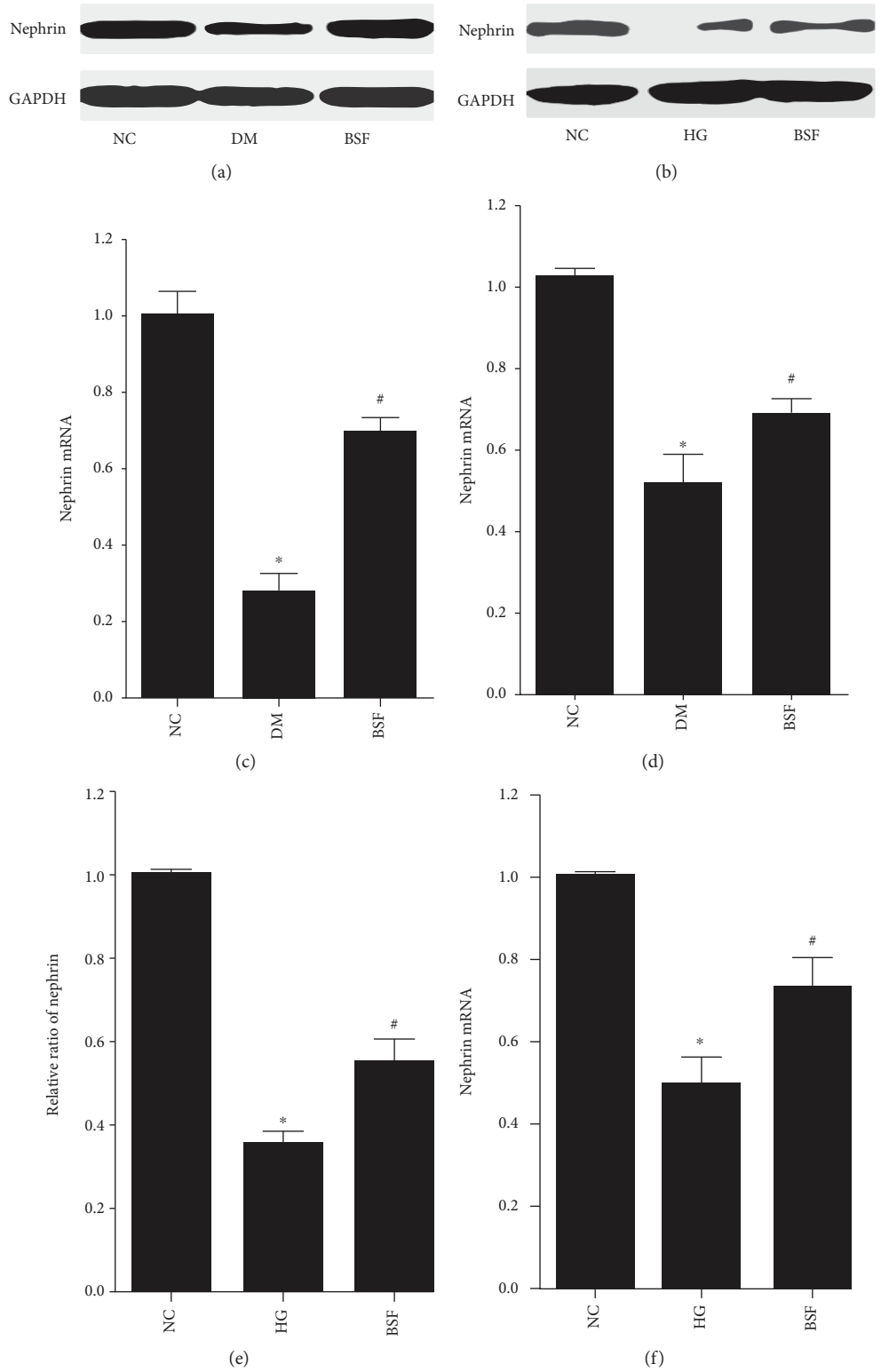

Figure 3: Effect of BSF on nephrin expression in podocyte in vivo and in vitro. (a) Representative band of nephrin protein in the cortex of rats. (b) Representative band of nephrin protein in cultured podocyte. (c) Comparison of the grey values of nephrin protein in podocyte of rats. (d) Comparison of mRNA levels of nephrin in podocyte of rats. (e) Comparison of the grey values of nephrin protein in cultured podocyte. (f) Comparison of mRNA levels of nephrin in cultured podocyte. Nephrin mRNA or protein level was significantly decreased in diabetic rats and high glucose (HG) cultured podocytes. BSF treatment significantly increased nephrin expression. $^{*}P < 0.05$, $^{**}P < 0.01$ versus normal control (NC), and $^{\#}P < 0.05$ versus DM or HG.

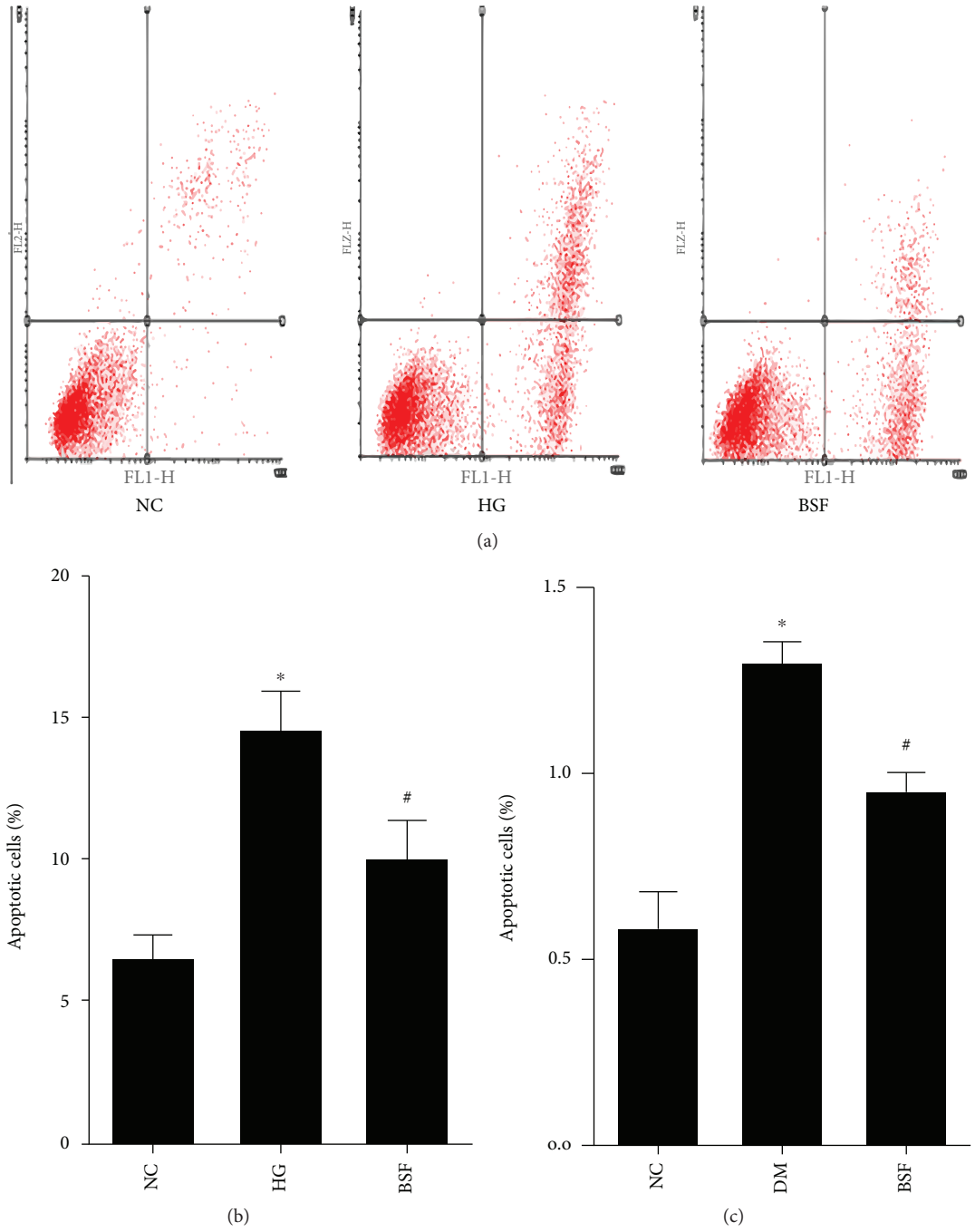

Figure 4: Effect of BSF on podocyte apoptosis in vivo and in vitro. (a) Representative photograph of flow cytometry analysis in vitro. (b) Comparison of apoptotic cells in cultured podocyte of different groups evaluated by flow cytometry. (c) Comparison of apoptotic index in glomerulus of different groups assayed by TUNEL. BSF treatment significantly decreased high glucose (HG) or hyperglycemia-induced cellular apoptosis. $^{*}P < 0.05$ versus normal control (NC) and $^{\#}P < 0.05$ versus DM or HG.

MDA, NOS, and ROS levels, a significant suppression of the T-SOD level. Compared with the HG group, MDA, NOS, and ROS levels were significantly decreased, while the T-SOD level was significantly increased in the BSF group (Figures 5(d)–5(g)). Moreover, the upregulated ROS level was significantly reduced by NOX-4 silencing (Figure 5(h)), suggesting that the antioxidation effect is NOX-4 blockage dependent.

3.7. BSF Inhibited Bcl-2 Family-Associated Apoptosis by Inactivating the p38 Pathway in High Glucose Cultured Podocyte. To explore the effect of BSF on the p38 pathway in podocyte, p38 and/or phospho-p38 (P-p38) protein expression was assessed by western blot and immunofluorescence. Western blot analysis showed that p38 protein expression had no significant difference among different groups. However, the P-p38 protein level was significantly increased

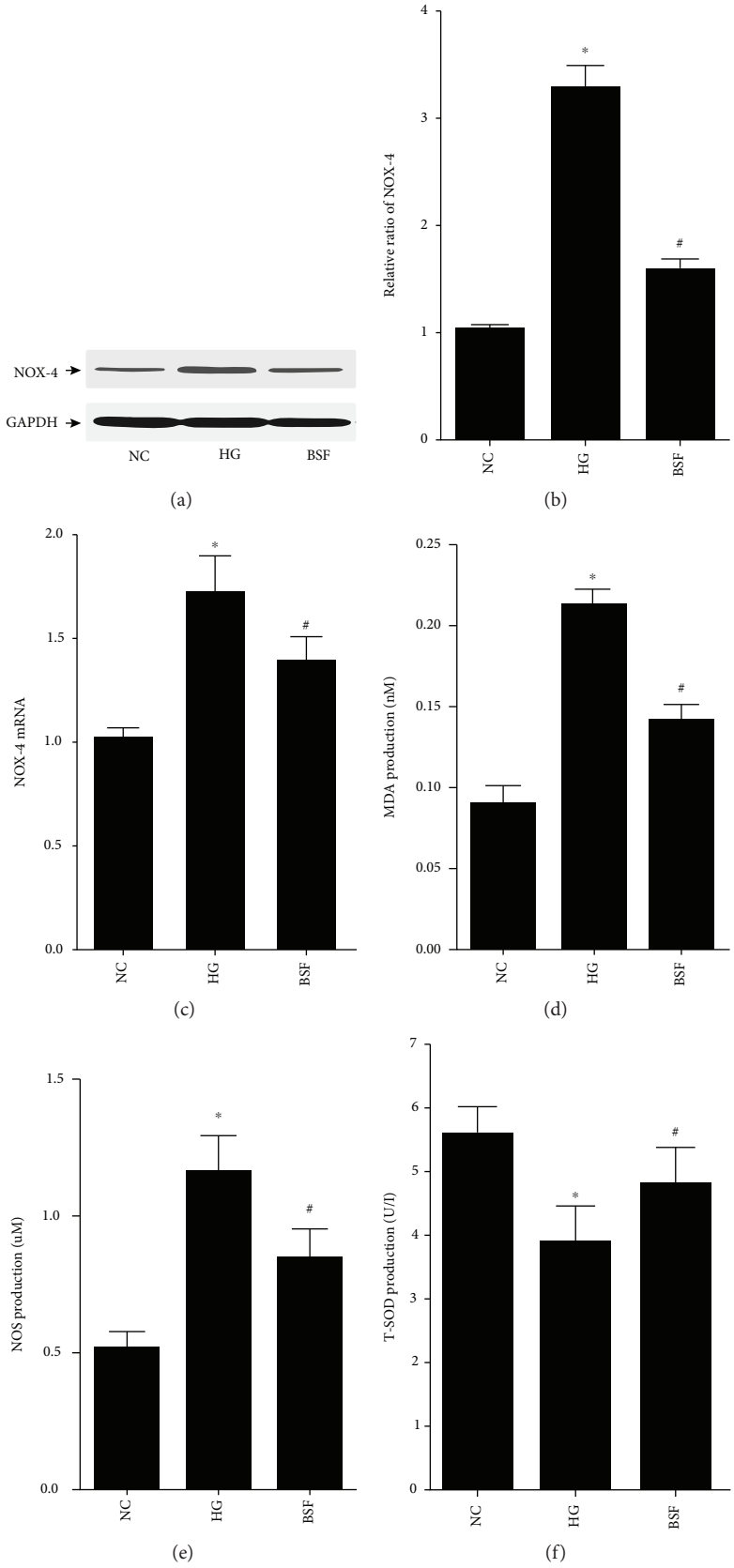

Figure 5: Continued.

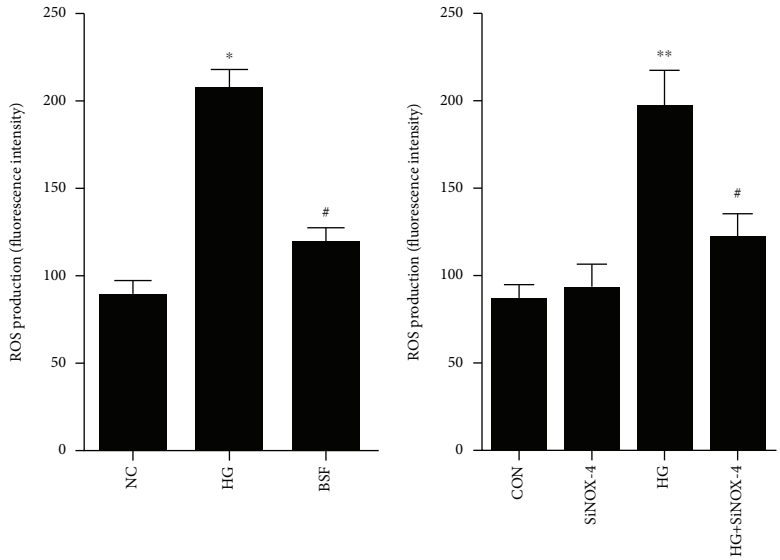

Figure 5: Effect of BSF on NOX-4-mediated oxidative stress in cultured podocyte. (a) Representative band of NOX-4 protein in cultured podocyte. (b) Comparison of the grey values of NOX-4 protein in cultured podocyte. (c) Comparison of mRNA levels of NOX-4 in cultured podocyte. BSF suppressed the upexpression of NOX-4 after exposure of podocyte to high glucose (HG). (d–f) Comparison of MDA, NOS, and T-SOD levels measured by ELISA in cultured podocyte. (g, h) Comparison of ROS production in cultured podocyte. High glucose induced a marked enhancement of MDA, NOS, and ROS levels, a significant suppression of T-SOD level. Compared with the HG group, MDA, NOS, and ROS levels were significantly decreased, while the T-SOD level was significantly increased in the BSF group. And the upregulated ROS production was suppressed by NOX-4 silencing. $^{*}P < 0.05$, $^{**}P < 0.01$ versus normal control (NC), $^{\#}P < 0.05$, and $^{\#\#}P < 0.01$ versus HG.

in the HG group. Interestingly, the high expression of P-p38 was also downregulated by BSF in an in vitro study (Figures 6(a)–6(c)). Moreover, the results of immunofluorescence indicated that HG promoted P-p38 protein nuclear translation, which was inhibited by BSF therapy (Figures 6(d) and 6(e)). The antiapoptotic protein Bcl-2 and proapoptotic protein Bax in the Bcl-2 family were then studied. Our results showed that Bax was significantly increased and Bcl-2 was significantly decreased in the HG group. BSF decreased Bax expression and increased Bcl-2 expression induced by HG in an in vitro study (Figures 6(f)–6(h)). Accordingly, HG-induced high caspase-3 activity was lowered by BSF treatment (Figure 6(i)). More importantly, we also found that the antiapoptotic effect of BSF was p38 pathway-dependent, since p38 pathway inhibitor SB203580 could suppress the podocyte apoptosis induced by HG (Figure 6(k)).

3.8. p38 Phosphorylation Induced Podocyte Apoptosis Was NOX-4-Dependent. To demonstrate the relationship between p38 phosphorylation and NOX-4 activation, the p38 pathway was studied after the podocytes were transfected with NOX-4 siRNA. In our study, NOX-4 silence significantly inhibited p38 phosphorylation induced by HG in cultured podocytes (Figures 7(a)–7(c)). Moreover, the high caspase-3 activity was significantly decreased by NOX-4 siRNA in HG-cultured podocytes (Figure 7(d)). It indicates that the antiapoptotic effect of BSF is NOX-4/p38 pathway-dependent.

4. Discussion

Diabetic nephropathy, as the most common microvascular complication of diabetic mellitus, has been the leading cause of end-stage renal disease [2]. Data from clinical trials indicates that 40% of end-stage renal disease patients and 50% of dialysis and kidney transplant patients are induced by DN [10]. However, the pathomechanism of DN has been unclear. Meanwhile, the effective clinical intervention is limited for DN patients. Thus, it is important for us to seek a potential therapeutic target of DN. As we know, microalbuminuria is the typical clinical symptom of the early stage of DN [11]. Microalbuminuria is also the key cause which can lead to rapid progression of DN [1]. Moreover, reducing urinary protein excretion has been the important therapeutic method in recent years. BSF, a kind of traditional Chinese medicine compound, has been widely used in treatment of DN in our clinical practice. BSF can significantly decrease proteinuria and serum creatinine of DN patients, although it has no obvious influence on eGFR (data was not shown). In our in vivo study, we found that BSF significantly decreased urinary albumin excretion of diabetic rats. Moreover, in the main substances of BSF, it has been demonstrated that quercetin [12], salvianolic acid B [13], and luteolin [14] can decrease oxidative stress in many diseases. Moreover, astragaloside IV could protect podocytes from injury via inhibiting oxidative stress, as demonstrated in a previous study [15]. It indicates that BSF probably prevents the progression of DN by offering antioxidative activity.

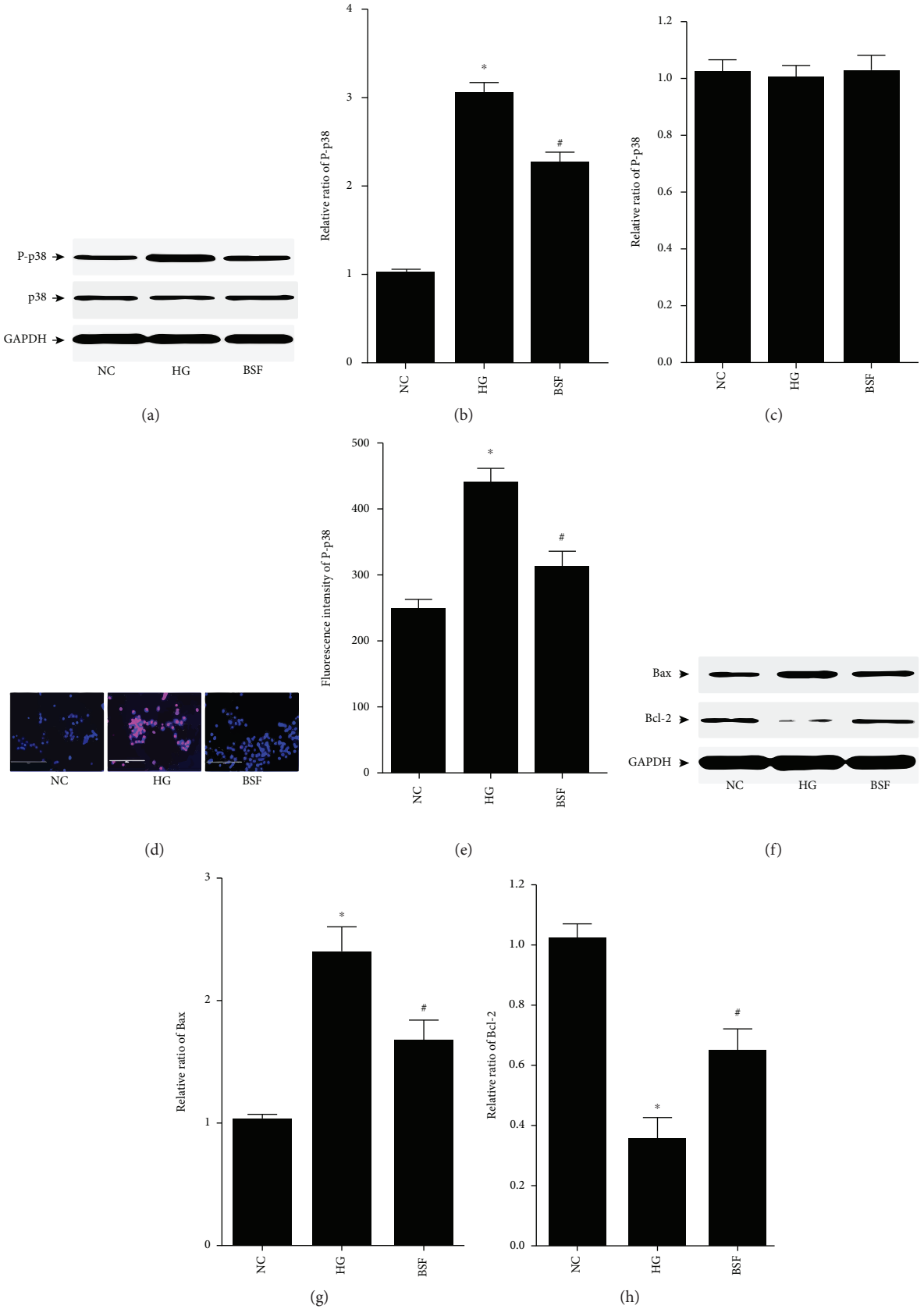

Figure 6: Continued.

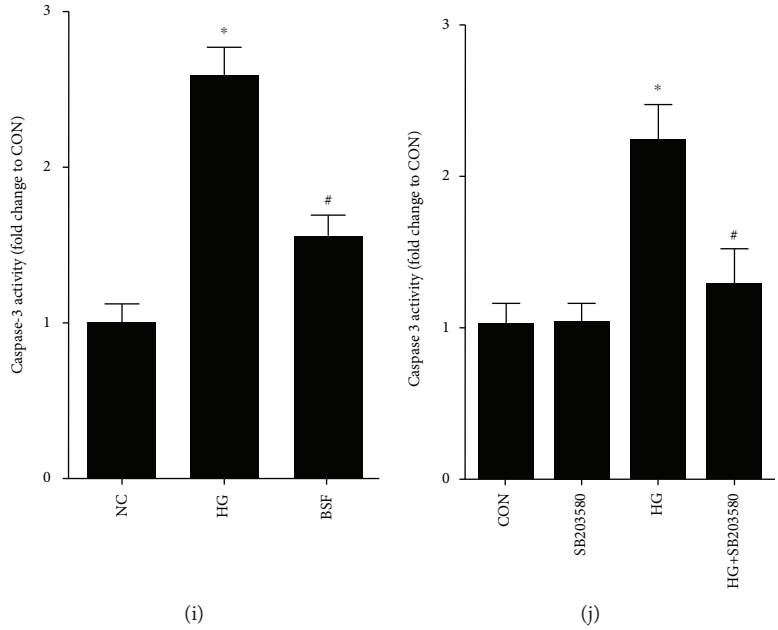

Figure 6: Effect of BSF on p38 pathway-induced apoptosis in HG cultured podocytes. (a) Representative band of p38 protein and P-p38 protein in cultured podocyte. (b, c) Comparison of the grey values of p38 and P-p38 protein in cultured podocytes. P-p38, but not p38 protein expression, was significantly increased in the HG group compared with the NC group. BSF decreased the expression of P-p38 protein. (d) Representative photograph of P-p38 staining (red) and cell nucleus (DAPI blue) in cultured podocyte. (e) Comparison of the fluorescence intensity of P-p38 protein in cultured podocyte. BSF significantly decreased the fluorescence intensity of P-p38 compared with the HG group. (f) Representative band of Bax protein and Bcl-2 protein in cultured podocyte. (g, h) Comparison of the grey values of Bax protein in cultured podocyte. HG upregulated the expression of Bax protein and downregulated the expression of Bcl-2 protein, which was reversed by BSF. (i, k) Comparison of caspase-3 activity in cultured podocyte. Either BSF or SB203580 could decrease the high caspase-3 activity induced by HG. $^{*}P < 0.05$ versus NG. $^{\#}P < 0.05$ versus HG.

Podocyte, as an important component of glomerular filtration membrane, has been the research focus and important potential therapeutic target of DN in recent years [16–18]. Meanwhile, podocyte injury plays a key role in increased urinary albumin in DN [19–22]. Nephrin, a signature molecule of podocyte, can regulate many pivotal functions of podocyte [5]. Research suggests that nephrin expression is important for signal transduction and cytoskeletal reorganization of podocyte [5]. Moreover, podocyte is a kind of terminal differentiation cell and has lost the ability for regenerative reparation. A decrease in the number of podocytes can lead to destruction of GBM and increased urinary albumin [23–25]. The previous study has demonstrated that podocyte apoptosis is the leading cause of the decrease in the number of podocytes in DN [19, 20]. Thus, decreased nephrin expression and increased podocyte apoptosis is a good marker of podocyte injury. Evidence suggests that nephrin expression is significantly decreased and podocyte apoptosis is significantly increased in DN. We also explored nephrin expression and podocyte apoptosis in diabetic rats and high glucose cultured podocyte in our study. In accordance with the previous study, nephrin expression is significantly decreased and podocyte apoptosis is significantly increased in DN. More importantly, BSF significantly increased nephrin expression and decreased podocyte apoptosis in diabetic rats and high glucose cultured podocytes. Our results indicate that BSF can protect podocytes from injury in DN.

Oxidative stress has been the central pathomechanism of podocyte injury in DN [7, 26]. ROS production is significantly increased in podocyte in DN, which has been demonstrated by many previous studies. Moreover, there are many ways involved in increased ROS production in podocyte. However, NADPH is the major source of ROS in podocyte in DN. NOX-4, as a member of the NADPH oxidase family, has been the key oxidase in increased ROS production in podocyte in DN [27]. It has been demonstrated that HG can increase NOX-4 expression and ROS production in podocyte, which is the major cause of podocyte apoptosis [7, 27]. Moreover, NOS, T-SOD, and MDA are also good markers of oxidative stress [15]. In order to explore the effect of BSF on podocyte oxidative stress, ROS, NOX-4, NOS, T-SOD, and MDA were detected in our in vivo and in vitro study. Our results showed that BSF significantly inhibited podocyte oxidative stress in DN.

The p38 pathway is an important mechanism of podocyte injury in DN [28]. Some reports suggest that the p38 pathway can be activated by oxidative stress in podocyte [9]. The p38 pathway has an intensive relationship with podocyte apoptosis [8]. The activated p38 pathway can lead to increased Bax expression and decreased Bcl-2 expression [29]. As we know, Bax is a kind of proapoptotic protein and Bcl-2 is a kind of inhibitor of apoptosis protein. Thus, increased podocyte apoptosis can be induced by the activated p38 pathway. Moreover, p38 pathway activation

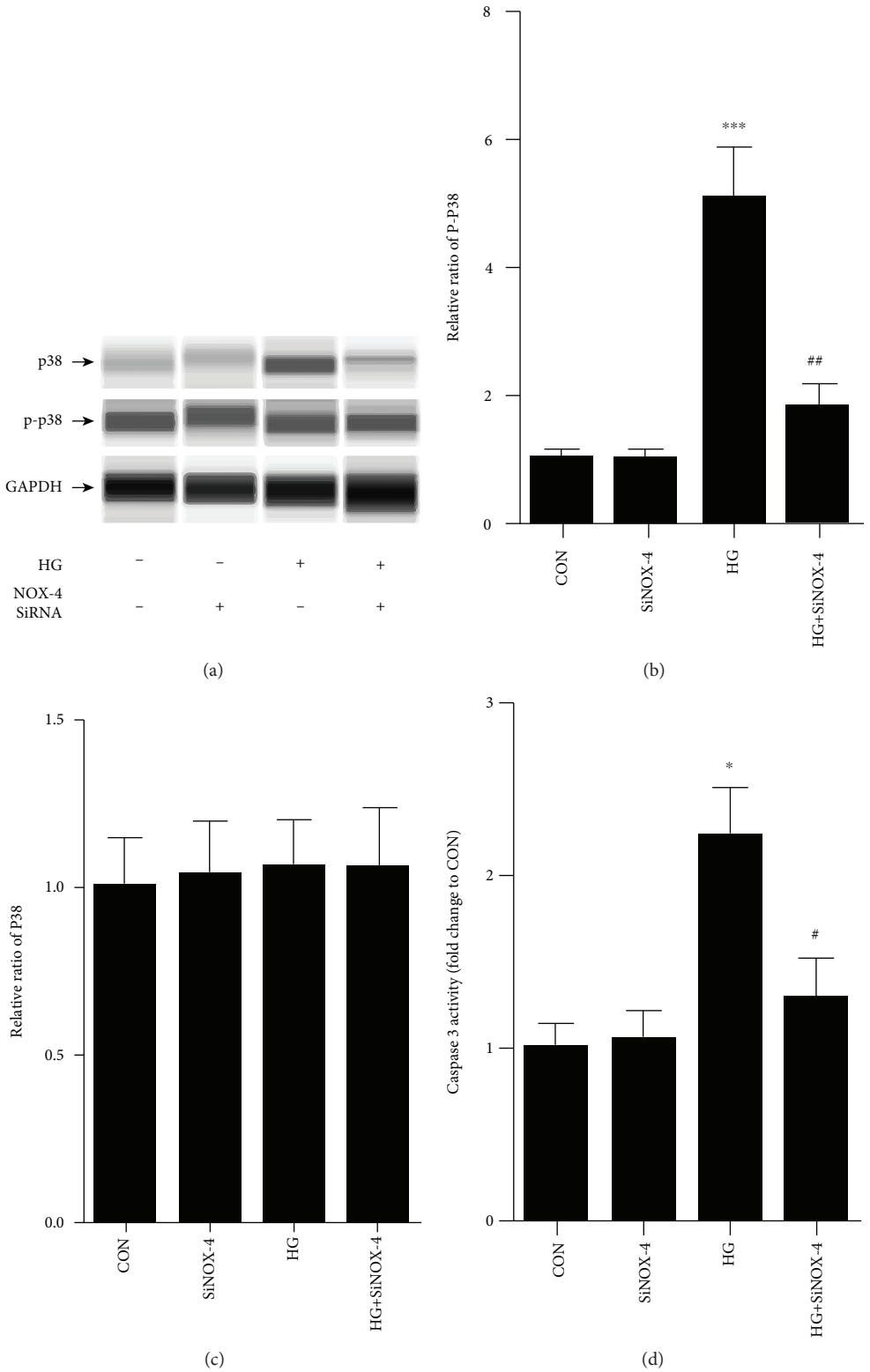

Figure 7: Effect of NOX-4 siRNA on p38 pathway-induced apoptosis in HG cultured podocytes. (a) Representative band of p38 and P-p38 protein in cultured podocyte. (b, c) Comparison of the grey values of P-p38 and p38 protein in cultured podocyte. NOX-4 siRNA significantly decreased the expression P-p38 protein compared with the HG group. (d) Comparison of caspase-3 activity in cultured podocyte. NOX-4 siRNA significantly decreased the caspase-3 activity in HG cultured podocytes. $^{*}P < 0.05$ and $^{***}P < 0.001$ versus NG. $^{\#}P < 0.05$ and $^{\#\#}P < 0.01$ versus HG.

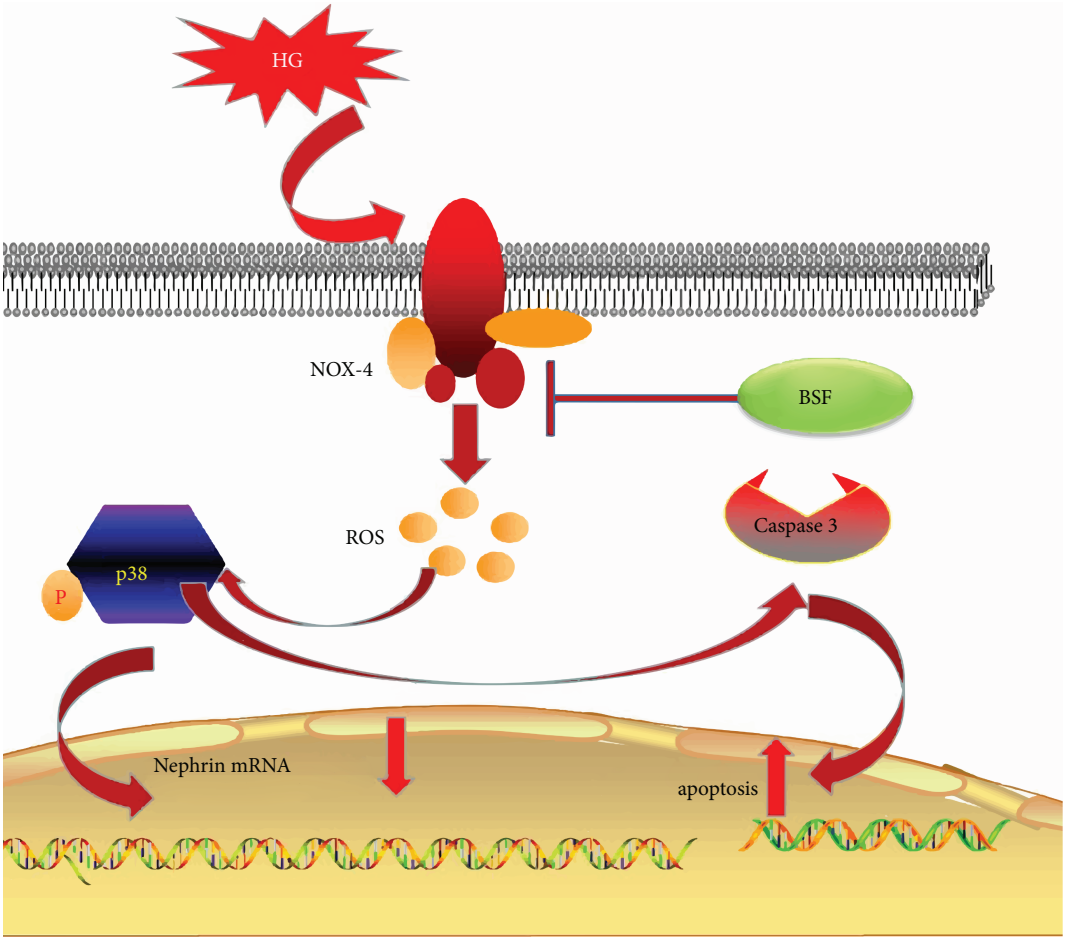

Figure 8: Schematic representation of the mechanisms of the NOX-4/ROS/p38 pathway in podocyte injury in high glucose condition. HG significantly increases NOX-4 expression in podocyte. And NOX-4-induced ROS overproduction triggers cascade phosphorylation reaction of the p38 pathway. Accordingly, activation of the p38 pathway can decrease nephrin expression and induce podocyte apoptosis. Baoshenfang formula might protect podocyte from HG-induced injury via inhibiting the NOX-4/ROS/p38 pathway.

decreases nephrin expression and induces podocyte injury, which has been demonstrated by previous studies. To explore the molecular mechanism of BSF on podocyte injury, p38 pathway, Bax, and Bcl-2 expression were detected in our study. Our results showed that P-p38 protein was significantly increased in podocyte of the HG group. Moreover, Bax protein was significantly increased and Bcl-2 protein was significantly decreased in podocyte of the HG group. More importantly, BSF could significantly decrease p38 phosphorylation after exposure of podocyte to HG. Bax expression was significantly decreased, and Bcl-2 expression was significantly increased in the BSF group compared with the HG group.

In conclusion, BSF could prevent the development of DN. The renoprotection might be attributed to an inhibitive effect of the NOX-4/ROS/p38 pathway in podocytes (Figure 8).

Data Availability

The data used to support the findings of this study are available from the corresponding author upon request.

Conflicts of Interest

The authors declare that they have no competing interests.

Authors' Contributions

Fang-qiang Cui and Long Tang contributed equally to this work.

Acknowledgments

This work was supported by grants from an open research program of the Key Lab of Capital Medical University, the National Natural Science Foundation of China (No. 81703989 and 81774278), and the Provincial Natural Science Foundation of Beijing (No. 7182069 and 7172096).

References

[1] J. Ahmad, "Management of diabetic nephropathy: recent progress and future perspective," *Diabetes & Metabolic Syndrome: Clinical Research & Reviews*, vol. 9, no. 4, pp. 343–358, 2015.

[2] H. Pavenstadt, W. Kriz, and M. Kretzler, "Cell biology of the glomerular podocyte," *Physiological Reviews*, vol. 83, no. 1, pp. 253–307, 2003.

[3] B. F. Palmer, "Supratherapeutic doses of angiotensin receptor blockers to decrease proteinuria in patients with chronic kidney disease," *American Journal of Nephrology*, vol. 28, no. 3, pp. 381–390, 2008.

[4] F. Cui, D. Zou, Y. Gao et al., "Effect of Tongxinluo on nephrin expression via inhibition of Notch1/snail pathway in diabetic rats," *Evidence-based Complementary and Alternative Medicine*, vol. 2015, Article ID 424193, 11 pages, 2015.

[5] G. I. Welsh and M. A. Saleem, "Nephrin—signature molecule of the glomerular podocyte?," *Journal of Pathology*, vol. 220, no. 3, pp. 328–337, 2010.

[6] A. Piwkowska, D. Rogacka, I. Audzeyenka, M. Jankowski, and S. Angielski, "High glucose concentration affects the oxidant-antioxidant balance in cultured mouse podocytes," *Journal of Cellular Biochemistry*, vol. 112, no. 6, pp. 1661–1672, 2011.

[7] K. Susztak, A. C. Raff, M. Schiffer, and E. P. Bottinger, "Glucose-induced reactive oxygen species cause apoptosis of podocytes and podocyte depletion at the onset of diabetic nephropathy," *Diabetes*, vol. 55, no. 1, pp. 225–233, 2006.

[8] M. Koshikawa, M. Mukoyama, K. Mori et al., "Role of p38 mitogen-activated protein kinase activation in podocyte injury and proteinuria in experimental nephrotic syndrome," *Journal of the American Society of Nephrology*, vol. 16, no. 9, pp. 2690–2701, 2005.

[9] K. Gao, Y. Chi, W. Sun, M. Takeda, and J. Yao, "5′-AMP-activated protein kinase attenuates adriamycin-induced oxidative podocyte injury through thioredoxin-mediated suppression of the apoptosis signal-regulating kinase 1-P38 signaling pathway," *Molecular Pharmacology*, vol. 85, no. 3, pp. 460–471, 2014.

[10] W. Lv, Y. Zhang, G. Guan, P. Li, J. Wang, and D. Qi, "Mycophenolate mofetil and valsartan inhibit podocyte apoptosis in streptozotocin-induced diabetic rats," *Pharmacology*, vol. 92, no. 3-4, pp. 227–234, 2013.

[11] B. F. Palmer, "Proteinuria as a therapeutic target in patients with chronic kidney disease," *American Journal of Nephrology*, vol. 27, no. 3, pp. 287–293, 2007.

[12] I. Ben Salem, M. Boussabbeh, I. Graiet, A. Rhouma, H. Bacha, and S. Abid Essefi, "Quercetin protects HCT116 cells from Dichlorvos-induced oxidative stress and apoptosis," *Cell Stress & Chaperones*, vol. 21, no. 1, pp. 179–186, 2016.

[13] D.-H. Zhao, Y.-J. Wu, S.-T. Liu, and R.-Y. Liu, "Salvianolic acid B attenuates lipopolysaccharide-induced acute lung injury in rats through inhibition of apoptosis, oxidative stress and inflammation," *Experimental and Therapeutic Medicine*, vol. 14, no. 1, pp. 759–764, 2017.

[14] M. Hytti, N. Piippo, E. Korhonen, P. Honkakoski, K. Kaarniranta, and A. Kauppinen, "Fisetin and luteolin protect human retinal pigment epithelial cells from oxidative stress-induced cell death and regulate inflammation," *Scientific Reports*, vol. 5, no. 1, article 17645, 2015.

[15] D. Gui, Y. Guo, F. Wang et al., "Astragaloside IV, a novel antioxidant, prevents glucose-induced podocyte apoptosis in vitro and in vivo," *PLoS One*, vol. 7, no. 6, article e39824, 2012.

[16] M. W. Steffes, D. Schmidt, R. McCrery, J. M. Basgen, and International Diabetic Nephropathy Study Group, "Glomerular cell number in normal subjects and in type 1 diabetic patients," *Kidney International*, vol. 59, no. 6, pp. 2104–2113, 2001.

[17] M. E. Pagtalunan, P. L. Miller, S. Jumping-Eagle et al., "Podocyte loss and progressive glomerular injury in type II diabetes," *The Journal of Clinical Investigation*, vol. 99, no. 2, pp. 342–348, 1997.

[18] T. W. Meyer, P. H. Bennett, and R. G. Nelson, "Podocyte number predicts long-term urinary albumin excretion in Pima Indians with type II diabetes and microalbuminuria," *Diabetologia*, vol. 42, no. 11, pp. 1341–1344, 1999.

[19] J. Xu, Z. Li, P. Xu, and Z. Yang, "Protective effects of leukemia inhibitory factor against oxidative stress during high glucose-induced apoptosis in podocytes," *Cell Stress and Chaperones*, vol. 17, no. 4, pp. 485–493, 2012.

[20] E. Riedl, F. Pfister, M. Braunagel et al., "Carnosine prevents apoptosis of glomerular cells and podocyte loss in STZ diabetic rats," *Cellular Physiology and Biochemistry*, vol. 28, no. 2, pp. 279–288, 2011.

[21] E. Sohn, J. Kim, C.-S. Kim, Y. S. Kim, D. S. Jang, and J. S. Kim, "Extract of the aerial parts of Aster koraiensis reduced development of diabetic nephropathy via anti-apoptosis of podocytes in streptozotocin-induced diabetic rats," *Biochemical and Biophysical Research Communications*, vol. 391, no. 1, pp. 733–738, 2010.

[22] H. Wang, T. Madhusudhan, T. He et al., "Low but sustained coagulation activation ameliorates glucose-induced podocyte apoptosis: protective effect of factor V Leiden in diabetic nephropathy," *Blood*, vol. 117, no. 19, pp. 5231–5242, 2011.

[23] C. Li and H. M. Siragy, "High glucose induces podocyte injury via enhanced (Pro)renin receptor-Wnt-β-catenin-snail signaling pathway," *PLoS One*, vol. 9, no. 2, article e89233, 2014.

[24] G. Li, Y. Li, S. Liu et al., "Gremlin aggravates hyperglycemia induced podocyte injury by a TGFβ/smad dependent signaling pathway," *Journal of Cellular Biochemistry*, vol. 114, no. 9, pp. 2101–2113, 2013.

[25] S. Doublier, G. Salvidio, E. Lupia et al., "Nephrin expression is reduced in human diabetic nephropathy: evidence for a distinct role for glycated albumin and angiotensin II," *Diabetes*, vol. 52, no. 4, pp. 1023–1030, 2003.

[26] A. A. Eid, Y. Gorin, B. M. Fagg et al., "Mechanisms of podocyte injury in diabetes: role of cytochrome P450 and NADPH oxidases," *Diabetes*, vol. 58, no. 5, pp. 1201–1211, 2009.

[27] J. Toyonaga, K. Tsuruya, H. Ikeda et al., "Spironolactone inhibits hyperglycemia-induced podocyte injury by attenuating ROS production," *Nephrology Dialysis Transplantation*, vol. 26, no. 8, pp. 2475–2484, 2011.

[28] F. Cui, Y. Gao, W. Zhao et al., "Effect of Tongxinluo on podocyte apoptosis via inhibition of oxidative stress and P38 pathway in diabetic rats," *Evidence-based Complementary and Alternative Medicine*, vol. 2016, Article ID 5957423, 10 pages, 2016.

[29] A. Van Laethem, S. Van Kelst, S. Lippens et al., "Activation of p38 MAPK is required for Bax translocation to mitochondria, cytochrome c release and apoptosis induced by UVB irradiation in human keratinocytes," *The FASEB Journal*, vol. 18, no. 15, pp. 1946–1948, 2004.

Hindawi
Journal of Diabetes Research
Volume 2019, Article ID 9489826, 16 pages
https://doi.org/10.1155/2019/9489826

Review Article

Myocardial Ischemia and Diabetes Mellitus: Role of Oxidative Stress in the Connection between Cardiac Metabolism and Coronary Blood Flow

Paolo Severino, Andrea D'Amato, Lucrezia Netti, Mariateresa Pucci, Fabio Infusino, Viviana Maestrini, Massimo Mancone, and Francesco Fedele

Department of Cardiovascular, Respiratory, Nephrology, Anesthesiology and Geriatric Sciences, Sapienza University of Rome, 00161 Rome, Italy

Correspondence should be addressed to Francesco Fedele; francesco.fedele@uniroma1.it

Received 10 December 2018; Revised 23 February 2019; Accepted 13 March 2019; Published 4 April 2019

Guest Editor: Julia M. dos Santos

Ischemic heart disease (IHD) has several risk factors, among which diabetes mellitus represents one of the most important. In diabetic patients, the pathophysiology of myocardial ischemia remains unclear yet: some have atherosclerotic plaque which obstructs coronary blood flow, others show myocardial ischemia due to coronary microvascular dysfunction in the absence of plaques in epicardial vessels. In the cross-talk between myocardial metabolism and coronary blood flow (CBF), ion channels have a main role, and, in diabetic patients, they are involved in the pathophysiology of IHD. The exposition to the different cardiovascular risk factors and the ischemic condition determine an imbalance of the redox state, defined as oxidative stress, which shows itself with oxidant accumulation and antioxidant deficiency. In particular, several products of myocardial metabolism, belonging to oxidative stress, may influence ion channel function, altering their capacity to modulate CBF, in response to myocardial metabolism, and predisposing to myocardial ischemia. For this reason, considering the role of oxidative and ion channels in the pathophysiology of myocardial ischemia, it is allowed to consider new therapeutic perspectives in the treatment of IHD.

1. Introduction

Myocardial ischemia represents a condition of sufferance for cardiomyocytes due to coronary blood flow reduction as compared to their metabolic requests, and it may exhibit through several clinical conditions [1]. From the epidemiological point of view, the mortality rate for ischemic heart disease (IHD) is about 12% of total death causes, and in a population aged between 35 and 74 years, myocardial infarction represents the main cause of death and morbidity [2]. Recent studies demonstrated that, in western countries, the mortality rate for IHD reduced over the past four decades, although it now represents one of the main causes of death in people over 35. Instead, in developing countries, the IHD death rate is expected to increase because of environmental pollution, increasing life expectancy and assumption of western habits such as western diet, smoking, alcohol assumption, and physical inactivity [3-6]. From the pathophysiological point of view, IHD may represent the consequence of both coronary artery disease (CAD) and coronary microvascular dysfunction (CMD) [7-11]. There are many regulatory mechanisms which, acting at coronary vasculature, are responsible for the adaptation of coronary blood flow (CBF) to the myocardial metabolic demand [7–10]. Ion channels represent the end effector of all these mechanisms because they regulate vassal tone through ion influx and efflux in both endothelial and smooth muscle cells [8–10]. Diabetes mellitus, such as other cardiovascular risk factors, may impair the function of these channels predisposing to CMD, and CAD and oxidative stress seem the main mechanisms through which diabetes mellitus acts [8].

2. Diabetes Mellitus and Oxidative Stress: Connection with Ischemic Heart Disease

2.1. Pathophysiological Basis of IHD. IHD may be the result of two pathophysiological mechanisms of action: CAD and CMD. CAD represents a condition defined by the presence of an atherosclerotic plaque which reduces the vessel diameter more than 50%, and it is usually the main, but not the only cause of IHD. Indeed, often the presence of CAD is not associated with the onset of IHD and conversely IHD may develop in the absence of angiographic relevant atherosclerotic plaques [7–9]. About that, the role of microcirculation may be crucial in the pathophysiology of IHD [7-11]. CMD, causing a reduced endothelial and nonendothelial response of coronary microvasculature to myocardial demands, is associated with coronary blood flow reduction and myocardial ischemia independently from CAD [10, 11]. From the opposite point of view, CMD promotes the development of atherosclerotic plaques too, altering physical coronary blood flow features and increasing epicardial vessel shear stress [7–11]. From the clinical point of view, IHD may exhibit with several conditions such as angina, acute coronary syndrome, sudden cardiac death, and heart failure [7, 9, 12–26] (Figure 1).

2.2. Diabetes Mellitus as Risk Factor for Ischemic Heart Disease. There are several cardiovascular risk factors which are involved in IHD and other cardiovascular diseases pathogenesis, and diabetes mellitus represents one of the most significative ones [8, 27]. Cardiovascular diseases, in particular IHD, represent the main long-term complication and death cause among diabetic patients [8]. Moreover, the risk to develop cardiovascular disease is similar for both type 2 diabetes mellitus (T2DM) and type 1 diabetes mellitus (T1DM) patients, even if there are gender and age differences between the two types [8, 27]. The main mechanism of diabetes mellitus pathophysiology is a condition of long-time insulin resistance which is strictly associated with hyperglycaemia followed by a compensatory hyperinsulinemia [27]. Hyperglycaemia, insulin resistance, and fatty acid excessive production lead to an increase in systemic oxidative stress, inflammatory response, and advanced glycation product (AGE) production [8, 27]. All these mechanisms contribute both to coronary atherosclerosis onset and progression and to coronary microvascular dysfunction [8, 27]. In particular, hyperglycaemia stimulates AGE production, accumulation of free radicals, polyol and hexosamine flux in endothelial cells, and an increase in intravascular inflammatory response through the overexpression of several factors, such as nuclear factor-κB, which is initially produced by endothelial cells, and it promotes the transcription of inflammatory response-associated genes and leukocyte recruitment near the vascular wall [28]. These mechanisms are shared between diabetes mellitus and other cardiovascular risk factors, promoting dysfunction and apoptosis of endothelial cells [29, 30]. Moreover, diabetes-related renal dysfunction promotes mineral metabolism imbalance, and it determines the accumulation of calcium in coronary arteries leading to an increase in arterial rigidity and atherosclerotic plaque burden [29, 30]. Regarding myocardial ischemia in patients with diabetes mellitus, its pathophysiology is not completely understood yet. Some diabetic patients show IHD due to the presence of coronary atherosclerotic plaques which obstruct the blood flow directly to the myocardium while others develop IHD due to CMD in the absence of atherosclerotic plaques in coronary epicardial vessels [7, 9]. As regard the CMD in diabetes mellitus, oxidative stress together with hyperglycaemia and inflammation response determines coronary vasomotion alteration through the impairment of both endothelium-dependent vasodilation, reducing NO production and increasing endothelin-1 release, and endothelium-independent vasodilation [31]. Moreover, Yokoyama et al. underlined an inverse relationship among myocardial flow reserve and haemoglobin A1C average levels and fasting glucose plasma values. Authors demonstrated the role of diabetes mellitus in the determinism of CMD and myocardial ischemia [32]. Endothelial, smooth muscle cells and cardiomyocyte death, autonomic dysregulation, lipotoxicity, and endomyocardial fibrosis are other mechanisms through which diabetes mellitus promotes IHD [33, 34]. In most cases, the impact of diabetes mellitus on IHD determinism is improved by the presence of other cardiovascular risk factors such as dyslipidemia, arterial hypertension, and inflammation [35–45] (Figure 2).

2.3. Role of Oxidative Stress in the Pathophysiological Continuum among Diabetes Mellitus and IHD. Oxidative stress is defined as a condition of oxidant molecule cellular excess compared to antioxidant ones [46]. The presence of oxidants is normally neutralized by the presence of antioxidant cell systems which include both enzymatic molecules, such as superoxide dismutase (SOD) and catalase, and nonenzymatic molecules, such as all trans-retinol 2 and ascorbic acid [46]. The activity of these systems and the regulation of redox cell state are crucial for cell function and survival. When produced in not excessive quantity, ROS are involved in several physiological mechanisms regarding the cardiovascular system [46, 47]. They stimulate angiogenesis via the vascular endothelial growth factor (VEGF) pathway, and they are involved in endothelial cell regeneration, proliferation, and migration. H2O2 is crucial for postischemic neovascularization, and they are also involved in the regulation of coronary endothelial-dependent and independent vasodilatation [7–9, 46, 47]. In pathological conditions, the damage and/or the overload of antioxidant systems make them unable to contrast the production of oxidants. Reactive oxygen species (ROS) play a central role as mediators of oxidative stress and its complications [46–48]. This term defines several agents among which there are both oxygen radicals as hydroxyl (OH-), superoxide (o2–), and peroxile (Ro2-) and several nonradical oxygen species as hydrogen peroxide (H2O2) [47, 48]. However, ROS are highly reactive molecules and in case of their accumulation, they may cause several modifications in the structure and function of DNA, proteins, and lipids [46, 48–50]. Metabolic cell activity and environmental factors, such as wrong diet and smoke, contribute to ROS production and therefore oxidative stress which may predispose to several pathological conditions as neurological

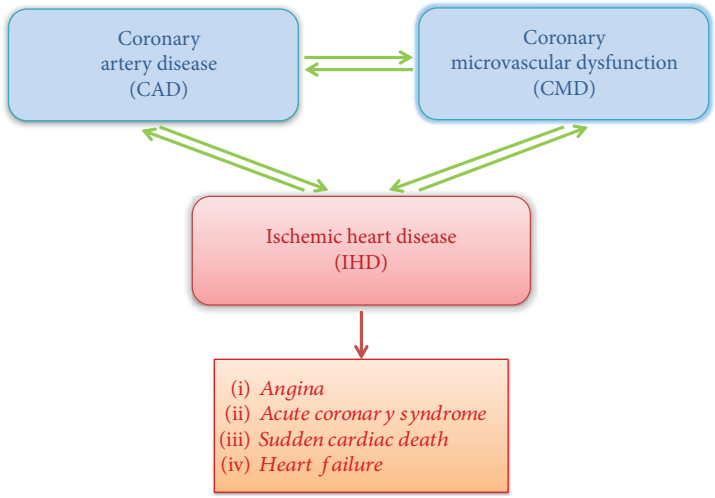

Figure 1: Pathophysiological basis of IHD and its clinical manifestations.

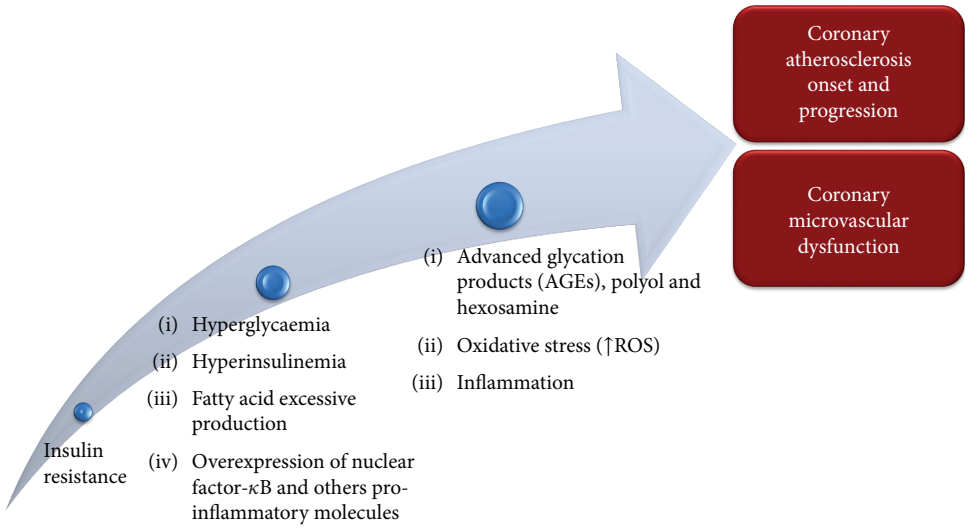

Figure 2: Pathophysiology of diabetes mellitus and its role in the determinism of IHD.

disease, cancer, atherosclerosis, hypertension, diabetes mellitus, and cardiovascular diseases [46, 47]. There is an important link between oxidative stress and the development of diabetes mellitus and its complications [51–53]. Indeed, in diabetic patients there is not only an excess of ROS production but also a damage of antioxidant mechanism function and a stronger and prolonged inflammatory response [51]. In diabetes mellitus, ROS together with inflammatory response and hyperglycaemia plays a central role in the initiation and progression of vascular damage, supporting the atherosclerosis process and microvascular dysfunction [51, 54]. These mechanisms are the basis of chronic kidney injury, myocardial ischemia, and retinopathy, the most important diabetes mellitus complications [51, 54–58]. Moreover, patients with diabetes mellitus who were already treated with percutaneous coronary intervention show an increased risk to develop stent restenosis, mostly by using bare-metal stents and previous generations of drug-eluting stents [59, 60]. In diabetes mellitus, hyperglycaemia represents a stimulus for ROS production [51, 61]. Hyperglycaemia and the excess of intravascular ROS may cause not only the elevation of low density lipoproteins (LDL), chylomicrons, and total cholesterol values but also the oxidation and glycation of lipoproteins increasing their atherogenicity and accelerating the atherosclerotic process [51, 61–63]. Hyperglycaemia increases advanced glycation product (AGE) production, and Giardino et al. demonstrated that also ROS represents a stimulus for AGE synthesis [51, 61]. From another point of view, Sima et al. showed a bidirectional link between the AGE-LDL complex and ROS, demonstrating that the AGE- LDL complex may stimulate ROS production and the subsequent inflammatory response activation which contributes to vascular damage, through the expression of IL-1β and TNF-α [51, 62]. There is a clear link among ROS, AGE, and oxidized LDL (Ox-LDL) [51, 64, 65]. Indeed, beyond the bidirectional link between AGE and ROS, these two agents

stimulate the oxidation of LDL. Ox-LDL causes a reduction in endothelial nitric oxide production and through the activation of caspase-3 and 9 stimulates endothelial cell apoptosis [51, 66, 67]. ROS contribute to atherosclerosis, also inducing the worsening of endothelial dysfunction, increasing the expression of adhesion molecules like intercellular adhesion molecule-1 (ICAM-1) and vascular adhesion molecule-1 (VCAM-1), and modulating the expression of different growth factors important in the proliferation of vascular smooth muscle cells (VSMCs) [68]. In diabetic patients, the main source of intravascular ROS is NADPH oxidase (NOS) whose expression is highly increased compared to nondiabetic patients [51, 69]. There are 4 isoforms of NOX, NOX1, NOX2, NOX4, and NOX5, which are overexpressed and play a crucial role in atherosclerosis progression in diabetic patients. NOX1 is expressed by endothelial cells. A decreased expression of NOX1 is associated with reduced leucocyte vascular wall adhesion and macrophage recruitment [51, 70]. NOX4 is expressed by endothelial and muscle cells, and it has a protective role for the wall vessel. The reduction in its expression supports the increase in inflammatory marker production such as IL-1 and MCP-1 and the progression of atherosclerosis [51, 71]. Moreover, the reduced expression of NOX4 on smooth muscle cells associates with reduced contractile gene expression and higher production and deposition of collagen [51, 72]. NOX5 may alter endothelial nitric oxide synthase (eNOS) activity contributing to endothelial dysfunction [51, 73, 74]. Inside the cell, the most important site of free radical production is mitochondria because they represent the energetic central point of the cell. Glucose from the blood circle enters inside the cell to be used for adenosine triphosphate (ATP) production. During glycolysis, pyruvate, ATP, nicotinamide adenine dinucleotide (NADH), and flavin adenine dinucleotide (FADH2) are produced. NADH and FADH2 are transferred inside mitochondria, and they have a role as electronic donors during oxidative phosphorylation. In the hyperglycaemic state, a lot of electrons are lost in the mitochondrial respiratory chain which become the most important source of the overproduction of O2- [75, 76]. Moreover, Azumi et al. highlighted an association between ROS production in human atherosclerotic coronary arteries and the NAPDH-oxidase subunit p22 phox [77]. Hyperglycaemia increases diacylglycerol (DAG) content by the activation of phospholipase C or D, which activates protein kinase C (PKC) [77]. PKC activates NADPH oxidase. The NADPH oxidase complex consists of the cytosolic components p47phox, p67phox, p40phox; a low-molecular-weight G-protein, Rac 1 or Rac 2; and the membrane-associated NOX2 and p22phox [77]. Activation of the enzyme complex requires translocation of the cytosolic components to the plasma membrane, and their association to NOX2 produces ROS [77]. Recently, particular attention was focused on the role of microRNA as a mediator of oxidative stress effects in the pathophysiology of diabetes mellitus and its complications [78–89] (Figure 3).

MicroRNAs (miRNAs) may play a role also in the regulation of protein expression such as ion channels and their subunits [78–89]. miRNAs represent noncoding RNA molecules of 21-23 nucleotides, and they are negative regulators of gene expression, modulating the stability of several messenger RNAs (mRNAs) before their translation in amino acids. Given that, miRNA takes part in several biological mechanisms such as apoptosis, proliferation, and differentiation, and it is clear how they may be also involved in pathological processes [78]. Several stimuli such as H2O2, ultraviolet (UV), and ionizing radiation may induce both ROS production and modification in miRNA expression [78, 79]. Magenta et al. demonstrated the strong upregulation of the miR-200 family in endothelial cells exposed to oxidative stress induced by hyperglycaemia and hyperlipidemia [78]. However, the miR-200 family may act also through another pathway. They reduce the p38alpha mitogen-activated protein (MAP) kinase expression, a protein involved in the regulation of the cellular cycle also important as an oxidative stress sensor [78, 80, 81]. Silent mating type information regulation 2 homolog (SIRT1) represents a histone deacetylase which is able to induce a lot of stress-responsive transcription factors, and it has also a strong anti-inflammatory and antioxidative effect for endothelial cells [78, 82]. In atherosclerosis, miR-217 and miR-200 targets SIRT1 causing its downregulation in endothelial cells. The reduction in SIRT1 expression is associated with senescence, apoptosis, and therefore endothelial dysfunction [78, 82]. miR-21 is upregulated in vascular smooth muscle cells in conditions of shear stress, and it protects cells from death through binding with programmed cell death 4 (PDCD4) [78, 82]. It determines an increase in NO production via activation of eNOS, but at the same time it reduces the expression of SOD-2 [78]. In case of ischemia, the reduced oxygen tension inside the cells determines the hypoxia-inducible factor (HIF) which is a transcription factor family involved in the shift from aerobic to anaerobic metabolism [78, 82–89].

3. Oxidative Stress and Ion Channel Function in the Regulation of Coronary Blood Flow

3.1. Coronary Blood Flow and Its Regulation. CBF has to satisfy myocardial metabolic and oxygen requests which continuously vary through a fine modulation of coronary resistances [90]. Microcirculation, characterized by small arteries and arterioles with a diameter included between 50 and 200 μm, represents the most important site of coronary total resistance regulation [9]. In the "cross-talk" between myocardium and coronary artery circulation, several mechanisms of vasal tone regulation act to guarantee an adequate CBF to the myocardium [7–9, 90] and their contribution changes according to the considered district [7–9, 90]. Microcirculation, which represents the distal district of coronary arterial circulation, is the main site where metabolic and myogenic regulation mechanisms act, while the epicardial artery district, which represents the proximal district of coronary arterial circulation, is the main site where neurohumoral and shear stress-related regulation mechanisms act [9]. At rest, the myocardium extracts about 80% from coronary circulation and the oxygen consumption amount to 10 mL of oxygen, per minute, per gram of myocardial tissue [90]. When myocardial oxygen consumption increases, coronary circulation has to modulate its vasal tone to guarantee

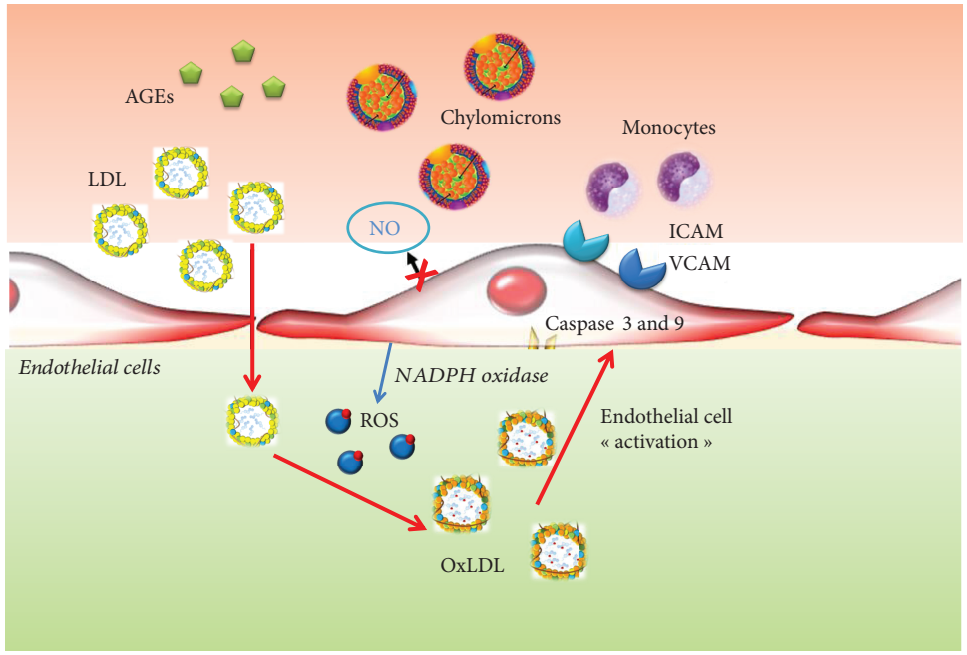

Figure 3: Role of oxidative stress in the pathogenesis of coronary artery disease and coronary microvascular dysfunction.

an adequate CBF to the myocardium. For these reasons, several vasal tone regulation mechanisms exist. Neurohumoral regulation acts through sympathetic and parasympathetic innervation which are both expressed on coronary arteries, and through their tonic activity, they determine vascular basal tone at rest [8, 9, 90]. The endothelium participates for CBF regulation producing several molecules with paracrine effects such as arachidonic acid metabolites and NO, which contributes to vasodilatation and endothelin which contribute to vasoconstriction [8, 9, 90]. Autoregulation acts myogenically, which, reducing vasal wall stress, guarantees a constant and sufficient CBF to the myocardium [8, 9, 90]. Myogenic response is mediated by variation of calcium values in smooth muscle cells which modulate their state of contraction [8, 9, 90]. CBF is also modulated by several hormones such as progesterone, testosterone, histamine, and antidiuretic hormone (ADH) which are vasodilators and angiotensin II which is a vasoconstrictor [91–94]. Insulin mediates both vasoconstriction, via activation of sympathetic fibers, and vasodilatation, via NO production stimulation [91]. Metabolic regulation acts mainly at microcirculation, and it is important for the quick adaptation of CBF to myocardial metabolic demand. The effect of metabolic regulation is mediated by several molecules produced by cardiomyocytes whose targets are represented by specific receptors and ion channels. Among these molecules, there are carbon dioxide (CO2), adenosine, oxygen, H2O2, superoxide, and other reactive oxygen species [90, 95–97] (Figure 4).

3.2. Coronary Ion Channels and Their Physiological Role. Coronary ion channels represent the crucial connectors in the cross-talk between myocardial metabolic demand and coronary blood flow regulation. They are the final effectors of several CBF regulatory mechanisms (nervous, metabolic, endothelial, and myogenic) which act in response to myocardial metabolism variations [8, 9, 90]. In coronary circulation, ion channels are expressed both by endothelial cells where they modulate the secretion of different vasoactive substances, among which there is nitric oxide (NO), and by arterial smooth muscle cells where they regulate the vascular tone, modulating ions fluxes through the cell membrane. The importance of ion channels in the regulation of coronary blood flow and the connection between their function and IHD was also underlined by us [7–9] with particular attention for several specific single-nucleotide polymorphisms (SNPs) of genes encoding for ion channel constitutive proteins. There are several types of ion channels involved in the regulation of vasal tone and endothelial function. Voltage-gated sodium channels are associated with a late Na^+ current which determines cell depolarization. The main function of these channels is to modulate endothelial NO production and release via endothelial Ca^{2+} levels and Na^+/Ca^{2+} exchange regulation [8, 98]. Vascular smooth muscle cells express chloride channels, and they can be both Ca^{2+}- and voltage-dependent. When these channels are opened, a Cl^- current moves out from the cells determining their depolarization and therefore vasoconstriction [8, 98]. Chloride channels determine the opposite effect when they are closed [9]. One of the main channels involved in the regulation of microvascular resistance are voltage-gated calcium channels (Cav). They regulate the Ca^{2+} current from the extracellular to intracellular environment. Their final effect is to increase vascular tone and determine a reduction of CBF [9]. Potassium channels are expressed both by endothelial cells, where they modulate the secretion of vasoactive substances such as NO, and by arterial smooth muscle cells, where they regulate cell state of contraction [7, 8]. The opening of the potassium channel determines the efflux of K^+

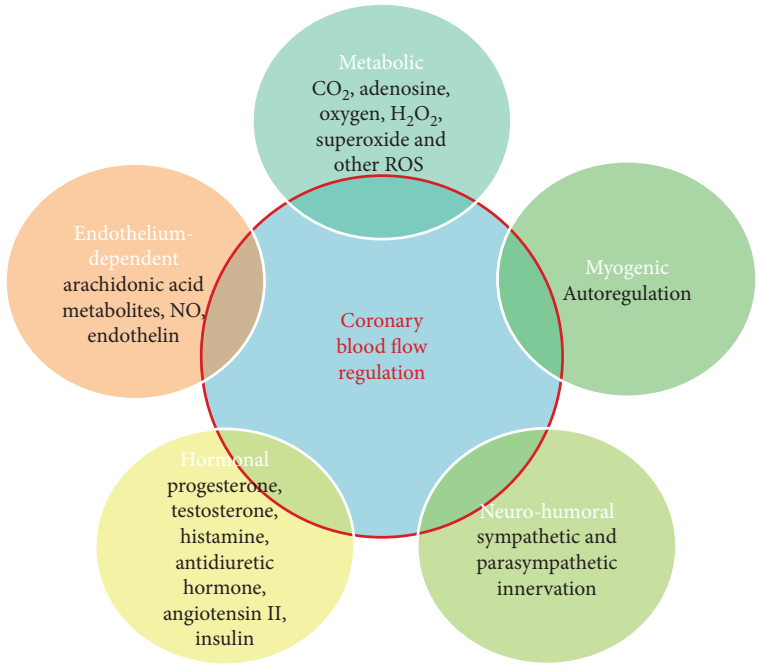

Figure 4: Different mechanisms involved in coronary blood flow regulation.

from the intracellular to extracellular environment, the membrane resting potential moves to more negative values, the cell is hyperpolarized, and the Ca^{2+} channels are closed. The final effect of this event is artery vasodilatation, thanks to smooth muscle cell relaxation. The closing of potassium channels, instead, determines cell depolarization and the activation of voltage-gated Ca^{2+} channels which determines the increase in calcium cell concentration. The final effect of this event is smooth muscle cell contraction and the increase in vasal tone [90]. In the coronary circulation, four types of potassium channels are described in literature: KATP, KCa, Kv, and inward rectifier potassium (Kir) channels. KATP channels are made up of two subunits: an inward rectifier-potassium channel (Kir subunit) and an ATP-binding cassette protein defined as sulfonylurea-binding subunit (SUR) [7, 8]. Kir subunits have a crucial role in maintaining resting membrane potential because they support a faster inward K^+ current than an outward one while SUR subunits bind ATP [7, 8]. Coronary KATP channels are involved in the metabolic regulation of coronary vascular tone [7, 8]. KATP channels open when intracellular ATP is reduced, and they allow the efflux of K^+ from the intracellular to extracellular environment [7, 8]. This condition associates with reduction of intracellular Ca^{2+} values and therefore vasodilatation [7]. KATP channels are mainly closed in normal metabolic conditions [7, 8]. The main represented KATP subunit combinations in coronary circulation are Kir6.2/SUR2A and Kir6.1/SUR2B [8]. Kv channels regulate CBF at rest and during cardiac stimulation [7, 8]. They are the targets of several vasoactive molecules, and for this reason they are involved in endothelial-dependent and -independent vasodilatation [8, 99]. Vasodilating molecules open Kv via the cAMP-dependent pathway while vasoconstrictor ones close Kv, increasing Ca^{2+} cell levels [8, 99]. Several channels of the Kv family, such as Kv1.5 and Kv1.3, are involved in H2O2-mediated CBF regulation [95, 100]. KCa channels are expressed by both endothelial and smooth muscle cells, and they have a crucial role in preserving the rest membrane potential [7, 8]. KCa channel activation, associated with the efflux of K^+ from the intracellular to extracellular space, is caused by two main stimuli: the increase in intracellular Ca^{2+} levels and membrane depolarization [7, 8, 90]. Three types of KCa channels are described in coronary artery circulation [7, 8, 90]. On the basis of their conductance, they are divided into small (S), intermediate (I), and big (B). KCa channels are redox-sensitive ones; in particular, they contribute to vasodilatation in response to endothelial-derived hyperpolarizing factor (EDHF), lipoxygenase metabolites, and H2O2 [101–104]. However, they are also involved in vasoconstriction, because they represent the target of several vasoconstrictor agents such as endothelin and angiotensin II which determine their inhibition [8, 105–108] (Figure 5 and Table 1).

Transient receptor potential vanilloid 1 (TRPV1) channels belong to the vanilloid TRP family, and they have permeability to several cations such as Mg^{2+}, Ca^{2+}, H^+, and Na^+ [109, 110]. In the cardiovascular system, TRPV1 channels are expressed by endothelial smooth muscle cells, by the myocardium, and by nerve myocardium nerve fibers [7, 8, 90]. TRPV1 channel activation is associated with coronary vasodilatation; they contrast atherosclerosis onset and progression and vascular and myocardium remodeling, and they reduce arterial pressure values, inducing endothelial NO release [109]. TRPV1 activation plays an important role against vascular oxidative stress effect because they increase mitochondrial Sirtuin 3, UCP2, and PPAR-γ expression [109].

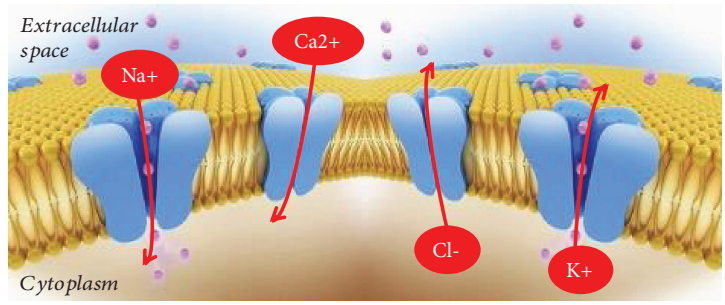

Figure 5: Schematic representation of ion movements through coronary ion channels.

Table 1: Coronary ion channels and their physiological role in the regulation of coronary vascular tone.

Ion channel	Membrane effect	Functions
Nav	Depolarization	Endothelial-dependent coronary vasodilation
Cl-	Depolarization	Endothelial-independent vasoconstriction
Cav	Depolarization	Coronary vasoconstriction; coronary autoregulation and control of coronary microvascular resistance
Kv	Hyperpolarization	Endothelial-dependent and -independent coronary vasodilation
KATP	Hyperpolarization	Coronary vasodilation and metabolic regulation of coronary blood flow
KCa	Hyperpolarization	Redox-sensitive channel, coronary dilatation in response to endothelial-derived hyperpolarizing factor (EDHF), lipoxygenase metabolites, and H_2O_2

3.3. Impact of Oxidative Stress on Ion Channel Function. Some products of myocardial metabolism mediate CBF according to myocardium metabolic demand. In this cross-talk, ROS, produced in not excessive quantities, may have an important physiological role interacting with ion channel function. H2O2 is a product of myocardial metabolism which is involved in coronary autoregulation [111]. It may represent an endothelial hyperpolarizing factor [112] which causes coronary dilatation [104] through its activation of K + channels. Saitoh et al. demonstrated that H2O2, produced in relation to cardiomyocyte oxygen consumption, represents a stimulus for arteriole dilatation and coronary blood flow increase [97]. They confirmed the role of H2O2 because they showed that catalase and 4-aminopyridine (4-AP) intracoronary infusion is associated with the intracoronary H2O2 levels and coronary blood flow reduction [97]. H2O2 may cause the modification of K^+ currents [97]. H2O2 and probably other types of ROS may also stimulate endothelial-independent vasodilatation because they act as smooth muscle BKca channel openers through a redox-induced G protein dimerization [90]. About that, several studies suggested a role for large-conductance Ca^{2+}/voltage-sensitive K^+ channels (BKCa) as a target of H2O2 [96, 101, 102, 104]. However, the only H2O2 activity on BKCa was not enough to cause coronary vasodilatation [97]. Kv channels may represent the main ones involved in ROS-mediated coronary vasodilatation [90] Rogers et al. studied other possible targets of H2O2 that may be involved in redox-mediated coronary vasodilatation [96]. They previously demonstrated that 4-AP, a voltage-gated K^+ channel (Kv) inhibitor, reduced H2O2 production and coronary vasodilatation [97]. For this reason, they focused on the possible role of the Kv channel as a redox-sensitive regulator of coronary blood flow [96]. Their results suggest that H2O2 acts through thiol oxidation and its effect on Kv channels developed quickly (2-3 minutes) [96] (Figure 6).

Thiol groups are probably contained in proteins involved in Kv channel regulation or they are inside the molecular structure of channels [96, 97]. Moreover, the intracoronary infusion of DTT, a thiol reductant, and NEM, a thiol-alkylating agent, reduces the effect of H2O2 on Kv channel activity [96]. As we previously described, ion channels play a crucial role in the cross-talk between myocardial metabolic demand and coronary blood flow [7–9]. The Kv channel family is expressed on endothelial and smooth muscle cells, and it fulfilled the role of coronary blood flow metabolic regulators [7–9, 90]. These channels are redox-sensitive ones, and H2O2, produced by mitochondria, determines their opening and the following cellular hyperpolarization which is associated with vascular dilatation [96, 97, 100]. Ohanyan et al. focused their attention on the Kv1.5 channels which are mainly expressed on smooth muscle cells, and they are both redox- and oxygen-sensitive channels [100]. They showed that Kv1.5 $^{-/-}$ mice had an impaired response of coronary blood flow to the increased myocardial work, leading to myocardial ischemia and heart pump failure through microvascular dysfunction and without the presence of atherosclerotic obstructive plaques [100]. Myocardial ischemia represents the final effect of Kv1.5 dysfunction [100]. Indeed, after the noradrenaline infusion in Kv1.5 $^{-/-}$ mice, there is an imbalance between oxygen delivery and oxygen consumption caused by the impaired response of coronary circulation, which is unable to sustain coronary arterial pressure and heart pump, to the increased cardiac work [100]. Myocardial

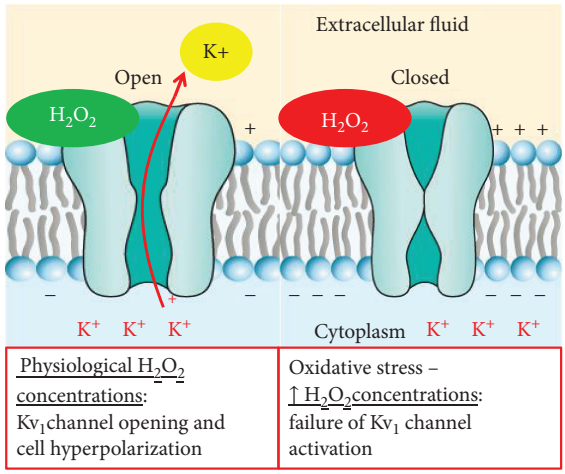

FIGURE 6: Physiological and pathophysiological roles of H2O2 on voltage-dependent potassium channel (Kv).

ischemia, pump efficiency, and arterial pressure reduction do not occur in wild-type mice [100]. However, Kv1.5 activity is not the only mechanism which guarantees an adequate blood flow in response to myocardial work [100]. There are other ion channels and mechanisms involved in this [90, 100]. Indeed, the absence of Kv1.5 in mice facilitates myocardial ischemia, but it is not lethal, coronary dilatation in response to H2O2 is not completely abolished in Kv1.5$^{-/-}$ mice, and moreover in Kv1.5$^{-/-}$ mice there is an upregulation of Kir6.2, Kir6.1, and Kv1.2, suggesting a compensative role of these channels for coronary blood flow regulation in the absence of Kv1.5 [100]. For this reason, it may be other ion channels involved in the oxygen and redox-sensitive coronary blood flow regulation [100, 113, 114]. For this reason, Ohanyan et al. focused on Kv1.3 channels and they demonstrated that these channels have a crucial role in the connection between cardiac metabolism and coronary blood flow [95]. Kv1.3 channels participate in H2O2-induced vasodilatation, but they did not involve in that one induced by adenosine and acetylcholine [95]. Indeed, Kv1.3$^{-/-}$ mice showed an impaired blood flow regulation in response to cardiac work increase [95]. Moreover, administration of correolide, a blocker of the Kv cannel family, in wild-type mice reproduces the same condition seen in Kv1.3$^{-/-}$ mice [95]. In the study of Ohanyan et al., Kv1.5$^{-/-}$ mice developed heart pump failure when they underwent a growing cardiac work [100]. In this case, coronary microvascular dysfunction and not the presence of an obstructive atherosclerotic plaque provoked heart failure. This study supports results [7–9] about the importance of microcirculation in the pathophysiology of IHD [115]. In obese and diabetic patients, diastolic dysfunction represents an early and frequent abnormality of heart function [116–118]. Insulin resistance and the renin angiotensin-aldosterone system (RAAS) had a crucial role in the determinism of diabetes complications and diastolic heart failure [116, 119, 120]. Jia et al. defined the role of coronary microvascular dysfunction in the determinism of diastolic heart failure in diabetes mellitus [116]. They demonstrated that administration of typical west diet in mice was associated with cardiac remodeling and fibrosis, accumulation of M1-polarized macrophages, and reduced occluding and claudin-5 expression, which belong to endothelial tight junctions, and they are markers of endothelium permeability [116]. However, their most important finding was that in these mice there was an upregulation of the endothelium epithelial sodium channel (EnNaC) [116]. In diabetic and obese female mice, the excess in dietary intake caused an overexpression of cardiac mineral-corticoid receptors which together with heightened oxidative stress and inflammation led to EnNaC overexpression, a condition which caused diastolic heart failure through microvascular dysfunction [116, 121, 122]. EnNaC determined the excessive endothelial intake of Na^+ which caused the reduction of NO production [123] and the polymerization of G-actin to F-actin that determined arterial stiffness [124]. The administration of low doses of amiloride, an antagonist of EnNaC, reduced the risk of LV diastolic heart failure in diabetic and obese female mice [116]. Dwenger et al. studied Kv1 channels, and they confirmed the crucial role of this type of channels in the connection between myocardial metabolism and coronary blood flow [125]. Moreover, they focused on the redox sensibility of these channels [125]. The regulation of Kv1 channel functions is determined by several posttranslational modifications on cysteine, tyrosine, and methionine residues belonging to the channel structure [125, 126]. A dual role of oxidative stress on Kv1 channels was supposed [125, 126]. Indeed, physiological levels of H2O2 represented a stimulus for channel activation and K^+ peak increase, conditions associated with smooth muscle cell hyperpolarization and coronary vascular dilatation [125, 127]. However, in condition of heightened H2O2 production such as diabetes mellitus, it failed Kv1 channel activation and it even determined their closure [125]. Peroxynitrite ($ONOO^-$) is produced from superoxide and NO [128]. Li et al. demonstrated that an excess of $ONOO^-$ led to Kv-mediated vasodilatation impairment through Kv1.2 tyrosine residue nitration [129]. Several authors focused on the role of the TRP channel family in the regulation of coronary blood flow in response to oxidative stress [130–132]. Guarini et al. had already demonstrated that the transient receptor potential vanilloid 1 (TRPV1) channels, belonging to the TRP channel family, are impaired in diabetic mice and they contributed to the development of microvascular dysfunction in these models [130, 133]. TRPV1 is expressed by the endothelium of coronary vasculature, and it represents an oxidative sensor which regulates coronary blood flow in relation to myocardial redox state [130, 132]. In diabetic patients, the persistent exposure to oxidative stress promotes lipid peroxidation and its by-product formation such as 4-hydroxynonenal (4-HNE) which causes posttranslational modifications through the interaction with several amino acid residues contained in the ion channel structure [130]. 4-HNE had a main role in the determinism of cardiomyocyte hypertrophy, onset and progression of atherosclerotic disease, and ischemia-reperfusion damage after myocardial ischemia [130, 134, 135]. DelloStritto et al. confirmed the contribution of 4-HNE also in the determinism of microvascular dysfunction in diabetes mellitus [130]. In particular, they demonstrated that the target of 4-HNE on the TRPV1

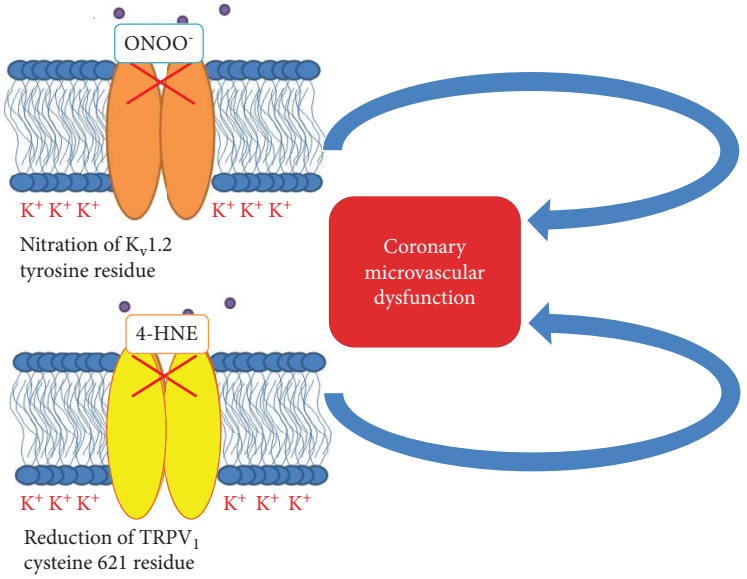

Figure 7: An excess of peroxynitrite (ONOO-) may lead to Kv-mediated vasodilatation impairment through Kv1.2 tyrosine residue nitration; 4-hydroxynonenal (4-HNE) targets a cysteine 621 residue of the TRPV1 coronary channel impairing its function and contributing to CMD in diabetes mellitus.

channel was the cysteine 621 residue. The final effect was the reduction of TRPV1-dependent coronary blood flow dilatation which may contribute to microvascular dysfunction in diabetes [130] (Figure 7).

4. Ion Channels as Target in the Therapy against Ischemic Heart Disease

Among potassium channels, KATP represents the main pharmacological target in the treatment of diabetes mellitus and cardiovascular diseases. In this context, it is involved in several pathophysiological processes, and for this reason, it shows a remarkable therapeutic potential [136]. In diabetic patients, pancreatic β-cell KATP, in particular SUR subunits, represents a target of sulphonylureas which act as antagonist of this channel, causing their closure [136]. Sulphonylureas promotes β-cell depolarization and the increase in insulin secretion [136]. Diazoxide is a Kir6.2/SUR1 KATP channel opener, and it is used in hypertensive crisis [136–139]. Pinacidil and cromakalim are Kir6.2/SUR2A KATP and Kir6.2/SUR2B KATP channel openers, and they determine arteriole resistance reduction, arterial blood pressure reduction, and vasodilatation [136–139]. In patients with IHD, coronary smooth muscle and myocardial KATP become therapeutic targets of several molecules such as nicorandil and levosimendan which cause the opening of these channels, a condition associated with higher CBF and better myocardial perfusion [140]. Nicorandil has a nitrate-like effect, and it also blocks calcium channels; for this reason, it is used in the treatment of stable angina [140]. Nicorandil may reduce the possibility of QT abnormalities and ventricular fibrillation in patients who underwent coronary angioplasty after acute myocardial infarction, and it is also used in the management of no-reflow phenomenon which may manifest after the same procedure [141]. Zhang et al. demonstrated that nicorandil, stimulating M2 macrophage polarization and inhibiting M1 macrophage polarization, reduces macrophage phagocytic activity and ROS and cytokine production [140]. Moreover, they demonstrated that nicorandil promotes endothelial reconstitution because, promoting M2 macrophage polarization, it increased VEGFA expression which has a proangiogenic effect [140]. In particular, nicorandil ameliorates cell redox state reducing ROS production and increasing mitochondrial membrane stability and Bcl-2/Bax ratio. NF-κB which is made up of two subunits, p50 and p65, represents a nuclear factor which promotes the transcription of several genes involved in inflammatory response and in M1 macrophage polarization [140]. Kupatt et al. demonstrated that NF-κB signaling pathway upregulation may aggravate myocardial ischemic damage [140, 142]. Nicorandil reduces NF-κB pathway activity, acting through the inhibition of the p65 subunit and therefore M1 macrophage polarization [140]. Moreover, angina IONA study demonstrated that nicorandil improved the prognosis of patients with stable angina [143]. Levosimendan beyond the action on KATP represents a calcium sensitizer, and it determines a remarkable reduction in pulmonary capillary wedge pressure in a patient who presents with heart failure with low output [136, 144]. Moreover, levosimendan has electrophysiological effects such as inhibitors of phosphodiesterase [145]. It is used to improve heart pump function, and it reduces the risk to develop arrhythmic events more than milrinone, after myocardial ischemia [146]. Bunte al. demonstrated that preconditioning with levosimendan may reduce myocardial ischemic area by about 50% [145]. This effect may be due to the activation of mBKCa channels by levosimendan. mBKCa channels are voltage-gated potassium channels involved in the regulation of intracellular calcium homeostasis and which are expressed on the inner mitochondrial membrane [145, 147, 148]. In levosimendan

Table 2: Main drugs and molecules which may have a role against IHD using ion channels as therapeutic target.

Drug	Biological effects	Functions
Sulphonylureas	Antagonist of the SUR subunit of pancreatic β-cell KATP	Promotion of β-cell depolarization and insulin secretion
Pinacidil and cromakalim	Kir6.2/SUR2A KATP and Kir6.2/SUR2B KATP channel openers	(i) Arteriole resistance reduction (ii) Arterial blood pressure reduction (iii) Vasodilatation
Nicorandil	Nitrate-like and proangiogenetic effect, calcium channel blocker, M2 macrophage polarization stimulator, M1 macrophage polarization inhibitor, and NF-κB p65 subunit inhibitor	(i) Prevention of ventricular arrhythmias in patients who underwent coronary angioplasty after acute myocardial infarction (ii) Reduction of macrophage phagocytic activity, ROS and cytokine production, and improvement of mitochondrial membrane stability and Bcl-2/Bax ratio (iii) Promotion of endothelial reconstitution (iv) Improvement of the prognosis of patients with stable angina
Levosimendan	mBKCa-channel activator and calcium sensitizer, KATP activator	(i) Heart pump function improvement and reduction of the risk to develop arrhythmic events after myocardial ischemia (ii) Vasodilatation and increase in CBF
Isosteviol sodium	ROS scavenger	(i) Inhibition of QTc prolongation related to ischemia/reperfusion injury and reduction of I_{kr} and I_{katp} channel inhibition during ischemia/reperfusion injury
N-3-PUFA	Coronary BK_{Ca} channel activation, Ca^{2+} concentration in coronary smooth muscle cell reduction	(i) Vasodilation and increase in CBF
NOX inhibitor	ROS reduction	
Nrf-2 activator	Catalase and erythrocyte SOD activity induction in vivo	
Vitamin E	Antioxidant activity	

preconditioning, coronary KATP channels seem to play an important role because their activation is associated with vasodilatation and increase in CBF [145]. Intermediate and small-conductance calcium-activated K^+ channels (IKCa and SKCa) have an important role in the metabolic regulation of coronary vasal tone, and they mediate endothelial NO release [149]. The impairment of the function of these channels by diabetes mellitus and other cardiovascular risk factors may contribute to endothelial dysfunction [149]. Wang et al. demonstrated that ischemia-reperfusion damage inhibits the IKCa and SKCa function impairing coronary EDHF-mediated vasodilatation, and it reduced TRPC3 expression, a channel belonging to the TRP family and which is involved in the metabolic regulation of CBF, through a calcium-related pathway, both stimulating NO release and mediating IKCa and SKCa function [150]. Wang et al. focused on the close relation between IKCa and SKCa channel dysfunction and TRPC3 channel impairment in the determinism of endothelial dysfunction and coronary microvascular one [150]. For this reason, they proposed TRPC3 as a new therapeutic target to improve CBF in ischemic conditions [150]. Isosteviol is a natural sweetener contained in Stevia rebaudiana Bertoni leaves, and from it, isosteviol sodium is obtained which is a beyeranediterpene with therapeutic effects against diabetes mellitus, cardiovascular diseases, and cancer [151]. Yin et al. demonstrated a double effect of isosteviol sodium on cardiomyocytes [151]. It contrasted QTc prolongation related to ischemia/reperfusion injury, and it reduced Ikr and Ikatp channel inhibition during ischemia/reperfusion injury through the scavenging of ROS [151]. N-3 polyunsaturated fatty acids (PUFA) represent essential fatty acids which play an important role against cardiovascular diseases. N-3-PUFA, in particular docosahexaenoic acid (DHA) and eicosapentaenoic acid (EPA), are important activators of coronary smooth muscle cell BKCa channels contributing therefore to coronary vasodilation, in normal coronary arteries [152–154]. Tang et al. demonstrated that diabetic patients who have an impaired coronary ion channel function may have benefits, regarding cardiovascular complications, from N-3-PUFA assumption because they promote coronary BKCa channel activation and increased expression and they reduce Ca^{2+} concentration in coronary smooth muscle cells, increasing CBF [155]. Moreover, several antioxidant agents may contrast the effect of ROS and may preserve ion channel function. Several studies described the protective role of some NOX inhibitors against DM complications [156–163]. They may act as reducing ROS production, and among these are probucol [156], apocynin [157], plumbagin [158], and GLX351322 [159]. Gray et al. demonstrated the renal and atheroprotective effect of GKT 137831, a NOX1-4 inhibitor in insulin

diabetes-deficient mouse [160]. It determines the reduction of atherosclerotic plaque diameter [160]. Nelson et al. demonstrated in a trial that the use of Protandim, an Nrf-2 activator, is associated with the induction of catalase and erythrocyte SOD activity in vivo and haem oxygenase 1 in vitro [161, 162]. Haem oxygenase 1 is an endogenous antioxidant which contrasts cardiomyocytes and endothelial apoptosis [161, 162]. Two different studies by Milman et al. and Blum et al. demonstrated that administration of vitamin E for 1.5 years may reduce cardiovascular events in patients with diabetes mellitus [163] (Table 2).

5. Conclusions

In conclusion, oxidative stress may represent a dangerous condition for organ and system function, and it is associated with several conditions such as diabetes mellitus, cardiovascular diseases, cancer, and neurological disorders. With this article, we aimed to investigate the physiological and pathophysiological role of oxidative stress in the connection between myocardial metabolism and CBF, with particular attention to patients with diabetes mellitus. There are several products of myocardial metabolism in the CBF regulation in relation with myocardial metabolic activity. However, the imbalance between oxidants and antioxidants, which defines the condition of oxidative stress, plays a crucial role in the alteration of CBF regulation in response to myocardial metabolism. In our previous studies [7–9], we already defined the importance of coronary ion channels as end effectors of CBF regulation mechanisms and the association between some SNPs of ion channel subunits and IHD. So, we investigated the impact of oxidative stress on ion channel function and the possibility to use them as therapeutic target in the treatment of IHD.

Conflicts of Interest

The authors declare no conflict of interests.

Authors' Contributions

Paolo Severino and Andrea D'Amato contributed equally.

References

[1] K. Thygesen, J. S. Alpert, A. S. Jaffe et al., "Fourth universal definition of myocardial infarction (2018)," *European Heart Journal*, vol. 40, no. 3, pp. 237–269, 2019.

[2] E. Perugini, A. P. Maggioni, A. Boccanelli, and G. Di Pasquale, "Epidemiology of acute coronary syndromes in Italy," *Giornale Italiano di Cardiologia*, vol. 11, no. 10, pp. 718–729, 2010.

[3] F. Sanchis-Gomar, C. Perez-Quilis, R. Leischik, and A. Lucia, "Epidemiology of coronary heart disease and acute coronary syndrome," *Annals of Translational Medicine*, vol. 4, no. 13, p. 256, 2016.

[4] J. Critchley, J. Liu, D. Zhao, W. Wei, and S. Capewell, "Explaining the increase in coronary heart disease mortality in Beijing between 1984 and 1999," *Circulation*, vol. 110, no. 10, pp. 1236–1244, 2004.

[5] K. S. Reddy, "Cardiovascular disease in non-Western countries," *The New England Journal of Medicine*, vol. 350, no. 24, pp. 2438–2440, 2004.

[6] K. Okrainec, D. K. Banerjee, and M. J. Eisenberg, "Coronary artery disease in the developing world," *American Heart Journal*, vol. 148, no. 1, pp. 7–15, 2004.

[7] F. Fedele, M. Mancone, W. M. Chilian et al., "Role of genetic polymorphisms of ion channels in the pathophysiology of coronary microvascular dysfunction and ischemic heart disease," *Basic Research in Cardiology*, vol. 108, no. 6, p. 387, 2013.

[8] P. Severino, A. D'Amato, L. Netti et al., "Diabetes mellitus and ischemic heart disease: the role of ion channels," *International Journal of Molecular Sciences*, vol. 19, no. 3, p. 802, 2018.

[9] F. Fedele, P. Severino, N. Bruno et al., "Role of ion channels in coronary microcirculation: a review of the literature," *Future Cardiology*, vol. 9, no. 6, pp. 897–905, 2013.

[10] P. G. Camici, G. D'Amati, and O. Rimoldi, "Coronary microvascular dysfunction: mechanisms and functional assessment," *Nature Reviews Cardiology*, vol. 12, no. 1, pp. 48–62, 2015.

[11] F. Crea, P. G. Camici, and C. N. Bairey Merz, "Coronary microvascular dysfunction: an update," *European Heart Journal*, vol. 35, no. 17, pp. 1101–1111, 2014.

[12] N. Bairey Merz, R. O. Bonow, G. Sopko et al., "Women's ischemic syndrome evaluation," *Circulation*, vol. 109, no. 6, pp. 805–807, 2004.

[13] C. Leuzzi and M. G. Modena, "Coronary artery disease: clinical presentation, diagnosis and prognosis in women," *Nutrition, Metabolism, and Cardiovascular Diseases*, vol. 20, no. 6, pp. 426–435, 2010.

[14] H. A. DeVon, C. J. Ryan, A. L. Ochs, and M. Shapiro, "Symptoms across the continuum of acute coronary syndromes: differences between women and men," *American Journal of Critical Care*, vol. 17, no. 1, pp. 14–24, 2008.

[15] C. N. Bairey Merz, L. J. Shaw, S. E. Reis et al., "Insights from the NHLBI-sponsored Women's Ischemia Syndrome Evaluation (WISE) study," *Journal of the American College of Cardiology*, vol. 47, no. 3, pp. S21–S29, 2006.

[16] S. W. Davies, "Clinical presentation and diagnosis of coronary artery disease: stable angina," *British Medical Bulletin*, vol. 59, no. 1, pp. 17–27, 2001.

[17] V. Čulić, D. Eterović, D. Mirić, and N. Silić, "Symptom presentation of acute myocardial infarction: influence of sex, age, and risk factors," *American Heart Journal*, vol. 144, no. 6, pp. 1012–1017, 2002.

[18] S. A. Stephen, B. G. Darney, and A. G. Rosenfeld, "Symptoms of acute coronary syndrome in women with diabetes: an integrative review of the literature," *Heart & Lung*, vol. 37, no. 3, pp. 179–189, 2008.

[19] S. E. Reis, R. Holubkov, A. J. Conrad Smith et al., "Coronary microvascular dysfunction is highly prevalent in women with chest pain in the absence of coronary artery disease: results from the NHLBI WISE study," *American Heart Journal*, vol. 141, no. 5, pp. 735–741, 2001.

[20] J. S. Hochman, C. H. McCabe, P. H. Stone et al., "Outcome and profile of women and men presenting with acute coronary syndromes: a report from TIMI IIIB. TIMI investigators. Thrombolysis in myocardial infarction," *Journal of the American College of Cardiology*, vol. 30, no. 1, pp. 141–148, 1997.

[21] L. J. Shaw, C. N. Bairey Merz, C. J. Pepine et al., "Insights from the NHLBI- sponsored Women's Ischemia Syndrome Evaluation (WISE) study," *Journal of the American College of Cardiology*, vol. 47, no. 3, pp. S4–S20, 2006.

[22] S. S. Rathore, J. Chen, Y. Wang, M. J. Radford, V. Vaccarino, and H. M. Krumholz, "Sex differences in cardiac catheterization," *Journal of the American Medical Association*, vol. 286, no. 22, pp. 2849–2856, 2001.

[23] F. Fedele, M. C. Gatto, A. D'Ambrosi, and M. Mancone, "TNM-like classification: a new proposed method for heart failure staging," *The Scientific World Journal*, vol. 2013, Article ID 175925, 8 pages, 2013.

[24] F. Fedele, P. Severino, S. Calcagno, and M. Mancone, "Heart failure: TNM-like classification," *Elsevier Journal of the American College of Cardiology*, vol. 63, no. 19, pp. 1959-1960, 2014.

[25] N. Koren-Morag, U. Goldbourt, and D. Tanne, "Poor functional status based on the New York Heart Association classification exposes the coronary patient to an elevated risk of ischemic stroke," *American Heart Journal*, vol. 155, no. 3, pp. 515–520, 2008.

[26] P. Moons, K. Van Deyk, and W. Budts, "The NYHA classification, employment, and physical activities are poor indicators of quality of life after congenital cardiac surgery," *The Annals of Thoracic Surgery*, vol. 82, no. 3, pp. 1167-1168, 2006.

[27] S. Chatterjee, K. Khunti, and M. J. Davies, "Type 2 diabetes," *The Lancet*, vol. 389, no. 10085, pp. 2239–2251, 2017.

[28] T. Nishikawa, D. Edelstein, X. L. du et al., "Normalizing mitochondrial superoxide production blocks three pathways of hyperglycaemic damage," *Nature*, vol. 404, no. 6779, pp. 787–790, 2000.

[29] K. Yahagi, F. D. Kolodgie, C. Lutter et al., "Pathology of human coronary and carotid artery atherosclerosis and vascular calcification in diabetes mellitus," *Arteriosclerosis, Thrombosis, and Vascular Biology*, vol. 37, no. 2, pp. 191–204, 2017.

[30] J. M. Van Werkhoven, F. Cademartiri, S. Seitun et al., "Diabetes: prognostic value of CT coronary angiography—-comparison with a nondiabetic population," *Radiology*, vol. 256, no. 1, pp. 83–92, 2010.

[31] M. F. di Carli, J. Janisse, G. Grunberger, and J. Ager, "Role of chronic hyperglycemia in the pathogenesis of coronary microvascular dysfunction in diabetes," *Journal of the American College of Cardiology*, vol. 41, no. 8, pp. 1387–1393, 2003.

[32] I. Yokoyama, S. Momomura, T. Ohtake et al., "Reduced myocardial flow reserve in non-insulin-dependent diabetes mellitus," *Journal of the American College of Cardiology*, vol. 30, no. 6, pp. 1472–1477, 1997.

[33] A. Kibel, K. Selthofer-Relatic, I. Drenjancevic et al., "Coronary microvascular dysfunction in diabetes mellitus," *The Journal of International Medical Research*, vol. 45, no. 6, pp. 1901–1929, 2017.

[34] M. Laakso, "Heart in diabetes: a microvascular disease," *Diabetes Care*, vol. 34, Supplement 2, pp. S145–S149, 2011.

[35] A. J. Flammer, T. Anderson, D. S. Celermajer et al., "The assessment of endothelial function," *Circulation*, vol. 126, no. 6, pp. 753–767, 2012.

[36] A. Virdis and S. Taddei, "Endothelial dysfunction in resistance arteries of hypertensive humans," *Journal of Cardiovascular Pharmacology*, vol. 67, no. 6, pp. 451–457, 2016.

[37] A. Lerman and A. M. Zeiher, "Endothelial function," *Circulation*, vol. 111, no. 3, pp. 363–368, 2005.

[38] M. Dessì, A. Noce, P. Bertucci et al., "Atherosclerosis, dyslipidemia, and inflammation: the significant role of polyunsaturated fatty acids," *ISRN Inflammation*, vol. 2013, Article ID 191823, 13 pages, 2013.

[39] A. Basoli, C. Cametti, F. G. Satriani, P. Mariani, and P. Severino, "Hemocompatibility of stent materials: alterations in electrical parameters of erythrocyte membranes," *Vascular Health and Risk Management*, vol. 8, pp. 197–204, 2012.

[40] B. W. Wong, A. Meredith, D. Lin, and B. M. McManus, "The biological role of inflammation in atherosclerosis," *The Canadian Journal of Cardiology*, vol. 28, no. 6, pp. 631–641, 2012.

[41] S. Balanescu, L. Calmac, D. Constantinescu, M. Marinescu, R. Onut, and M. Dorobantu, "Systemic inflammation and early atheroma formation: are they related?," *Maedica*, vol. 5, no. 4, pp. 292–301, 2010.

[42] A. Farzaneh-Far, M. J. Roman, M. D. Lockshin et al., "Relationship of antiphospholipid antibodies to cardiovascular manifestations of systemic lupus erythematosus," *Arthritis and Rheumatism*, vol. 54, no. 12, pp. 3918–3925, 2006.

[43] A. L. Catapano, F. M. Maggi, and E. Tragni, "Low density lipoprotein oxidation, antioxidants, and atherosclerosis," *Current Opinion in Cardiology*, vol. 15, no. 5, pp. 355–363, 2000.

[44] P. Matzinger, "Tolerance, danger, and the extended family," *Annual Review of Immunology*, vol. 12, no. 1, pp. 991–1045, 1994.

[45] F. Martinon, K. Burns, and J. Tschopp, "The inflammasome: a molecular platform triggering activation of inflammatory caspases and processing of proIL-β," *Molecular Cell*, vol. 10, no. 2, pp. 417–426, 2002.

[46] E. Birben, U. M. Sahiner, C. Sackesen, S. Erzurum, and O. Kalayci, "Oxidative stress and antioxidant defense," *World Allergy Organization Journal*, vol. 5, no. 1, pp. 9–19, 2012.

[47] H. Bayr, "Reactive oxygen species," *Critical Care Medicine*, vol. 33, no. 12, pp. S498–S501, 2005.

[48] B. Halliwell and J. M. C. Gutteridge, *Free Radicals in Biology and Medicine*, Humana Press, Clifton, NJ, USA, 1984.

[49] M. Valko, C. J. Rhodes, J. Moncol, M. Izakovic, and M. Mazur, "Free radicals, metals and antioxidants in oxidative stress-induced cancer," *Chemico-Biological Interactions*, vol. 160, no. 1, pp. 1–40, 2006.

[50] M. Wang, K. Dhingra, W. N. Hittelman, J. G. Liehr, M. de Andrade, and D. Li, "Lipid peroxidation-induced putative malondialdehyde-DNA adducts in human breast tissues," *Cancer Epidemiology, Biomarkers & Prevention*, vol. 5, no. 9, pp. 705–710, 1996.

[51] J. C. Jha, F. Ho, C. Dan, and K. Jandeleit-Dahm, "A causal link between oxidative stress and inflammation in cardiovascular and renal complications of diabetes," *Clinical Science*, vol. 132, no. 16, pp. 1811–1836, 2018.

[52] K. Maiese, "New insights for oxidative stress and diabetes mellitus," *Oxidative Medicine and Cellular Longevity*, vol. 2015, Article ID 875961, 17 pages, 2015.

[53] A. Alwan, *Global Status Report on Noncommunicable Diseases 2010*, World Health Organization, 2011, http://www.cabdirect.org/cabdirect/abstract/20113168808.

[54] A. Dinesh Shah, C. Langenberg, E. Rapsomaniki et al., "Type 2 diabetes and incidence of a wide range of cardiovascular

diseases: a cohort study in 1·9 million people," *The Lancet*, vol. 385, article S86, 2015.

[55] J. C. Jha, C. Banal, B. S. M. Chow, M. E. Cooper, and K. Jandeleit-Dahm, "Diabetes and kidney disease: role of oxidative stress," *Antioxidants & Redox Signaling*, vol. 25, no. 12, pp. 657–684, 2016.

[56] J. C. Jha, C. Banal, J. Okabe et al., "NADPH oxidase Nox5 accelerates renal injury in diabetic nephropathy," *Diabetes*, vol. 66, no. 10, pp. 2691–2703, 2017.

[57] J. C. Jha, S. P. Gray, D. Barit et al., "Genetic targeting or pharmacologic inhibition of NADPH oxidase Nox4 provides renoprotection in long-term diabetic nephropathy," *Journal of the American Society of Nephrology*, vol. 25, no. 6, pp. 1237–1254, 2014.

[58] J. C. Jha, V. Thallas-Bonke, C. Banal et al., "Podocyte-specific Nox4 deletion affords renoprotection in a mouse model of diabetic nephropathy," *Diabetologia*, vol. 59, no. 2, pp. 379–389, 2016.

[59] G. Sardella, P. Stella, M. Chiarito et al., "Clinical outcomes with reservoir-based polymer-free amphilimus-eluting stents in real-world patients according to diabetes mellitus and complexity: the INVESTIG8 registry," *Catheterization and Cardiovascular Interventions*, vol. 91, no. 5, pp. 884–891, 2018.

[60] G. Sardella, M. Mancone, R. E. Stio et al., "Prasugrel or ticagrelor in ST-segment–elevation myocardial infarction patients with diabetes mellitus," *Circulation*, vol. 136, no. 6, pp. 602–604, 2017.

[61] I. Giardino, D. Edelstein, and M. Brownlee, "BCL-2 expression or antioxidants prevent hyperglycemia-induced formation of intracellular advanced glycation endproducts in bovine endothelial cells," *The Journal of Clinical Investigation*, vol. 97, no. 6, pp. 1422–1428, 1996.

[62] A. V. Sima, G. M. Botez, C. S. Stancu, A. Manea, M. Raicu, and M. Simionescu, "Effect of irreversibly glycated LDL in human vascular smooth muscle cells: lipid loading, oxidative and inflammatory stress," *Journal of Cellular and Molecular Medicine*, vol. 14, no. 12, pp. 2790–2802, 2010.

[63] L. Park, K. G. Raman, K. J. Lee et al., "Suppression of accelerated diabetic atherosclerosis by the soluble receptor for advanced glycation endproducts," *Nature Medicine*, vol. 4, no. 9, pp. 1025–1031, 1998.

[64] A. Ungurianu, D. Margină, D. Grădinaru et al., "Lipoprotein redox status evaluation as a marker of cardiovascular disease risk in patients with inflammatory disease," *Molecular Medicine Reports*, vol. 15, no. 1, pp. 256–262, 2017.

[65] K. Sugimoto, T. Ishibashi, T. Sawamura et al., "LOX-1-MT1-MMP axis is crucial for RhoA and Rac1 activation induced by oxidized low-density lipoprotein in endothelial cells," *Cardiovascular Research*, vol. 84, no. 1, pp. 127–136, 2009.

[66] J. Galle, A. Heinloth, C. Wanner, and K. Heermeier, "Dual effect of oxidized LDL on cell cycle in human endothelial cells through oxidative stress," *Kidney International*, vol. 59, pp. S120–S123, 2001.

[67] J. Chen, J. L. Mehta, N. Haider, X. Zhang, J. Narula, and D. Li, "Role of caspases in ox-LDL–induced apoptotic cascade in human coronary artery endothelial cells," *Circulation Research*, vol. 94, no. 3, pp. 370–376, 2004.

[68] P. Delafontaine and L. Ku, "Reactive oxygen species stimulate insulin-like growth factor I synthesis in vascular smooth muscle cells," *Cardiovascular Research*, vol. 33, no. 1, pp. 216–222, 1997.

[69] T. J. Guzik, S. Mussa, D. Gastaldi et al., "Mechanisms of increased vascular superoxide production in human diabetes mellitus: role of NAD(P)H oxidase and endothelial nitric oxide synthase," *Circulation*, vol. 105, no. 14, pp. 1656–1662, 2002.

[70] S. P. Gray, E. di Marco, J. Okabe et al., "NADPH oxidase 1 plays a key role in diabetes mellitus–accelerated atherosclerosis," *Circulation*, vol. 127, no. 18, pp. 1888–1902, 2013.

[71] S. P. Gray, E. di Marco, K. Kennedy et al., "Reactive oxygen species can provide atheroprotection via NOX4-dependent inhibition of inflammation and vascular remodeling," *Arteriosclerosis, Thrombosis, and Vascular Biology*, vol. 36, no. 2, pp. 295–307, 2016.

[72] P. Hu, X. Wu, A. R. Khandelwal et al., "Endothelial Nox4-based NADPH oxidase regulates atherosclerosis via soluble epoxide hydrolase," *Biochimica et Biophysica Acta (BBA) - Molecular Basis of Disease*, vol. 1863, no. 6, pp. 1382–1391, 2017.

[73] Q. Zhang, P. Malik, D. Pandey et al., "Paradoxical activation of endothelial nitric oxide synthase by NADPH oxidase," *Arteriosclerosis, Thrombosis, and Vascular Biology*, vol. 28, no. 9, pp. 1627–1633, 2008.

[74] T. Münzel, C. Sinning, F. Post, A. Warnholtz, and E. Schulz, "Pathophysiology, diagnosis and prognostic implications of endothelial dysfunction," *Annals of Medicine*, vol. 40, no. 3, pp. 180–196, 2009.

[75] S. Sifuentes-Franco, D. E. Padilla-Tejeda, S. Carrillo-Ibarra, and A. G. Miranda-Díaz, "Oxidative stress, apoptosis, and mitochondrial function in diabetic nephropathy," *International Journal of Endocrinology*, vol. 2018, Article ID 1875870, 13 pages, 2018.

[76] F. Addabbo, M. Montagnani, and M. S. Goligorsky, "Mitochondria and reactive oxygen species," *Hypertension*, vol. 53, no. 6, pp. 885–892, 2009.

[77] H. Azumi, N. Inoue, Y. Ohashi et al., "Superoxide generation in directional coronary atherectomy specimens of patients with angina pectoris: important role of NAD(P)H oxidase," *Arteriosclerosis, Thrombosis, and Vascular Biology*, vol. 22, no. 11, pp. 1838–1844, 2002.

[78] A. Magenta, S. Greco, C. Gaetano, and F. Martelli, "Oxidative stress and microRNAs in vascular diseases," *International Journal of Molecular Sciences*, vol. 14, no. 9, pp. 17319–17346, 2013.

[79] A. Magenta, C. Cencioni, P. Fasanaro et al., "miR-200c is upregulated by oxidative stress and induces endothelial cell apoptosis and senescence via ZEB1 inhibition," *Cell Death and Differentiation*, vol. 18, no. 10, pp. 1628–1639, 2011.

[80] L. Hui, L. Bakiri, A. Mairhorfer et al., "p38α suppresses normal and cancer cell proliferation by antagonizing the JNK–c-Jun pathway," *Nature Genetics*, vol. 39, no. 6, pp. 741–749, 2007.

[81] I. Dolado, A. Swat, N. Ajenjo, G. De Vita, A. Cuadrado, and A. R. Nebreda, "p38α MAP kinase as a sensor of reactive oxygen species in tumorigenesis," *Cancer Cell*, vol. 11, no. 2, pp. 191–205, 2007.

[82] H. Zhang, P. Gao, R. Fukuda et al., "HIF-1 inhibits mitochondrial biogenesis and cellular respiration in VHL-deficient renal cell carcinoma by repression of C-MYC activity," *Cancer Cell*, vol. 11, no. 5, pp. 407–420, 2007.

[83] M.-G. Perrelli, P. Pagliaro, and C. Penna, "Ischemia/reperfusion injury and cardioprotective mechanisms: role of mitochondria and reactive oxygen species," *World Journal of Cardiology*, vol. 3, no. 6, pp. 186–200, 2011.

[84] C. Devlin, S. Greco, F. Martelli, and M. Ivan, "miR-210: more than a silent player in hypoxia," *IUBMB Life*, vol. 63, no. 2, 2011.

[85] S. Y. Chan and J. Loscalzo, "MicroRNA-210: a unique and pleiotropic hypoxamir," *Cell Cycle*, vol. 9, no. 6, pp. 1072–1083, 2010.

[86] S. Y. Chan, Y.-Y. Zhang, C. Hemann, C. E. Mahoney, J. L. Zweier, and J. Loscalzo, "MicroRNA-210 controls mitochondrial metabolism during hypoxia by repressing the iron-sulfur cluster assembly proteins ISCU1/2," *Cell Metabolism*, vol. 10, no. 4, pp. 273–284, 2009.

[87] P. Fasanaro, S. Greco, M. Lorenzi et al., "An integrated approach for experimental target identification of hypoxia-induced miR-210," *The Journal of Biological Chemistry*, vol. 284, no. 50, pp. 35134–35143, 2009.

[88] L. Cicchillitti, V. di Stefano, E. Isaia et al., "Hypoxia-inducible factor 1-α induces miR-210 in normoxic differentiating myoblasts," *The Journal of Biological Chemistry*, vol. 287, no. 53, pp. 44761–44771, 2012.

[89] R. K. Mutharasan, V. Nagpal, Y. Ichikawa, and H. Ardehali, "microRNA-210 is upregulated in hypoxic cardiomyocytes through Akt- and p53-dependent pathways and exerts cytoprotective effects," *American Journal of Physiology-Heart and Circulatory Physiology*, vol. 301, no. 4, pp. H1519–H1530, 2011.

[90] A. G. Goodwill, G. M. Dick, A. M. Kiel, and J. D. Tune, "Regulation of coronary blood flow," *Comprehensive Physiology*, vol. 7, pp. 321–382, 2017.

[91] C. Molinari, A. Battaglia, E. Grossini et al., "Effects of insulin on coronary blood flow in anesthetized pigs," *Journal of Vascular Research*, vol. 39, no. 6, pp. 504–513, 2002.

[92] K. G. Lamping, H. Kanatsuka, C. L. Eastham, W. M. Chilian, and M. L. Marcus, "Nonuniform vasomotor responses of the coronary microcirculation to serotonin and vasopressin," *Circulation Research*, vol. 65, no. 2, pp. 343–351, 1989.

[93] M. J. Kern, "Histaminergic modulation of coronary vascular resistance: are we missing a therapeutic adjunct for the treatment of myocardial ischemia?," *Journal of the American College of Cardiology*, vol. 17, no. 2, pp. 346-347, 1991.

[94] C. Zhang, J. D. Knudson, S. Setty et al., "Coronary arteriolar vasoconstriction to angiotensin II is augmented in prediabetic metabolic syndrome via activation of AT1 receptors," *American Journal of Physiology-Heart and Circulatory Physiology*, vol. 288, no. 5, pp. H2154–H2162, 2005.

[95] V. Ohanyan, L. Yin, R. Bardakjian et al., "Kv1.3 channels facilitate the connection between metabolism and blood flow in the heart," *Microcirculation*, vol. 24, no. 4, article e12334, 2017.

[96] P. A. Rogers, W. M. Chilian, I. N. Bratz, R. M. Bryan Jr., and G. M. Dick, "H_2O_2 activates redox- and 4-aminopyridine-sensitive K_v channels in coronary vascular smooth muscle," *American Journal of Physiology-Heart and Circulatory Physiology*, vol. 292, no. 3, pp. H1404–H1411, 2007.

[97] S. Saitoh, C. Zhang, J. D. Tune et al., "Hydrogen peroxide: a feed-forward dilator that couples myocardial metabolism to coronary blood flow," *Arteriosclerosis, Thrombosis, and Vascular Biology*, vol. 26, no. 12, pp. 2614–2621, 2006.

[98] S. O. Sage, C. van Breemen, and M. B. Cannell, "Sodium-calcium exchange in cultured bovine pulmonary artery endothelial cells," *The Journal of Physiology*, vol. 440, no. 1, pp. 569–580, 1991.

[99] G. M. Dick, I. N. Bratz, L. Borbouse et al., "Voltage-dependent K^+ channels regulate the duration of reactive hyperemia in the canine coronary circulation," *American Journal of Physiology-Heart and Circulatory Physiology*, vol. 294, no. 5, pp. H2371–H2381, 2008.

[100] V. Ohanyan, L. Yin, R. Bardakjian et al., "Requisite role of Kv1.5 channels in coronary metabolic dilation," *Circulation Research*, vol. 117, no. 7, pp. 612–621, 2015.

[101] R. S. Barlow and R. E. White, "Hydrogen peroxide relaxes porcine coronary arteries by stimulating BK_{Ca}channel activity," *American Journal of Physiology-Heart and Circulatory Physiology*, vol. 275, no. 4, pp. H1283–H1289, 1998.

[102] R. S. Barlow, A. M. El-Mowafy, and R. E. White, "H_2O_2 opens BK_{Ca} channels via the PLA_2-arachidonic acid signaling cascade in coronary artery smooth muscle," *American Journal of Physiology-Heart and Circulatory Physiology*, vol. 279, no. 2, pp. H475–H483, 2000.

[103] G. M. Dick and J. D. Tune, "Role of potassium channels in coronary vasodilation," *Experimental Biology and Medicine*, vol. 235, no. 1, pp. 10–22, 2010.

[104] N. Thengchaisri and L. Kuo, "Hydrogen peroxide induces endothelium-dependent and -independent coronary arteriolar dilation: role of cyclooxygenase and potassium channels," *American Journal of Physiology-Heart and Circulatory Physiology*, vol. 285, no. 6, pp. H2255–H2263, 2003.

[105] S. L. Hu, H. S. Kim, and A. Y. Jeng, "Dual action of endothelin-1 on the Ca^{2+}-activated K^+ channel in smooth muscle cells of porcine coronary artery," *European Journal of Pharmacology*, vol. 194, no. 1, pp. 31–36, 1991.

[106] F. S. Scornik and L. Toro, "U46619, a thromboxane A2 agonist, inhibits KCa channel activity from pig coronary artery," *American Journal of Physiology-Cell Physiology*, vol. 262, no. 3, pp. C708–C713, 1992.

[107] L. Toro, M. Amador, and E. Stefani, "ANG II inhibits calcium-activated potassium channels from coronary smooth muscle in lipid bilayers," *American Journal of Physiology-Heart and Circulatory Physiology*, vol. 258, no. 3, pp. H912–H915, 1990.

[108] K. Minami, Y. Hirata, A. Tokumura, Y. Nakaya, and K. Fukuzawa, "Protein kinase C-independent inhibition of the Ca^{2+}-activated K^+ channel by angiotensin IIand endothelin-1," *Biochemical Pharmacology*, vol. 49, no. 8, pp. 1051–1056, 1995.

[109] P. K. Randhawa and A. S. Jaggi, "TRPV 1 channels in cardiovascular system: a double edged sword?," *International Journal of Cardiology*, vol. 228, pp. 103–113, 2017.

[110] S. Qin, S. Liu, and R. Wang, "Protective effect of capsaicin on against myocardial ischemia-reperfusion injury of rat in vivo," *Sichuan Da Xue Xue Bao Yi Xue Ban*, vol. 39, no. 4, pp. 550–554, 2008.

[111] T. Yada, H. Shimokawa, O. Hiramatsu et al., "Hydrogen peroxide, an endogenous endothelium-derived hyperpolarizing factor, plays an important role in coronary autoregulation in vivo," *Circulation*, vol. 107, no. 7, pp. 1040–1045, 2003.

[112] T. Matoba, H. Shimokawa, K. Morikawa et al., "Electron spin resonance detection of hydrogen peroxide as an endothelium-derived hyperpolarizing factor in porcine

coronary microvessels," *Arteriosclerosis, Thrombosis, and Vascular Biology*, vol. 23, no. 7, pp. 1224–1230, 2003.

[113] N. B. Standen and J. M. Quayle, "K^+ channel modulation in arterial smooth muscle," *Acta Physiologica Scandinavica*, vol. 164, no. 4, pp. 549–557, 1998.

[114] L. Conforti, I. Bodi, J. W. Nisbet, and D. E. Millhorn, "O_2-sensitive K^+ channels: role of the Kv1.2 α-subunit in mediating the hypoxic response," *The Journal of Physiology*, vol. 524, no. 3, pp. 783–793, 2000.

[115] F. Fedele, M. Mancone, F. Adamo, and P. Severino, "Heart failure with preserved, mid-range, and reduced ejection fraction: the misleading definition of the new guidelines," *Cardiology in Review*, vol. 25, no. 1, pp. 4-5, 2017.

[116] G. Jia, J. Habibi, A. R. Aroor et al., "Enhanced endothelium epithelial sodium channel signaling prompts left ventricular diastolic dysfunction in obese female mice," *Metabolism*, vol. 78, pp. 69–79, 2018.

[117] B. Bostick, J. Habibi, L. Ma et al., "Dipeptidyl peptidase inhibition prevents diastolic dysfunction and reduces myocardial fibrosis in a mouse model of Western diet induced obesity," *Metabolism*, vol. 63, no. 8, pp. 1000–1011, 2014.

[118] B. Bostick, A. R. Aroor, J. Habibi et al., "Daily exercise prevents diastolic dysfunction and oxidative stress in a female mouse model of western diet induced obesity by maintaining cardiac heme oxygenase-1 levels," *Metabolism*, vol. 66, pp. 14–22, 2017.

[119] C. H. Mandavia, L. Pulakat, V. DeMarco, and J. R. Sowers, "Over-nutrition and metabolic cardiomyopathy," *Metabolism*, vol. 61, no. 9, pp. 1205–1210, 2012.

[120] A. Tomaschitz, E. Ritz, B. Pieske et al., "Aldosterone and parathyroid hormone interactions as mediators of metabolic and cardiovascular disease," *Metabolism*, vol. 63, no. 1, pp. 20–31, 2014.

[121] G. Jia, J. Habibi, V. G. DeMarco et al., "Endothelial mineralocorticoid receptor deletion prevents diet-induced cardiac diastolic dysfunction in females," *Hypertension*, vol. 66, no. 6, pp. 1159–1167, 2015.

[122] S. Kenchaiah, J. C. Evans, D. Levy et al., "Obesity and the risk of heart failure," *The New England Journal of Medicine*, vol. 347, no. 5, pp. 305–313, 2002.

[123] J. Fels, P. Jeggle, K. Kusche-Vihrog, and H. Oberleithner, "Cortical actin nanodynamics determines nitric oxide release in vascular endothelium," *PLoS One*, vol. 7, no. 7, article e41520, 2012.

[124] Y. Zeng, M. Waters, A. Andrews et al., "Fluid shear stress induces the clustering of heparan sulfate via mobility of glypican-1 in lipid rafts," *American Journal of Physiology-Heart and Circulatory Physiology*, vol. 305, no. 6, pp. H811–H820, 2013.

[125] M. M. Dwenger, V. Ohanyan, M. F. Navedo, and M. A. Nystoriak, "Coronary microvascular Kv1 channels as regulatory sensors of intracellular pyridine nucleotide redox potential," *Microcirculation*, vol. 25, no. 1, article e12426, 2018.

[126] M. W. Weiner and H. A. Lardy, "Reduction of pyridine nucleotides induced by adenosine diphosphate in kidney mitochondria. The influence of sodium, magnesium, and inhibitors of oxidative phosphorylation," *The Journal of Biological Chemistry*, vol. 248, no. 22, pp. 7682–7687, 1973.

[127] F. Dayanikli, D. Grambow, O. Muzik, L. Mosca, M. Rubenfire, and M. Schwaiger, "Early detection of abnormal coronary flow reserve in asymptomatic men at high risk for coronary artery disease using positron emission tomography," *Circulation*, vol. 90, no. 2, pp. 808–817, 1994.

[128] M. Kelm, "Nitric oxide metabolism and breakdown," *Biochimica et Biophysica Acta (BBA) - Bioenergetics*, vol. 1411, no. 2-3, pp. 273–289, 1999.

[129] H. Li, D. D. Gutterman, N. J. Rusch, A. Bubolz, and Y. Liu, "Nitration and functional loss of voltage-gated K^+ channels in rat coronary microvessels exposed to high glucose," *Diabetes*, vol. 53, no. 9, pp. 2436–2442, 2004.

[130] D. J. DelloStritto, P. Sinharoy, P. J. Connell et al., "4-Hydroxynonenal dependent alteration of TRPV1-mediated coronary microvascular signaling," *Free Radical Biology & Medicine*, vol. 101, pp. 10–19, 2016.

[131] H. Chuang and S. Lin, "Oxidative challenges sensitize the capsaicin receptor by covalent cysteine modification," *Proceedings of the National Academy of Sciences of the United States of America*, vol. 106, no. 47, pp. 20097–20102, 2009.

[132] D. A. Andersson, C. Gentry, S. Moss, and S. Bevan, "Transient receptor potential A1 is a sensory receptor for multiple products of oxidative stress," *The Journal of Neuroscience*, vol. 28, no. 10, pp. 2485–2494, 2008.

[133] G. Guarini, V. A. Ohanyan, J. G. Kmetz et al., "Disruption of TRPV1-mediated coupling of coronary blood flow to cardiac metabolism in diabetic mice: role of nitric oxide and BK channels," *American Journal of Physiology-Heart and Circulatory Physiology*, vol. 303, no. 2, pp. H216–H223, 2012.

[134] S. J. Chapple, X. Cheng, and G. E. Mann, "Effects of 4-hydroxynonenal on vascular endothelial and smooth muscle cell redox signaling and function in health and disease," *Redox Biology*, vol. 1, no. 1, pp. 319–331, 2013.

[135] V. R. Mali and S. S. Palaniyandi, "Regulation and therapeutic strategies of 4-hydroxy-2-nonenal metabolism in heart disease," *Free Radical Research*, vol. 48, no. 3, pp. 251–263, 2014.

[136] H. N. Rubaiy, "The therapeutic agents that target ATP-sensitive potassium channels," *Acta Pharmaceutica*, vol. 66, no. 1, pp. 23–34, 2016.

[137] M. Matsuo, K. Tanabe, N. Kioka, T. Amachi, and K. Ueda, "Different binding properties and affinities for ATP and ADP among sulfonylurea receptor subtypes, SUR1, SUR2A, and SUR2B," *The Journal of Biological Chemistry*, vol. 275, no. 37, article 28757- 28763, pp. 28757–28763, 2000.

[138] S. Isomoto and Y. Kurachi, "Molecular and biophysical aspects of potassium channels," *Nihon Rinsho*, vol. 54, no. 3, pp. 660–666, 1996.

[139] M. Schwanstecher, C. Sieverding, H. Dörschner et al., "Potassium channel openers require ATP to bind to and act through sulfonylurea receptors," *The EMBO Journal*, vol. 17, no. 19, pp. 5529–5535, 1998.

[140] F. Zhang, Y. Xuan, J. Cui, X. Liu, Z. Shao, and B. Yu, "Nicorandil modulated macrophages activation and polarization via NF-κb signaling pathway," *Molecular Immunology*, vol. 88, pp. 69–78, 2017.

[141] S. H. Rezkalla, R. V. Stankowski, J. Hanna, and R. A. Kloner, "Management of no-reflow phenomenon in the catheterization laboratory," *JACC Cardiovascular Interventions*, vol. 10, no. 3, pp. 215–223, 2017.

[142] C. Kupatt, H. Habazettl, A. Goedecke et al., "Tumor necrosis factor-alpha contributes to ischemia- and reperfusion-induced endothelial activation in isolated hearts," *Circulation Research*, vol. 84, no. 4, pp. 392–400, 1999.

[143] IONA Study Group, "Effect of nicorandil on coronary events in patients with stable angina: the Impact Of Nicorandil in Angina (IONA) randomised trial," *The Lancet*, vol. 359, no. 9314, pp. 1269–1275, 2002.

[144] M. S. Nieminen, M. Buerke, J. Parissis et al., "Pharmacoeconomics of levosimendan in cardiology: a European perspective," *International Journal of Cardiology*, vol. 199, pp. 337–341, 2015.

[145] S. Bunte, F. Behmenburg, A. Bongartz et al., "Preconditioning by levosimendan is mediated by activation of mitochondrial Ca^{2+}-sensitive potassium (mBK_{Ca}) channels," *Cardiovascular Drugs and Therapy*, vol. 32, no. 5, pp. 427–434, 2018.

[146] J. G. Papp, P. Pollesello, A. F. Varró, and Á. S. Végh, "Effect of levosimendan and milrinone on regional myocardial ischemia/reperfusion-induced arrhythmias in dogs," *Journal of Cardiovascular Pharmacology and Therapeutics*, vol. 11, no. 2, pp. 129–135, 2006.

[147] W. Xu, Y. Liu, S. Wang et al., "Cytoprotective role of Ca^{2+}-activated K^+ channels in the cardiac inner mitochondrial membrane," *Science*, vol. 298, no. 5595, pp. 1029–1033, 2002.

[148] C. C. Shieh, M. Coghlan, J. P. Sullivan, and M. Gopalakrishnan, "Potassium channels: molecular defects, diseases, and therapeutic opportunities," *Pharmacological Reviews*, vol. 52, no. 4, pp. 557–594, 2000.

[149] I. Grgic, B. P. Kaistha, J. Hoyer, and R. Köhler, "Endothelial Ca^{2+}-activated K^+ channels in normal and impaired EDHF-dilator responses - relevance to cardiovascular pathologies and drug discovery," *British Journal of Pharmacology*, vol. 157, no. 4, pp. 509–526, 2009.

[150] X.-C. Wang, W.-T. Sun, J. Fu et al., "Impairment of coronary endothelial function by hypoxia-reoxygenation involves TRPC3 inhibition-mediated KCa channel dysfunction: implication in ischemia-reperfusion injury," *Scientific Reports*, vol. 7, no. 1, p. 5895, 2017.

[151] C. Yin, Y. Chen, H. Wu, D. Xu, and W. Tan, "Attenuation of ischemia/reperfusion- induced inhibition of the rapid component of delayed rectifier potassium current by Isosteviol through scavenging reactive oxygen species," *Biochimica et Biophysica Acta (BBA) - Biomembranes*, vol. 1859, no. 12, pp. 2447–2453, 2017.

[152] L. Lai, R. Wang, W. Jiang et al., "Effects of docosahexaenoic acid on large-conductance Ca^{2+}-activated K^+ channels and voltage-dependent K^+ channels in rat coronary artery smooth muscle cells," *Acta Pharmacologica Sinica*, vol. 30, no. 3, pp. 314–320, 2009.

[153] X. Li, S. Hong, P.-L. Li, and Y. Zhang, "Docosahexanoic acid-induced coronary arterial dilation: actions of 17S-hydroxy docosahexanoic acid on K^+ channel activity," *The Journal of Pharmacology and Experimental Therapeutics*, vol. 336, no. 3, pp. 891–899, 2011.

[154] R. Wang, Q. Chai, T. Lu, and H.-C. Lee, "Activation of vascular BK channels by docosahexaenoic acid is dependent on cytochrome P450 epoxygenase activity," *Cardiovascular Research*, vol. 90, no. 2, pp. 344–352, 2011.

[155] X. Tang, L. L. Qian, R. X. Wang et al., "Regulation of coronary arterial large conductance Ca^{2+}-activated K^+ channel protein expression and function by n-3 polyunsaturated fatty acids in diabetic rats," *Journal of Vascular Research*, vol. 54, no. 6, pp. 329–343, 2017.

[156] G. Zhou, Y. Wang, P. He, and D. Li, "Probucol inhibited Nox2 expression and attenuated podocyte injury in type 2 diabetic nephropathy of db/db mice," *Biological & Pharmaceutical Bulletin*, vol. 36, no. 12, pp. 1883–1890, 2013.

[157] K. Susztak, A. C. Raff, M. Schiffer, and E. P. Böttinger, "Glucose-induced reactive oxygen species cause apoptosis of podocytes and podocyte depletion at the onset of diabetic nephropathy," *Diabetes*, vol. 55, no. 1, pp. 225–233, 2006.

[158] Y. Ding, Z.-J. Chen, S. Liu, D. Che, M. Vetter, and C.-H. Chang, "Inhibition of Nox-4 activity by plumbagin, a plant-derived bioactive naphthoquinone," *The Journal of Pharmacy and Pharmacology*, vol. 57, no. 1, pp. 111–116, 2005.

[159] E. Anvari, P. Wikström, E. Walum, and N. Welsh, "The novel NADPH oxidase 4 inhibitor GLX351322 counteracts glucose intolerance in high-fat diet-treated C57BL/6 mice," *Free Radical Research*, vol. 49, no. 11, pp. 1308–1318, 2015.

[160] S. P. Gray, J. C. Jha, K. Kennedy et al., "Combined NOX1/4 inhibition with GKT137831 in mice provides dose-dependent reno- and atheroprotection even in established micro- and macrovascular disease," *Diabetologia*, vol. 60, no. 5, pp. 927–937, 2017.

[161] S. K. Nelson, S. K. Bose, G. K. Grunwald, P. Myhill, and J. M. McCord, "The induction of human superoxide dismutase and catalase in vivo: a fundamentally new approach to antioxidant therapy," *Free Radical Biology & Medicine*, vol. 40, no. 2, pp. 341–347, 2006.

[162] E. L. Donovan, J. M. McCord, D. J. Reuland, B. F. Miller, and K. L. Hamilton, "Phytochemical activation of Nrf2 protects human coronary artery endothelial cells against an oxidative challenge," *Oxidative Medicine and Cellular Longevity*, vol. 2012, Article ID 132931, 9 pages, 2012.

[163] U. Milman, S. Blum, C. Shapira et al., "Vitamin E supplementation reduces cardiovascular events in a subgroup of middle-aged individuals with both type 2 diabetes mellitus and the haptoglobin 2-2 genotype," *Arteriosclerosis, Thrombosis, and Vascular Biology*, vol. 28, no. 2, pp. 341–347, 2008.

Hindawi
Journal of Diabetes Research
Volume 2019, Article ID 2583047, 11 pages
https://doi.org/10.1155/2019/2583047

Research Article

A New Way for Beta Cell Neogenesis: Transdifferentiation from Alpha Cells Induced by Glucagon-Like Peptide 1

Zhen Zhang,[1] Yinghui Hu,[2] Ningning Xu,[1] Wenjun Zhou,[1] Lei Yang,[3] Rongping Chen,[1] Rui Yang,[1] Jia Sun,[1] and Hong Chen[1]

[1]*Department of Endocrinology, Zhujiang Hospital, Southern Medical University, Guangzhou, China*
[2]*Department of International Medical Center, The First Affiliated Hospital of Xi'an Jiaotong University, Shangxi, China*
[3]*Department of Nephrology, Zhujiang Hospital, Southern Medical University, Guangzhou, China*

Correspondence should be addressed to Jia Sun; sunjia@smu.edu.cn and Hong Chen; chenhong82330@163.com

Received 27 June 2018; Revised 14 November 2018; Accepted 21 November 2018; Published 13 March 2019

Guest Editor: Roberta H. Mendes

Recent studies showed that alpha cells, especially immature cells and proalpha cells, might be the precursors of beta cells. Exposure to glucagon-like peptide 1 (GLP1) can ameliorate hyperglycemia in diabetic mice and restore the beta cell mass. In the present study, we adopted single high-dose (60 mg/kg, i.p.) streptozotocin (STZ) to model diabetes mellitus (DM) and randomly assigned short-tail (SD) rats to a normal group, a diabetic group, GLP1 groups (50 μg/kg, 100 μg/kg, and 200 μg/kg), a GLP1 (200 μg/kg) with exendin (9-39) group, and a GLP1 with LY294002 group. We found that the pancreatic insulin-glucagon-positive cell populations increased according to the increase in GLP1 exposure. By contrast, no insulin-amylase-positive cell populations or insulin/pan-cytokeratin cells were observed in the pancreatic sections. The GLP1 receptor antagonist exendin (9-39) and the phosphatidylinositol-4,5-bisphosphate 3-kinase (PI3K) family inhibitor LY294002 not only suppressed protein kinase B (*Akt*), pancreatic and duodenal homeobox 1 (*Pdx1*), forkhead box O 1 (*FoxO1*), and mast cell function-associated antigen A (*MafA*) mRNA expression but also increased *MAFB* expression. We concluded that treatment with GLP1 might result in beta cell neogenesis by promoting the transdifferentiation of alpha cells but not by pancreatic acinar cells, ductal cells, or the self-replication of beta cells. The regulation on the GLP1 receptor and its downstream transcription factor PI3K/AKT/FOXO1 pathway, which causes increased pancreatic and duodenal homeobox 1 (*Pdx1*) and *MafA* mRNA expression but causes decreased *MAFB* expression, may be the mechanism involved in this process.

1. Introduction

The impoverishment or functional decline in pancreatic beta cells is the main cause of all forms of diabetes [1]. Currently, therapy for diabetes comprises drug therapy or pancreatic islet transplantation. The influences of the environment and other exogenous factors mean that a transplanted pancreas does not play a good role in regulating blood glucose. Thus, endogenous proliferation of functional islet beta cells has become a focus of research attention [2]. Pancreatic exocrine cells (pancreatic ductal cells and pancreatic acinar cells) and pancreatic cells (liver cells) can be transformed into islet cells [3]. In experimental transgenic models of diphtheria toxin- (DT-) induced acute selective near-total beta cell ablation, researchers observed beta cell regeneration. They used lineage tracing to label the glucagon-producing alpha cells and found that beta cell regeneration was largely derived from alpha cells before beta cell ablation, revealing previously unrecognized pancreatic cell plasticity [4]. Other studies observed a large number of glucagon-insulin-positive cells with extreme beta cell loss induced by streptozotocin (STZ), which is considered an important process to transform alpha cells into beta cells [5, 6]. Such spontaneous conversion of adult pancreatic alpha cells into beta cells could be harnessed to treat diabetes.

Glucagon-like peptide 1 (GLP1) is a gut-derived hormone secreted by intestinal L cells in response to food intake. GLP1 has been a prospective target for type 2 diabetes therapy [7]. Numerous studies have shown that infusion of GLP1 can efficiently ameliorate hyperglycemia in diabetic

models. Animal models demonstrated increasing and restored beta cell mass via beta cell regeneration, proliferation, and neogenesis after GLP1 administration [8]. Other studies showed that GLP1 acts mainly by activating GLP1 receptors, which upregulates the levels of pancreatic and duodenal homeobox 1 (PDX1) through the phosphatidylinositol-4,5-bisphosphate 3-kinase (PI3K)/AKT kinase (AKT) pathway. PDX1, known as a master regulator of the beta cell phenotype, plays a prominent role as an activator of genes essential for beta cell identity, along with the suppression of alpha cell identity [9, 10]. However, it remains unknown whether the augmentation of beta cell mass induced by GLP1 acts, at least in part, through transdifferentiation from alpha cells within the pancreas.

Therefore, the present study was aimed at investigating whether GLP1 could promote the regeneration of beta cells by the endogenous neogenesis of beta cells from the transdifferentiation of alpha cells in rat pancreatic islets and its possible mechanism.

2. Materials and Methods

2.1. Animals and Treatments. Sixty specific pathogen-free (SPF) level male Sprague-Dawley (SD) rats at eight to ten weeks old with a weight of 180–220 g were purchased from the Laboratory Animal Center of the Southern Medical University. The rats were housed in groups with an artificial 12 h dark-light cycle and with free access to food and water. The animals were treated by intraperitoneal injection with 60 mg/kg STZ (Sigma-Aldrich, St. Louis, MO, USA) dissolved in 50 mM citrate buffer (pH 4.5). Blood glucose levels, body weights, and diabetes incidence were monitored weekly. Only rats with a blood glucose level greater than 28 mmol/L (measured after 72 hours of STZ injection) were selected for the experiments [11]. These rats ($n = 60$) were divided into a normal group ($n = 6$); a diabetic group ($n = 9$); GLP1 groups treated with subcutaneous injections of GLP1 50 μg/kg/12 h ($n = 9$), 100 μg/kg/12 h ($n = 9$), or 200 μg/kg/12 h ($n = 9$); a GLP1 (200 μg/kg) with exendin (9-39) group ($n = 9$); and a GLP1 with LY294002 group ($n = 9$) for 12 weeks [12]. Numerous studies have shown that infusion of GLP1 can efficiently ameliorate hyperglycemia in diabetic models [13, 14]. GLP1 has been shown to increase beta cell mass, based on *in vitro* studies. It has also been shown to increase beta cell mass in animal models through beta cell regeneration, proliferation, and neogenesis and through the inhibition of apoptosis [15]. Miao et al. [8] indicated that treatment with 100 nM liraglutide (a GLP1 derivative) for 24–72 h promoted cell proliferation in the presence of 30 mM glucose, and the liraglutide increased beta cell viability at an optimum concentration of 100 nM in the presence of 11.1 or 30 mM glucose. After confirming previous evidence that GLP1 reduced blood glucose level and body weight, we chose the GLP1 concentrations utilized in the present study. All animal experiments were approved by the Committee on Animal Experimentation of Southern Medical University, Guangzhou, China and performed in compliance with the university's Guidelines for the Care and Use of Laboratory Animals. The Ethics Committee approval number is L2015106.

2.2. Antibodies and Reagents. GLP1 was obtained from Novo Nordisk A/S (Bagsvaerd, Denmark). Insulin and the C-peptide assay (enzyme-linked immunosorbent assay (ELISA)) kit were from Mercodia (Uppsala, Sweden). The anti-insulin mouse monoclonal antibody (SAB4200691) and anti-forkhead box O 1 (FOXO1) antibody (AV32107) were from Sigma-Aldrich. The anti-glucagon antibody (2760S) was from CST Biological Reagents Company Limited (Shanghai, China). The anti-mast cell function-associated antigen B (MAFB) antibody (DF8895) and anti-PDX1 antibody (DF7170) were from Affinity Biosciences (Cincinnati, OH, USA). The anti-neurogenin 3 (NGN3) antibody (GTX60254) was from GeneTex Inc. (Irvine, CA, USA). The primary antibodies against MAFA (sc-390491), pan-Cytokeratin (sc-8018), AKT1/2/3 (sc-81434), exendin (9-39) (SC-364387), and amylase were from Santa Cruz Biotechnology Inc. (Santa Cruz, CA, USA). The PI3K inhibitor LY294002 hydrochloride was also from Sigma-Aldrich.

2.3. Measurement of Metabolic and Biochemical Parameters. Body weight was measured weekly in each group for the entire duration of the study. The fasting glucose level (12-hour food deprivation) was measured using a glucometer (FreeStyle Optium; Abbot Laboratories, Italy) in blood taken weekly from the tail vein from rats in each experimental group. Plasma insulin concentrations and C-peptide levels were determined using ELISA assays after the intervention. At the end of the study period, all rats were anesthetized using pentobarbital (0.1 mg/g intraperitoneal injection) and sacrificed.

2.4. Immunofluorescence Analysis and Immunohistochemistry. After double-labeling immunofluorescence, areas labeled for insulin (green) and glucagon (red) in pancreatic islets were assessed, as described previously [16]. Pancreatic sections (6 μm thick) of normal and diabetic rats were deparaffinized with xylene and rehydrated with descending concentrations of ethanol. Antigen retrieval was then conducted by boiling the slides in citrate buffer, followed by gradual cooling. The sections were treated with a blocking agent (0.5% bovine serum albumin) for 45 minutes at room temperature after washing in phosphate-buffered saline (PBS), and then they were incubated overnight at 4°C with anti-insulin antibodies (1 : 1000 dilution) followed by the corresponding fluorescein isothiocyanate- (FITC-) conjugated anti-guinea pig secondary antibody after washing in PBS. The sections were then incubated overnight at 4°C with anti-glucagon, amylase, and pan-Cytokeratin antibodies (prediluted) followed by the anti-rabbit tetramethylrhodamine- (TRITC-) conjugated secondary antibody. Finally, the sections were mounted using Immu-Mount® (Thermo Electron Corporation, Waltham, MA, USA) and viewed with a Carl Zeiss fluorescent microscope.

Proliferation of pancreas islets was analyzed by immunohistochemical staining of proliferating cell nuclear antigen (PCNA) using anti-PCNA antibodies. The slides were

Table 1: List of primer sequences used for RT-PCR.

ID	Sequence (5′-3′)	Product length (bp)
β-Actin F	GGAGATTACTGCCCTGGCTCCTA	150
β-Actin R	GACTCATCGTACTCCTGCTTGCTG	
GLP1 F	TCGTGGCTGGATTGTTTGTA	143
GLP1 R	ATGGCGTTTGTCTTCGTTTAT	
AKT F	TCCCTTCCTTACAGCCCT	285
AKT R	TCCTTGATACCCTCCTTGC	
PDX1 F	GCCAGAGTTCAGTGCTAATCC	106
PDX1 R	TCCCTGTTCCAGCGTTCC	
MafA F	TTCAGCAAGGAGGAGGTCAT	117
MafA R	CTCGCTCTCCAGAATGTGC	
MafB F	GCTGGTGTCCATGTCCGT	245
MafB R	TGACCTTGTAGGCGTCTCTCT	
FOXO1 F	GTGGATGGTGAAGAGTGTGC	275
FOXO1 R	CGGACTGGAGAGATGCTTT	

incubated with primary antibodies for 1 hour at room temperature. After washing, secondary antibodies (1 : 500, biotin-conjugated goat anti-rabbit IgG) were applied for 30 min at room temperature. The number of PCNA-positive cells in each islet section was counted under a microscope. Three islets were randomly selected for analysis in each rat [17].

2.5. RNA Extraction and Quantitative Real-Time Reverse Transcriptase Polymerase Chain Reaction (qRT-PCR). Total RNA was isolated from the pancreatic tissue mentioned above using the TRIzol reagent (Takara Bio Inc., Dalian, China) according to the manufacturer's instructions, after which the RNA quantity and purity were evaluated using a model ND-2000 apparatus (Thermo Fisher Scientific NanoDrop 2000, Waltham, MA, USA). The integrity of the RNA was confirmed by agarose-formaldehyde gel electrophoresis. Using a cDNA Reverse Transcription Kit (Promega Corporation, Madison, WI, USA), first-strand cDNA was synthesized from individual samples in 20 μL reactions using 200 ng of total RNA, following the manufacturer's instructions. The integrity of the cDNA was confirmed by amplifying the *Atcb* (beta-actin) gene. Real-time PCR was conducted using a LightCycler 96 (Roche Applied Science, Rotkreuz, Switzerland) employing SYBR Green I as the dsDNA-specific binding dye for continuous fluorescence monitoring. The reverse transcription protocol was as follows: 5 min at 95°C, followed by 45 cycles of 15 s at 95°C, 15 s at 58°C, and 15 s at 72°C. The primers were synthesized by Takara Bio Inc. (Table 1).

2.6. Western Blotting Analysis. Total protein extracts to detect PDX1, MAFA, MAFB, AKT, and FOXO1 levels were obtained as previously described [12], pancreatic tissues were homogenized in lysis buffer (0.25 mol/L sucrose, 1 mmol/L EDTA) supplemented with protease inhibitor cocktail (Sigma-Aldrich) and phosphatase inhibitors (Sigma-Aldrich), and then the samples were centrifuged for 10 min at 16,000 × g. Protein concentrations were determined using a BCA Protein Assay Kit (Pierce Biotechnology, Rockford, IL, USA). Subsequently, the protein samples (20 μg) were separated on a 10% SDS-PAGE gel at 80 V (stacking gel) and 100 V (separating gel) and transferred onto nitrocellulose membranes. The membranes were blocked with PBS-Tween (PBS-T) containing 5% nonfat milk for 1 hour at room temperature. After blocking nonspecific binding, the membranes were incubated overnight at 4°C with mouse monoclonal primary antibodies against PDX1 (diluted 1 : 4000), MAFA (diluted 1 : 1000), MAFB (diluted 1 : 800), AKT (diluted 1 : 800), FOXO1 (diluted 1 : 1000), and glyceraldehyde-3-phosphate dehydrogenase (GAPDH) (diluted 1 : 10,000). Subsequently, the membranes were washed with PBS-T three times and incubated for 1 hour with a goat anti-mouse IgG antibody conjugated to horseradish peroxidase (HRP) (1 : 1000; catalog no. sc-2031; Santa Cruz Biotechnology Inc.). Lastly, the membranes were washed three times with PBS-T, and the immunoreactive proteins were visualized using an enhanced chemiluminescence-(ECL-) detection system (Beyotime Institute of Biotechnology, Jiangsu, China).

2.7. Statistical Analysis. All data are expressed as the means ± standard error of the mean (SEM). Statistical analysis was performed using Student's t-test and one-way analysis of variance (ANOVA), followed by a post hoc Fisher protected least significant difference (Fisher PLSD) test. A value of $P < 0.05$ was considered statistically significant. Statistical analyses were conducted using SPSS 16.0 software (IBM Corp., Armonk, NY, USA).

3. Results

3.1. Establishment of an Extreme Beta Cell Loss Rat Model Induced by STZ. Thorel et al. demonstrated that after extreme beta cell loss, a proportion of new beta cells transdifferentiated from alpha cells via a bihormonal glucagon/insulin (Gcg/Ins) coexpressing transitional state [4]. Thus, the present study was conducted using a single high dose of STZ (60 mg/kg) injection to induce a near-total beta cell ablation diabetic rat model to investigate the role of GLP1 in the neogenesis of beta cells. The results of double-labeled immunofluorescence in rat pancreatic slices showed that the pancreatic islets of the SD rats were significantly reduced, and the results also showed 95% insulin-positive beta cell ablation (Figures 1(a) and 1(b)). The islets showed the serious structural damage of beta cells, with alpha cell invasion into the center of the islets; very few residual beta cells were found scattered around the alpha cells. To confirm that the endogenous beta cell regeneration induced by GLP1 mainly occurs by transdifferentiation from alpha cells, we used double-labeled immunofluorescence technology to trace the development of different types of islet cells. The results demonstrated that after intervention with GLP1, insulin-glucagon-positive cells appeared in the islets of the pancreas in the diabetic rats and increased in a dose-dependent and statistically significant manner ($P < 0.05$) compared with those in the normal control group and the diabetic model group (Figures 1(c)–1(h)).

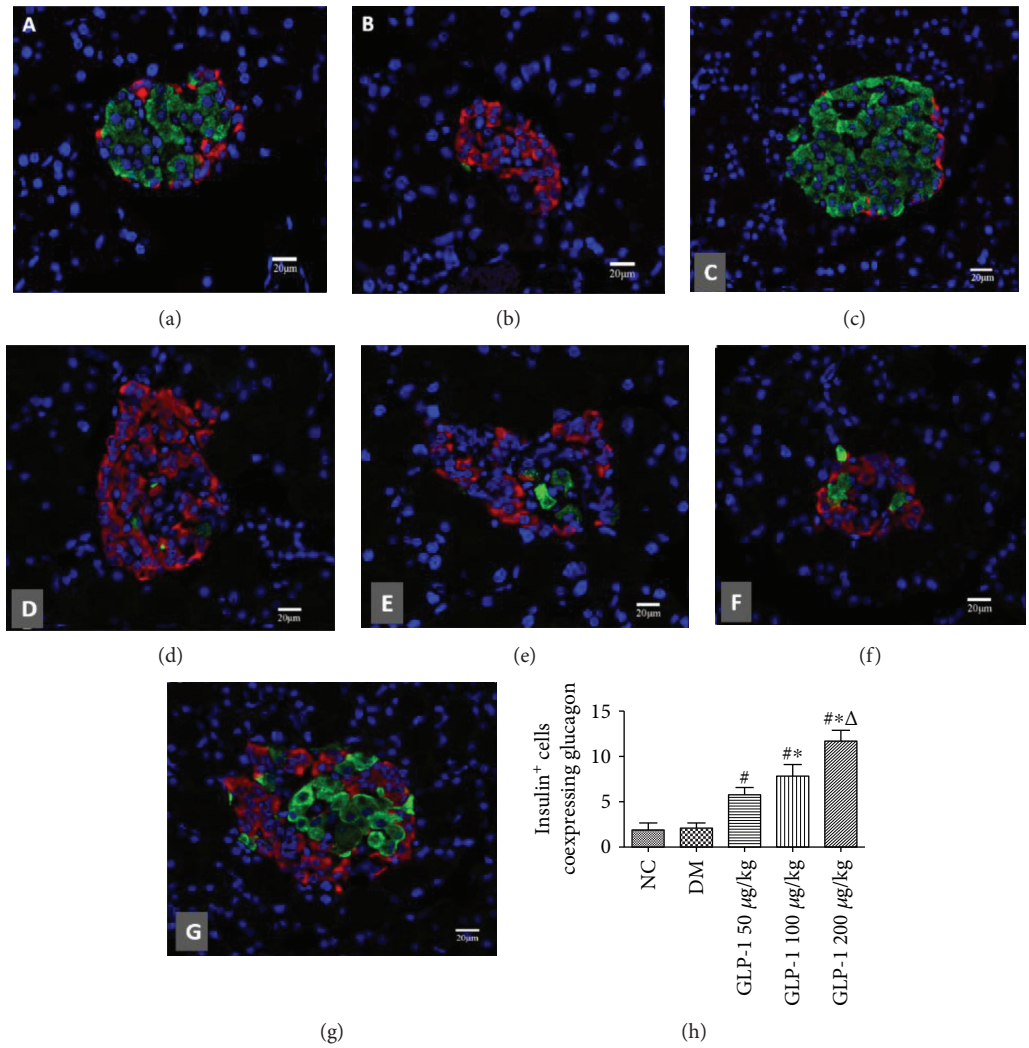

Figure 1: GLP1 reversed STZ-induced compromised β cell identity by inducing α cell transdifferentiation into β cells. Diabetic groups received an intravenous injection with STZ (35 mg/kg). Where indicated, GLP1 (50, 100, or 200 μg/kg per rat) was also administered. (a–g) Confocal images of pancreatic islet sections double-labeled via immunofluorescence for insulin and glucagon. Insulin$^+$ cells' immunoreactivity was distinguished by green fluorescence, while glucagon$^+$ cells were identified using FITC immunofluorescence (red) in the same slices. Scale bar = 20 μm. (h) Ratio of insulin$^+$-glucagon$^+$ cells to insulin$^+$-glucagon$^-$ cells. Data are presented as the mean ± SEM ($n \geq 6$ rats per group), $P < 0.01$, one-way ANOVA. GLP1, glucagon-like peptide 1; STZ, streptozotocin; FITC, fluorescein isothiocyanate; SEM, standard error of the mean; ANOVA, analysis of variance; NC, negative control; DM, diabetes mellitus.

3.2. GLP1 Protects Beta Cells against Glucose Toxicity in Diabetic Rats. After confirming the previous observation [4] that GLP1 reduced blood glucose level and body weight (data not shown), we investigated its effects in STZ-DM rats (the blood glucose level and weight were detected every week). After GLP1 intervention, insulin and C-peptide were measured using ELISA, and the number of endocrine cells was analyzed using double immunofluorescence. As expected, we found that GLP1 induced a significant decrease in the weight and blood glucose level in a dose-dependent manner compared with that in the control group (Figures 2(a) and 2(b)). However, even when treated with the maximum dose of GLP1 (200 μg/kg), the blood glucose level of the diabetic rats stayed at a high level (>19 mmol/L). Meanwhile, GLP1 resulted in a significant increase in insulin and C-peptide levels (Figures 2(c) and 2(d)).

3.3. Evidence for Endogenous Beta Cell Regeneration from Alpha Cells in Rat Pancreatic Islets Induced by GLP1. Under specific conditions, the rodent pancreas is capable of regeneration and cell plasticity. Many studies have shown that pancreatic epithelial cells (ductal, acinar, alpha, and beta cells) are potential alternatives to pluripotent stem cells because of the tremendous differentiation capacities of beta cells and their lower safety concerns [2]. The results demonstrated that after intervention with GLP1, insulin-glucagon-positive cells are at an intermediate state of transformation from alpha cells to beta cells. By contrast, no insulin-amylase-positive and insulin-pan-CK-positive cells were found in pancreases of all groups (Figure 3) indicating that subcutaneous injection of GLP1 did not promote pancreatic acinar cells or ductal cells of the STZ-induced diabetic rats to transform into islet beta cells. We also used

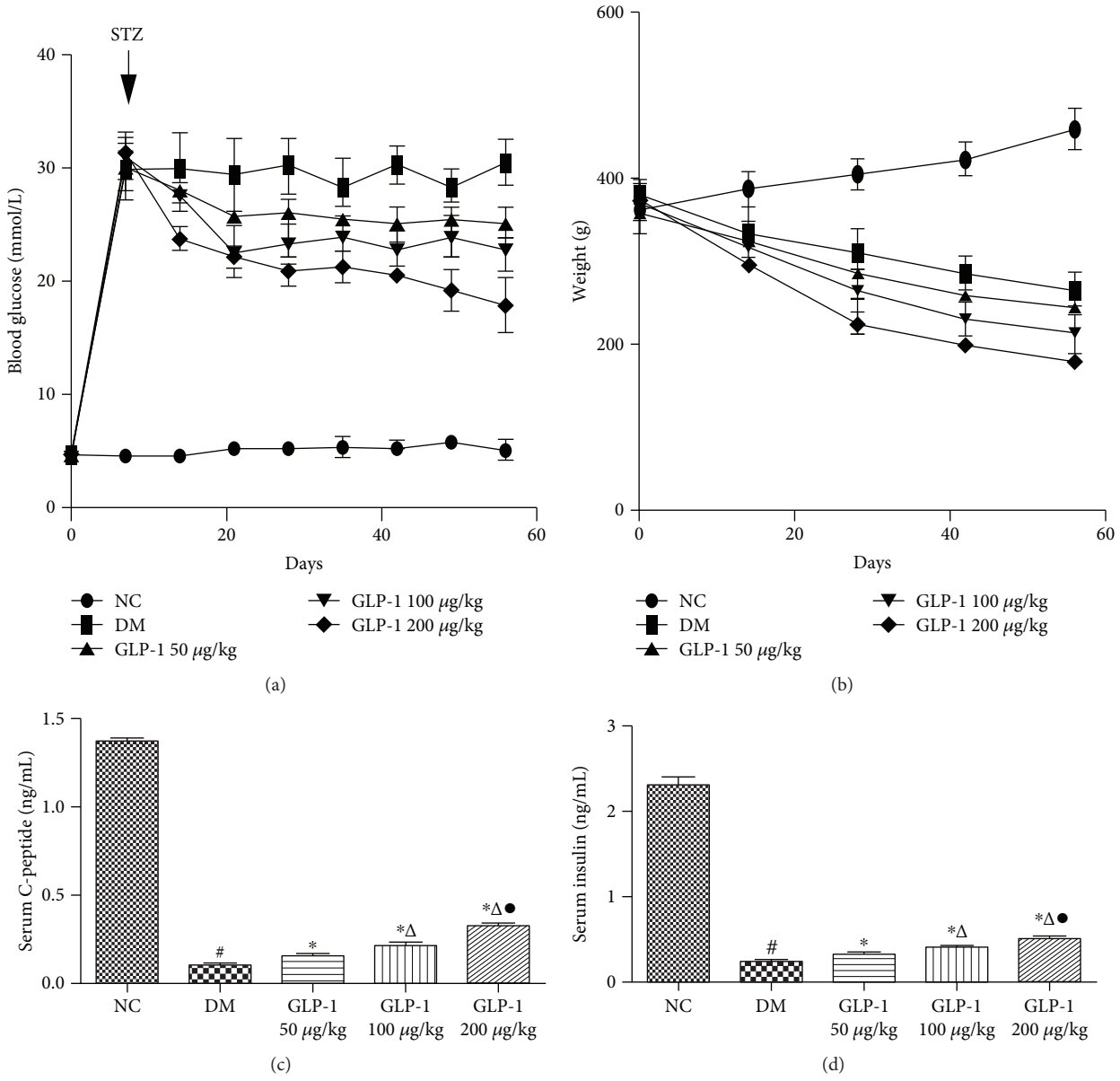

Figure 2: Fasting blood glucose, weight, and serum C-peptide, together with insulin levels, in rats from different treatment groups. (a). Profiles of 60-day fasting blood glucose and weight. (b). Serum C-peptide and insulin levels after 60 days. Data are presented as the mean ± SEM ($n \geq 6$ rats per group), $P < 0.05$, one-way ANOVA. GLP1, glucagon-like peptide 1; SEM, standard error of the mean; ANOVA, analysis of variance; NC, negative control; DM, diabetes mellitus.

PCNA immunohistochemistry to assess the proliferation of rat pancreatic beta cells after GLP1 intervention. We found that the region of PCNA-stained cells was coincident with the distribution of islet beta cells in the normal rat pancreas, whereas in the diabetic model group and the GLP1 groups, the PCNA-stained cells were mainly located in the region containing alpha cells, and there were no significant differences in PCNA-stained cells between the diabetic model group and the GLP1 groups ($P < 0.05$) (Figure 3). These results indicated that the endogenous beta cell regeneration and increase in beta cell number induced by GLP1 did not occur by the replication of beta cells but mainly from alpha cell transdifferentiation.

3.4. Effect of GLP1 Treatment on Expressions of the Key Genes Related to Beta Cell Development. To investigate the possible mechanism by which GLP1 promotes alpha cells to transdifferentiate into beta cells, the mRNA and protein expressions of AKT, PDX1, MAFA, MAFB, and FOXO1 were detected by qRT-PCR and western blotting in rat pancreatic islets. The results showed that the expression levels of AKT, PDX1, FOXO1, MAFA, and MAFB in the diabetic model group were significantly lower than those in the normal group ($P < 0.05$). The addition of GLP1 induced significant increases in the expression levels of FOXO1, AKT, PDX1, and MAFA in a dose-dependent manner compared with those in the diabetic model group ($P < 0.05$) (Figures 4 and 5).

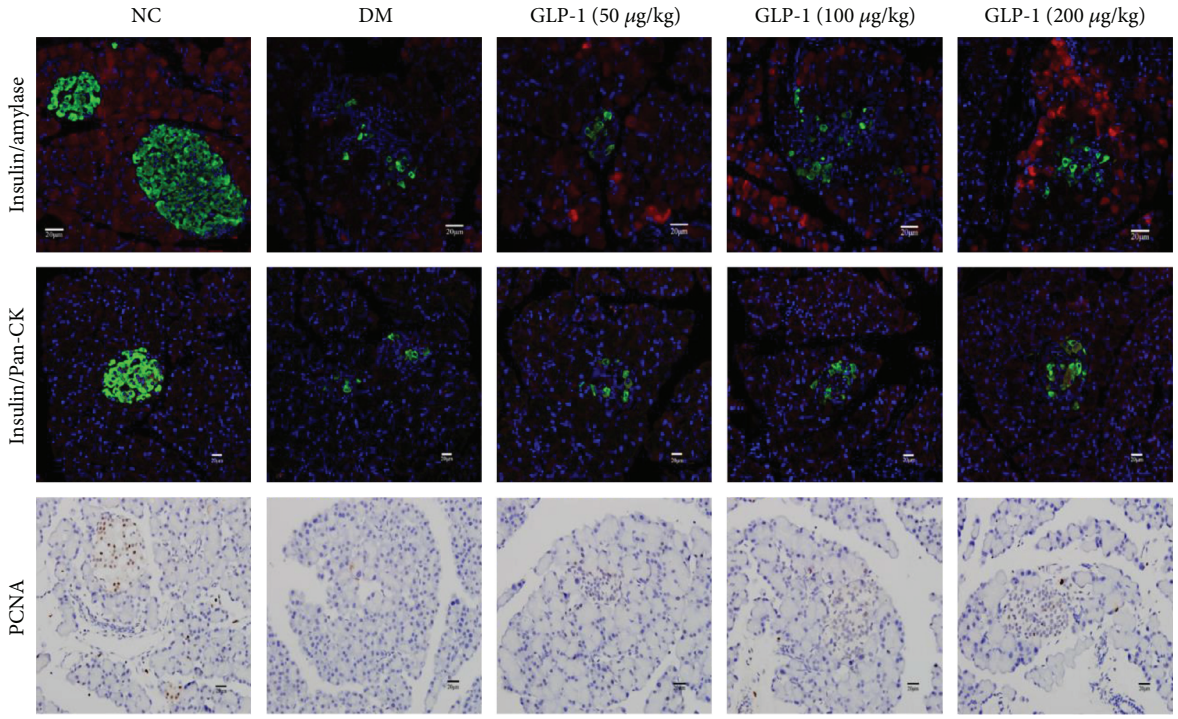

Figure 3: GLP1 did not promote pancreatic acinar or ductal cells to transform into islet β cells. (a) Pancreatic frozen sections were immunolabeled for insulin (green), amylase, or Pan-CK (red) as indicated. (b) PCNA immunohistochemical staining for pancreatic paraffin-embedded slices. Pan-CK; pan-cytokeratin; GLP1, glucagon-like peptide 1; NC, negative control; DM, diabetes mellitus; PCNA, proliferating cell nuclear antigen.

The expression of MAFB showed an interesting expression pattern. At first, the injection of GLP1 (50 μg/kg) also induced a marked increase compared with that in the diabetic model group. However, as the dose of GLP1 increased, the expression of MAFB decreased significantly in a dose-dependent manner. All of these effects could be attenuated using the GLP1 receptor blocker exendin (9-39) or the PI3K inhibitor LY294002 ($P < 0.05$) (Figures 4 and 5).

4. Discussion

Streptozotocin (STZ), an antibiotic extracted from *Streptomyces achromogenes*, can invade beta cells in rats, causing extreme DNA damage and cell death, resulting in hyperglycemia [18]. There are three main factors affecting the diabetic models induced by STZ, including the frequency, dose, and time of STZ injection [19]. High-fat diet/low-dose STZ injections induce models of type 2 diabetes mellitus (T2DM) [20], while two days of injection with STZ (45 mg/kg) into rats severely impaired insulin secretion and produced type 1 diabetes [21]. To exclude insulin resistance and self-immunity as possible confounders and to investigate the effects of GLP1 on rat pancreatic islets, we constructed severe insulin-deficient diabetic rat models induced by injecting a single dose of intraperitoneal STZ (60 mg/kg). The results showed that the pancreatic islets of the SD rats were significantly reduced, and the results also showed 95% insulin-positive beta cell ablation. We also observed that beta cells were seriously structurally damaged, with alpha cells invading into the center of the islets and very few residual beta cells being found scattered around the alpha cells. The blood glucose levels of diabetic rats stayed at a high level, with no spontaneous recovery, which implied that these rats are ideal models for the study of beta cell regeneration.

Similar to a previous study [22], we found that GLP1 induced a significant decrease of blood glucose and an increase of insulin and C-peptide levels in a dose-dependent manner compared with those in the control group. However, even when treated with GLP1 at the maximum dose of 200 μg/kg, the blood glucose level of the diabetic rats stayed at a high level (>19 mmol/L), which indicated that in rats with type 1 diabetes mellitus, the effects of GLP1 on decreasing blood glucose level and improving beta cell function are limited. Meanwhile, we found that GLP1 induced a significant decrease in the weight of the rats in a dose-dependent manner compared with the control group, which agreed with previous studies [23] that showed that GLP1 might help to suppress appetite and induce body weight loss in the obese rats.

The appearance of insulin-glucagon-positive cells, which might be an intermediate state of transformation from alpha cells to beta cells, was found in the progenitor cells of the rat pancreatic islets [6]. Our results demonstrated that after intervention with GLP1, insulin-glucagon-positive cells appeared in the islets of the pancreases of diabetic rats and increased in a dose-dependent manner, which means that our observations are easily reconciled with the common view that GLP1 could promote beta cell neogenesis by promoting the transdifferentiation of alpha cells.

Hui et al. [24] observed that in *in vitro* studies, the GLP1 receptor agonist, exendin-4, and GLP1 promoted pancreatic

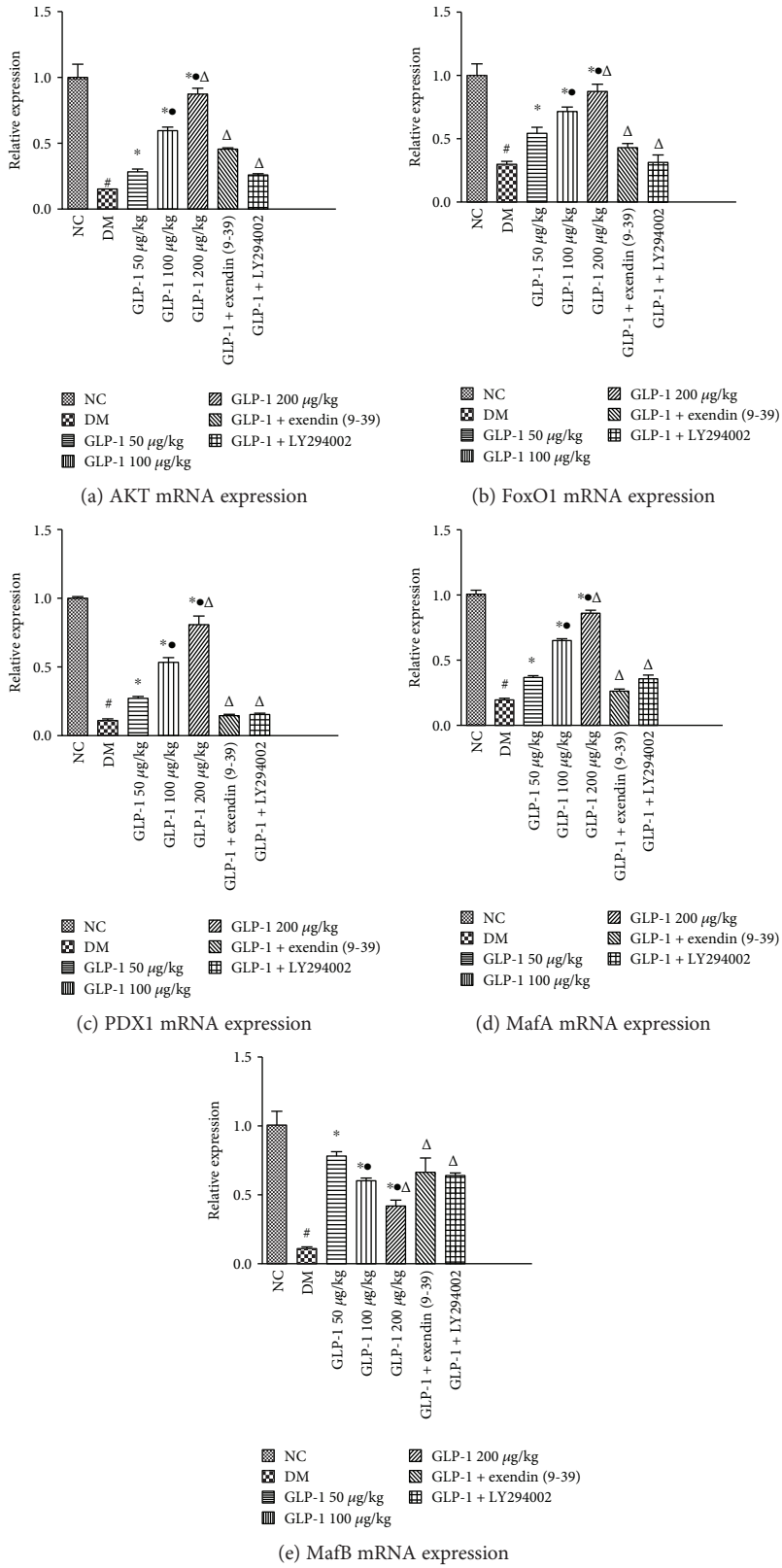

Figure 4: Quantitative real-time reverse transcription PCR (qRT-PCR) analyses for markers of β cell identity genes (*Akt*, *FoxO1*, *Pdx1*, *MafA*, and *MafB*) in rat islets. Data are presented as the mean ± SEM ($^{\#}P < 0.05$ *vs*. NC; $^{*}P < 0.05$ *vs*. DM; $^{\bullet}P < 0.05$ *vs*. GLP1 50 μg/kg; and $^{\Delta}P < 0.05$ *vs*. GLP1 100 μg/kg). GLP1, glucagon-like peptide 1; NC, negative control; DM, diabetes mellitus; SEM, standard error of the mean; Akt, AKT kinase; FoxO1, forkhead box O 1; Pdx1, pancreatic and duodenal homeobox 1; MafA, MAF BZIP transcription factor A; MafB, MAF BZIP transcription factor B.

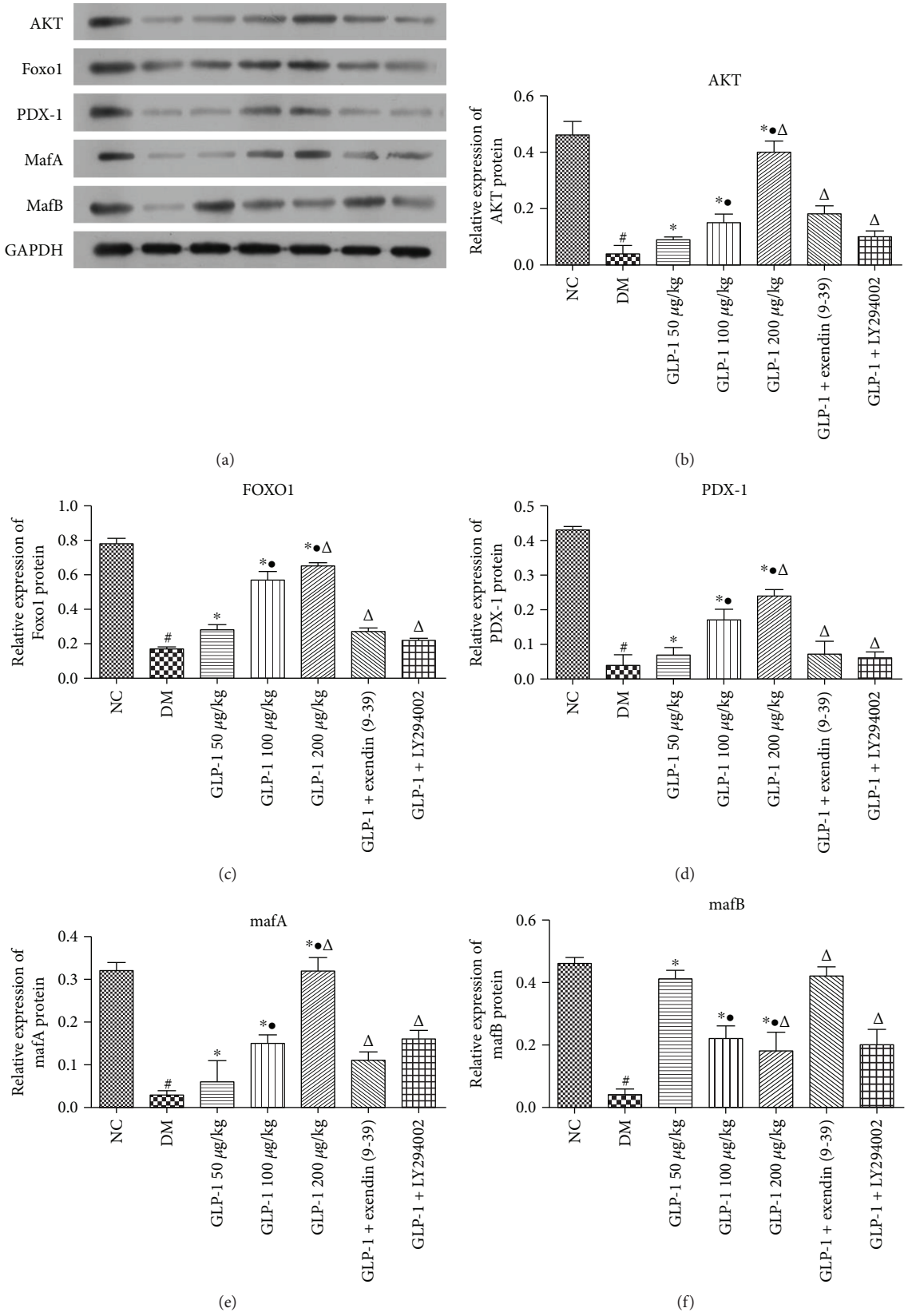

Figure 5: Western blotting analysis for Akt, FoxO1, Pdx1, MafA, and MafB in rat islets. GAPDH was used as a loading control ($^{\#}P < 0.05$ *vs.* NC; $^{*}P < 0.05$ *vs.* DM; $^{\bullet}P < 0.05$ *vs.* GLP1 50 μg/kg; and $^{\Delta}P < 0.05$ *vs.* GLP1 100 μg/kg). GLP1, glucagon-like peptide 1; NC, negative control; DM, diabetes mellitus; Akt, AKT kinase; FoxO1, forkhead box O 1; Pdx1, pancreatic and duodenal homeobox 1; MafA, MAF BZIP transcription factor A; MafB, MAF BZIP transcription factor B; GAPDH, glyceraldehyde-3-phosphate dehydrogenase.

acinar cells into insulin-producing cells via the PKC-MAPK signaling pathway. Bonner-Weir et al. [25] have provided evidence that the formation of islet-like cell clusters occurs after culturing ductal cells derived from human pancreas, and these cell clusters can secrete a small amount of insulin under stimulation by glucose. Gao et al. [26] used the bromodeoxyuridine (BrdU) marker to show that part of the pancreatic ductal cells transformed into islet endocrine cells, resulting in the alleviation of hyperglycemia in diabetic rats [27]. To determine the source of beta cell neogenesis, we used double-labeled immunofluorescence technology. Our discovery of the lack of insulin-amylase-positive and insulin-Pan-CK-positive cells in specimens of the pancreas of all groups indicated that the subcutaneous injection of GLP1 did not promote pancreatic acinar cells or ductal cells of STZ-induced diabetic rats to transform into islet beta cells.

Esteban et al. suggested that the replication of beta cells plays an important role in endogenous neogenesis of beta cells [28]. To test this hypothesis, we used PCNA immunohistochemistry to assess the proliferation of rat pancreatic beta cells. We found that the region of PCNA-stained cells was coincident with the distribution of islet beta cells in the normal rat pancreas (Figure 4), while in the diabetic model group and the GLP1 group, the cells were mainly located in the region showing alpha cell distribution, and there were no significant differences in PCNA-stained cells between the diabetic model group and the GLP1 group. These results indicated that the endogenous beta cell regeneration and increase in the number of beta cells induced by GLP1 was not derived from the replication of beta cells but was derived mainly from alpha cell transdifferentiation.

The MAF family is subdivided into two groups, according to their structure: the large and small MAF transcription factors [29–31]. In adult mammals, MAFA, which is essential in maintaining pancreatic islet structure and beta cell function, stimulates insulin gene expression and promotes insulin secretion [32]. When the insulin gene is transcribed, MAFA, as the insulin gene promoter, acts on the cis-regulatory element, termed RIPE3b/C1, located in the insulin gene promoter. The expression levels of transcription factors such as PDX1, Beta2, and NeuroD were reduced in rats displaying low expression of the *MafA* gene, and the number of cells and the secretion of insulin were reduced as well [33, 34]. MAFB is only expressed in mature alpha cells, and MAFA is a marker of mature beta cells. In the process of alpha cells' transformation into beta cells, the expression level of MAFB gradually changed from high to low, while that of MAFA showed the opposite trend [35].

The results showed that the expression levels of AKT, PDX1, FOXO1, MAFA, and MAFB in the diabetic model group was significantly lower than those in the normal group. The injection of GLP1 resulted in a dose-dependent increase in AKT, PDX1, FOXO1, and MAFA expression, but it resulted in a decrease in MAFB expression. From these results, we concluded that GLP1 promotes beta cell function but inhibits alpha cells. The GLP1 receptor antagonist exendin (9-39) and the PI3K family inhibitor LY294002 suppressed *Akt*, *Pdx1*, *FoxO1*, and *MafA* mRNA expression; however, *MAFB* expression increased, indicating that GLP1 enhances the reactivity of PDX1 and MAFA, which are markers of beta cells via the GLP1 receptor and its downstream pathway. In addition, these results suggested that GLP1 regulates the expression of pancreas-specific transcription factors by binding to the GLP1 receptor located on the membrane surface and activating the downstream PI3K-AKT-FOXO1 signaling pathway. The western blotting results were consistent with those of the qRT-PCR results, which led us to believe that GLP1 promotes the transformation from alpha cells to beta cells, and this positive action of GLP1 is mediated by the activation of the PI3K/AKT/FOXO1 pathway, which results in the upregulation of PDX1 and MAFA.

However, there were some limitations in our research. First, some researchers insist that insulin-glucagon-positive cells are an intermediate state of transformation from alpha cells to beta cells, whereas others suggest that insulin-glucagon-positive cells, which are immature pancreatic endocrine cells, tend to develop into alpha cells in the early development of the rat endocrine pancreas. In addition, MAFB is only expressed in mature alpha cells and PDX1 is a marker of mature beta cells. Thus PDX1/glucagon and MAFB/insulin double-positive cells are also an intermediate state in the transformation of alpha cells to beta cells [36]. If we conducted more thorough double-labeled immunofluorescence technology using insulin/MAFB and glucagon/PDX1, the outcomes would be more convincing. Second, our research was an experimental validation based on a hypothesis; therefore, we propose to construct *Pdx1* gene knockout animal models by genetic engineering and use them to confirm the role of PDX1 in the transformation of alpha cells into beta cells.

In recent years, research on promoting beta cell regeneration has provided new methods for the treatment of diabetes. Our findings indicated that GLP1 treatment might result in beta cell neogenesis by promoting the transdifferentiation of alpha cells. The regulation of the GLP1 receptor and its downstream transcription factor pathway (PI3K/AKT/FOXO1), which causes increased *Pdx1* and *MafA* mRNA expression, but decreased *MAFB* expression, may be the mechanism involved in this process. The results of the present study may be useful to study cellular and molecular mechanisms that regulate adult pancreatic differentiation and will increase our understanding of pancreatic diseases, such as cancer and diabetes.

Data Availability

The data used to support the findings of this study are available from the corresponding author upon request.

Conflicts of Interest

None of the authors of this paper has any financial or personal relationships with other people or organizations that could influence (bias) the research results. No conflicts of interest exist for the authors of this study.

Authors' Contributions

Zhen Zhang and Yinghui Hu contributed equally to this work. Yinghui Hu prepared the constructs to generate the transgenic animals. Zhen Zhang wrote the manuscript together with Yinghui Hu. Yinghui Hu performed most the experiments and performed the analyses. Ningning Xu conducted the gene expression analyses, and Wenjun Zhou performed immunofluorescence microscopy. Lei Yang, Rui Yang, and Rongping Chen conceived the experiments. Zhen Zhang and Yinghui Hu are co-first authors.

Acknowledgments

This work was supported by the Science and Technology Planning Project of Guangdong Province, China (grant number 2014A020212177) and the National Natural Science Foundation of China (grant numbers 81500623 and 81770804).

References

[1] L. Blaabjerg, G. L. Christensen, M. Matsumoto et al., "CRFR1 activation protects against cytokine-induced β-cell death," *Journal of Molecular Endocrinology*, vol. 53, no. 3, pp. 417–427, 2014.

[2] P. A. Lysy, G. C. Weir, and S. Bonner-Weir, "Making β cells from adult cells within the pancreas," *Current Diabetes Reports*, vol. 13, no. 5, pp. 695–703, 2013.

[3] L. Bouwens, I. Houbracken, and J. K. Mfopou, "The use of stem cells for pancreatic regeneration in diabetes mellitus," *Nature Reviews Endocrinology*, vol. 9, no. 10, pp. 598–606, 2013.

[4] F. Thorel, V. Népote, I. Avril et al., "Conversion of adult pancreatic α-cells to β-cells after extreme β-cell loss," *Nature*, vol. 464, no. 7292, pp. 1149–1154, 2010.

[5] S. Lenzen, "The mechanisms of alloxan- and streptozotocin-induced diabetes," *Diabetologia*, vol. 51, no. 2, pp. 216–226, 2008.

[6] Y.-P. Yang, F. Thorel, D. F. Boyer, P. L. Herrera, and C. V. E. Wright, "Context-specific α-to-β-cell reprogramming by forced PDX1 expression," *Genes & Development*, vol. 25, no. 16, pp. 1680–1685, 2011.

[7] Y. Ying, H. Zhu, Z. Liang, X. Ma, and S. Li, "GLP1 protects cardiomyocytes from palmitate-induced apoptosis via Akt/GSK3b/b-catenin pathway," *Journal of Molecular Endocrinology*, vol. 55, no. 3, pp. 245–262, 2015.

[8] X. Y. Miao, Z. Y. Gu, P. Liu et al., "The human glucagon-like peptide-1 analogue liraglutide regulates pancreatic beta-cell proliferation and apoptosis via an AMPK/mTOR/P70S6K signaling pathway," *Peptides*, vol. 39, pp. 71–79, 2013.

[9] L. Yang, D. Yao, H. Yang et al., "Puerarin protects pancreatic β-cells in obese diabetic mice via activation of GLP-1R signaling," *Molecular Endocrinology*, vol. 30, no. 3, pp. 361–371, 2016.

[10] S. Sasaki, T. Miyatsuka, T. A. Matsuoka et al., "Activation of GLP-1 and gastrin signalling induces in vivo reprogramming of pancreatic exocrine cells into beta cells in mice," *Diabetologia*, vol. 58, no. 11, pp. 2582–2591, 2015.

[11] N. J. Johansen, T. Frugier, B. Hunne, and J. A. Brock, "Increased peripherin in sympathetic axons innervating plantar metatarsal arteries in STZ-induced type I diabetic rats," *Frontiers in Neuroscience*, vol. 8, p. 99, 2014.

[12] T. Inoue, T. Inoguchi, N. Sonoda et al., "GLP-1 analog liraglutide protects against cardiac steatosis, oxidative stress and apoptosis in streptozotocin-induced diabetic rats," *Atherosclerosis*, vol. 240, no. 1, pp. 250–259, 2015.

[13] L. Farilla, H. Hui, C. Bertolotto et al., "Glucagon-like peptide-1 promotes islet cell growth and inhibits apoptosis in Zucker diabetic rats," *Endocrinology*, vol. 143, no. 11, pp. 4397–4408, 2002.

[14] A. Pick, J. Clark, C. Kubstrup et al., "Role of apoptosis in failure of beta-cell mass compensation for insulin resistance and beta-cell defects in the male Zucker diabetic fatty rat," *Diabetes*, vol. 47, no. 3, pp. 358–364, 1998.

[15] J. Zhou, X. Wang, M. A. Pineyro, and J. M. Egan, "Glucagon--like peptide 1 and exendin-4 convert pancreatic AR42J cells into glucagon- and insulin-producing cells," *Diabetes*, vol. 48, no. 12, pp. 2358–2366, 1999.

[16] L. Amiri, A. John, J. Shafarin et al., "Enhanced glucose tolerance and pancreatic beta cell function by low dose aspirin in hyperglycemic insulin-resistant type 2 diabetic Goto-Kakizaki (GK) rats," *Cellular Physiology and Biochemistry*, vol. 36, no. 5, pp. 1939–1950, 2015.

[17] Y.-x. Wu, R. Q. Sun, G. S. Yin et al., "Different effect of handle region peptide on β-cell function in different sexes of rats neonatally treated with sodium L-glutamate," *Medical Science Monitor Basic Research*, vol. 21, pp. 33–40, 2015.

[18] D. A. Rees and J. C. Alcolado, "Animal models of diabetes mellitus," *Diabetic Medicine*, vol. 22, no. 4, pp. 359–370, 2005.

[19] W. Zhu and X. Liu, "Optimization and evaluation of type 2 diabetes induced by high-fat diet and low dose of STZ in C57BL/6J mouse model," *China Tropical Medicine*, vol. 10, no. 5, pp. 529–613, 2010.

[20] M. Zhang, X.-Y. Lv, J. Li, Z.-G. Xu, and L. Chen, "The characterization of high-fat diet and multiple low-dose streptozotocin induced type 2 diabetes rat model," *Experimental Diabetes Research*, vol. 2008, Article ID 704045, 9 pages, 2008.

[21] S. Raghunathan, P. Tank, S. Bhadada, and B. Patel, "Evaluation of buspirone on streptozotocin induced type 1 diabetes and its associated complications," *BioMed Research International*, vol. 2014, Article ID 948427, 9 pages, 2014.

[22] T. H. Meek, M. D. Dorfman, M. E. Matsen et al., "Evidence that in uncontrolled diabetes, hyperglucagonemia is required for ketosis but not for increased hepatic glucose production or hyperglycemia," *Diabetes*, vol. 64, no. 7, pp. 2376–2387, 2015.

[23] H. H. Hansen, G. Hansen, S. Paulsen et al., "The DPP-IV inhibitor linagliptin and GLP-1 induce synergistic effects on body weight loss and appetite suppression in the diet-induced obese rat," *European Journal of Pharmacology*, vol. 741, pp. 254–263, 2014.

[24] H. Hui, Y. G. Tang, L. Zhu et al., "Glucagon like peptide-1-directed human embryonic stem cells differentiation into insulin-producing cells via hedgehog, cAMP, and PI3K pathways," *Pancreas*, vol. 39, no. 3, pp. 315–322, 2010.

[25] S. Bonner-Weir, M. Taneja, G. C. Weir et al., "In vitro cultivation of human islets from expanded ductal tissue," *Proceedings of the National Academy of Sciences of the United States of America*, vol. 97, no. 14, pp. 7999–8004, 2000.

[26] R. Gao, J. Ustinov, M. A. Pulkkinen, K. Lundin, O. Korsgren, and T. Otonkoski, "Characterization of endocrine progenitor cells and critical factors for their differentiation in human adult pancreatic cell culture," *Diabetes*, vol. 52, no. 8, pp. 2007–2015, 2003.

[27] K. al-Hasani, A. Pfeifer, M. Courtney et al., "Adult duct-lining cells can reprogram into β-like cells able to counter repeated cycles of toxin-induced diabetes," *Developmental Cell*, vol. 26, no. 1, pp. 86–100, 2013.

[28] M. A. Esteban, T. Wang, B. Qin et al., "Vitamin C enhances the generation of mouse and human induced pluripotent stem cells," *Cell Stem Cell*, vol. 6, no. 1, pp. 71–79, 2010.

[29] H. Ogino and K. Yasuda, "Induction of lens differentiation by activation of a bZIP transcription factor, L-Maf," *Science*, vol. 280, no. 5360, pp. 115–118, 1998.

[30] S. Benkhelifa, S. Provot, O. Lecoq, C. Pouponnot, G. Calothy, and M. P. Felder-Schmittbuhl, "mafA, a novel member of the maf proto-oncogene family, displays developmental regulation and mitogenic capacity in avian neuroretina cells," *Oncogene*, vol. 17, no. 2, pp. 247–254, 1998.

[31] A. M. Abdellatif, K. Ogata, T. Kudo et al., "Role of large MAF transcription factors in the mouse endocrine pancreas," *Experimental Animals*, vol. 64, no. 3, pp. 305–312, 2015.

[32] K. Kataoka, S. I. Han, S. Shioda, M. Hirai, M. Nishizawa, and H. Handa, "MafA is a glucose-regulated and pancreatic β-cell-specific transcriptional activator for the insulin gene," *Journal of Biological Chemistry*, vol. 277, no. 51, pp. 49903–49910, 2002.

[33] H. Kaneto, T. A. Matsuoka, Y. Nakatani et al., "A crucial role of MafA as a novel therapeutic target for diabetes," *Journal of Biological Chemistry*, vol. 280, no. 15, pp. 15047–15052, 2005.

[34] J. M. Moates, S. Nanda, M. A. Cissell, M. J. Tsai, and R. Stein, "*BETA2* activates transcription from the upstream glucokinase gene promoter in islet β-cells and gut endocrine cells," *Diabetes*, vol. 52, no. 2, pp. 403–408, 2003.

[35] T. van der Meulen and M. O. Huising, "Role of transcription factors in the transdifferentiation of pancreatic islet cells," *Journal of Molecular Endocrinology*, vol. 54, no. 2, pp. R103–R117, 2015.

[36] H. Kaneto, T. Miyatsuka, D. Kawamori et al., "PDX-1 and MafA play a crucial role in pancreatic β-cell differentiation and maintenance of mature β-cell function," *Endocrine Journal*, vol. 55, no. 2, pp. 235–252, 2008.

Hindawi
Journal of Diabetes Research
Volume 2019, Article ID 7457295, 17 pages
https://doi.org/10.1155/2019/7457295

Review Article

Evidence in Practice of Tissue Healing with Latex Biomembrane: Integrative Review

Suélia de Siqueira Rodrigues Fleury Rosa,[1] **Mário Fabrício Fleury Rosa**,[2] **Marcos Augusto Moutinho Fonseca**,[1] **Glécia Virgolino da Silva Luz**,[1] **Carlos Federico Domínguez Avila**,[3] **Aldira Guimarães Duarte Domínguez**,[4] **Aldene Guimarães Duarte Dantas**,[1] **and Von Braun Richter**[1]

[1]*Postgraduate Program in Biomedical Engineering-PPGEB at Gama-FGA, University of Brasília-UnB, Brasília 72.444-240, Brazil*
[2]*Postgraduate Technology and Health Program, University of Brasília-UnB at Ceilândia-FCE, Brasília 72220-275, Brazil*
[3]*Postgraduate Program in Human Rights, Citizenship and Violence/Political Science, University Center Unieuro, Brasília 70.200-001, Brazil*
[4]*University of Brasília at Ceilândia-FCE, Brasília 72220-275, Brazil*

Correspondence should be addressed to Suélia de Siqueira Rodrigues Fleury Rosa; suelia@unb.br

Received 17 September 2018; Revised 21 November 2018; Accepted 26 December 2018; Published 3 March 2019

Guest Editor: Roberta H. Mendes

Wound healing is a perfectly coordinated cascade of cellular, molecular, and biochemical events which interact in tissue reconstitution. Chronic diseases such as pressure ulcers (PU) and diabetes mellitus (DM) are considered risk factors for wound healing. Patients with such diseases often have higher sepsis, infection, and complication rates, since they have revascularization inhibition and low growth factor expression. Thus, latex biomembrane (LBM), a biocompatible material, derived from the latex of the rubber tree (*Hevea brasiliensis*) appears to create tendencies as an angiogenic-inducing tissue healing agent and as biomaterial, resulting from its structural qualities and its low cost when compared to conventional treatments. Therefore, this work aims at summarizing the results, experiments, and scientific findings that certify or recommend the use of LBM as a new technique to be applied effectively in the treatment of wounds. An integrative review was held in the BIREME, LILACS, Burns, MEDLINE, PubMed, and SciELO databases, from 2000 to 2016, using the following descriptors: "healing," "diabetes mellitus," "wounds," and "latex membrane." As a result, 600 experiments (out of 612) presented satisfactory results; however, 33% of the cases received explicit recommendations, 11% required more studies on the subjects, and 1% was denied. On the other hand, half of the studies did not expressly endorse its use, despite presenting satisfactory results. The LBM was characterized as a good therapeutic alternative in cases of wounds, including chronic diseases, such as diabetes mellitus and PU, due to its relevant potential for wound healing stimulation, acceleration of cell tissue mending and revascularization, or the reestablishment of angiogenic functions (creation of new blood vessels). The LBM was also confirmed to be safe as a biocompatible material whose structural qualities (elasticity, adaptability, impermeability, and possibility of suture), devoid of toxicity, allowed interaction between tissues and presented no hypersensitivity inducer and no antimicrobial effect.

1. Introduction

Wound treatment has been evolving since 3,000 BC, when hemorrhagic wounds were treated with cauterization. There are evidences of the use of tourniquets that date back to 400 BC, while suture is from the 3rd century BC. In the Middle Ages, with the creation of gunpowder, wounds became a more serious matter. Nowadays, chronic wounds caused by pressure ulcers (PU), vascular ulcers, and neuropathic ulcers (diabetes mellitus (DM) and leprosy) associated with complications in ambulatory therapeutic efficiency are quite challenging to treat [1–3].

The most common chronic wounds in the American population are chronic ulcers in the lower limbs (80 to

90%), and its etiology is venous stasis, at 5% arterial insufficiency and 2% neuropathy [4]. According to information from the International Diabetes Federation (IDF), 80% of the people with diabetes live in low- and middle-income countries. For example, in South and Central America, there were 26 million patients diagnosed with diabetes in 2017, and it is predicted that this number will increase to 42 million until 2045 [5]. Specifically in Brazil, the amount of patients diagnosed with diabetes has increased 61.8% between the years of 2006 and 2016 [6]. The World Health Organization (WHO) informs that roughly 422 million of adults have diabetes and that 2% of the population of the planet have complications in healing chronic wounds [7].

In Costa et al.'s survey [8] on the cost for PU treatment, treatment material costs were calculated around R$ 10,989.00 per year per patient. When combining this cost to the information we have on the treatment of DM-originated wounds, it is stated that about R$ 59.4 billion/year is spent on it [3].

Scientific communities have been making multiple efforts in order to test new techniques and discoveries that aim at contributing to the improvement of this scenario. In 1996, the latex biomembrane (LBM) emerged as a promising element, because besides it being quite affordable, it also has physical and chemical characteristics that aid in healing with its neoangiogenic activity [9, 10].

LBM is a polyisoprene derivative, made of rubber latex (*Hevea brasiliensis*), a whitish secretion (also called "coagulated milky sap") produced by the stem of the tree when it undergoes an incision in the bark, called "sangria." This natural latex is composed of rubbery, nongummy hydrocarbon particles suspended in an aqueous serum phase, in which there is an occurrence of (on average) 36% hydrocarbons, 1.6% carbohydrates, 1.4% protein, 1% neutral lipids, 0.6% glycolipids plus phospholipids, 0.5% inorganic components, 58.5% water, and 0.4% other substances. Therefore, *Hevea brasiliensis* latex is a compound cytoplasmic system in which rubber particles and nonrubbery particles are dispersed in an aqueous cytosol phase [3, 11].

Mrue et al. [12] emphasize that the great secret for LBM's angiogenesis (formation of new blood vessels) stimulation was only discovered because the polymer was not obtained through the traditional vulcanization method, which involves temperatures of 110°C to 125°C. In order to obtain the polymer, latex was collected with ammonia as the sole preservative, and centrifugation was then used to diminish its protein content, principally allergenic proteins. A sulfur composition was then added as the sole recovery agent; then, the latex was polymerized at low temperatures in a glass mold and then sterilized in ethylene oxide [3]. The result of this process is a biomembrane. The biomembrane is thin and elastic, has micropores that resemble human skin, and is easy to maneuver, as can be seen in Figure 1.

These characteristics help out in the wound repair process, particularly at the granulation tissue growth phase. This process can be divided into spatially and temporarily overlapping phases: (1) coagulation, (2) inflammation, (3) formation of granulation tissue (proliferative phase), and (4) remodeling or scar formation phase [14]. The endothelial cells are digested by molecules that make cell-cell and cell-matrix interactions. The endothelial cells are grouped and make a protrusion through the fragments of the basal membrane, at first forming solid rows of cells. Endothelial cells then begin to introduce cytoplasmic vacuoles, which are fused together at first among themselves and then with the neighboring cells, giving rise to new light. Factors by macrophages (factor of angiogenesis-derived macrophages), mast cells (heparin), platelets (platelet-derived growth factor, transforming growth factor beta), and fibroblasts (fibroblast growth factor) have all presented a positive effect on angiogenesis [14–16].

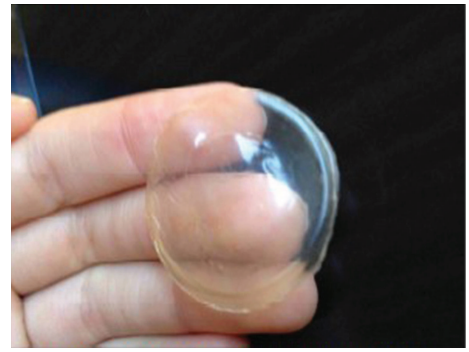

Figure 1: Latex biomembrane. This figure is reproduced from Ribeiro et al. [13], public domain.

Latex, one of the materials used for the production of the therapeutic insoles features the advantages of its low market price, low pathogen transmission risk, neovascularization and tissue regeneration properties, and wide clinical-social applicability. Latex is extracted from the rubber tree *Hevea brasiliensis*, and it is both a healing substance and defense mechanism for this organism [17]. Numerous research which used natural latex as an implant on different tissues have presented satisfactory results, which motivate the development of new works in the area [13, 17–20]. Regarding this scope, personalized insoles made with natural latex have been used as an important tool for the reduction of plantar pressure in the treatment of patients with a diabetic foot [12, 17]. The research of Duff A. C. indicates that one in four of young diabetics (age 11-24) has increased plantar pressure and/or plantar blister (lump, tissue thickening—lat. plantar callus) [13, 20, 21]. The impacted areas are high-risk areas for development of some variety of foot conditions in adulthood. Biomechanical alterations increase the occurrence of development of fissures, blisters, and deformities. Limited range of motion in joints is commonly seen in diabetic patients [21]. Natural latex biomembrane (NLB) was proven to be an effective material in the reconstruction of the pericardium of dogs [22], in iatrogenic defects in the abdominal wall of rats [23], and in a neoangiogenic inductor in rabbit corneas [24, 25]. According to Balabanian et al. [26], granules of natural latex implanted inside the alveolar sockets of rats immediately after dental extraction demonstrated biocompatibility and become integrated with the alveolar bone, simultaneously accelerating bone formation

Table 1: Publication research.

Author	Study	Objective	Number of experiments	Results
Araujo et al. [34]	Anatomical and functional evaluation of tympanoplasty with the use of the transitional implant of the natural latex biomembrane from the rubber tree *Hevea brasiliensis*	This work aims at investigating the effects of the latex and silicone biomembrane in tympanic perforation restoration	107 humans	There was greater vascularity in the group with the transitional latex biomembrane implant. They presented good biocompatibility with the use of latex and silicone implants without affecting the rates of occurrence of infection, otorrhea, or otorrhagia. The proportion of tympanic membrane healing was equivalent in three groups, as well as the hearing improvement. Thus, the use of the implant caused a bigger graft vascularity process, with satisfactory interaction with human tympanic membrane tissues
Ganga et al. [35]	Sciatic nerve regeneration in rats through a conduit made from a natural latex membrane	To evaluate the NLB's capacity to accelerate and improve the quality of regeneration of a sciatic nerve cut in rats	40 Wistar rats	All morphological and functional analyses have shown that rats with the latex membrane recovered better than those with the autologous nerve: quality of printed shoeprints, treadmill performance, electrophysiological response, and histological quality of nerve regeneration. Thus, the data presented depicted behavioral and functional recovery in the rats that were implanted with the latex conduit through a complete morphological and physiological restoration of the sciatic nerve
Sousa et al. [36]	Morphological evaluation of the use of latex prosthesis in videolaparoscopic inguinoplasty: an experimental study in dogs	To evaluate (through videolaparoscopic inguinoplasty) the morphological aspects of the behavior of 4 types of latex biomembranes preperitoneally put in dogs	12 dogs	The biomembranes maintain the induction of the healing process fibrosis-free. They undergo encasement and, with the exception of the thin porous polyamide membrane, they are not incorporated in neighboring tissues. The latex biomembrane, alone, be it with or without polyamide, is not recommended for preperitoneal inguinoplasty
Frade et al. [37]	Vegetal biomembrane bandage and hypersensitivity	To evaluate bandage and hypersensitivity in the treatment of wounds with the latex membrane	67 humans	The biomembrane proved to be safe as bandaging, as it did not induce hypersensitivity
Talieri [38]	Natural latex graft in the healing of lamellar and	This study aim at investigating the effects of natural latex with the 0.1%	24 rabbits	Great adhesion of the latex graft to the receptor's sclera

Table 1: Continued.

Author	Study	Objective	Number of experiments	Results
	penetrating sclerectomies in rabbits	polylysine on the healing process of lamellar and penetrating sclerectomies in rabbits		
Quege et al. [39]	Comparison of the activity of essential fatty acids and the biomembrane on the microbiota of infected chronic wounds	To evaluate the highest efficiency between the latex membrane (Biocure) and AGE-based product (Dersani) in postleprosy treatment ulcers	8 humans	Dersani: positive antimicrobial effect in Enterobacter aerogenes Biocure: positive antimicrobial effect in *Pseudomonas aeruginosas*
Brandão et al. [40]	Latex-derived vascular prosthesis	To develop a new microperforated vascular prosthesis model, made of fabric covered with a natural rubber tree (*Hevea brasiliensis*) latex-derived compound, and to assess its patency rates, thrombogenicity, biocompatibility, and the process of healing, in addition to some mechanical properties (elasticity, adaptability, impermeability, and possibility of suture), using the expanded polytetrafluoroethylene prosthesis as a control in the same animal	15 dogs	The tissue and microperforated latex graft demonstrated structural qualities (adaptability, elasticity, impermeability, and possibility of suture) that were satisfying as a vascular substitute. It stimulated endothelial growth beyond the contact with the regions on the anastomosis and it was biocompatible with the dogs' arterial system, presenting appropriate tissue integration
Sousa et al. [41]	Latex biomembrane: new method for cavity flooring opened in tympanomastoidectomy	To study the performance of the biomembrane as an interface between the bone rim and the buffering material and to analyze its role in the epithelialization of the neocavity	54 humans	The use of the latex biomembrane proved to be an effective method in the neocavity coating, facilitating the removal of the cap and the epithelialization of the neocavity
Pinho et al. [24]	Experimental use of latex biomembrane in conjunctival reconstruction	To check the effect of the latex biomembrane in the conjunctival repair process	15 rabbits	As described in the literature for other tissues, the natural latex biomembrane also seems to favor the conjunctival scarring and neoangiogenesis. If these results repeat themselves in humans, the biomembrane could become a promising therapeutic feature in conjunctival reconstruction, particularly in cases where tissue revascularization is important
Reis [42]	Tissue neoformation-inducing system for diabetic feet with LED light circuit and use of natural latex	The goal is to evaluate the efficiency of the tissue neoformation-inducing system in the healing of diabetic foot ulcers. This system has been tested in patients with diabetic foot ulcer. Six patients with 11 ulcers were selected and then	6 humans	The clinical findings were analyzed qualitatively and quantitatively, demonstrating that the experimental group has higher results than the control group. Thus, tissue neoformation-inducing system may be considered an effective alternative for

Table 1: Continued.

Author	Study	Objective	Number of experiments	Results
		seen in the Diabetic Foot Center of HRT/DF. They constituted two distinct groups of treatment and study: control group and experimental group Diabetes (related to cellular stress) changes considerably the skin ulcer's healing process. The rubber tree *Hevea brasiliensis* latex has presented itself as especially relevant as an inducer of diabetes' compromised ulceration healing. It was clinically observed that the latex completely stimulates full reepithelialization. Tissue modifications were evaluated, as well as the latex protein fraction (F1) action mechanisms in the healing of skin ulcers in diabetic and nondiabetic rats. Initially, it was tested on the cytotoxicity of F1 in human fibroblast and keratinocyte cultures through the MTT colorimetric method		diabetic foot ulcer treatment, once it showed a high potential in healing induction
Andrade [43]	Tissue modifications and rubber latex *Hevea brasiliensis* F1 fraction action mechanisms in the healing of skin ulcers in diabetic rats		80 Wistar rats	Essential factors which enabled the reepithelization of the total skin ulcers treated with F1 in diabetic rats were a large recruitment of inflammatory cells, stimulation of the production of growth factors and cytokines, oxidative stress triggered until the 14th day, and the induction of collagenase and fibroplasia, as well as the significant activation of insulin signaling, once lowered in diabetics
Nogueira [44]	Oronasal fistula in dog: repair with a simple flap associated with a protein-purified angiogenic factor of hevea latex, aired with collagen sponge array—an experimental study	This experiment intended to use the purified protein fraction of hevea latex on the repair of inflicted oronasal communications, for experimental simulation of fistula, after the dogs' upper canines' dental extraction	6 dogs	The results were better quality healing, less inflammatory processes at the end of 21 days, less occurrence of suture dehiscence, and a greater amount of bone tissue in the alveoli, concluding that the use of the protein factor helps the repair process, making it faster and more efficient
Herculano [45]	Development of natural latex membranes for medical applications	In this work, we tested the latex biomembrane as an occlusive membrane for GBR with promising results	*In vitro* laboratory tests	The result indicated that the latex biomembrane could be used as an active membrane to fasten the healing process
Friolani [46]	The use of the latex hevea biomembrane (*Hevea brasiliensis*) in rabbits' diaphragmatic lesions: an experimental study	Considering the healing process accelerating properties the latex biomembrane has presented, this work aimed at evaluating the behavior of a natural latex biomembrane flap in diaphragmatic lesions experimentally induced in rabbits	15 rabbits	It was possible to conclude that the use of the latex membrane in repairing diaphragmatic lesions, due to its low cost and subsequent easiness to obtain and be used, not to mention its strength, presented a satisfactory answer in relation to the time of healing
Matos [47]	Effects of the natural latex biomembrane (*Hevea brasiliensis*) in Wistar rats submitted to body heat injury by scalding	Latex membrane biocompatibility	21 Wistar rats	The LBM (latex biomembrane) improved the healing in burned areas and stimulated neoangiogenesis, appearing then to be a

Table 1: Continued.

Author	Study	Objective	Number of experiments	Results
				promising therapeutic resource for healing of burned skin, in which tissue revascularization is important
Borsari [48]	Effects of the application of the natural latex biomembrane and frog skin extract (*Lithobates catesbiana*) (Shaw, 1802) in Wistar rats surgical wounds	A comparison between natural latex biomembrane's reaction whether isolated or with frog skin extract in cutaneous wounds. This work aims at evaluating the tissue reparation in the following aspects: biocompatibility, healing capacity, and possible complications	60 Wistar rats	All showed positive healing signs
Andrade [49]	Natural rubber tree *Hevea brasiliensis* latex biomembrane's activity in tissue neoformation in mice	The natural rubber tree *Hevea brasiliensis* latex biomembrane, used as a bandage in the treatment of chronic ulcers in humans, proves to be effective in debridement and to stimulate granulation and accelerating healing. Its mechanism of action is still unknown, making it important to evaluate its activity as an implant in tissue induction by comparing it to other implants and normal healing	60 C57BL/6 mice	It is concluded that the natural rubber tree *Hevea brasiliensis* latex biomembrane plays a significant role in the inflammatory phase of wound healing, thus being important in the neurophilic recruiting in the wound site, confirmed quantitatively by the concentration of myeloperoxidase and interleukin and immunohistochemistry. This fact seems to influence directly the subsequent phases of the healing process, confirmed by its ability to stimulate angiogenesis, which is probably not influenced by VEGF, and by stimulating fibroplasia TGF1 independent and with no modification on collagen production
Frade [50]	Foot ulcer: clinical characterization and immunohistopathological profile of healing in the presence of the natural rubber tree *Hevea brasiliensis* latex biomembrane	Foot ulcer is a very common disease in the elderly population. Numerous types of bandages are currently used for foot ulcer treatment with different indications, advantages and disadvantages, and which effectiveness is not well comprehended due to the discontinuity of the treatments and the costs involved in some situations. This work aims at evaluating the action of the latex biomembrane (LBM) in treating foot ulcers, which behaved like an efficient healing tissue inducer	21 humans	The global analysis of the data suggests that treatment with the biomembrane leads to scar tissue organization consequent to the increased production of cellular growth factors. Thus, the biomembrane is characterized as a good therapeutic option for foot ulcer due to the practicality of its application, low cost, and high potential in the induction of healing

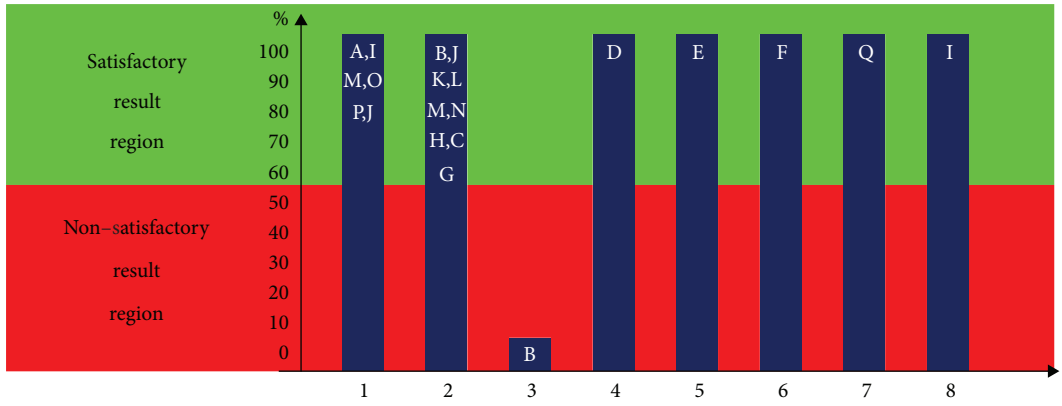

1–Vascularization, angiogenisis, neoangiogenisis, VEGF
2–Healing improvements
3–Inguinoplasty adhesion to the graft
4–Hypersensitive non–inducer
5–Graft adhesion to recipient sclera
6–Antimicrobial effect
7–Sciatic nerve repair
8–Fibroplasty stimulation

Label

A–Araujo (2012)
B–Sousa (2011)
C–Ries (2013)
D–Frade (2011)
E–Talieri (2009)
F–Quege (2008)
G–Sousa (2007)
H–Pinho (2004)
I–Andrade (2012)
J–Nogueira (2009)
K–Herculano(2009)
L–friolani (2008)
M–Matos (2008)
N–Borsasi (2008)
O–Andrade (2007)
P–Frade (2003)
Q–Ganga (2012)

Figure 2: Main results obtained with the use of LBM in direct application, checked in the publication-surveyed 1 frame.

undergoes and playing an important role in the healing process. Domingos et al. [27] have also demonstrated NLB's biocompatibility as a matrix for bladder augmentation in rabbits. The researchers affirm that it allows a progressive ingrowth of all layers of the bladder wall, raising epithelium and muscle regeneration without postoperative urinary leakage and with a slow rate of stone formation [25, 27].

Patients with chronic wounds come across multiple difficulties in this stage, such as vascular problems, atherosclerosis predisposition, renal insufficiency, and poor infection response [28, 29]. Diabetes mellitus (DM) is a set of metabolic alterations, whose main characteristic is the decompensation of glucose levels in the bloodstream, characterized as hyperglycemia or hypoglycemia [30]. There is a raised risk of infection due to the diabetic's inability to control the bacterial colonization site, and obviously, if the situation is not controlled, it will lead to a vicious circle, which will fatally evolve to the amputation stage. That being said, early intervention is essential in the wound-healing treatment's success [31, 32].

Candido ([33], p. 80) makes the following approach: antibiotics can produce toxic effects and inhibit healing and thus should be administered only when there is infection, and anti-inflammatories cause microcirculation vasoconstriction, reducing the inflammatory response and collagen synthesis, and should be used only when there is pain or inflammation. This analysis is important because otherwise there is a bigger probability of delay in the healing process and the rise of resistant bacteria.

It is at this healing stage that the LBM can contribute the most. From 1998 to 2000, this peptide- and angiogenesis-inducing material started being successfully used in some hospitals in the treatment of chronic wound patients suffering from diabetes. In some cases, the biomaterial is sprinkled on the wound, and a substance very similar to the VEGF (Vascular Endothelial Growth Factor) is released, rebuilding veins and arteries and carrying fuel so that the wound site can heal [12]. Therefore, this article intends to contribute to these studies through the gathering and exposition of scientific evidences on the successful use of LBM in the healing process, as well as its recommendations and prohibitions.

2. Materials and Methods

We conducted a study to review the scientific literature using the following databases: BIREME, LILACS, Burns, MEDLINE, PubMed, and SciELO. Publications from 2000 to 2016 were selected with the following keywords: "healing," "diabetes mellitus," "wounds," and "latex biomembrane." The inclusion criteria for the selection of publications were the publications in their entirety, being published and/or indexed in these databases in the period of 2000 to 2016, and that they addressed the issues of use of the rubber tree (*Hevea brasiliensis*) latex-derived biomembrane and being of free access. Articles published before 2000, articles that have not addressed the rubber tree (*Hevea brasiliensis*) latex-derived biomembrane, articles that presented DM-related issues that were not correlated to LBM, and those discussing issues related to healing and wounds without the use of the latex biomembrane were not considered for this study, thus being the exclusion criteria.

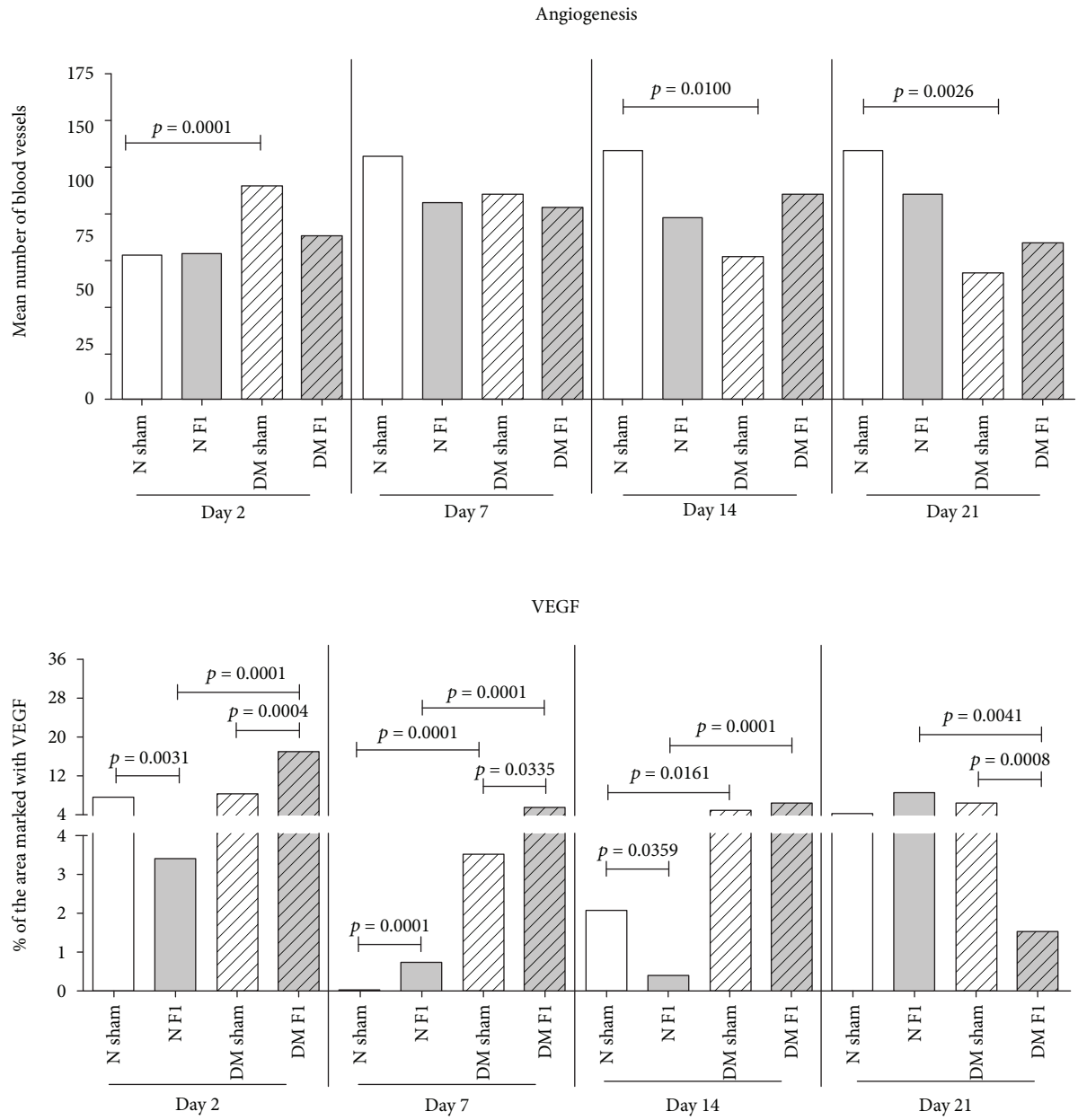

Figure 3: Characterization of angiogenesis increase and VEGF. This figure is adapted from Andrade [43], public domain.

3. Results

Table 1 presents the results of the integrative review of the scientific literature. With the works selected through the inclusion and exclusion criteria, there were 18 publications found, among which were selected tests with 611 subjects that varied between humans, animals, and laboratory tests.

4. Discussion

Out of the 18 publications found, 17 papers presented satisfactory results with tests on 600 subjects (263 in humans, 1 laboratory test, and 336 in animals), i.e., 98% of cases with LBM implementation presented satisfactory results.

Sousa et al. [36], in 12 experiments with dogs, do not recommend the LBM for preperitoneal inguinoplasty due to encasement formation. However, the authors state that the biomembranes keep influencing the process of scarring with no fibrosis, no bruising, and no seroma and infection and with the induction of vascular neoformation and collagen deposition.

The publication results have been synthesized in Figure 2, featuring broadly the main contributions of the LBM.

It is observed that the latex biomembrane is highly recommended, because of the results acquired in the different publications. Six publications, with 128 human studies and 295 animal studies, refer to the LBM as a vascularization-, angiogenesis-, and VEGF-inducing agent, as well as eight publications (with 60 human studies, one

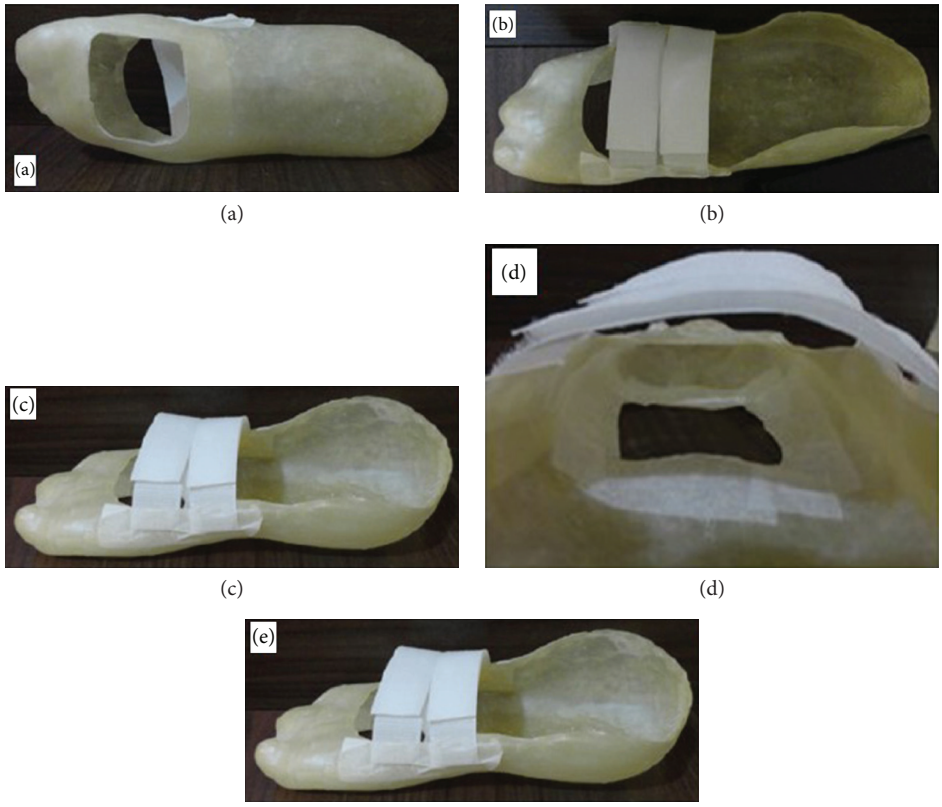

FIGURE 4: Healing insole: (a–c) various views of the sock with the gap; (d) microporous tape glued around the gap; (e) patient using the insole healing with tissue regeneration electronic circuit (circuit off). This figure is reproduced from Reis [42], public domain.

laboratory test, and 129 animal studies) showing improvements in the healing process. Nevertheless, it still presents an antimicrobial effect, it encourages wound healing and the adherence to recipient sclerae, and it was proven to be as safe as a nonhypersensitivity-inducing bandage.

Frade [50] conducted clinical and immunohistopathological assessments in 21 casually selected patients, subject to the LBM application (14 patients), in a comparison with the classical treatment (7 patients), which consisted of an ointment with chloramphenicol and proteolytic enzymes (Fibrase) with the purpose of analyzing and comparing the histopathological and immunohistochemical alterations when it comes to different treatments.

In order to analyze the two scenarios, the biopsies were collected before and 30 days after Grochocki treatments. Biopsies were then split into two fragments: one for the immunohistopathological study and the other frozen at -70°C for immunohistochemical analysis. The results revealed that the use of the latex biomembrane facilitated the Grochocki care, and it was also proven to be an adequate alternative, due to its low cost and practicality of application. It was also observed that LBM induces a clinical and histopathological differentiation of healing points, with improved detection of growth factors such as VEGF and TGF1 (transforming growth factor 1).

A similar fact is evidenced in Andrade [43], where, in the assessing of skin ulcers due to diabetes mellitus (DM) in rats, it was found that the LBM performed as an important healing inducer where a latex stimulus to full reepithelialization was clinically observed. This stimulating inflammatory and oxidative stress phase favored the subsequent phases of wound healing, enhancing angiogenesis and VEGF in the 14th and 21st days, which certainly favored the reepithelialization. It is also assumed that there was a stimulus for fibroplasia in the 14th and 21st days and collagenase, as shown in Figure 3.

Thus, the essential factors which enabled the complete reepithelization of skin ulcers treated with F1 in diabetic rats, showing that the biomembrane (LBM) contributed favorably, were a larger recruitment of inflammatory cells, stimulation of the production of growth factors and cytokines, oxidative stress triggered until the 14th day, and the important fibroplasia and collagenase stimulus as well as the important signaling insulin activation, once reduced in diabetics.

In Frade et al. [37], there was an evaluation of the vegetable biomembrane's safety as a bandage in relation to latex hypersensitivity. Patients with cutaneous ulcers were selected, with the groups being control: low exposure to latex (sample = 17), high exposure to latex (sample = 14), and ulcerated using vegetable biomembrane (sample = 13) and experimental: ulcerated with no vegetable biomembrane (sample = 14) and new cases (sample = 9), all submitted for evaluation before and after 3 months using the biomembrane. All of them were submitted to clinical and epidemiological assessment regarding latex hypersensitivity and to a

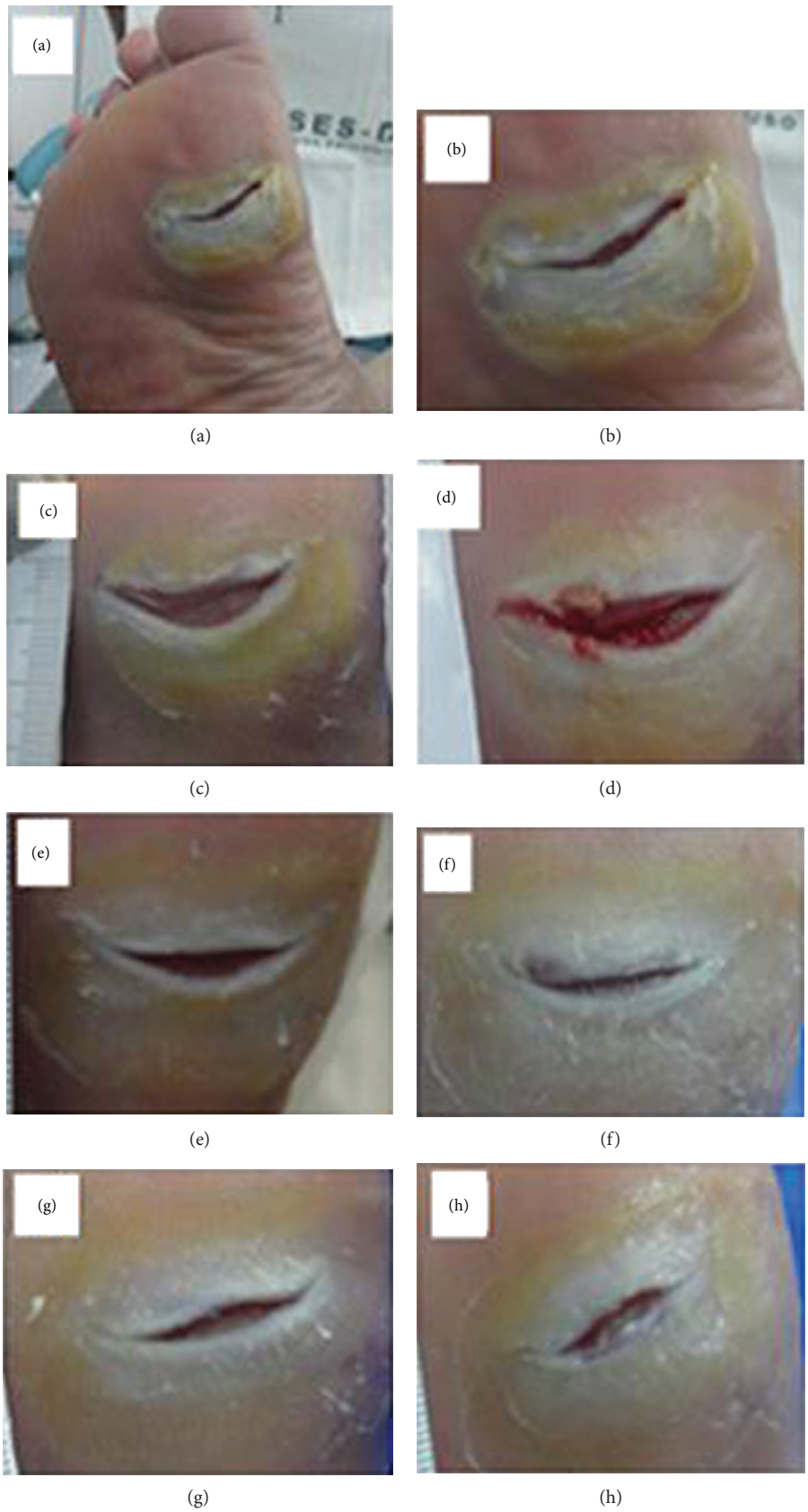

Figure 5: Continued.

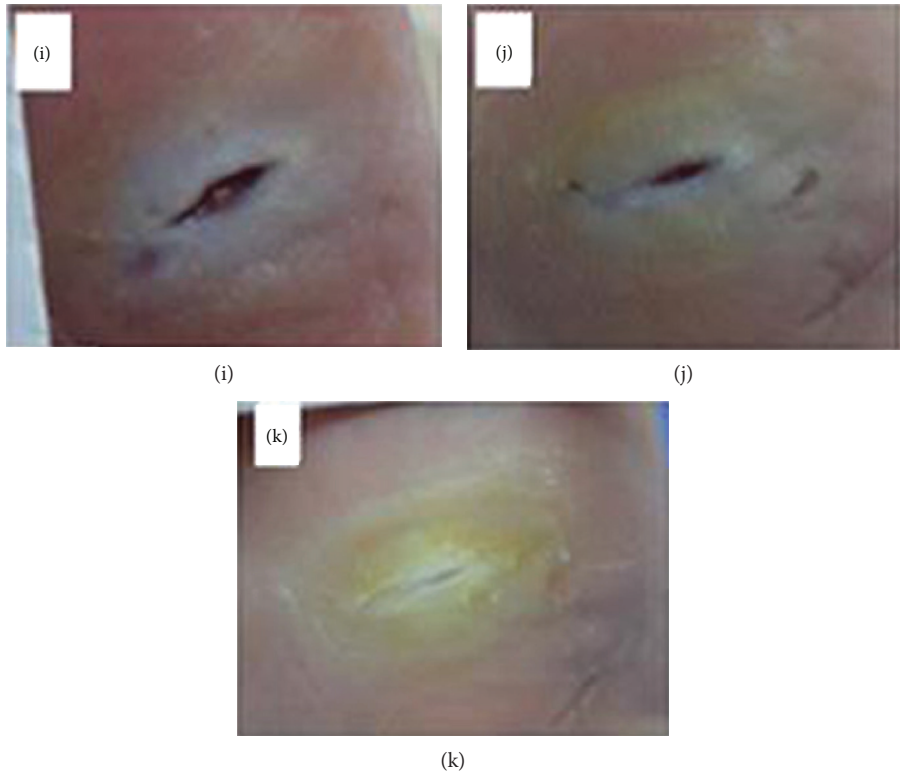

Figure 5: Photo clinical follow-up. Patient 1: control group: (a) ulcerated foot region; (b) pretreatment (initial); (c) posttreatment (1 week); (d) 2 weeks; (e) 3 weeks; (f) 4 weeks; (g) 5 weeks; (h) 6 weeks; (i) 7 weeks; (j) 8 weeks; (k) 9 weeks. This figure is reproduced from Reis [42], public domain.

contact test ("patch test"). The study concluded that the vegetable biomembrane was safe to be used as a bandage, as it did not induce hypersensitivity reactions in the volunteers submitted to the "patch test."

In Soares et al. [51], the treatment and healing of pressure ulcers using the latex biomembrane was studied, with substantial reduction of treatment time. Reis [42] presents the search for a new possibility for the healing of diabetic foot ulcers. In this sense, a then-unheard-of tissue neoformation-inducing system was developed for a diabetic foot, with a LED light circuit and using natural latex. This system involves a healing insole and an electronic tissue regeneration circuit. The insole's scarring effect is derived from the natural latex rubber tree *Hevea brasiliensis* and was individually custom made. This diabetic foot ulcer healing method is composed of the cooperative and simultaneous action of both biomaterial latex and the light irradiation of low-intensity LED lights.

Both features have properties and agents capable of inducing regeneration and tissue neoformation. When the patient is using the healing insole and the tissue regeneration electronic circuit, both of them will engage in the healing of the diabetic foot ulcer. This happens for two reasons: full contact of the ulcerated area with the latex and the low-intensity LED lights irradiating on the entire extent of the wound.

The insole's design was one of the important requirements throughout this project's preparation process. Since this is an insole that can be used either in hospitals or in everyday life, it is essential that it can provide the patient with the maximum possible comfort, softness, and well-being. Therefore, the making of this healing insole is personalized and individualized in its entirety, considering the anatomy and the specific features of the patient's foot such as size, shape, and proportion. This allows the LED light irradiation force cell (which is customized) to be installed in the exact wound spot in order to promote direct healing. In addition, customizing the insole makes it possible to perfectly accommodate the patient's feet possible deformities (foot dig or plan, bunions, claw-like fingers, and hammer, among others) if there is any, as shown in Figure 4.

Commercially sold insoles are made following just the numbering system and a standard model. They are not properly built for this, even if they may accommodate other foot health complications, and consequently, it is nearly impossible for them to be properly useful in the treatment of diabetic foot ulcers.

Another positive point of this invention is the low production cost, due to the material used in the making (biomaterial latex) and the fact that the tissue regeneration electronic circuit consists of LED lights. This invention has had satisfactory results, especially when it comes to reducing healing time, as demonstrated in Figures 5, 6, and 7.

In Figure 8, the black dashes belong to the control group (CG), while the colored lines are the experimental group (EG). As it can be seen in this figure, in the second week of treatment, the EG's patient 2 had presented full reepithelization. Three patients (1 ulcer-CG; 2-EG ulcer), 1 (EG),

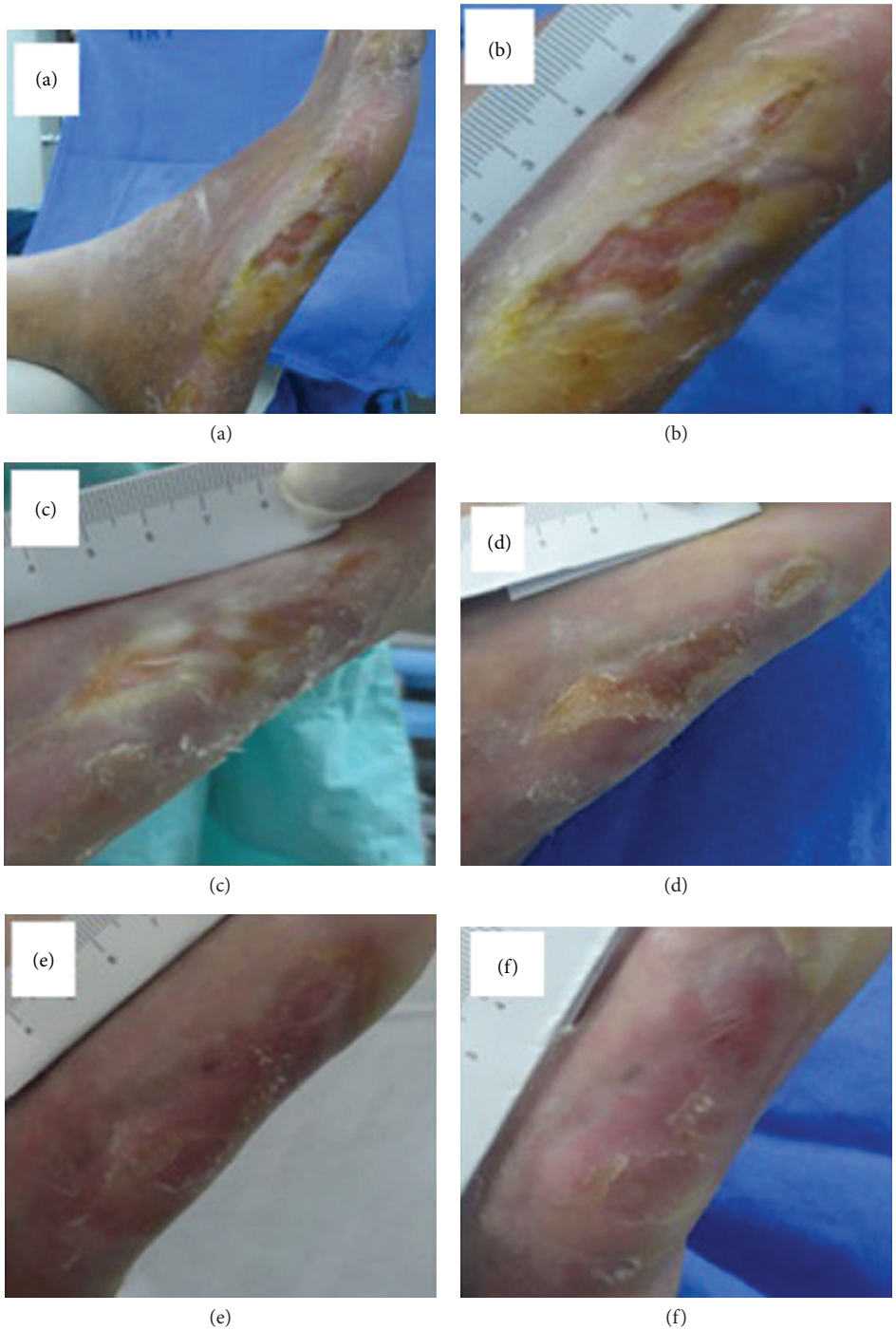

Figure 6: Photo clinical follow-up. Patient 2: experimental group: (a) ulcerated foot region; (b) early (before the tissue neoformation-inducing system); (c) posttreatment (after using the tissue neoformation-inducing system) (1 week); (d) 2 weeks; (e) 3 weeks; (f) 4 weeks. This figure is reproduced from Reis [42], public domain.

and 1 (CG) also presented full reepithelization in the 4th, 6th, 8th, and 9th weeks. All patients showed healing evolution in all weeks, some with less and others with more intensity, except for patient 1 (CG), who in fact got worse between the 4th and 6th weeks. When comparing the two groups in the second week of treatment, it is possible to see that the best UHRs belonged to the 2 patients (EG), 1 (EG), 3 (CG and EG), and 5 (EG), while the other patients had UHRs below 0.4. It should be noted that patient 3's ulcer (1 ulcer-CG) was the smaller and the most superficial out of all ulcers in this study. When making the same comparison in week 4, it is possible to see that the highest UHRs belonged to patients 3 (CG and EG), 1 (EG), and 5 (EG). The worst result in all weeks was patient 4 (EG), whose

Figure 7: Continued.

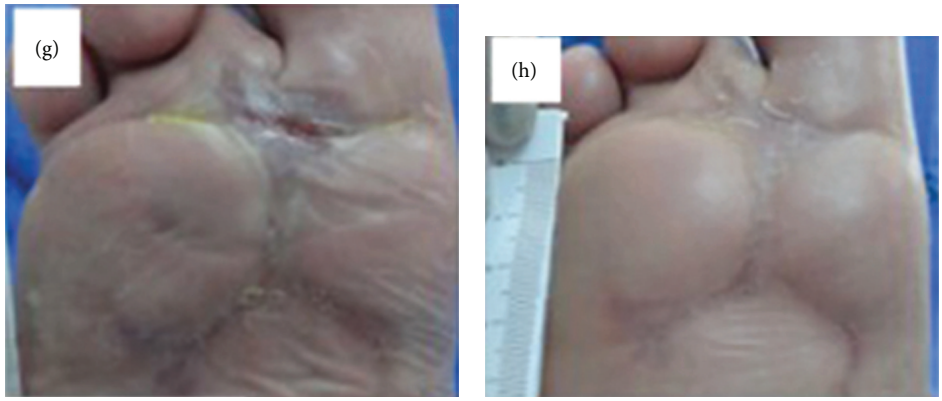

Figure 7: Photo clinical follow-up. Patient 3 (2 ulcer): experimental group: (a) ulcerated foot region; (b) early (before the tissue neoformation-inducing system); (c) posttreatment (after using the tissue neoformation-inducing system) (1 week); (d) 2 weeks; (e) 3 weeks; (f) 4 weeks; (g) 5 weeks; (h) 6 weeks. This figure is reproduced from Reis [42], public domain.

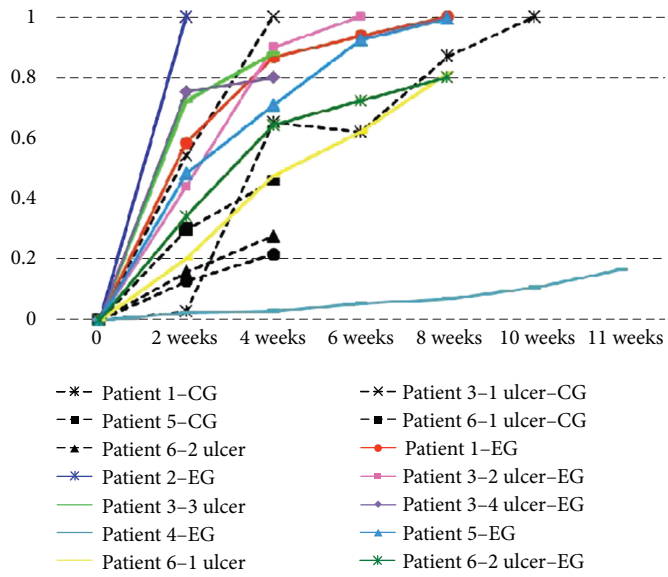

Figure 8: Evolution of the Ulcer Healing Rates (UHRs) in relation to the treatment time (in weeks) for the control group (CG) and the experimental group (EG). This figure is reproduced from Reis [42], public domain.

chronic ulcer is harder to heal and has been there for the past 16 years. Despite all that, a small evolution in the healing process of their wounds was observed.

One of the reviews of this study was a comparison of the behavior of two different healing methods in the same patient. This refers to the patient 1, which was submitted to silver foam (CG) in their right foot ulcer (the metatarsals) and a neoformation tissue inducer system (EG) on their left foot ulcer (calcaneal region). Comparing the UHRs in both cases in the 2nd, 4th, 6th, and 8th weeks, patient 1 presented the best results in EG. This reveal that the tissue neoformation-inducing system favored an increase of healing better than foam with silver and in less time.

Costa et al. [8] made a survey on the cost of pressure ulcer (PU) treatment, which was calculated around R$ 915.75 per patient monthly and R$ 10,989.00 yearly in a hospital unit in Minas Gerais. The cost for the hospital is proportionally higher due to the number of patients that show up with PU and due to the possibility that the available resources might be used inappropriately. Considering the high investment in this treatment, it is important to properly control the materials needed in the care of PU; after all, the actions in these treatments should aim at cost reduction, the reduction of patient's suffering, and the possibility to provide them with humanized assistance.

The population with a higher risk of presenting pressure ulcer is, in most cases, people over 60 years old, because the skin becomes then much more sensitive due to the changes that come with the process of aging; white people, because "the black skin is more resistant to external damage"; the bedridden and/or restricted-to-wheelchair people; the malnourished; and those with very dry or very wet skin.

In Brazil, Biocure® is a registered trademark for the first national application of latex (Biomembrane® is manufactured by Pelenova Biotechnology S/A), which was founded in 2003. According to the directors of Pelenova, Freitas and Silva (2003), the Biocure® box with 20 units costs approximately U$ 30.00 (updated value, 2004 reference; R$ 28.50).

The similar products that come from the international market are much more expensive because they are based on the production of living cells, which involves very high industrial effort and expenses. In Japan, this medicine costs around U$ 500.00. Healing ointment gel with human hormone compounds (Becaplermin, Johnson & Johnson) is worth nearly U$ 350.00 and can only last for a few days of treatment. A human skin transplant patented by Novartis costs around U$ 1200.00, plus surgical expenses and the risk of it being rejected by the patient's body.

Therefore, it can be concluded that the cost for obtaining the LBM for tissue-healing treatment is considered low when compared with other traditional methods available on the market that are expensive and often end up in interrupted treatment, thus possibly worsening the patients' situations.

5. Final Considerations

By analyzing the experiments' results, it is possible to conclude that there are practical evidences of tissue healing with the use of the latex biomembrane, including in cases of chronic wounds from diabetes mellitus [39, 42, 43] and pressure ulcers [49, 50].

There were several cases that presented tissues' cellular reconstitution, revascularization, and function reestablishment after the burns, acting and reducing healing times in the inflammatory phase.

LBM's low production cost (and it is already being manufactured in Brazil by Pelenova Biotechnology S/A (Terenos/MS)) is another favorable aspect for this method to be made more popular. It is more affordable than traditional methods, and it also presents favorable results in a shorter period of time and in adverse conditions of treatments for healing.

The satisfying results make it possible to elucidate that there is still much to be studied and analyzed regarding the LBM besides the direct use in tissue healing processes. There is also the indirect use, with new applications, in order to take advantage of their biocompatible material properties, which demonstrated structural qualities (adaptability, elasticity, impermeability, and possibility of suture) and the absence of toxicity and allowed interaction between tissues (as demonstrated by the study on vascular prostheses [40]), whether as an inductor of sciatic nerve regeneration [35] or in bandages [37] for not inducing hypersensitivity and for having an antimicrobial effect [39].

All this considered, it is believed that the current results, as well as the forthcoming ones, will contribute considerably to the advancement of medicine, as well as in the treatment of many patients by giving them a faster healing time and an affordable cost that the majority of the population can afford.

Conflicts of Interest

The authors declare that there are no conflicts of interest.

Acknowledgments

This study was financed in part by the *Coordenação de Aperfeiçoamento de Pessoal de Nível Superior*, *Brasil* (CAPES), Finance Code 001. We thank the University of Brasília (UnB) for all the support granted.

References

[1] S. Sarabahi, V. K. Tiwari, and S. P. Bajaj, *Principles and Practice of Wound Care*, Jaypee Brothers Medical Publishers (P) LTD, New Delli, Panama City and London, 2012.

[2] I. Peate and W. Glencross, *Wound Care at a Glance*, John Wiley & Sons, Ltd., Chichester, UK, 2015.

[3] V. B. Richter, *Evidências na Prática de Cicatrização Tecidual com Biomembrana de Látex*, Campus Gama/FGA, Programa de Pós-Graduação em Engenharia Biomédica, University of Brasília/UnB, 2016, http://repositorio.unb.br/bitstream/10482/22449/1/2016_VonBraunRichte.pdf.

[4] P. F. d. A. G. Rittes, "Stasis ulcers of the lower limbs: a new therapy," *Anais Brasileiros de Dermatologia*, vol. 71, no. 4, pp. 295–297, 2005.

[5] International Diabetes Federation, *IDF Diabetes Atlas*, International Diabetes Federation, Brussels, Belgium, 8th edition, 2017.

[6] Ministério da Saúde, *SAGE-Sala de Apoio à Gestão Estratégica*, Ministério da Saúde, Brasília, Brazil, 2018.

[7] World Health Organization, *Global Report on Diabetes*, World Health Organization, Geneva, Switzerland, 2016.

[8] A. M. Costa, A. C. S. Matozinhos, P. D. S. Trigueiro, R. C. G. Cunha, and L. R. Moreira, "Costs of treatment pressure ulcers in long-term care unit in an institution of Minas Gerais," *Enfermagem Revista*, vol. 18, no. 1, pp. 58–74, 2015.

[9] F. Mrué, *Substituição do esôfago cervical por prótese biossintética de látex. Estudo experimental em cães*, University of São Paulo, Ribeirão Preto, Brazil, 1996, http://www.scielo.br/scielo.php?script=sci_nlinks&ref=000107&pid=S0365-05962012000100005000006&lng=en.

[10] F. Mrué, *Neoformação tecidual induzida por biomembrana de látex natural com polilisina: aplicabilidade na neoformação esofágica e da parede abdominal. Estudo experimental em cães*, Faculdade de Medicina Ribeirão Preto, University of São Paulo, Ribeirão Preto, Brazil, 2000, http://dedalus.usp.br/F/N465C3LQTU7JPUHYEVC1P612IH9NXEL7VINQI4SN71IQ2T13E5-33251?func=full-set-set&set_number=000444&set_entry=000008&format=999.

[11] A. C. C. Peres, L. M. A. Lopes, L. L. Y. Visconte, and R. C. R. Nunes, "Uso de DSC na determinação de parâmetros de vulcanização de látex de borracha natural," *Polímeros*, vol. 16, no. 1, pp. 61–65, 2006.

[12] F. Mrue, J. C. Netto, R. Ceneviva, J. J. Lachat, J. A. Thomazini, and H. Tambelini, "Evaluation of the biocompatibility of a new biomembrane," *Materials Research*, vol. 7, no. 2, pp. 277–283, 2004.

[13] J. A. Ribeiro, S. S. R. F. Rosa, and D. S. Oliveira, "Biomaterial latex manufactured occlusion contact lens: proposal for

amblyopia treatment," *International Journal of Advanced Engineering Research and Science*, vol. 2, pp. 65–69, 2015.

[14] T. N. Demidova-Rice, M. R. Hamblin, and I. M. Herman, "Acute and impaired wound healing: pathophysiology and current methods for drug delivery, part 1 normal and chronic wounds biology, causes, and approaches to care," *Advances in Skin & Wound Care*, vol. 25, no. 7, pp. 304–314, 2012.

[15] A. J. Singer and R. A. F. Clark, "Cutaneous wound healing," *New England Journal of Medicine*, vol. 341, no. 10, pp. 738–746, 1999.

[16] J. Folkman and M. Klagsbrun, "Angiogenic factors," *Science*, vol. 235, no. 4787, pp. 442–447, 1987.

[17] P. B. Aielo, F. A. Borges, K. M. Romeira et al., "Evaluation of sodium diclofenac release using natural rubber latex as carrier," *Materials Research*, vol. 17, Supplement 1, pp. 146–152, 2014.

[18] Y. Zhang, J. Leclercq, and P. Montoro, "Reactive oxygen species in *Hevea brasiliensis* latex and relevance to tapping panel dryness," *Tree Physiology*, vol. 37, no. 2, pp. 261–269, 2017.

[19] J. Pirrello, J. Leclercq, F. Dessailly et al., "Transcriptional and post-transcriptional regulation of the jasmonate signalling pathway in response to abiotic and harvesting stress in *Hevea brasiliensis*," *BMC Plant Biology*, vol. 14, no. 1, p. 341, 2014.

[20] L. Bolognesi, F. Borges, J. Cinman, R. Silva, A. Santos, and R. Herculano, "Natural latex films as carrier for *Casearia sylvestris* Swartz extract associated with ciprofloxacin," *American Chemical Science Journal*, vol. 5, no. 1, pp. 17–25, 2015.

[21] S. Zimny, H. Schatz, and M. Pfohl, "The role of limited joint mobility in diabetic patients with an at-risk foot," *Diabetes Care*, vol. 27, no. 4, pp. 942–946, 2004.

[22] S. L. Sader, J. Coutinho Netto, J. Barbieri Neto et al., "Partial replacement of dog pericardium with a natural latex membrane," *Revista Brasileira de Cirurgia Cardiovascular*, vol. 15, no. 4, pp. 338–344, 2000.

[23] N. M. Paulo, F. G. d. Lima, J. T. d. Siqueira Júnior et al., "Seringueira's latex membrane (*Hevea brasiliensis*) with and without polylysine 0,1% and marlex mesh for the reconstruction of iatrogenics abdominal wall defects in rats," *Acta Cirurgica Brasileira*, vol. 20, no. 4, pp. 305–310, 2005.

[24] E. C. C. M. de Pinho, S. J. de e Faria Sousa, F. Schaud, J.-J. Lachat, and J. Coutinho-Netto, "Experimental use of latex biomembrane in conjunctival reconstruction," *Arquivos Brasileiros de Oftalmologia*, vol. 67, no. 1, pp. 27–32, 2004.

[25] T. A. M. Andrade, A. Iyer, P. K. Das et al., "The inflammatory stimulus of a natural latex biomembrane improves healing in mice," *Brazilian Journal of Medical and Biological Research*, vol. 44, no. 10, pp. 1036–1047, 2011.

[26] C. A. C. A. Balabanian, J. Coutinho-Netto, T. L. Lamano-Carvalho, S. A. Lacerda, and L. G. Brentegani, "Biocompatibility of natural latex implanted into dental alveolus of rats," *Journal of Oral Science*, vol. 48, no. 4, pp. 201–205, 2006.

[27] A. L. A. Domingos, S. Tucci Jr, S. B. Garcia, J. d. Bessa Jr, A. J. Cologna, and A. C. P. Martins, "Use of a latex biomembrane for bladder augmentation in a rabbit model: biocompatibility, clinical and histological outcomes," *International Brazilian Journal of Urology*, vol. 35, no. 2, pp. 217–226, 2009.

[28] P. Heher, S. Mühleder, R. Mittermayr, H. Redl, and P. Slezak, "Fibrin-based delivery strategies for acute and chronic wound healing," *Advanced Drug Delivery Reviews*, vol. 129, pp. 134–147, 2018.

[29] R. Zhao, H. Liang, E. Clarke, C. Jackson, and M. Xue, "Inflammation in chronic wounds," *International Journal of Molecular Sciences*, vol. 17, no. 12, p. 2085, 2016.

[30] A. Kumar, S. K. Bharti, and A. Kumar, "Therapeutic molecules against type 2 diabetes: what we have and what are we expecting?," *Pharmacological Reports*, vol. 69, no. 5, pp. 959–970, 2017.

[31] I. Uçkay, J. Aragón-Sánchez, D. Lew, and B. A. Lipsky, "Diabetic foot infections: what have we learned in the last 30 years?," *International Journal of Infectious Diseases*, vol. 40, pp. 81–91, 2015.

[32] J. Jneid, J. P. Lavigne, B. la Scola, and N. Cassir, "The diabetic foot microbiota: a review," *Human Microbiome Journal*, vol. 5-6, pp. 1–6, 2017.

[33] L. C. Candido, *Nova Abordagem no Tratamento de Feridas*, SENAC, São Paulo, Brazil, 2001.

[34] M. M. Araujo, E. T. Massuda, and M. A. Hyppolito, "Anatomical and functional evaluation of tympanoplasty using a transitory natural latex biomembrane implant from the rubber tree Hevea brasiliensis," *Acta Cirurgica Brasileira*, vol. 27, no. 8, pp. 566–571, 2012.

[35] M. V. M. Ganga, J. Coutinho-Netto, B. O. Colli et al., "Sciatic nerve regeneration in rats by a nerve conduit engineering with a membrane derived from natural latex," *Acta Cirurgica Brasileira*, vol. 27, no. 12, pp. 885–891, 2012.

[36] L. H. Sousa, R. Ceneviva, J. Coutinho Netto, F. Mrué, L. H. de Sousa Filho, and O. de Castro e Silva, "Morphologic evaluation of the use of a latex prosthesis in videolaparoscopic inguinoplasty: an experimental study in dogs," *Acta Cirurgica Brasileira*, vol. 26, Supplement 2, pp. 84–91, 2011.

[37] M. A. C. Frade, J. Coutinho Netto, F. G. Gomes, E. L. Mazzucato, T. A. M. . Andrade, and N. T. Foss, "Curativo de biomembrana vegetal e hipersensibilidade," *Anais Brasileiros de Dermatologia*, vol. 86, no. 5, pp. 885–891, 2011.

[38] I. C. Talieri, J. L. Laus, J. Coutinho-Netto, M. C. R. Luvizotto, and M. C. . Paula, "Natural latex graft in lamellar and penetrating sclerectomies in rabbits," *Ciência Rural*, vol. 39, no. 6, pp. 1815–1822, 2009.

[39] G. E. Quege, M. M. Bachion, R. d. S. L. Junior et al., "Comparison of the activity of fatty essential acids and biomembrane in the microbiota of infected chronic wounds," *Revista Eletrônica de Enfermagem*, vol. 10, no. 4, pp. 890–905, 2008.

[40] M. L. Brandão, J. Coutinho Netto, J. A. Thomazini, J. J. Lachat, V. F. Muglia, and C. E. Piccinato, "Prótese vascular derivada do látex," *Jornal Vascular Brasileiro*, vol. 6, no. 2, pp. 130–141, 2007.

[41] L. C. A. de Sousa, M. R. de Toledo Piza, J. Coutinho-Netto, D. B. Ruiz, and V. B. Schmidt, "Biomembrana de látex: novo método para o revestimento da cavidade aberta nas timpanomastoidectomia," *Revista Brasileira de Otorrinolaringologia*, vol. 73, no. 3, pp. 331–336, 2007.

[42] M. d. C. d. Reis, *Sistema indutor de neoformação tecidual para pé diabético com circuito emissor de luz de LEDs e utilização do látex natural*, Universidade de Brasília, 2013, http://repositorio.unb.br/handle/10482/15212.

[43] T. A. M. Andrade, *Modificações teciduais e mecanismos de ação da fração F1 do látex da seringueira Hevea brasiliensis na cicatrização de úlceras cutâneas em ratos diabéticos*, Biblioteca Digital de Teses e Dissertações da Universidade de São Paulo, Ribeirão Preto, Brazil, 2012, http://www.teses.usp.br/teses/disponiveis/17/17138/tde-22022012-094819/.

[44] R. d. M. Nogueira, *Oronasal Fistula in Dog. Single Flap Repair Associated with Angiogenic Protein Factor from Seringueira Latex, in a Collagen Sponge Matrix. Experimental Study*, Universidade Estadual Paulista (UNESP), 2009, https://repositorio.unesp.br/handle/11449/89032.

[45] R. Herculano, *Desenvolvimento de membrana de látex natural para aplicações médicas*, University of São Paulo, 2009, http://www.teses.usp.br/teses/disponiveis/59/59135/tde-05082009-141412/publico/Herculano_RD.pdf.

[46] M. Friolani, *The Use of Rubber Tree Latex Bio-Membrane (Hevea Brasiliensis) in Diaphragmatic Lesion in Rabbits–An Experimental Study*, Universidade Estadual Paulista (UNESP), 2008, https://repositorio.unesp.br/handle/11449/89027.

[47] R. d. S. B. Matos, *Effects of the Natural Latex Biomembrane (Hevea brasiliensis) in Wistar Rat Skin Submitted to Body Thermal Injury by Scalding*, Universidade de São Paulo, 2008, http://www.teses.usp.br/teses/disponiveis/10/10132/tde-23042009-091225/pt-br.php.

[48] F. N. Borsari, *Effect of Implementation of the Membrane of Natural Latex and Extract the Skin of Frogs (Lithobates catesbiana) (Shaw, 1802), in Surgical Wound in Wistar Rats*, Universidade Estadual Paulista (UNESP), 2008, https://repositorio.unesp.br/handle/11449/89058.

[49] T. A. M. de Andrade, *The Activity of the Natural Latex Biomembrane from Hevea brasiliensis Rubber Tree in the New Tissue Formation in Mice*, Biblioteca Digital de Teses e Dissertações da Universidade de São Paulo, Ribeirão Preto, Brazil, 2007, http://www.teses.usp.br/teses/disponiveis/17/17138/tde-08072008-143229/.

[50] M. A. C. Frade, *Leg Ulcer: Clinical Caracterization and Immunohistopathologic Profile on Wound Healing in the Presence of Natural Latex Biomembrane of Rubber Tree Hevea brasiliensis*, Biblioteca Digital de Teses e Dissertações da Universidade de São Paulo, Ribeirão Preto, Brazil, 2003, http://www.teses.usp.br/teses/disponiveis/17/17138/tde-17042012-215000/.

[51] S. C. Soares, I. B. Cursi, F. F. Andrade et al., "Úlceras de perna: Tratamento e cicatrização," *Revista Médica Oficial do Hospital Universitário da UFJF*, vol. 30, no. 2, pp. 16–19, 2004.

Hindawi
Journal of Diabetes Research
Volume 2019, Article ID 9426014, 10 pages
https://doi.org/10.1155/2019/9426014

Research Article

Glucagon-Like Peptide-1 Receptor Agonist Protects Dorsal Root Ganglion Neurons against Oxidative Insult

Mohammad Sarif Mohiuddin,[1] Tatsuhito Himeno,[1] Rieko Inoue,[1] Emiri Miura-Yura,[1] Yuichiro Yamada,[1] Hiromi Nakai-Shimoda,[1] Saeko Asano,[1] Makoto Kato,[1] Mikio Motegi,[1] Masaki Kondo,[1] Yusuke Seino,[2] Shin Tsunekawa,[1] Yoshiro Kato,[1] Atsushi Suzuki,[2] Keiko Naruse,[3] Koichi Kato,[4] Jiro Nakamura,[1] and Hideki Kamiya[1]

[1]*Division of Diabetes, Department of Internal Medicine, Aichi Medical University School of Medicine, Nagakute, Japan*
[2]*Division of Endocrinology and Metabolism, Department of Internal Medicine, Fujita Health University School of Medicine, Toyoake, Aichi, Japan*
[3]*Department of Internal Medicine, Aichi Gakuin University School of Dentistry, Nagoya, Japan*
[4]*Department of Medicine, Aichi Gakuin University School of Pharmacy, Nagoya, Japan*

Correspondence should be addressed to Hideki Kamiya; hkamiya@aichi-med-u.ac.jp

Received 15 August 2018; Revised 23 November 2018; Accepted 30 December 2018; Published 21 February 2019

Guest Editor: Julia M. dos Santos

Objective. Diabetic polyneuropathy (DPN) is one of the most prevalent diabetic complications. We previously demonstrated that exendin-4 (Ex4), a glucagon-like peptide-1 receptor agonist (GLP-1RA), has beneficial effects in animal models of DPN. We hypothesized that GLP-1 signaling would protect neurons of the peripheral nervous system from oxidative insult in DPN. Here, the therapeutic potential of GLP-1RAs on DPN was investigated in depth using the cellular oxidative insult model applied to the dorsal root ganglion (DRG) neuronal cell line. *Research Design and Methods*. Immortalized DRG neuronal 50B11 cells were cultured with and without hydrogen peroxide in the presence or absence of Ex4 or GLP-1(7-37). Cytotoxicity and viability were determined using a lactate dehydrogenase assay and MTS (3-(4,5-dimethylthiazol-2-yl)-5-(3-carboxymethoxyphenyl)-2-(4-sulfophenyl)-2H-tetrazolium inner salt), respectively. Antioxidant enzyme activity was evaluated using a superoxide dismutase assay. Alteration of neuronal characteristics of 50B11 cells induced by GLP-1RAs was evaluated with immunocytochemistry utilizing antibodies for transient receptor potential vanilloid subfamily member 1, substance P, and calcitonin gene-related peptide. Cell proliferation and apoptosis were also examined by ethynyl deoxyuridine incorporation assay and APOPercentage dye, respectively. The neurite projection ratio induced by treatment with GLP-1RAs was counted. Intracellular activation of adenylate cyclase/cyclic adenosine monophosphate (cAMP) signaling was also quantified after treatment with GLP-1RAs. *Results*. Neither Ex4 nor GLP-1(7-37) demonstrated cytotoxicity in the cells. An MTS assay revealed that GLP-1RAs amended impaired cell viability induced by oxidative insult in 50B11 cells. GLP-1RAs activated superoxide dismutase. GLP-1RAs induced no alteration of the distribution pattern in neuronal markers. Ex4 rescued the cells from oxidative insult-induced apoptosis. GLP-1RAs suppressed proliferation and promoted neurite projections. No GLP-1RAs induced an accumulation of cAMP. *Conclusions*. Our findings indicate that GLP-1RAs have neuroprotective potential which is achieved by their direct actions on DRG neurons. Beneficial effects of GLP-1RAs on DPN could be related to these direct actions on DRG neurons.

1. Introduction

Among many significant diabetic complications, diabetic polyneuropathy (DPN) is one of the most prevalent complications and causes nontraumatic amputations of lower limbs [1]. Due to the lack of therapies to address the etiology of neurodegeneration in the peripheral nervous system (PNS) of diabetic patients, glucose-lowering therapy is

the only effective therapy to prevent the onset and progression of DPN [2]. In the current study, we investigated the beneficial effects of glucagon-like peptide-1 (GLP-1) signaling in neurons of the PNS using an *in vitro* model of DPN.

GLP-1, an incretin hormone which lowers blood glucose levels through enhancement of glucose-stimulated insulin secretion (GSIS), also has pleiotropic effects. In nervous systems, GLP-1 has a regulatory effect on food intake through the intermediary of the vagus nerve and the central nervous system (CNS) [3–7]. It is known that GLP-1 activates adenylate cyclase and employs cAMP as a second messenger to enhance GSIS in pancreatic beta cells [8, 9]. The cAMP signaling has been proven to stimulate neurite outgrowth [10, 11] and antagonize apoptosis of PNS neurons or PC12 cells [12]. In some kinds of nonneural cells including pancreatic beta cells and cardiomyocytes, antiapoptotic effects of GLP-1 receptor agonists (GLP-1RAs) have been also shown [13–16]. Additionally, it has been reported that activation of GLP-1 signaling modified cell fate and differentiation in pancreatic beta cells [17, 18]. GLP-1 signaling induced *in vivo* reprogramming of pancreatic exocrine cells into beta cells [17] and *in vitro* differentiation of human embryonic stem cells into insulin-producing cells [19].

Previously, we reported the beneficial effects of exendin-4 (Ex4) (also known as exenatide), a GLP-1RA, in the PNS of diabetic mice [20]. In that prior study, we indicated the improvement of DPN using an *in vivo* model but the mechanism of the favorable effects on the PNS has not yet been identified. Although we have proven that the elongation of neurite outgrowth using a tissue culture system of mouse dorsal root ganglion (DRG) was accelerated by supplementation of Ex4 or GLP-1, detailed effects of GLP-1RAs in the DRG should be still elucidated.

Among various mechanisms of pathogenesis in DPN, chronic inflammation followed by oxidative stress has been highlighted by several researchers [21, 22]. For instance, cyclooxygenase-2-deficient mice were protected from dysfunction of the PNS in experimental diabetes [23]. Given that oxidative stress due to various biological pathways, including chronic low-grade inflammation, has been suggested as a pathogenesis and a therapeutic target of DPN [21, 24, 25], we attempted to provide oxidative stress in our culture system. However, it remains to be clarified which factor is crucial in the pathology of DPN, e.g., glucotoxicity, insulin resistance, or lipotoxicity [21]. Therefore, we provided oxidative insult by hydrogen peroxide, which is a widely used oxidant in experimental settings and converts into the stronger oxidant hydroxyl radical, in the cell culture system of the DRG neuron cell line to reproduce DPN pathology in this study.

2. Materials and Methods

Unless noted otherwise, all reagents and materials were purchased from Thermo Fisher Scientific (Waltham, MA, USA).

2.1. Cell Culture. The DRG neuronal cell line (50B11) established and kindly provided by Dr. A. Höke (Johns Hopkins University, Baltimore, MD, USA) [26] was incubated at 37°C under 5% CO_2 in media consisting of Neurobasal™ medium supplemented with 5% fetal bovine serum, 2 mM L-glutamine, and B-27 supplement. 50B11 cells were kept in uncoated plastic tissue culture dishes and regularly passaged once a week with a 1 : 10-1 : 20 split ratio. For each experiment as described in the sections, cells were treated with Ex4 (0.1 nM, 1 nM, 10 nM, and 100 nM), human GLP-1(7-37) (1 nM, 10 nM), or 10 μM forskolin. Oxidative insult was induced by hydrogen peroxide (0.01 mM, 0.05 mM, and 0.1 mM).

2.2. Cell Cytotoxicity Assay. Cells were seeded into 96-well plates at a density of 1×10^4 cells/well in 100 μl medium. Cell cytotoxicity was assessed using lactate dehydrogenase (LDH) assay (Cytotoxicity LDH Assay Kit-WST, Dojindo Laboratories, Mashiki, Japan) following the manufacturer's instructions. The absorbance at 490 nm was measured on a microplate reader (VersaMax, Molecular Devices, Sunnyvale, CA, USA). Cytotoxicity was calculated by the following formula: cytotoxicity (%) = (sample OD – low control OD)/(high control OD – low control OD) × 100 (OD: optical density). Each OD value was calculated by subtracting the background value from each absorbance value.

2.3. Immunocytochemistry. To exclude the possibility of alteration in neuronal characteristics by GLP-1RAs which might induce a reprogramming of cell fate, the characteristics as a sensory neuronal cell were evaluated with the distribution of neuronal markers: transient receptor potential vanilloid subfamily member 1 (TRPV1), substance P, and calcitonin gene-related peptide (CGRP). After a 36-hour culture with or without 100 nM Ex4 or 10 nM GLP-1, DRG cells were fixed with 4% paraformaldehyde for 15 minutes. The cells were blocked with 1% bovine serum albumin, and the following primary antibodies were applied at 4°C overnight: rabbit polyclonal anti-TRPV1 antibody (1 : 200; Neuromics, Northfield, MN, USA), goat polyclonal anti-substance P antibody (1 : 200; Santa Cruz, Santa Cruz, CA, USA), and goat polyclonal anti-CGRP antibody (1 : 200; Santa Cruz). After washing, the following secondary antibodies were loaded for 1 hour at room temperature in a dark box: Alexa Fluor™ 594-coupled goat anti-rabbit IgG antibody (1 : 500) or Alexa Fluor™ 488-coupled donkey anti-goat antibody (1 : 500). Images were captured by a charge-coupled device (CCD) camera using a fluorescence microscope (IX73, Olympus Optical, Tokyo, Japan).

2.4. Cell Viability Assay. To elucidate the effects of GLP-1RAs in DRG neurons under oxidative stress, cell viability of DRG neurons cultured with or without hydrogen peroxide in the presence or absence of GLP-1RAs was assessed. A 3-(4,5-dimethylthiazol-2-yl)-5-(3-carboxymethoxyphenenyl)-2-(4-sulfophenyl)-2H-tetrazolium inner salt (MTS) assay, which correlated mitochondrial activity, was employed to measure cell viability in DRG neurons. Cells were seeded into 96-well plates at a density of 1×10^4 cells/well in 100 μl medium. Cell viability was determined 24 hours after treatment using the CellTiter96™ AQueous One Solution Cell Proliferation Assay (Promega Corporation, Madison, WI, USA), which employed

tetrazolium compound MTS, according to the manufacturer's protocol. The absorbance at 490 nm was measured on a microplate reader (VersaMax).

2.5. Superoxide Dismutase- (SOD-) Like Activity. To evaluate antioxidant activity, SOD-like activity was measured using an SOD-like assay kit (Dojindo Inc., Kumamoto, Japan) according to the manufacturer's instructions [27]. Equal amounts of protein, as determined using a bicinchoninic acid protein assay (Wako Pure Chemical Inc., Osaka, Japan), were applied. Cells were seeded into 96-well plates at a density of 1×10^4 cells/well in 100 μl medium. After 24 hours, cells were supplemented with GLP-1RAs (10 nM GLP-1, 100 nM Ex4) or left untouched. After 12 hours of treatment with/without GLP-1RAs, the media were replaced with media containing 0.1 mM hydrogen peroxide. SOD-like activity was determined 30 minutes after the exposure with hydrogen peroxide.

2.6. Apoptosis Assay. For the apoptosis assay, 50B11 cells were seeded into 24-well plates at a density of 5×10^4 cells/-well. Apoptosis was induced by 0.1 mM hydrogen peroxide. The degree of apoptosis was assessed using the APOPercentage assay (Biocolor, Belfast, Northern Ireland, UK), which was performed according to the manufacturer's instructions. The APOPercentage assay is a dye uptake assay, which stains only the apoptotic cells with a purple dye [28]. Apoptotic cells were assessed after a 3-hour exposure to hydrogen peroxide with or without GLP-1RAs (GLP-1, Ex4) and forskolin. Absorption was measured at 550 nm using a microplate reader (VersaMax).

2.7. Cell Proliferation Assay. An ethynyl deoxyuridine (EdU) incorporation assay was performed using the Click-iT Plus EdU Proliferation Kit (Life Technologies Inc., Gaithersburg, MD). Cells were treated with 10 μM EdU for 24 hours, then harvested, and fixed with 4% paraformaldehyde for 20 minutes. For EdU detection, cells were incubated with Alexa Fluor™ 488 Azide for 15 minutes and then counter stained with 4′,6-diamidino-2-phenylindole (DAPI) [29, 30]. The rate of proliferating cells was determined by the number of EdU-incorporating cells divided by that of DAPI-positive cells.

2.8. Neurite Outgrowth Assay in 50B11 Cells. As it has been verified that the 50B11 neuronal cell line can elongate neurites by stimulation with forskolin, the neurite outgrowth induced by GLP-1RAs was also examined to afford collateral evidence of the neuroregenerative ability in DRG neurons. 50B11 cells were plated into 6-well plates at a density of 1×10^4 cells/well. Twenty-four hours after the passage of the cells, cells were unexposed or exposed to the indicated compounds for 24 h. Images of the cells were captured by a contrast-phase microscope equipped with a CCD camera and counted for neurite outgrowth which was defined as a process equal to or greater than cell bodies in length [31].

2.9. Cyclic Adenosine Monophosphate (cAMP) Assay. Cellular cAMP production was measured using an enzyme immunoassay kit (Cayman Chemical, Ann Arbor, MI, USA) [32, 33]. Cells were seeded into 6-well plates at a density of 5×10^5 cells/well. The media were aspirated 20 or 120 minutes after exposure to test substances, and 250 μl of 0.1 N HCl was introduced. After 20 minutes incubation at room temperature, cells were scraped and centrifuged. The supernatants were stored at -80°C until the time of measurement. For the experiment with 120-minute exposure to test substances, the medium contained 0.5 mM 3-isobutyl-1-methyl xanthine (IBMX), a phosphodiesterase inhibitor, to inhibit cAMP degradation.

2.10. Statistical Analysis. All the group values were expressed as means ± standard deviation. Data are representative of at least three independent experiments. The normality of distribution was tested by the Kolmogorov-Smirnov test using R version 3.4.3 (http://www.r-project.org/, Vienna, Austria,). Statistical analyses were made by Student's t-test or one-way ANOVA with the Bonferroni correction for multiple comparisons using StatView version 5.0 (SAS Institute, Cary, NC). The threshold of statistical significance was taken as a value of $p < 0.05$. All analyses were performed by personnel unaware of the identities of culture conditions.

3. Results

3.1. No Cytotoxicity Was Introduced by GLP-1RAs in DRG Neurons. There was no significant cytotoxicity induced after 24 hour exposure to Ex4 (0.1 mM, 1 nM, 10 nM, or 100 nM) or GLP-1 (1 nM, 10 nM) (absorbance at 490 nm: control 0.449 ± 0.023, 0.1 nM Ex4 0.414 ± 0.027, 1 nM Ex4 0.355 ± 0.020, 10 nM Ex4 0.433 ± 0.129, 100 nM Ex4 0.444 ± 0.034, 1 nM GLP-1 0.408 ± 0.064, and 10 nM GLP-1 0.424 ± 0.046) (Figure 1). Neurons were also exposed to an adenylate cyclase activator, forskolin. The treatment with 10 μM forskolin did not induce any significant difference in cytotoxicity (10 μM forskolin 0.371 ± 0.029).

3.2. Sensory Neuronal Characteristics in Protein Marker Expressions Were Not Affected by GLP-1RAs. Ex4 or GLP-1 (data not shown) induced no evident changes in the distribution pattern of these sensory neuronal markers compared with neurons without those treatments (Figure 2).

3.3. Cell Viability Was Enhanced in DRG Neurons Cultured with GLP-1RAs. The cell viability of DRG neurons treated with 0.1 mM hydrogen peroxide for 4 hours was significantly decreased compared with that of cells cultured with no hydrogen peroxide (control 100 ± 8.1%, 0.1 mM hydrogen peroxide 54.3 ± 2.1, $p < 0.01$) (Figure 3). However, the treatment with Ex4 or GLP-1 significantly ameliorated cell viability compared with cells with no treatment (0.1 nM Ex4 85.1 ± 13.3, 1 nM Ex4 86.0 ± 6.4, 10 nM Ex4 86.9 ± 6.5, 100 nM Ex4 87.5 ± 3.2, 1 nM GLP-1 94.3 ± 11.7, and 10 nM GLP-1 92.6 ± 2.9). The supplementation with 10 μM forskolin also inhibited the decrease of cell viability (84.5 ± 2.6, $p < 0.005$).

3.4. SOD-Like Activity Increased in the Sensory Neurons Supplemented with GLP-1RAs. Following exposure to oxidative insult with hydrogen peroxide, SOD-like activity

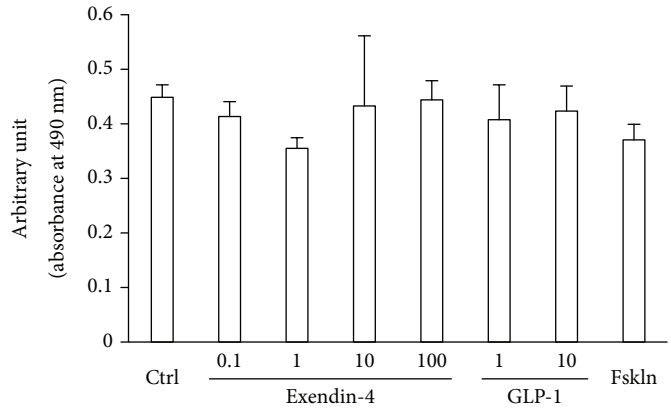

Figure 1: Cell cytotoxicity of GLP-1 receptor agonists (GLP-1RAs) in dorsal root ganglion (DRG) neurons. Cytotoxicity was determined 24 hours after treatment with GLP-1RAs or forskolin using LDH assay. No significant difference was detected between neurons treated with GLP-1RAs or forskolin and those without treatment (control). Concentrations of GLP-1RAs; exendin-4: 0.1, 1, 10, and 100 nM; GLP-1: 1, 10 nM. Ctrl: control; Fskln: forskolin; error bar: standard deviation. $n = 3$ in each group.

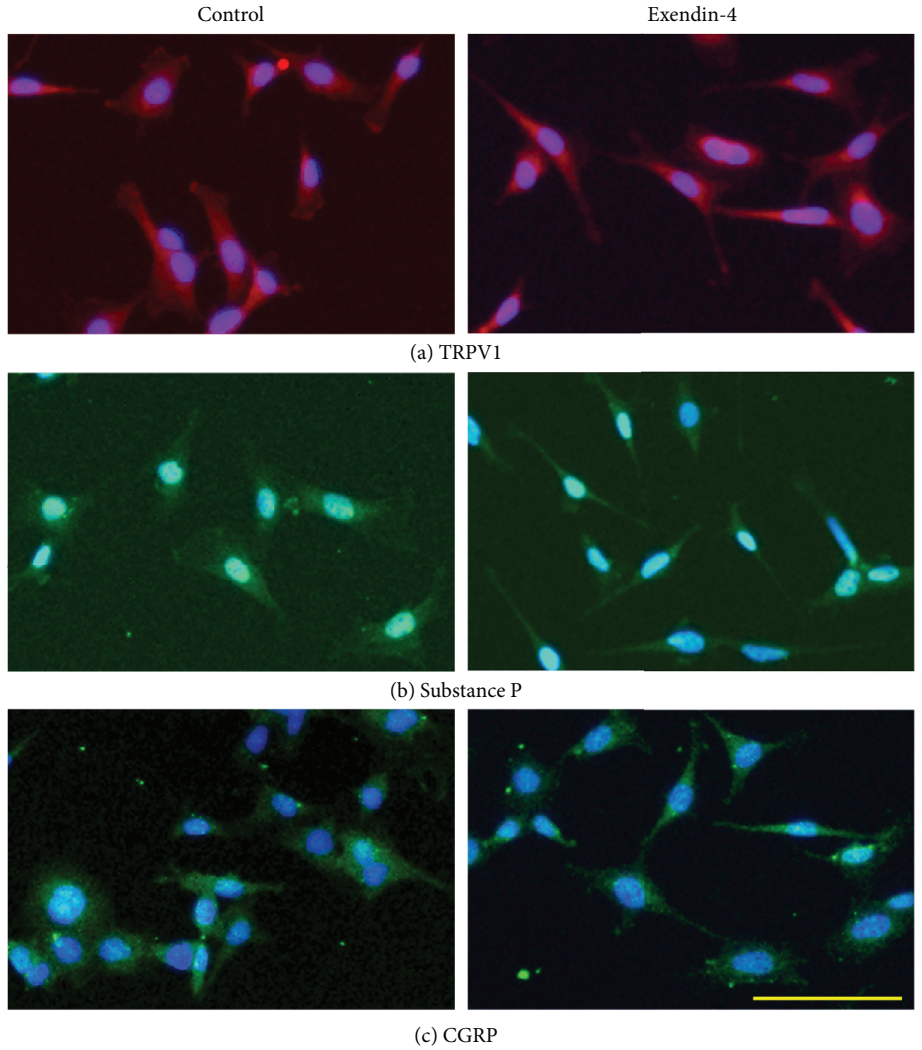

Figure 2: Distribution of sensory neuronal markers in the dorsal root ganglion (DRG) neuron cell line treated with exendin-4. Pictures on the left side are neurons without any treatment. Pictures on the right side are neurons treated with 100 nM exendin-4 for 36 hours. TRPV1: red (a), substance P: green (b), CGRP: green: DAPI (c), scale 100 μm.

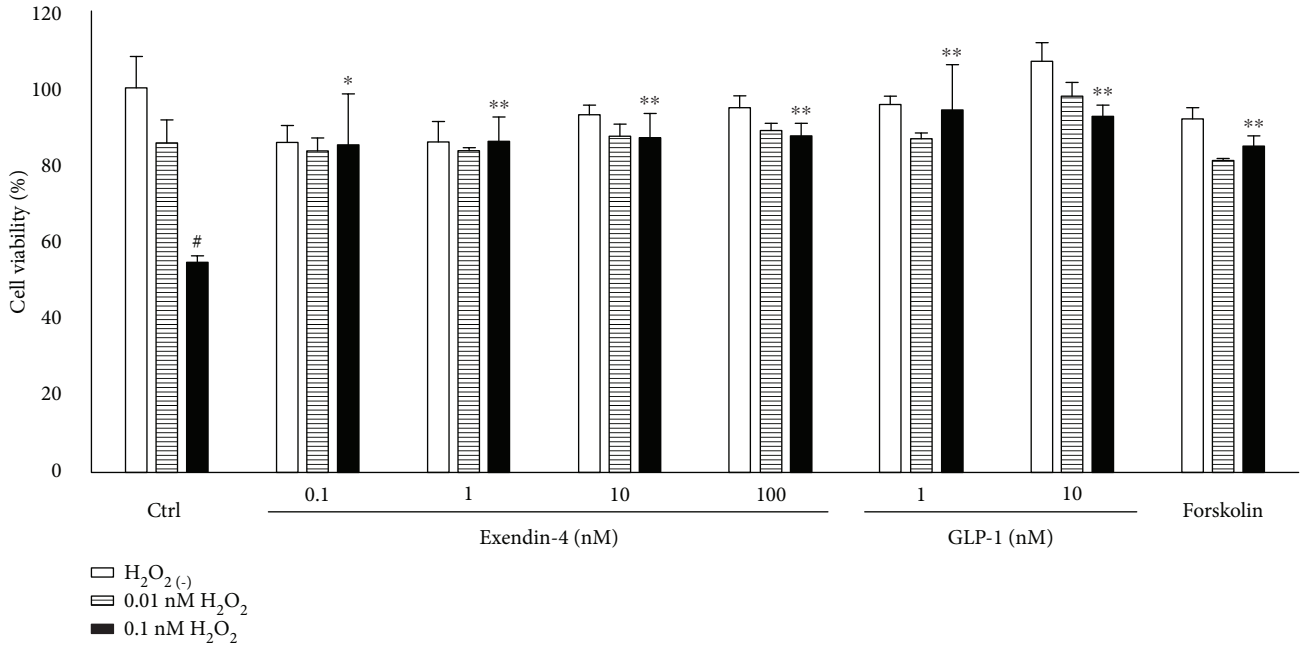

Figure 3: Cell viability in dorsal root ganglion (DRG) neurons treated with GLP-1 receptor agonists. Cell viability was quantified using 3-(4,5-dimethylthiazol-2-yl)-5-(3-carboxymethoxyphenenyl)-2-(4-sulfophenyl)-2H-tetrazolium inner salt (MTS). Although hydrogen peroxide (H_2O_2) significantly decreased the cell viability of DRG neurons, GLP-1 receptor agonists, exendin-4 and GLP-1, and forskolin, an activator of adenylate cyclase, prevent the reduction of cell viability induced by H_2O_2. White bar: no supplementation of H_2O_2; hatched bar: 0.01 mM H_2O_2; filled bar: 0.1 mM H_2O_2; Ctrl: control; H_2O_2: hydrogen peroxide; $^{\#}p < 0.01$ versus control without H_2O_2; $^{*}p < 0.05$ versus control with 0.1 mM H_2O_2; $^{**}p < 0.005$ versus control with 0.1 mM H_2O_2; error bar: standard deviation. $n = 3$ in each group.

increased in neurons supplemented with GLP-1 or Ex4 (cells with no hydrogen peroxide 40.4 ± 6.7%, 10 nM GLP-1 with 0.1 mM hydrogen peroxide 54.3 ± 5.8, and 100 nM Ex4 with 0.1 mM hydrogen peroxide 59.9 ± 8.4, $p < 0.001$ versus cells with no hydrogen peroxide in each GLP-1RA-supplemented group) (Figure 4).

3.5. Apoptosis Was Prevented in the Neurons Supplemented with Ex4. Apoptosis evoked by 0.1 mM hydrogen peroxide was detected using the APOPercentage assay (Figure 5). The degree of apoptosis was significantly decreased in the neurons supplemented with 100 nM Ex4 (absorbance at 550 nm: control 0.304 ± 0.017, 100 nM Ex4 0.250 ± 0.014, $p < 0.0001$) and 10 μM forskolin (0.199 ± 0.016, $p < 0.0001$). However, GLP-1 produced no significant change in the apoptosis assay (0.299 ± 0.03, $p = 0.623$).

3.6. Cell Proliferation Was Suppressed by GLP-1RAs. The EdU incorporation assay revealed a decrease of proliferation rate of neurons cultured with 10 nM GLP-1 or 100 nM Ex4 (control 87.7%±5.6%, GLP-1 75.5 ± 10.4, and Ex4 74.1 ± 14.4) (Figure 6). However, forskolin had no significant effect on the proliferation rate (forskolin: 86.9 ± 6.2).

3.7. Neurite Outgrowth Was Induced with GLP-1RAs. The percentage of neurons with neurite(s) increased in the neurons cultured with Ex4 or GLP-1 compared with the control (control 8.7%±5.1%, 100 nM Ex4 28.2 ± 4.0, and 10 nM GLP-1 23.3 ± 6.5, $p < 0.0001$ for both cases versus control) (Figure 7).

3.8. The Adenylate Cyclase/cAMP Pathway Was Not Activated by GLP-1RAs in DRG Neurons. Cyclic AMP levels after stimulation with GLP-1RAs and forskolin were determined. After 20 minutes of stimulation with 10 μM forskolin, cAMP had accumulated in the neurons (control: 5.3 ± 0.3 pmol/ml, 10 μM forskolin: 234.5 ± 6.3, $p < 0.0001$) (Figure 8). However, no accumulation of cAMP was detected in the neurons treated with Ex4 and GLP-1 (10 nM GLP-1: 3.3 ± 0.4, 100 nM Ex4: 4.0 ± 0.4). Longer exposure to GLP-1RAs supplemented with a phosphodiesterase inhibitor also generated no significant cAMP accumulation (Supplemental figure available here).

4. Discussion

In this decade, drug development targeting GLP-1 signaling has been considered as a prospective therapy of type 2 diabetes. A novel GLP-1RA semaglutide which can be orally administered would accelerate popularization of GLP-1RAs in clinical settings [34]. Furthermore, the neuroprotective effects of Ex4 have been already proven in one clinical trial of Parkinson's disease [35]. Therefore, if the neuroprotective effects of GLP-1RAs are accepted amongst the scientific community, a drug repositioning strategy of GLP-1RAs targeting other diseases will be promising, especially in diabetic complications including DPN.

In the current study, we investigated the neuroprotective effects of GLP-1RAs in the DRG neuronal cell line. First, we examined the neurotoxicity of GLP-1RAs in the DRG neurons. Second, we examined the effect of GLP-1RA on cell

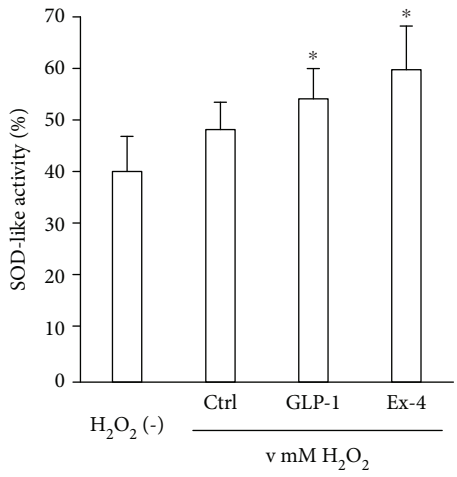

Figure 4: Superoxide dismutase- (SOD-) like activity in dorsal root ganglion (DRG) neurons treated with glucagon-like peptide-1 (GLP-1) receptor agonists. Oxidative insult induced by 30-minute treatment with 0.1 mM hydrogen peroxide increased SOD-like activity in the neurons supplemented with 10 nM GLP-1 or 100 nM exendin-4. $^*p < 0.001$ versus no treated cell with H_2O_2. H_2O_2: hydrogen peroxide; Ctrl: control; GLP-1: cells supplemented with 10 nM GLP-1; Ex-4: cells supplemented with 100 nM exendin-4. Error bar means standard deviation. $n = 6$ or 7 in each group.

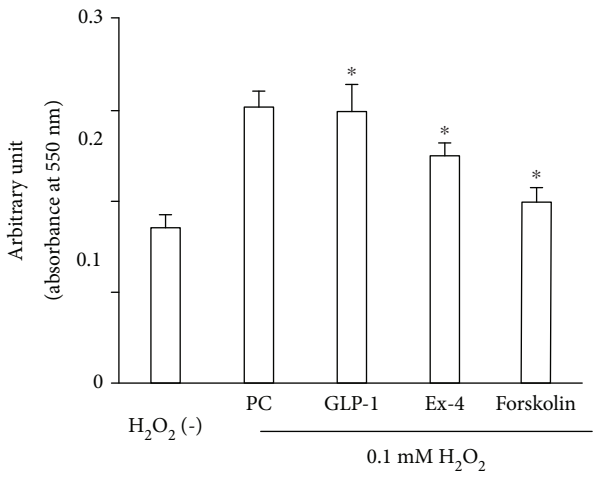

Figure 5: Apoptosis in dorsal root ganglion (DRG) neurons treated with exendin-4. Apoptosis induced by 3-hour treatment with 0.1 mM hydrogen peroxide was partially inhibited in the neurons supplemented with 100 nM exendin-4 or 10 μM forskolin. $^*p < 0.05$ versus control; H_2O_2: hydrogen peroxide; PC: positive control of apoptosis; GLP-1: glucagon-like peptide-1; Ex-4: exendin-4. Error bar means standard deviation. $n = 8$ in each group.

viability, antioxidant enzyme activity, and apoptosis in the DRG neurons. We confirmed enhanced cell viability, increased activity of antioxidant enzyme SOD, and inhibition of apoptosis with GLP-1RA supplementation. We then demonstrated that treatment with GLP-1RAs reduced cell proliferation and promoted neurite outgrowth of DRG neurons. Although these significant changes were seemed to be evoked

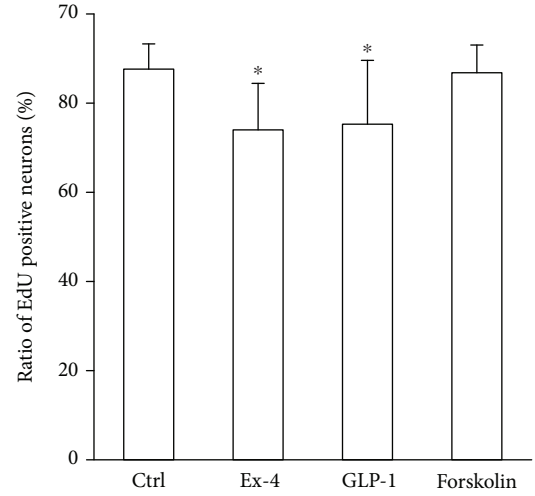

Figure 6: Proliferation rate of dorsal root ganglion (DRG) neurons treated with GLP-1 receptor agonists. Proliferation rate assessed by EdU assay revealed that both GLP-1 receptor agonists, exendin-4 and GLP-1, suppressed proliferation of DRG neurons. Ctrl: control; Ex-4: cells supplemented with 100 nM exendin-4; GLP-1: cells supplemented with 10 nM GLP-1; $^*p < 0.05$ versus control; error bar: standard deviation. $n = 9$ in each group.

by activation of the adenylate cyclase/cAMP pathway, no evident accumulation of intracellular cAMP was generated by stimuli with GLP-1RAs.

GLP-1RAs have previously been shown to promote neurite outgrowth in PC12 cells, a rat pheochromocytoma cell type [36, 37]. However, no report has investigated the direct pharmacological function of GLP-1RAs in the cells of the PNS, e.g. DRG neurons, Schwann cells, vascular endothelial cells in peripheral nerves. Some research studies, including our previous study, have already reported *in vivo* beneficial effects of GLP-1RAs in the disorders of the PNS [20, 38]. The current study would support these beneficial effects through verification of the direct effects of GLP-1RAs on DRG neurons.

A number of DPN pathogenesis mechanisms have been postulated in experimental studies, including the polyol pathway, advanced glycation end products, poly ADP-ribose polymerase, the protein kinase C pathway, and oxidative stress [39, 40]. In the current study, we chose oxidative stress to represent an *in vitro* DPN model. To verify the novel *in vitro* experimental system for investigation of DPN, we confirmed the characteristics of a 50B11 cell line as DRG neurons and induced oxidative insult on the cell line. After the confirmation of no cytotoxicity of GLP-1RAs and forskolin in 50B11, we evaluated the neuronal characteristics of the cells. The markers of a primary sensory neuron including TRPV1, substance P, and CGRP were expressed in 50B11 even after the treatment with GLP-1RAs. Furthermore, we successfully performed the neurite outgrowth assay, which is accepted as one of the crucial neuronal assays in a sympathetic-like neuron cell line PC12 [31]. As oxidative stress is one of the primary factors according to the prevailing views of DPN pathogenesis [39], we attempted to produce the pathogenesis utilizing hydrogen peroxide in the neuronal

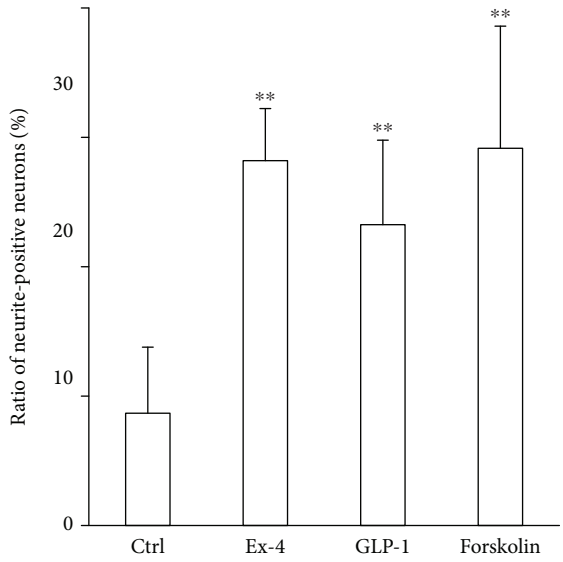

Figure 7: Neurite outgrowth of dorsal root ganglion (DRG) neurons. The ratio of neurite-positive neurons increased in cells supplemented with GLP-1 receptor agonists, exendin-4 and GLP-1, as well as cells which were supplemented with forskolin. Ctrl: control; Ex-4: cells supplemented with 100 nM exendin-4; GLP-1: cells supplemented with 10 nM GLP-1; forskolin: cells supplemented with 10 nM forskolin; $^{**}p < 0.001$ versus control; error bar: standard deviation. $n = 9$ or 15 in each group.

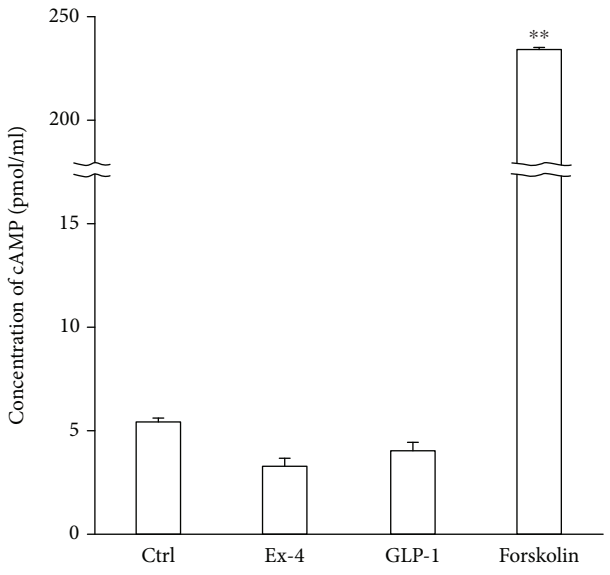

Figure 8: Intracellular cyclic adenylate monophosphate (cAMP) accumulation in neurons treated with GLP-1 receptor agonists. The cAMP accumulation was measured 20 minutes after exposure to 100 nM exendin-4, 10 nM GLP-1, or 10 μM forskolin. Both GLP-1 receptor agonists, exendin-4 and GLP-1, provoked no significant cAMP accumulation. Ex-4: cells supplemented with 100 nM exendin-4; $^{**}p < 0.001$ versus control; error bar: standard deviation. $n = 5$ or 6 in each group.

cell culture. Although, in clinical settings, several factors including dyslipidemia, hyperglycemia, hypertension, and smoking are considered to be risk factors of DPN [41], the significance of each oxidation mechanism derived from glucose, proteins, or lipids is unclear in the pathogenesis of DPN. Therefore, we utilized hydrogen peroxide, which is considered to be one of the most important reactive oxygen species because it crosses membranes and yields hydroxyl radicals via Fenton reaction in cells [42], as an oxidative insult-mimicking oxidative stress in DPN. As a result, hydrogen peroxide provoked an increase of antioxidant SOD in 50B11 cells. These experiments verified our experimental system as a novel approach to investigate DPN.

However, we must recognize some limitations of our study. As it is known that the incretin/adenylate cyclase/-cAMP pathway is critical for insulin secretion in pancreatic beta cells [43] and neuroprotective effect in the CNS neurons [9], we compared pharmacological effects of GLP-1RAs with those of forskolin, an activator of adenylate cyclase, in DRG neurons. We proved the antiapoptotic effect of Ex4 and forskolin and the decrease of cell proliferation by GLP-1RAs. These findings were consistent with the previous report in which liraglutide, another GLP-1RA, potentiated cell viability and prevented apoptosis via cAMP signaling in SH-SY5Y neuroblastoma cells [44]. Furthermore, neurite outgrowth was induced by GLP-1RAs and forskolin. Given that background, these changes appear to indicate the activation of intracellular adenylate cyclase/cAMP signaling by GLP-1RAs as well as forskolin. However, unexpectedly, cAMP accumulation was not evident in the neurons cultured with GLP-1RAs for 20 or 120 minutes. This unexpected finding could be caused by the experimental limitation that our cAMP measurement kit was able to examine only the endpoint accumulation of cAMP. The activation of adenylate cyclase induced by GLP-1RAs might be more transient than we expected. Therefore, in the future, we would like to measure cAMP accumulation utilizing a real-time detection system.

Furthermore, we should consider scrutinizing other signaling pathways which have been reported to be initiated by GLP-1RAs. It is known that p44/42 mitogen-activated protein kinase (also called ERK1/2) can be also activated by GLP-1 in pancreatic beta cells [45]. It is also shown that the antiapoptotic effect of GLP-1 is mediated by ERK1/2 activation in beta cells [46]. Therefore, the antiapoptotic effect shown in the current study might be mediated by activation of ERK1/2 signaling.

Another limitation is the immortalization of the neurons. As the DRG neuronal cell line 50B11 cells are immortalized neurons, the differences between nonproliferative neurons collected from mammalians and the genetically engineered neurons should be taken into account. It was reported that an activation of phosphoinositide-3-kinase (PI3K) induced by GLP-1 in the beta cell line accelerated mitosis of the cells [47]. However, in this study, EdU incorporation was decreased by administration of GLP-1RAs. To address this conflict, in the future, we would clarify the involvement of PI3K signaling in sensory neurons [45, 46, 48].

5. Conclusions

This study is the first report to investigate the neuroprotective effects of GLP-1RAs on DRG neurons. The beneficial

effects of GLP-1RAs in DPN might be attributable to the direct neuroprotective effects of GLP-1RAs on DRG neurons through protection from cellular oxidative insult.

At the same time, we successfully verified the novel *in vitro* experimental system for investigation of DPN.

Abbreviations

cAMP: Cyclic adenosine monophosphate
CCD: Charge-coupled device
CGRP: Calcitonin gene-related peptide
CNS: Central nervous system
DAPI: 4′,6-Diamidino-2-phenylindole
DRG: Dorsal root ganglion
DPN: Diabetic polyneuropathy
EdU: Ethynyl deoxyuridine
Ex4: Exendin-4
GLP-1: Glucagon-like peptide-1
GLP-1RA: GLP-1 receptor agonist
GSIS: Glucose-stimulated insulin secretion
IBMX: 3-Isobutyl-1-methyl xanthine
LDH: Lactate dehydrogenase
MTS: 3-(4,5-Dimethylthiazol-2-yl)-5-(3-carboxymethoxyphenenyl)-2-(4-sulfophenyl)-2H-tetrazolium inner salt
PNS: Peripheral nervous system
SOD: Superoxide dismutase
TRPV1: Transient receptor potential vanilloid subfamily member 1.

Data Availability

The whole data used to support the findings of this study are available from the corresponding author upon request.

Conflicts of Interest

The authors declare that there is no conflict of interest regarding the publication of this paper.

Acknowledgments

This research was supported in part by the Grant-in-Aid for Scientific Research (15H06720) from the Ministry of Education, Culture, Sports, Science and Technology (MEXT) and Grants for Young Researchers from the Japan Association for Diabetes Education and Care. TH was supported by the Manpei Suzuki Diabetes Foundation, Japan Diabetes Foundation, and Aichi Medical University Aikeikai. The authors wish to acknowledge helpful comments and discussions from Prof. Eva L. Feldman. The authors would like to thank Prof. A. Höke for kindly providing 50B11 neuronal cells and Crystal Pacut, Carey Backus, and John M. Hayes for preparing the cell culture system using the 50B11 neuronal cell line.

Supplementary Materials

Supplemental figure: intracellular cyclic adenylate monophosphate (cAMP) accumulation in neurons treated with GLP-1 receptor agonists and a cAMP/cGMP-phosphodiesterase inhibitor. *(Supplementary Materials)*

References

[1] J. R. Singleton and A. G. Smith, "The diabetic neuropathies: practical and rational therapy," *Seminars in Neurology*, vol. 32, no. 3, pp. 196–203, 2012.

[2] S. Genuth, "Insights from the diabetes control and complications trial/epidemiology of diabetes interventions and complications study on the use of intensive glycemic treatment to reduce the risk of complications of type 1 diabetes," *Endocrine Practice*, vol. 12, Supplement 1, pp. 34–41, 2006.

[3] D. Yabe, Y. Seino, and Y. Seino, "Incretin concept revised: the origin of the insulinotropic function of glucagon-like peptide-1 - the gut, the islets or both?," *Journal of Diabetes Investigation*, vol. 9, no. 1, pp. 21–24, 2018.

[4] E. K. Williams, R. B. Chang, D. E. Strochlic, B. D. Umans, B. B. Lowell, and S. D. Liberles, "Sensory neurons that detect stretch and nutrients in the digestive system," *Cell*, vol. 166, no. 1, pp. 209–221, 2016.

[5] Y. Li, S. Chigurupati, H. W. Holloway et al., "Exendin-4 ameliorates motor neuron degeneration in cellular and animal models of amyotrophic lateral sclerosis," *PLoS One*, vol. 7, no. 2, article e32008, 2012.

[6] S. Yamane and N. Inagaki, "Regulation of glucagon-like peptide-1 sensitivity by gut microbiota dysbiosis," *Journal of Diabetes Investigation*, vol. 9, no. 2, pp. 262–264, 2018.

[7] T. Okawa, H. Kamiya, T. Himeno et al., "Sensory and motor physiological functions are impaired in gastric inhibitory polypeptide receptor-deficient mice," *Journal of Diabetes Investigation*, vol. 5, no. 1, pp. 31–37, 2014.

[8] X. Xu, J. Chen, L. Hu et al., "Liraglutide regulates the viability of pancreatic α-cells and pancreatic β-cells through cAMP-PKA signal pathway," *Life Sciences*, vol. 195, pp. 87–94, 2018.

[9] M. Kawatani, Y. Yamada, and M. Kawatani, "Glucagon-like peptide-1 (GLP-1) action in the mouse area postrema neurons," *Peptides*, vol. 107, pp. 68–74, 2018.

[10] A. Piiper, I. Dikic, M. P. Lutz et al., "Cyclic AMP induces transactivation of the receptors for epidermal growth factor and nerve growth factor, thereby modulating activation of MAP kinase, Akt, and neurite outgrowth in PC12 cells," *The Journal of Biological Chemistry*, vol. 277, no. 46, pp. 43623–43630, 2002.

[11] M. G. Sabbir and P. Fernyhough, "Muscarinic receptor antagonists activate ERK-CREB signaling to augment neurite outgrowth of adult sensory neurons," *Neuropharmacology*, vol. 143, pp. 268–281, 2018.

[12] N. K. Huang, Y. W. Lin, C. L. Huang, R. O. Messing, and Y. Chern, "Activation of protein kinase A and atypical protein kinase C by A(2A) adenosine receptors antagonizes apoptosis due to serum deprivation in PC12 cells," *The Journal of Biological Chemistry*, vol. 276, no. 17, pp. 13838–13846, 2001.

[13] X. M. Wu, Q. Y. Ou, W. Zhao, J. Liu, and H. Zhang, "The GLP-1 analogue liraglutide protects cardiomyocytes from high glucose-induced apoptosis by activating the Epac-1/Akt pathway," *Experimental and Clinical Endocrinology & Diabetes*, vol. 122, no. 10, pp. 608–614, 2014.

[14] C. Wang, Q. Li, W. Wang et al., "GLP-1 contributes to increases in PGC-1α expression by downregulating miR-23a

to reduce apoptosis," *Biochemical and Biophysical Research Communications*, vol. 466, no. 1, pp. 33–39, 2015.

[15] Y. Zhao, H. Li, F. Fang et al., "Geniposide improves repeated restraint stress-induced depression-like behavior in mice by ameliorating neuronal apoptosis via regulating GLP-1R/AKT signaling pathway," *Neuroscience Letters*, vol. 676, pp. 19–26, 2018.

[16] K. Kapodistria, E. P. Tsilibary, E. Kotsopoulou, P. Moustardas, and P. Kitsiou, "Liraglutide, a human glucagon-like peptide-1 analogue, stimulates AKT-dependent survival signalling and inhibits pancreatic β-cell apoptosis," *Journal of Cellular and Molecular Medicine*, vol. 22, no. 6, pp. 2970–2980, 2018.

[17] S. Sasaki, T. Miyatsuka, T. A. Matsuoka et al., "Activation of GLP-1 and gastrin signalling induces in vivo reprogramming of pancreatic exocrine cells into beta cells in mice," *Diabetologia*, vol. 58, no. 11, pp. 2582–2591, 2015.

[18] A. Suzuki, H. Nakauchi, and H. Taniguchi, "Glucagon-like peptide 1 (1-37) converts intestinal epithelial cells into insulin-producing cells," *Proceedings of the National Academy of Sciences of the United States of America*, vol. 100, no. 9, pp. 5034–5039, 2003.

[19] H. Hui, Y. G. Tang, L. Zhu et al., "Glucagon like peptide-1-directed human embryonic stem cells differentiation into insulin-producing cells via hedgehog, cAMP, and PI3K pathways," *Pancreas*, vol. 39, no. 3, pp. 315–322, 2010.

[20] T. Himeno, H. Kamiya, K. Naruse et al., "Beneficial effects of exendin-4 on experimental polyneuropathy in diabetic mice," *Diabetes*, vol. 60, no. 9, pp. 2397–2406, 2011.

[21] R. Pop-Busui, L. Ang, C. Holmes, K. Gallagher, and E. L. Feldman, "Inflammation as a therapeutic target for diabetic neuropathies," *Current Diabetes Reports*, vol. 16, no. 3, p. 29, 2016.

[22] E. Akude, E. Zherebitskaya, S. K. R. Chowdhury, D. R. Smith, R. T. Dobrowsky, and P. Fernyhough, "Diminished superoxide generation is associated with respiratory chain dysfunction and changes in the mitochondrial proteome of sensory neurons from diabetic rats," *Diabetes*, vol. 60, no. 1, pp. 288–297, 2011.

[23] A. P. Kellogg, T. D. Wiggin, D. D. Larkin, J. M. Hayes, M. J. Stevens, and R. Pop-Busui, "Protective effects of cycloo xygenase-2 gene inactivation against peripheral nerve dysfunction and intraepidermal nerve fiber loss in experimental diabetes," *Diabetes*, vol. 56, no. 12, pp. 2997–3005, 2007.

[24] L. M. Hinder, C. Figueroa-Romero, C. Pacut et al., "Long--chain acyl coenzyme A synthetase 1 overexpression in primary cultured Schwann cells prevents long chain fatty acid-induced oxidative stress and mitochondrial dysfunction," *Antioxidants & Redox Signaling*, vol. 21, no. 4, pp. 588–600, 2014.

[25] M. Kobayashi and D. W. Zochodne, "Diabetic neuropathy and the sensory neuron: new aspects of pathogenesis and their treatment implications," *Journal of Diabetes Investigation*, vol. 9, no. 6, pp. 1239–1254, 2018.

[26] W. Chen, R. Mi, N. Haughey, M. Oz, and A. Hoke, "Immortalization and characterization of a nociceptive dorsal root ganglion sensory neuronal line," *Journal of the Peripheral Nervous System*, vol. 12, no. 2, pp. 121–130, 2007.

[27] A. V. Peskin and C. C. Winterbourn, "A microtiter plate assay for superoxide dismutase using a water-soluble tetrazolium salt (WST-1)," *Clinica Chimica Acta*, vol. 293, no. 1-2, pp. 157–166, 2000.

[28] A. C. Uguz and M. Naziroglu, "Effects of selenium on calcium signaling and apoptosis in rat dorsal root ganglion neurons induced by oxidative stress," *Neurochemical Research*, vol. 37, no. 8, pp. 1631–1638, 2012.

[29] A. Salic and T. J. Mitchison, "A chemical method for fast and sensitive detection of DNA synthesis in vivo," *Proceedings of the National Academy of Sciences of the United States of America*, vol. 105, no. 7, pp. 2415–2420, 2008.

[30] A. Moutal, L. S. Villa, S. K. Yeon et al., "CRMP2 phosphorylation drives glioblastoma cell proliferation," *Molecular Neurobiology*, vol. 55, no. 5, pp. 4403–4416, 2018.

[31] N. M. Radio, J. M. Breier, T. J. Shafer, and W. R. Mundy, "Assessment of chemical effects on neurite outgrowth in PC12 cells using high content screening," *Toxicological Sciences*, vol. 105, no. 1, pp. 106–118, 2008.

[32] P. Pradelles, J. Grassi, D. Chabardes, and N. Guiso, "Enzyme immunoassays of adenosine cyclic 3′,5′-monophosphate and guanosine cyclic 3′,5′-monophosphate using acetylcholinesterase," *Analytical Chemistry*, vol. 61, no. 5, pp. 447–453, 1989.

[33] T. Iwai, S. Ito, K. Tanimitsu, S. Udagawa, and J. I. Oka, "Glucagon-like peptide-1 inhibits LPS-induced IL-1β production in cultured rat astrocytes," *Neuroscience Research*, vol. 55, no. 4, pp. 352–360, 2006.

[34] M. Davies, T. R. Pieber, M. L. Hartoft-Nielsen, O. K. H. Hansen, S. Jabbour, and J. Rosenstock, "Effect of oral semaglutide compared with placebo and subcutaneous semaglutide on glycemic control in patients with type 2 diabetes: a randomized clinical trial," *JAMA*, vol. 318, no. 15, pp. 1460–1470, 2017.

[35] D. Athauda, K. Maclagan, S. S. Skene et al., "Exenatide once weekly versus placebo in Parkinson's disease: a randomised, double-blind, placebo-controlled trial," *The Lancet*, vol. 390, no. 10103, pp. 1664–1675, 2017.

[36] R. Kimura, M. Okouchi, H. Fujioka et al., "Glucagon-like peptide-1 (GLP-1) protects against methylglyoxal-induced PC12 cell apoptosis through the PI3K/Akt/mTOR/GCLc/redox signaling pathway," *Neuroscience*, vol. 162, no. 4, pp. 1212–1219, 2009.

[37] T. Perry, D. K. Lahiri, D. Chen et al., "A novel neurotrophic property of glucagon-like peptide 1: a promoter of nerve growth factor-mediated differentiation in PC12 cells," *Journal of Pharmacology and Experimental Therapeutics*, vol. 300, no. 3, pp. 958–966, 2002.

[38] T. Perry, H. W. Holloway, A. Weerasuriya et al., "Evidence of GLP-1-mediated neuroprotection in an animal model of pyridoxine-induced peripheral sensory neuropathy," *Experimental Neurology*, vol. 203, no. 2, pp. 293–301, 2007.

[39] R. Pop-Busui, A. J. M. Boulton, E. L. Feldman et al., "Diabetic neuropathy: a position statement by the American Diabetes Association," *Diabetes Care*, vol. 40, no. 1, pp. 136–154, 2017.

[40] S. Sifuentes-Franco, F. P. Pacheco-Moisés, A. D. Rodríguez--Carrizalez, and A. G. Miranda-Díaz, "The role of oxidative stress, mitochondrial function, and autophagy in diabetic polyneuropathy," *Journal Diabetes Research*, vol. 2017, article 1673081, 15 pages, 2017.

[41] B. C. Callaghan, H. T. Cheng, C. L. Stables, A. L. Smith, and E. L. Feldman, "Diabetic neuropathy: clinical manifestations and current treatments," *Lancet Neurology*, vol. 11, no. 6, pp. 521–534, 2012.

[42] J. A. Imlay, S. M. Chin, and S. Linn, "Toxic DNA damage by hydrogen peroxide through the Fenton reaction in vivo and in vitro," *Science*, vol. 240, no. 4852, pp. 640–642, 1988.

[43] M. Iwasaki, K. Minami, T. Shibasaki, T. Miki, J. I. Miyazaki, and S. Seino, "Establishment of new clonal pancreatic β-cell

lines (MIN6-K) useful for study of incretin/cyclic adenosine monophosphate signaling," *Journal of Diabetes Investigation*, vol. 1, no. 4, pp. 137–142, 2010.

[44] Y. Li, M. Bader, I. Tamargo et al., "Liraglutide is neurotrophic and neuroprotective in neuronal cultures and mitigates mild traumatic brain injury in mice," *Journal of Neurochemistry*, vol. 135, no. 6, pp. 1203–1217, 2015.

[45] D. Arnette, T. B. Gibson, M. C. Lawrence et al., "Regulation of ERK1 and ERK2 by glucose and peptide hormones in pancreatic beta cells," *The Journal of Biological Chemistry*, vol. 278, no. 35, pp. 32517–32525, 2003.

[46] J. Quoyer, C. Longuet, C. Broca et al., "GLP-1 mediates antiapoptotic effect by phosphorylating Bad through a beta-arrestin 1-mediated ERK1/2 activation in pancreatic beta-cells," *The Journal of Biological Chemistry*, vol. 285, no. 3, pp. 1989–2002, 2010.

[47] J. Buteau, R. Roduit, S. Susini, and M. Prentki, "Glucagon-like peptide-1 promotes DNA synthesis, activates phosphatidylinositol 3-kinase and increases transcription factor pancreatic and duodenal homeobox gene 1 (PDX-1) DNA binding activity in beta (INS-1)-cells," *Diabetologia*, vol. 42, no. 7, pp. 856–864, 1999.

[48] S. Park, X. Dong, T. L. Fisher et al., "Exendin-4 uses Irs2 signaling to mediate pancreatic β cell growth and function," *Journal of Biological Chemistry*, vol. 281, no. 2, pp. 1159–1168, 2006.

Hindawi
Journal of Diabetes Research
Volume 2019, Article ID 4858740, 13 pages
https://doi.org/10.1155/2019/4858740

Research Article

Effects of High-Fat Diet on eHSP72 and Extra-to-Intracellular HSP70 Levels in Mice Submitted to Exercise under Exposure to Fine Particulate Matter

Iberê Machado Kostrycki,[1,2] Guilherme Wildner,[1] Yohanna Hannah Donato,[1] Analú Bender dos Santos,[1,3] Lílian Corrêa Costa Beber,[1,3] Matias Nunes Frizzo,[1,3] Mirna Stela Ludwig,[1,3] Kevin Noel Keane,[4] Vinicius Cruzat,[5] Cláudia Ramos Rhoden,[2] and Thiago Gomes Heck[1,3]

[1]*Research Group in Physiology, Department of Life Sciences, Regional University of Northwestern Rio Grande do Sul State (UNIJUI), Ijuí, RS, Brazil*
[2]*Laboratory of Oxidative Stress and Air Pollution, Postgraduate Program in Health Sciences, Federal University of Health Sciences of Porto Alegre (UFCSPA), Porto Alegre, RS, Brazil*
[3]*Postgraduate Program in Integral Attention to Health (PPGAIS-UNIJUÍ/UNICRUZ), Ijuí, RS, Brazil*
[4]*School of Pharmacy and Biomedical Sciences, Curtin Health Innovation Research Institute, Curtin University, Perth 6102, Australia*
[5]*Faculty of Health, Torrens University Australia, Melbourne, Victoria 3065, Australia*

Correspondence should be addressed to Thiago Gomes Heck; thiago.heck@unijui.edu.br

Received 10 August 2018; Accepted 23 October 2018; Published 6 January 2019

Guest Editor: Julia M. dos Santos

Obesity, air pollution, and exercise induce alterations in the heat shock response (HSR), in both intracellular 70 kDa heat shock proteins (iHSP70) and the plasmatic extracellular form (eHSP72). Extra-to-intracellular HSP70 ratio (H-index = eHSP70/iHSP70 ratio) represents a candidate biomarker of subclinical health status. This study investigated the effects of moderate- and high-intensity exercise in the HSR and oxidative stress parameters, in obese mice exposed to fine particulate matter ($PM_{2.5}$). Thirty-day-old male isogenic $B6_{129}F_2/J$ mice were maintained for 16 weeks on standard chow or high-fat diet (HFD). Then, mice were exposed to either saline or 50 μg of $PM_{2.5}$ by intranasal instillation and subsequently maintained at rest or subjected to moderate- or high-intensity swimming exercise. HFD mice exhibited high adiposity and glucose intolerance at week 16th. HFD mice submitted to moderate- or high-intensity exercise were not able to complete the exercise session and showed lower levels of eHSP70 and H-index, when compared to controls. $PM_{2.5}$ exposure modified the glycaemic response to exercise and modified hematological responses in HFD mice. Our study suggests that obesity is a critical health condition for exercise prescription under $PM_{2.5}$ exposure.

1. Introduction

Obesity is an increasing worldwide issue and is associated with comorbidities, such as insulin resistance, dyslipidemia, hypertension, cancer, and cardiovascular disease [1]. Overnutrition and physical inactivity are the primary factors that contribute to the burden of obesity. Interestingly, in animal models of obesity [2] and also in humans [3] exposed to a high-caloric intake diet, physical exercise can attenuate the effects of diet-induced obesity. Conversely, the importance of exercise continues to be undervalued despite evidence of its protective effects. It is estimated that >30% of the global adult population does not meet the minimum levels of daily exercise and can be defined as physically inactive [4]. The metabolic alterations resulting from this sedentary lifestyle, along with overnutrition include an increased abdominal

and visceral adiposity, which significantly contributes to insulin resistance chronic low-grade inflammation [5] and oxidative stress [6, 7].

Obesity and associated comorbidities are more prevalent in urban areas, where individuals are also exposed to another major global health problem, the air pollution exposure, mainly represented by a fine particulate matter ($PM_{2.5}$) [8, 9]. $PM_{2.5}$ is formed from the combustion processes, including vehicles, power plants, and burning related to agricultural or industrial work. As $PM_{2.5}$ is inhaled, it invades the respiratory tract and the vascular system [10] promoting oxidative stress in tissues such as the lungs and heart which has been associated with the development of pulmonary inflammation [11, 12]. In overweight and obese individuals, $PM_{2.5}$ exposure has been strongly associated with the risk of cardiovascular disease, stroke, and insulin resistance, which is potentiated by the rising inflammatory effects of adiposity, increased BMI and increased waist-to-hip ratio [9, 13–15].

At the most basic level, mammalian cells have developed a range of adaptations to survive and respond to these different types of hostile situations such as heat shock, oxidative stress, and inflammation, by changing the expression of heat shock proteins (HSPs). HSPs are a family of polypeptides clustered according to their molecular weight and have many intracellular functions. The most important is to act as a molecular chaperone and prevent inappropriate protein interactions and degradation. Also, recent studies have demonstrated that the intracellular 70 kDa heat shock protein (iHSP70) can act as an important anti-inflammatory agent particularly in stressful cellular situations [16, 17]. Conversely, HSP70 can be released into the extracellular space (i.e., eHSP70), where it functions as a stress signal and a proinflammatory molecule [18–20]. For example, the chronic exposure to $PM_{2.5}$ increases plasma levels of eHSP70 which can contribute to vascular dysfunction and the increased susceptibility to cardiovascular disease [21, 22]. In obesity and type 2 diabetes, eHSP70 has been negatively correlated with iHSP70 in skeletal muscles and led to impaired glucose handling. Indeed, elevated levels of eHSP70 are associated with insulin resistance and beta cell failure in elderly volunteers [18].

Although the precise regulation of extra-to-intracellular HSP70 ratio (H-index = eHSP70/iHSP70) is still unknown [15, 23], exercise is a potent mediator of the heat shock response (HSR) [17], when under exposure to $PM_{2.5}$ [24]. Thus, in the present study, we aimed to investigate the effects of high-fat diet consumption on eHSP70 and H-index, in mice submitted to acute moderate- and high-intensity exercise, following exposure to $PM_{2.5}$. The impact of these conditions on oxidative, glycaemic, and hematological parameters was also assessed.

2. Material and Methods

2.1. Animals, Diet, and Experimental Design. Thirty-day-old male isogenic $B6_{129}F_2/J$ mice weighing about 18 g were obtained from the Animal Facility of the Regional University of Northwestern of Rio Grande do Sul State (UNIJUÍ) and maintained in semimetabolic cages on a 12 h light/dark cycle (lights on at 07:00) and at a room temperature of $22 \pm 2^{\circ}C$ with 60% relative humidity. The animals were randomly housed in two groups: mice receiving standard laboratory mouse chow (CTRL, $n = 29$) or those on a high-fat diet (HFD, $n = 31$) for 16 weeks. All animals had free access to water and were ad libitum fed with CTRL or HFD chow. Animals from the CTRL group received a pelleted diet, consisting of crude protein, fibrous matter, and minerals (provided by NUVILAB CR1, NuVital Nutrients, Curitiba, Brazil) with a total energy of 16.6 MJ/kg and specifically included 11.4% fats, 62.8% carbohydrates, and 25.8% proteins. The HFD group received a lard-based diet (37.4% *w*/*w*) with a total energy of 22.8 MJ/kg and specifically included 58.3% fats, 24.5% carbohydrates, and 17.2% proteins (Bock et al. 2015; Goettems-Fiorin et al. [15]). After 16 weeks, CTRL and HFD mice were randomly subdivided and exposed to a nasotropic instillation of $PM_{2.5}$ or saline solution and were rested or submitted to moderate- or high-intensity physical exercise. The mice were euthanized by decapitation, and blood was collected for the determination of eHSP70 concentration in plasma. Also, the lungs were dissected for oxidative stress determination and the expression of iHSP70, allowing the calculation of the H-index. Epididymal white adipose tissue (WAT) was removed for adiposity analysis, and blood was collected for hematological analysis. The detailed experimental design and flow diagram is provided in Figure 1. All the procedures were approved by the Animal Ethics Committee of UNIJUÍ (CEUA 011/13), according to the guidelines of the Brazilian College on Animal Experimentation.

2.2. Characterization and Exposure to $PM_{2.5}$. The pollutant $PM_{2.5}$ was collected in a polycarbonate filter through a gravimetric collector on the terrace of the Faculty of Medicine, University of São Paulo (USP), in São Paulo, Brazil, as previously described [25]. The exposure site was located close to a monitoring station of the State of São Paulo Sanitation Agency. It is estimated that at least 100000 vehicles circulate daily on the main and lateral streets (~83% cars, ~10% diesel vehicles, and ~6% motorcycles). There are no industries or significant biomass sources in the surrounding area. $PM_{2.5}$ trace element content was determined by neutron activation analysis, and their concentrations were as follows: arsenic = 12.91 ± 0.53; bromine = 8.88 ± 0.39; cobalt = 1.14 ± 0.04; iron = 1.15 ± 0.03; lanthanum = 2.33 ± 0.29; manganese = 27.5 ± 2.2; antimony = 8.73 ± 0.08; scandium = 0.141 ± 0.009; and thorium = 0.351 ± 0.50 (all expressed as $ng \cdot m^{-3}$ of air). Likewise, the $PM_{2.5}$ sulphur concentration, determined by X-ray fluorescence analysis, was $1.424 \pm 0.08\ \mu m \cdot m^{-3}$. Almost all particles had a diameter of less than 10 μm ($1.2 \pm 2.18\ \mu$m), and about 98% of particles had a diameter of less than 2.5 μm. Briefly, after exposure (24 h), the filter was removed and retained. Particles were obtained by sonication, with an ultrasound bath in seven sessions (50 min each) and suspended in saline solution at a concentration of 50 μg of $PM_{2.5}$ in 10 μL of saline.

The nasotropic instillation of $PM_{2.5}$ occurred immediately before the exercise session with a 10 μL dose of the

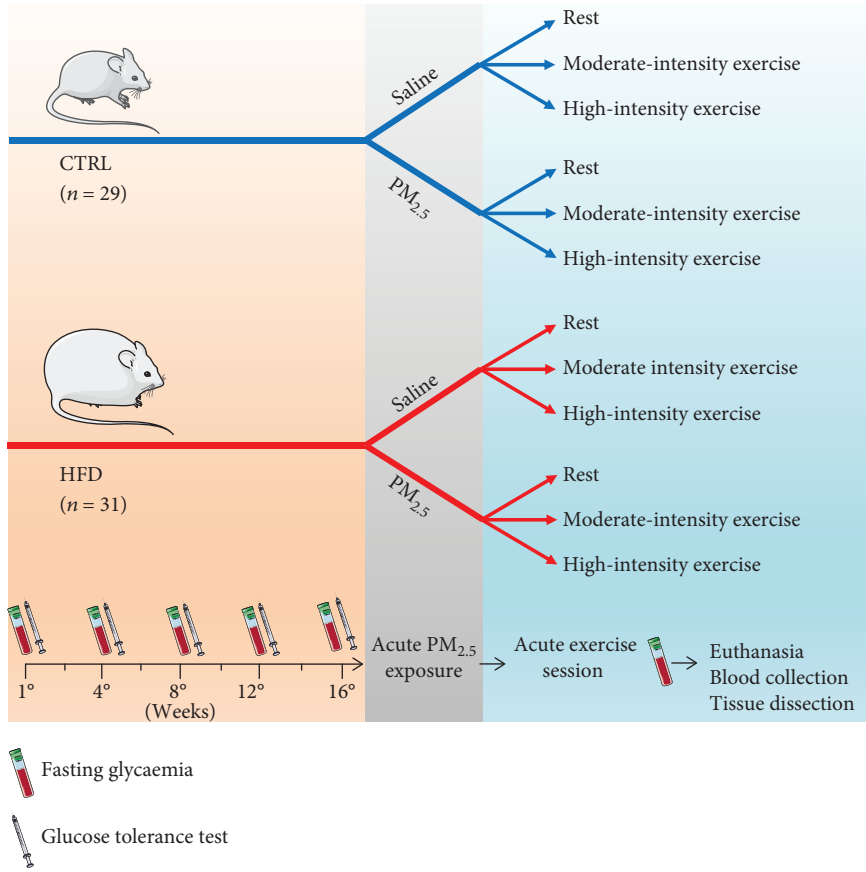

Figure 1: Experimental design. Thirty-day-old male mice were randomly housed in two groups: mice receiving standard chow (CTRL, $n = 29$) or high-fat diet (HFD, $n = 31$) for 16 weeks. After 16 weeks, CTRL and HFD mice were randomly subdivided and exposed to a nasotropic instillation of $PM_{2.5}$ or saline solution, then rested, or subjected to moderate- or high-intensity physical exercise. The mice were euthanized by decapitation, and blood and lungs were collected for biochemical analyses.

solution in the nostril of the animal. This procedure induced an apnoea reflex which promoted inhalation of the pollutant. Before instillation procedure, the particle suspension was submitted to a new sonication process for 10 minutes in a water bath ultrasound and was mixed 0 seconds in a vortex and, thus, immediately administrated. The intranasal dose of 50 μg represents a high exposure to the particle and is equivalent to an urban environment exposure of approximately 50 $\mu g/m^3$.

2.3. Moderate- and High-Intensity Exercise Protocols. All animals were allowed to acclimatize to the water environment before the exercise protocol to avoid any stress response related to the new environment and situation. The adaptation period consisted of 8 min in individual swimming pool chambers (10 cm × 10 cm × 30 cm) filled with water (20 cm depth) at 31 ± 1°C for three consecutive days and without any weight attached to the tail. Individual swimming pool chambers with 20 cm of water prevented jumping and diving behavior and allowed energy expenditure higher than three metabolic equivalents (METs) [26]. In the subsequent week, animals were randomly assigned to each exercise intensity protocol for 20 minutes or the swimming time was recorded until the animals were fatigued (8 seconds below water surface) due to the exercise burden imposed by weight (i.e., 4% or 8% of body weight) attached to the base of the tail. All experiments were carried out between 1:00 and 3:00 p.m., and the room temperature was kept at 24°C. Sedentary animals (CTRL, HFD, $PM_{2.5}$, and HFD + $PM_{2.5}$ groups) remained at rest in shallow water. All the procedures were in accordance with those prescribed in The American Physiological Society's Resource Book for the Design of Animal Exercise Protocols [26], and an experienced researcher was present at all times to prevent drowning. The exercise intensity was evaluated by caudal venous lactate concentrations (~25 μL of blood) using a lactate analyzer (Accutrend® Plus System, Roche Diagnostics®, Indiana, USA.).

2.4. Measurement of Plasma Glucose, GTT, and Adiposity. Throughout the 16 weeks, the total body weight, fasting glycaemia, and glucose tolerance test (GTT) were evaluated at the 30th day and at the 4th, 8th, 12th, and 16th week. Blood glucose concentrations were measured at rest, before and after exercise using an Optium Xceed glucometer (Abbott Diabetes Care, Alameda, USA). For the GTT, food was withdrawn 12 h before the test and glycaemia was measured immediately before and at 30 and 120 min post glucose (1 g/kg in saline solution, i.p.) administration. The glycaemic response during the GTT was evaluated by IAUC method.

Total body adiposity was measured at the end of the 16th week to better characterize the installation of obesity. At the end of the experiment, adiposity was evaluated by dissecting and weighing WAT buying an analytical balance and the adiposity was expressed as a percentage of total body weight (WAT weight/total body weight).

2.5. eHSP70 Concentration in Plasma. Animals were euthanized immediately after the exercise session, and blood was collected in EDTA-treated tubes. The samples were then centrifuged at $2000 \times g$, at room temperature for 15 min to obtain plasma samples. The HSP70 plasma concentration (eHSP70) was measured by using a high-sensitivity HSPA1A-specific HSP70 ELISA Kit (Enzo Life Sciences, EKS-715, Farmingdale, USA) in diluted (1 : 4) plasma samples as recommended by the manufacturer. Absorbance was measured at 450 nm using a microplate reader (Mindray MR-96A) and a standard curve constructed from known dilutions of recombinant 72 kDa heat shock protein (HSP72) to allow quantitative assessment of eHSP70 plasma concentration. The intra-assay coefficient of variation was identified as being <2%. Although there are at least two isoforms of HSP70 (the 72 and 73 kDa HSPs, which are well known as the HSPA1A-inducible form and the cognate HSPA8 constitutive form, respectively), the levels of HSPA1A (eHSP72) can be used as representative of total eHSP70 secretion [23]. It is expected that both the inducible and constitutive forms should be delivered into the extracellular space after stressful conditions as acute exercise; however, eHSP72 has been used as biomarker of stress situations in previous studies related to particulate matter pollution, diabetes, and exercise [15, 17, 24]. Also, only HSPA1A ELISA kits have been sufficiently tested worldwide and are accepted to possess enough sensitivity (pg·mL−1 range) to detect minute quantities of HSP70 in plasma.

2.6. iHSP70, TBARS, and SOD in the Lungs. The lungs were dissected and freeze clamped in liquid nitrogen for further homogenization and analysis of the iHSP70 levels, the antioxidant activity of total superoxide dismutase (SOD), and thiobarbituric acid reactive substances (TBARS). iHSP70 expression was evaluated in the lungs by immunoblot analyses. Equivalent amounts of protein from each sample (~40 μg) were mixed with Laemmli's gel loading buffer (50 mM Tris, 10% (*w*/*v*) SDS, 10% (*v*/*v*) glycerol, 10% (*v*/*v*) 2-mercaptoethanol, and 2 mg/mL bromophenol blue) in a ratio of 1 : 1, boiled for 5 min, and electrophoresed in a 10% polyacrylamide gel (5 h in 15 mA/gel). After the proteins were transferred onto a nitrocellulose membrane (GE Healthcare) by electrotransfer (1 h in 100 V), the subsequently transferred bands were visualized with 3% (*w*/*v*) Red Ponceau S (Sigma-Aldrich). The procedures were performed with the SNAP i.d. (Merck Millipore) vacuum system for rapid immunoblotting. Membranes were washed with water and then blocked with 0.5% (*w*/*v*) fat-free milk buffer (TEN-Tween 20 solution (0.1%, *w*/*v*); TEN is 50 mM Tris, 5 mM EDTA, 150 mM NaCl, and pH 7.4). Membranes were then washed three times with wash buffer and incubated for 15 min with the monoclonal anti-HSP70 antibody (Sigma-Aldrich H5147, 1 : 1000). After three consecutive washes with wash buffer, peroxidase-labelled rabbit anti-mouse IgG (Sigma-Aldrich A9044) was utilized as a secondary antibody, at 1 : 15000 dilution. For gel loading control, Coomassie Blue staining (0.1% Coomassie Blue, 40% methanol, and 10% acetic acid) was used. Blot visualization was performed using ECL Prime Western Blotting Reagent (GE Healthcare). Quantification of bands was determined using the ImageJ® software. The data was presented in arbitrary units of iHSP70, normalized by β-actin expression.

For TBARS and total SOD analysis, a portion of the lung tissue was homogenized in potassium phosphate buffer at pH 7.4 containing the protease inhibitor PMSF (phenylmethylsulfonyl fluoride, 100 μM). Afterwards, the homogenates were centrifuged at $1200 \times g$ for 10 min at room temperature and the supernatant fractions were saved for protein determination by a spectrophotometric method [27] at 595 nm, using bovine serum albumin as standard. Homogenates were precipitated with 10% trichloroacetic acid (3 : 1 *v*/*v*), centrifuged, and incubated with 0.67% thiobarbituric acid (1 : 1 *v*/*v*) (T5500, Sigma) for 15 min at 100°C. The absorbance was measured at 535 nm. The amount of TBARS formed was expressed in nanomoles of malondialdehyde per milligram of protein (nmol MDA·mg prot^{-1}). The MDA standard was prepared from 1,1,3,3,-tetramethoxypropane (Fluka, USA). Total SOD activity was determined by inhibition of autooxidation of pyrogallol [28]. Briefly, in a cuvette, 970 μL of 50 mM Tris/1 mM EDTA buffer (pH 8.2), 4 μL of catalase (CAT) (30 μM), and 10 μL of homogenate were added together and mixed. After that, 16 μL of pyrogallol (24 mM in 10 mM HCl) was added and total SOD activity was determined at 36°C in a spectrophotometer (420 nm) for 120 s. Results were expressed in units of SOD per milligram of protein (U SOD·mg prot^{-1}).

2.7. Hematological Analysis. After decapitation, blood was immediately collected into heparinized (30 IU·mL^{-1} final volume) tubes (for metabolite measurements) or in disodium EDTA-treated tubes (2 mg·mL^{-1} final volume). Hematological parameters were investigated in EDTA samples in a Horiba ABX Micros 60 hematology analyzer (for quantitative cell analysis) [24].

2.8. H-Index (eHSP72/iHSP70 Ratio). Extracellular-to-intracellular HSP70 ratio index (H-index) has been described as a novel and overall index of the immunoinflammatory status of an individual. The rationale for H-index is that the higher the level of eHSP70 is, the greater the inflammatory signal is, due to the proinflammatory nature of the protein. Conversely, if cells are able to respond to stressful stimuli by enhancing iHSP70 production, they simultaneously enter a state of anti-inflammation. First, by definition, the eHSP70 and iHSP70 levels and the eHSP70/iHSP70 ratio in control groups (Rc) were considered as a baseline (Rc = 1.0). Thereafter the eHSP70/iHSP70 ratio in a stressful situation such as that in the experimental groups (Rexp) can be calculated as the quotient of different values relative to the Rc. Hence, the H-index (Rexp/Rc) allows comparisons between any stressful situation and the control [15, 17, 24].

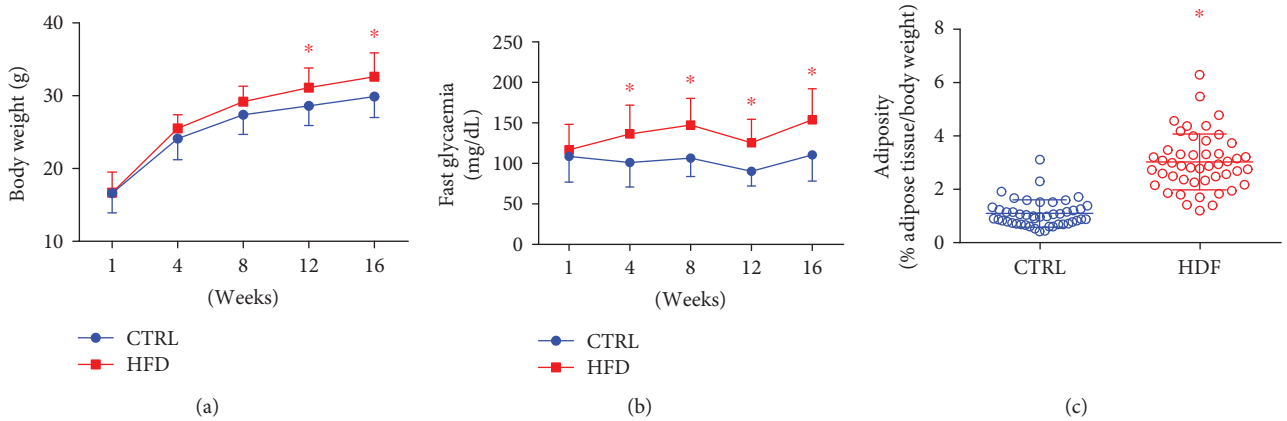

FIGURE 2: Effects of HFD consumption on body weight, fasting glycaemia, and adiposity in mice. Mice received standard chow (CTRL, $n = 29$) or high-fat diet (HFD, $n = 31$) over 16 weeks. HFD increased body weight (a), fasting glycaemia (b), and adiposity (c) of mice. Data are expressed as mean ± standard deviation. $^*P < 0.05$ compared to the control. Two-way ANOVA with repeated measures followed by post hoc Tukey's test (a, b). $^*P < 0.05$ vs. CTRL Student's t-test in (c).

2.9. Statistical Analyses. Statistical analysis was developed using two-way ANOVA with repeated measures followed by Tukey's post hoc test for differences in body weight, fasting glycaemia, glycaemia during GTT, and glycaemia during exercise. One-way ANOVA was used for comparison of IAUC results. Student's t-test was used to analyze all other variables. All statistical analyses were performed using GraphPad 7.0 for Windows. The level of significance was set to $P < 0.05$, and the results were expressed as mean ± Sd.

3. Results

At 30 days old, the mice were randomly separated in two groups, receiving the standard diet or HFD for 16 weeks. HFD treatment increased body weight, fasting glycaemia, and adiposity of mice compared to normally fed mice (Figure 2). Also, HFD mice presented with glucose intolerance via GTT, from the 4th week of HFD consumption (Figure 3).

At the end of the 16th week, mice received either saline or $PM_{2.5}$ by intranasal instillation and were submitted to moderate- or high-intensity exercise or remained at rest. Rested mice were left for 20 min after saline or $PM_{2.5}$ instillation (Figure 4), and we observed that mice that received normal chow were able to swim for 20 min with moderate intensity workload and without any effect from $PM_{2.5}$ instillation (Figure 4). However, at moderate-intensity workload, HFD mice did not reach 20 minutes of exercise, performing only 13.3 ± 4.6 and 12.0 ± 6.9 minutes of exercise (HFD and HFD + $PM_{2.5}$, respectively; see Figure 4). Also, all mice submitted to high-intensity exercise did not reach 20 minutes of exercise and HFD mice presented the lowest physical capacity in comparison to control mice in both situations: Without pollution, control mice swam for 15.9 ± 5.6 minutes, while HFD-treated mice swam for only 5.4 ± 3.6 minutes. Under $PM_{2.5}$ exposure, control mice swam for 11.4 ± 6.4 minutes, while HFD-treated mice swam for only 2.5 ± 0.7 minutes (Figure 4).

Mice remaining at rest in shallow water showed an increase in glycaemia, but it was higher in HFD mice than normal-chow mice (Figure 5). Moderate exercise did not modify the mice glycaemia, but the values in the HFD were above that of normal-chow mice, while the high-intensity exercise decreased the glycaemia in HFD mice (Figure 5). The $PM_{2.5}$ inhalation had no influence in rested mice or those submitted to moderate exercise since the results were similar to that of the saline administration group (Figure 5). However, under $PM_{2.5}$ exposure, HFD mice submitted to high-intensity exercise showed no decrease in glycaemia as that observed in the saline administration group (Figure 5).

There was no difference in eHSP72 levels in HFD mice when compared to normal-chow mice at rest and when submitted to moderate exercise or upon exposure to $PM_{2.5}$ (Figure 6). However, high-intensity exercise decreased eHSP72 levels in HFD mice but this effect was not observed in animals exposed to $PM_{2.5}$ (Figure 6).

HFD increased iHSP70 levels in the lung of rested mice (Table 1, and the representative blot is in Figure 7). Lower levels of lipid peroxidation were observed in HFD mice submitted to moderate-intensity exercise in comparison with CTRL (Table 1). Also, high-intensity exercise decreased eHSP70/iHSP70 ratio levels (plasma/lung HSP70 ratio) in HFD mice but this effect was not observed in animals exposed to $PM_{2.5}$ (Table 1). Total SOD antioxidant enzyme activity was not influenced in any experimental group (Table 1).

Changes in hematological parameters are shown in Table 2. The majority of parameters were not modified in our study. HFD induced an increase in lymphocyte count (vs. CTRL in resting groups). Moderate exercise increased the neutrophil count in HFD in comparison with CTRL animals, and high-intensity exercise increased red blood cell count and lymphocyte count in the HFD group (vs. CTRL in the same intensity).

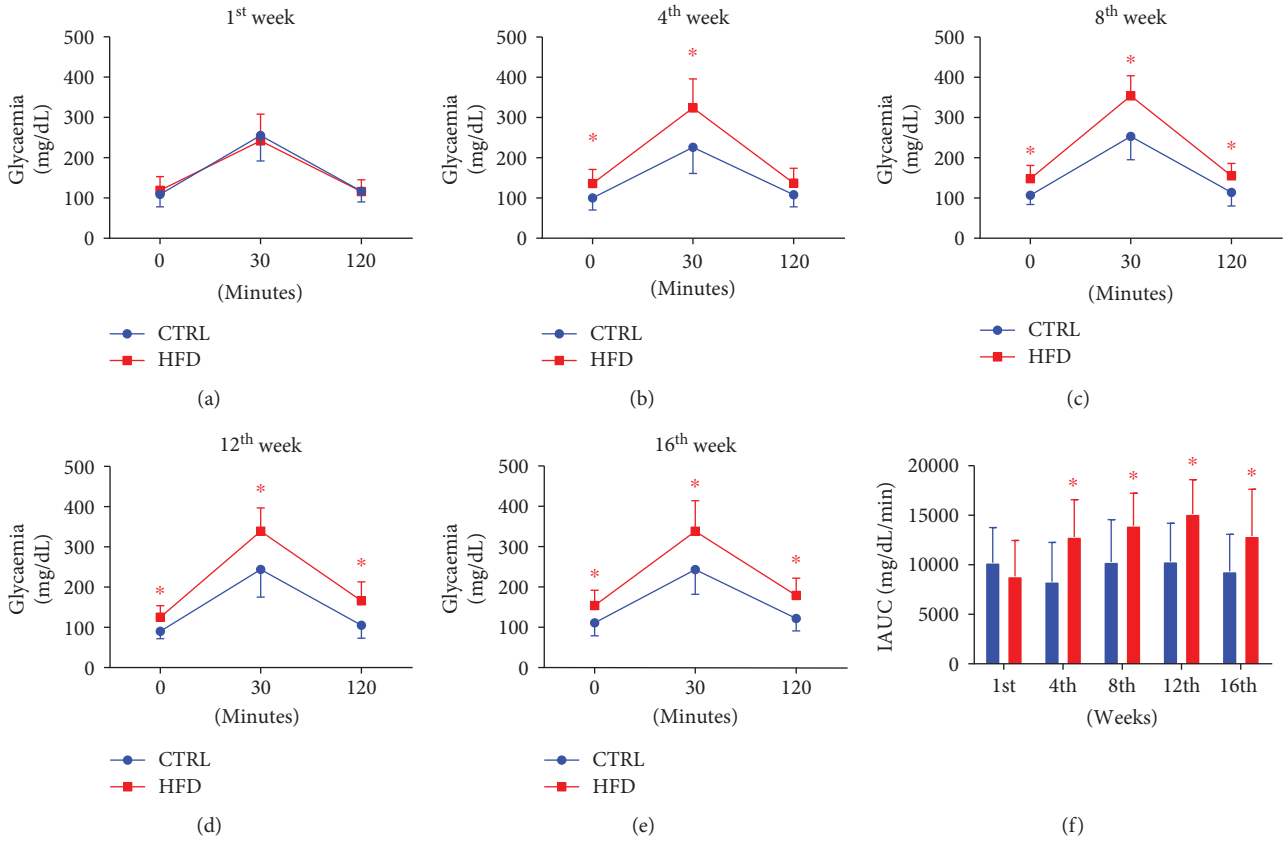

Figure 3: Effects of HFD on glucose tolerance test response in mice. Mice received standard chow (CTRL, $n = 29$) or high-fat diet (HFD, $n = 31$) over 16 weeks. Glucose tolerance test (GTT) was performed by administration (i.p.) of glucose (1 g/kg) before HFD intake in the first week (a), then following HFD in the 4th (b), 8th (c), 12th (d), and 16th (e) week. Glucose intolerance was confirmed based on the IAUC calculation (f). Data was expressed as mean ± standard deviation. $^*P < 0.05$ vs. the CTRL group. Two-way ANOVA with repeated measures followed by post hoc Tukey's test (a–e) and one-way ANOVA followed by post-hoc Tukey's test (f).

4. Discussion

In our study, we studied the effects of HFD on subclinical and clinical parameters, in mice submitted to exercise under $PM_{2.5}$ exposure. HFD mice presented an expected increase in body weight and adiposity, with an impaired glucose tolerance. This profile was accompanied by a poorer exercise performance, along with lower eHSP70 and eHSP70/iHSP70 ratio levels in comparison to the CTRL group. High-intensity exercise decreased glycaemia in HFD mice only and in the absence of $PM_{2.5}$ exposure. The $PM_{2.5}$ exposure promoted more hematological effects in HFD mice in comparison to CTRL, and this occurred in mice submitted to moderate- or high-intensity exercise. Thus, our study showed novelty in terms of the HSR as follows: (a) the influence of obesity/T2DM in eHSP70 plasma concentration and H-index (eHSP72/iHSP70 ratio) after exercise was dependent on exercise intensity, (b) acute environmental air pollution exposure modified the effects of exercise in obesity, and (c) these effects on HSP70 were not accompanied by altered oxidative stress biomarkers or by hematological changes.

The first step of our study was to induce obesity and glucose intolerance in $B6._{129}SF2/J$ mice by HFD. It was suggested that B6 mice used in our study should be more resistant to the effects of HFD due to decreased intestinal absorption of lipids, which would characterize the strain as less susceptible to the effects of HFD [29]. In the study of Bock et al. [29], lower responsiveness to GTT and alterations in fasting glucose were observed after four weeks of HFD intake in adult animals. In contrast, in the present study, we exposed the animals to HDF after weaning (four weeks old). The data presented herein, confirm previous findings, were the effects of HFD following weaning result in a greater adiposity and metabolic disorder profile, and therefore, this experimental design can be considered suitable for the of obesity [24]. In addition to the promotion of obesity (increased body mass and adipose tissue), this experimental protocol has also been used for the study of chronic and low-grade inflammation, and altered HSP70 expression [15, 16].

The second step of our study was to submit HFD and CTRL mice to 50 μg of $PM_{2.5}$ exposure (or saline). A single administration of particle suspension into the nostril of mice is aimed at simulating an acute exposure to an environment similar to that proposed by interim target 2 from the World Health Organization 24-hour concentration air quality guidelines. Based on published risk

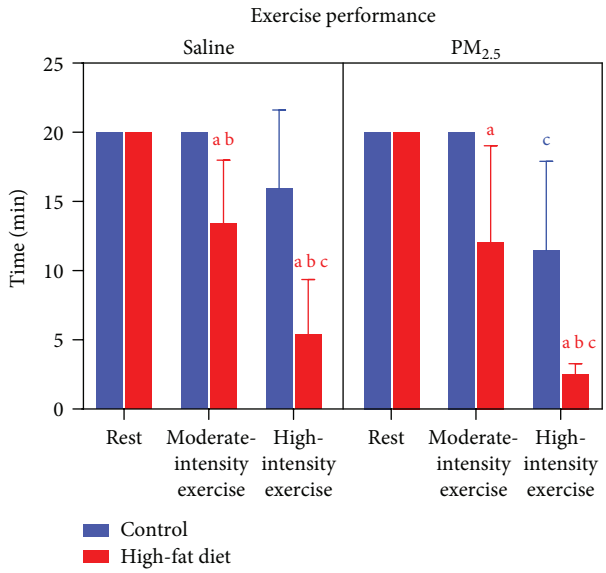

Figure 4: Effects of exercise under $PM_{2.5}$ exposure on swim performance of HFD-treated mice. Mice received standard chow (CTRL, $n = 29$) or high-fat diet (HFD, $n = 31$) over 16 weeks. After animals received saline or $PM_{2.5}$ by intranasal instillation, they were rested or submitted to exercise at moderate or high intensity. Data expressed was mean ± standard deviation. "a" means difference vs. the CTRL group in the same intensity, "b" means difference vs. the moderate-intensity group in the same diet treatment, and "c" means difference vs. the group that remained at rest in the same diet treatment. Two-way ANOVA $P < 0.05$.

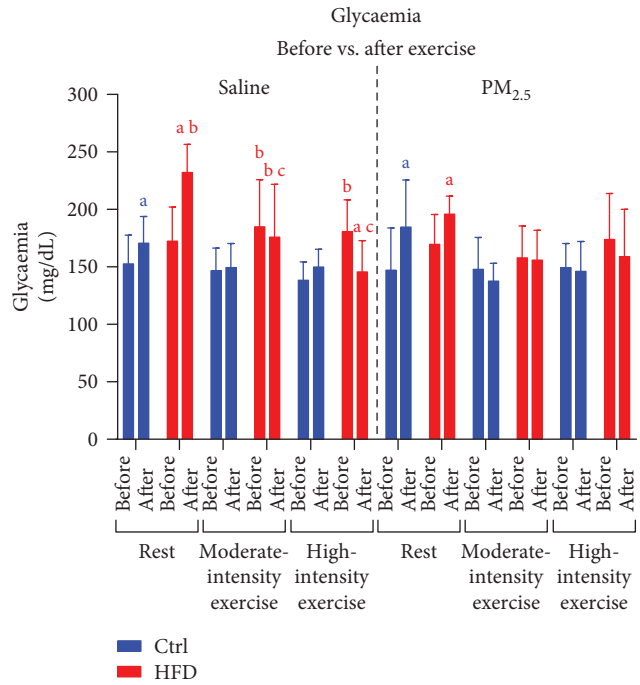

Figure 5: Effects of exercise under $PM_{2.5}$ exposure on glycaemia of HFD-treated mice. Mice received standard chow (CTRL, $n = 29$) or high-fat diet (HFD, $n = 31$) over 16 weeks. After animals received saline or $PM_{2.5}$ by intranasal instillation, they were rested or submitted to exercise at moderate or high intensity. Data expressed was mean ± standard deviation. "a" means statistical difference in the comparison before vs. after in the same group. "b" means the statistical difference in comparison with the CTRL group in the same intensity. "c" means the statistical difference in comparison with the moderate-intensity and rest groups in the same diet treatment. Two-way ANOVA, $P < 0.05$.

coefficients from multicenter studies and meta-analyses, urban $PM_{2.5}$ concentration of 50 $\mu g/m^3$ represents about 2.5% increase of short-term mortality than 25 $\mu g/m^3$ $PM_{2.5}$ concentration; limits are proposed by the Air Quality Guideline [4]. A previous study used the same dose to represent a particle concentration of 29 $\mu g/m^3$ in an urban area, which is the value found in a polluted city [30]. Thus, our protocol was elaborated to simulate closer a "real-world" exposure study (because of the dose, the source—urban area of Sao Paulo, Brazil—and the complex mix of metal adsorbed in the particles) than a more specifically toxicological study, evaluating the effect of each component of particle.

It is important to highlight that the majority of experimental studies regarding adverse effects of $PM_{2.5}$ on oxidative stress parameters (and others) are conducted with animals under rest conditions and use higher levels of particle exposure. Usually, oxidative stress is observed in experimental designs that expose mice or rats to high levels of concentrated particles [12], higher levels of aerosol suspension, or intratracheal particle instillation [25, 31]. In the same strain of mice used herein ($B6_{129}SF2/J$) and in a similar $PM_{2.5}$ exposure protocol (intranasal instillation of 5 μg $PM_{2.5}$, daily for 12 weeks), no increase in oxidative stress was observed in the $PM_{2.5}$ exposure group [15]. Considering that upper airway filtration in mice can prevent up to 50% of particle deposition in alveolar spaces, the dose of 50 μg of $PM_{2.5}$ used herein represents a low-to-moderate level of environmental air pollution exposure. During exercise, breath frequency ($n \cdot min^{-1}$) and minute ventilation ($mL \cdot min^{-1}$) increased and were dependent on exercise intensity and also possibly on particle deposition within the lungs [32]. In comparison to rest conditions, exercise can increase particle deposition up to 6.0-fold in rodents [33]. However, even at high levels of particles, one exposure alone may not induce clinical effects after exercise, but only subclinical effects [31, 34]. In our study, $PM_{2.5}$ exposure increased leukocytosis induced by exercise in HFD mice and this may represent a proinflammatory predisposition profile in HFD mice [35].

After $PM_{2.5}$ instillation (or saline), the mice were submitted to one bout of moderate- or high-intensity exercise or remained at rest. Our high-intensity exercise protocol was performed by the attachment of an overload weight on the tail (8% of body weight) during the swimming exercise session. The fatigability of this protocol was previously tested in mice and rats with this workload. Indeed, this swimming time (20 min) was chosen because this is the time limit within which an untrained animal really swims before learning how to perform bobbing, which is a survival strategy used to conserve energy without doing exercise. On the other hand, with 4% body weight attached to the tail, mice can swim for 60 minutes or more. For this reason, the workloads used herein characterized adequately two distinct exercise intensities. It may be questioned whether the effects observed in the

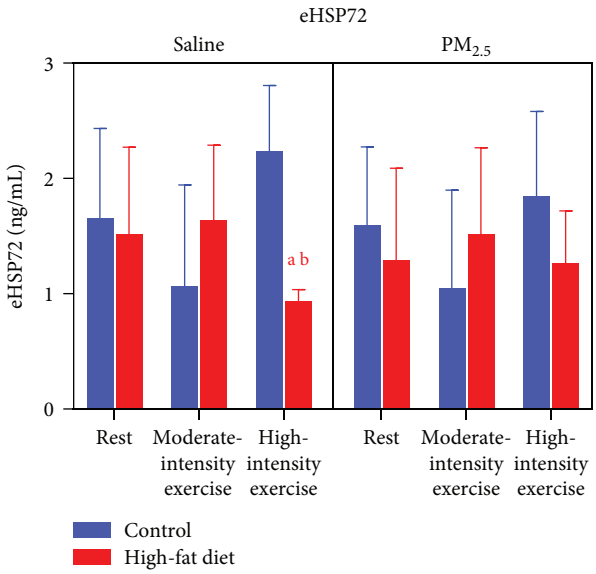

Figure 6: Effects of exercise under $PM_{2.5}$ exposure on plasma eHSP70 levels of HFD-treated mice. Mice received standard chow (CTRL, $n = 29$) or high-fat diet (HFD, $n = 31$) over 16 weeks. After animals received saline or $PM_{2.5}$ by intranasal instillation, they were rested or submitted to exercise at moderate or high intensity. Data expressed was mean ± standard deviation. "a" means the statistical difference in comparison with the CTRL group in the same intensity and "b" means the statistical difference in comparison with the moderate-intensity group in the same diet treatment. Two-way ANOVA, $P < 0.05$.

high-intensity exercise groups were induced by higher total energy expended during exercise than those observed in the moderate-intensity exercise groups. However, a moderate-intensity range of 60–75% of VO_2max at 4.0–4.6% workloads has been suggested for swimming mice [26]. Additionally, an 8% workload may represent a high-intensity swimming exercise estimated as representing more than 90% of VO_2max [36]. Despite this, the estimated total energy expended by animals from the high-intensity exercise groups (x min × 8% workload) was similar to that from the moderate-intensity groups (x min × 4% workload). Assuming 4.8 kcal (20 kJ) of energy equivalent of consumed O_2 and 100 mL·kg^{-1}·min^{-1} as mouse VO_2max [26, 37], the total energy expended in each exercise session for the moderate intensity groups was between 0.08 and 0.18 kcal (assuming 10–20 min × 0.025 kg × 60–75 mL·kg^{-1}·min^{-1}), while in the high-intensity exercise groups, it was 0.05–0.16.5 kcal (considering 5–15 min × 0.025 kg × 90 mL·kg^{-1}·min^{-1}). Since HFD mice presented low VO_{2max} [37], the performance of HFD mice in the swimming test was observed in our study during one swimming exercise session, in both moderate- and high-intensity exercise.

In our study, we observed that rested mice increased glycaemia and that this effect was more pronounced in HFD mice. Also, the decrease in glycaemia after high-intensity exercise in HFD mice was not observed under $PM_{2.5}$ exposure in HFD mice. These results may be explained by the effects of swimming exercise, HFD, and $PM_{2.5}$ on the autonomic nervous system: first, swimming performance in the rodents is known to be dramatically influenced by hot or cold water temperature generating early fatigue [26]. Although the water temperature range chosen herein (31 ± 1°C) has been suggested to be the optimal water temperature to exercise, animals that remained in rest have different responses than exercising animals in the same water temperature [17], which suggests a difference in the sympathetic stimulation and vascular response in these situations. Added to this, HFD mice presents a reduced vascular adrenergic contractility [38]. This situation may evoke an overstimulation of the sympathetic nervous system that was more evident with the HFD mice. Second, the catecholamine response to exercise may be blunted in obese/diabetic subjects, presumably indicating autonomic dysfunction during moderate-intensity exercise, resulting in mild hyperglycaemia, associated with defects in hepatic glucokinase activity [39]. Finally, particle inhalation may cause autonomic nervous system imbalance [11, 12], and, although not causing hemodynamic altered responses during exercise [31], the $PM_{2.5}$ effects may be influenced by early vascular inflammation and endothelial dysfunction observed in HFD mice that present reduced nitric oxide production-impaired insulin signal [40]. In this way, $PM_{2.5}$ exposure is associated with increases in systemic cytokines as TNF-α and IL-6 levels, evoking a pronounced pulmonary and systemic inflammatory response [41] that in our work may be a reason for altered exercise performance and glycaemia response in HFD mice.

After the exercise session, mice were euthanized and eHSP70 and eHSP70/iHSP70 levels were determined. Under stress conditions, cells from different tissues increase iHSP70 expression (cellular stress response) and also export this protein to the circulation [42]. High plasma levels of eHSP70 are correlated with energetic balance impairment, alteration of pro-/anti-inflammatory status, and redox homeostasis [15, 42–44]. On the other hand, absence or inhibition of HSP70 expression is associated with increased cell vulnerability and decreased ability to cope with stress [45], which may promote apoptosis [46]. In our study, we observed an increase in lung iHSP70 levels in HFD mice when compared to control and this may indicate that the lungs are under stress induced by HFD but they were still able to maintain the HSR, essential for lung protection against oxidative stress induced by $PM_{2.5}$. In other tissues such as muscle, low iHSP70 levels were observed in animals chronically exposed to the HFD intake [16]. A similar profile was also observed in the liver and adipose tissue [47]. This decrease in iHSP70 was correlated with glucose intolerance and insulin resistance in obese mice [16]. This defect in HSR, as commonly observed in chronic cases of inflammation, has been associated with many obesity-related diseases and dysfunctions including insulin resistance, T2DM, and nonalcoholic hepatic steatosis [47, 48]. In the other side, eHSP72 is related to immune system activation. Indeed, eHSP72 has been reported as an inductor of different immune cell activations attributed to its known capacity to bind to Toll-like receptors 2 and 4 (TLR2 and TLR4) [19, 20]. However, assuming that exercise, a known inducer of eHSP72 release [17, 18, 20, 23, 49], induces an anti-inflammatory response,

Table 1: Effects of exercise under $PM_{2.5}$ exposure on lung oxidative stress, iHSP70 levels, and eHSP70/iHSP70 ratio levels of HFD-treated mice.

	Rest			Moderate-intensity exercise			High-intensity exercise		
	Control	HFD	*t*-test	Control	HFD	*t*-test	Control	HFD	*t*-test
TBARS	0.18 ± 0.06	0.13 ± 0.03	$P = 0.112$	0.32 ± 0.10	0.14 ± 0.02	$P = 0.0004^*$	0.17 ± 0.02	0.14 ± 0.04	$P = 0.134$
SOD	0.17 ± 0.01	0.19 ± 0.02	$P = 0.068$	0.19 ± 0.02	0.19 ± 0.02	$P = 0.874$	0.20 ± 0.02	0.19 ± 0.03	$P = 0.562$
iHSP70	1.02 ± 0.02	1.27 ± 0.14*	$^*P = 0.034$	1.26 ± 0.27	1.29 ± 0.14	$P = 0.861$	1.08 ± 0.09	1.36 ± 0.24	$P = 0.129$
eHSP70/iHSP70 ratio	1.00 ± 0.31	0.65 ± 0.32	$P = 0.248$	0.94 ± 0.76	0.67 ± 0.39	$P = 0.608$	1.40 ± 0.47	0.42 ± 0.09*	$^*P = 0.023$
	Rest + $PM_{2.5}$			Moderate Intensity Exercise + $PM_{2.5}$			High-Intensity Exercise + $PM_{2.5}$		
	Control	HFD	*t*-test	Control	HFD	*t*-test	Control	HFD	*t*-test
TBARS	0.33 ± 0.14	0.13 ± 0.02*	$P = 0.003^*$	0.29 ± 0.07	0.12 ± 0.02*	$P = 0.0001^*$	0.14 ± 0.02	0.16 ± 0.06	$P = 0.670$
SOD	0.20 ± 0.01	0.19 ± 0.03	$P = 0.417$	0.17 ± 0.02	0.19 ± 0.04	$P = 0.401$	0.17 ± 0.02	0.18 ± 0.03	$P = 0.378$
iHSP70	1.15 ± 0.05	1.45 ± 0.26	$P = 0.118$	1.30 ± 0.32	1.48 ± 0.19	$P = 0.447$	1.27 ± 0.12	1.20 ± 0.17	$P = 0.587$
eHSP70/iHSP70 ratio	0.76 ± 0.28	0.36 ± 0.09	$P = 0.074$	0.33 ± 0.18	0.65 ± 0.33	$P = 0.211$	0.52 ± 0.06	0.81 ± 0.22	$P = 0.089$

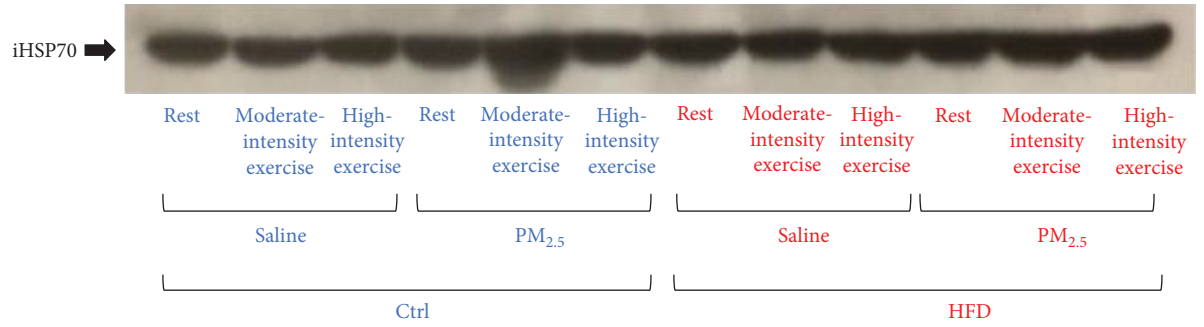

Figure 7: Effects of exercise under $PM_{2.5}$ exposure on plasma iHSP70 lung levels of HFD-treated mice. Mice received standard chow (CTRL, $n = 29$) or high-fat diet (HFD, $n = 31$) over 16 weeks. After animals received saline or $PM_{2.5}$ by intranasal instillation, they were rested or submitted to exercise at moderate or high intensity. This is a representative blot for HSP70 detection in mice lungs.

each single bout of exercise may induce an acute activation of inflammatory response followed by a membrane downregulation of Toll-like receptors resulting in a posterior anti-inflammatory response. Thus, the lower capacity to release eHSP72 of HFD mice under high-intensity exercise could result in a higher cellular response to inflammatory mediators in long term, worsening glucose unbalance. In this way, our study showed that a lower concentration of plasma eHSP70 was present in HFD mice submitted to high-intensity exercise, in comparison to CTRL mice. Since HFD mice were not able to swim for 20 minutes, the lower eHSP70 levels in plasma may represent an insufficient accumulation of exercise effort (time × load). These data are in agreement with the hypothesis that a minimum amount of exercise effort is necessary to promote health effects [50]. Thus, the minimum of level physical activity may not be reached due early fatigue and this represents a key limitation in the obese condition.

In our study, the glycaemia and eHSP70 levels decreased in the HFD group after high-intensity exercise and this effect was not observed in other groups (moderate-intensity exercise or $PM_{2.5}$ groups). It was demonstrated that eHSP70 increased throughout exercise and was attenuated by glucose ingestion, mainly by inhibition of hepatosplanchnic eHSP70 release [51]. Thus, the lower levels of eHSP70 in HFD submitted to exercise can be possibly explained by the hyperglycaemic state of mice. Also, in the presence of $PM_{2.5}$, the control of eHSP70 release may be related to glycaemia which may also be affected by liver stress induced by $PM_{2.5}$. In this way, $PM_{2.5}$ exposure induces endoplasmic reticulum stress in the lung and liver [52]. Endoplasmic reticulum stress, also called the unfolded protein response (UPR), is an intracellular stress signaling cascade that protects cells from stress caused by the accumulation of unfolded or misfolded proteins and is very sensitive to changes of intracellular homeostasis. Physiological states that increase protein folding demand or stimulate the disruption of protein folding reactions create an imbalance between the protein folding load and capacity of the endoplasmic reticulum. The UPR is related to many alterations in heat shock protein families, including the HSP70 family, and is associated with diabetic complications [53].

Due to the versatility of HSP70 to induce different responses related to inflammation according to its location, it is proposed that this protein may represent an important marker for the immunoinflammatory state during exercise [17, 20]. Also, HSP70 balance measured by mathematical calculation of the H-index as reported in other studies

Table 2: Effects of exercise under $PM_{2.5}$ exposure on the hematological profile of HFD-treated mice.

	Rest			Moderate-intensity exercise			High-intensity exercise		
	Control ($n = 5$)	HFD ($n = 7$)	t-test	Control ($n = 7$)	HFD ($n = 8$)	t-test	Control ($n = 8$)	HFD ($n = 8$)	t-test
RBC (10^6/mm^3)	8.4 ± 0.5	8.3 ± 1.0	*0.842*	8.0 ± 1.0	8.1 ± 0.9	*0.841*	8.4 ± 0.7	8.0 ± 1.2	*0.429*
HGB (g/dL)	13.8 ± 1.5	13.2 ± 1.3	*0.475*	12.4 ± 2.4	12.6 ± 1.0	*0.832*	13.8 ± 1.1	12.3 ± 2.1	*0.095*
HCT (%)	37.0 ± 3.2	36.6 ± 4.5	0.868	34.7 ± 4.6	35.6 ± 4.2	*0.698*	37.2 ± 3.2	35.1 ± 5.9	*0.391*
PLT (10^3/mm^3)	958 ± 120	896 ± 256	*0.628*	831 ± 154	879 ± 144	*0.543*	889 ± 191	820 ± 283	0.576
Neutr (10^3/mm^3)	0.32 ± 0.09	0.47 ± 0.16	*0.089*	0.28 ± 0.19	0.31 ± 0.19	*0.765*	0.36 ± 0.10	0.35 ± 0.26	0.920
Monoc (10^3/mm^3)	0.27 ± 0.07	0.39 ± 0.14	*0.110*	0.28 ± 0.06	0.27 ± 0.19	*0.896*	0.32 ± 0.11	0.31 ± 0.16	0.886
Lymph (10^3/mm^3)	5.18 ± 0.56	7.64 ± 1.93	*0.021* *	6.94 ± 2.02	8.50 ± 1.9	*0.147*	7.59 ± 1.72	8.0 ± 2.87	0.734
Neutr/lymph	0.05 ± 0.01	0.056 ± 0.016	*0.478*	0.054 ± 0.02	0.038 ± 0.02	*0.146*	0.043 ± 0.019	0.043 ± 0.02	0.999
	Rest + $PM_{2.5}$			Moderate-intensity exercise + $PM_{2.5}$			High-intensity exercise + $PM_{2.5}$		
	Control ($n = 7$)	HFD ($n = 7$)	t-test	Control ($n = 5$)	HFD ($n = 7$)	t-test	Control ($n = 8$)	HFD ($n = 8$)	t-test
RBC (10^6/mm^3)	8.1 ± 1.3	8.3 ± 0.7	*0.726*	8.6 ± 0.4	8.0 ± 0.9	*0.197*	7.2 ± 2.1	9.2 ± 1.2	*0.034* *
HGB (g/dL)	13.2 ± 2.2	13.2 ± 1.1	*0.999*	13.7 ± 1.7	12.7 ± 1.6	*0.322*	12.2 ± 3.2	14.0 ± 2.5	*0.230*
HCT (%)	35.7 ± 4.9	36.1 ± 2.8	*0.854*	37.8 ± 3.3	35.6 ± 3.6	*0.306*	36.7 ± 3.1	39.1 ± 5.9	*0.325*
PLT (10^3/mm^3)	807 ± 128	897 ± 140	*0.233*	934 ± 85	924 ± 100	*0.859*	960 ± 174	875 ± 150	*0.313*
Neutr (10^3/mm^3)	0.285 ± 0.073	0.390 ± 0.20	*0.216*	0.336 ± 0.183	0.540 ± 0.105	*0.033* *	0.348 ± 0.145	0.443 ± 0.327	*0.465*
Monoc (10^3/mm^3)	0.228 ± 0.083	0.315 ± 0.121	*0.142*	0.279 ± 0.115	0.388 ± 0.136	*0.176*	0.292 ± 0.130	0.418 ± 0.129	*0.072*
Lymph (10^3/mm^3)	5.922 ± 1.84	7.614 ± 2.67	*0.192*	8.091 ± 0.93	9.72 ± 2.29	*0.167*	5.874 ± 3.28	10.764 ± 2.74	*0.006* *
Neutr/lymph	0.055 ± 0.018	0.055 ± 0.024	*0.999*	0.043 ± 0.020	0.045 ± 0.016	*0.850*	0.060 ± 0.020	0.0375 ± 0.020	*0.037* *

[15, 17, 23, 24] may represent an important biomarker of the health/disease process, as well as serve as a reference in subclinical biological processes that occur in the body. In other words, it is expected that acute exercise bouts signal a "stressful situation" to all physiological systems [20], leading to transient but augmented eHSP70 plasma levels, and regular exercise training may lead to an overall decrease in eHSP70 levels [49], as a "heat shock tolerance" phenomenon or exercise-induced stress adaptation. These effects support the prescription of exercise as a tool to decrease or maintain the normal eHSP70 and eHSP70/iHSP70 ratio values and, consequently, to promote optimum glucose metabolism. It is also well known that during physical exercise, IL-6 can be expressed and released by the skeletal muscle, and within the extracellular space, it binds to the IL-6 receptor in an autocrine action. Interestingly, the "myokine" IL-6 has also been found to induce HSF-1 translocation to the nucleus upregulating heat-induced HSP70 gene and protein expression. Since the anti-inflammatory response to acute exercise is attributed to increased circulating levels of known anti-inflammatory cytokines that are dependent on exercise effort [49, 54], our data suggested that as obese subjects find it difficult to reach adequate levels of exercise, this may also cause an impairment in appropriate adaptive HSR responses and subsequent metabolic benefits to obese/T2DM subjects.

5. Conclusion

Our study showed that HFD impaired exercise performance and weakened the standard heat shock response to exercise, as observed by lower levels of eHSP70 and extra-to-intracellular HSP70 ratio levels. $PM_{2.5}$ exposure modified glycaemic response to exercise and altered hematological responses in HFD mice. Our data indicated that obesity is a critical health condition for exercise prescription under $PM_{2.5}$ exposure.

Abbreviations

AUC: Area under the curve
eHSP70: Extracellular 70 kDa heat shock proteins
GTT: Glucose tolerance test
HFD: High-fat diet
HSP70: 70 kDa heat shock proteins
H index: eHSP70/iHSP70 ratio
iHSP70: Intracellular 70 kDa heat shock proteins
$PM_{2.5}$: Fine particulate matter
T2DM: Type 2 diabetes.

Data Availability

The data used to support the findings of this study are available from the corresponding author upon request.

Conflicts of Interest

The authors declare that they do not have competing financial interests.

Authors' Contributions

IMK completed all the experiments described in this manuscript. GW and YHD performed biometric and metabolic profiles. IMK, GW, and YHD performed the exercise

protocol. LCB and ABS performed experiments on oxidative stress parameters. ABS and GW performed Western blot analyses. MNF performed hematological procedures. TGH performed eHSP70 and eHSP70/iHSP70 procedures. All authors were involved in analyzing the results. TGH, IMK, KK, and VC cowrote and revised the paper. Figure 1 was designed by TGH and VC. TGH, MSL, and CRR designed the study. TGH, MSL, and CRR provided experimental advice and helped with manuscript revision. All the authors had final approval of the submitted and published versions.

Acknowledgments

This work was supported by the Regional University of Northwestern Rio Grande do Sul State (UNIJUI) and Federal University of Health Sciences of Porto Alegre (UFCSPA). This also was supported by grants from the Fundação de Amparo à Pesquisa do Estado do Rio Grande do Sul (#PqG-2013—FAPERGS, process 002106-2551/13-5 and #ARD/PPP/FAPERGS/CNPq 08/2014, process 16/2551-0000196-0, both to TGH) and from the Conselho Nacional de Desenvolvimento Científico e Tecnológico (CNPq) (#MCTI/CNPq no. 01/2016—CNPq, process 407329/2016-1 to TGH). IMK, ABS, and LCB were recipients of scholarships from the Coordination for the Improvement of Higher Education Personnel (CAPES) and GW from the Research Support Foundation of the State of Rio Grande do Sul (FAPERGS). The authors would like to thank colleagues from the Laboratory of Oxidative Stress and Atmospheric Pollution (UFCSPA), all students from the Research Group in Physiology (UNIJUI), and Prof. Paulo Ivo Homem de Bittencourt Jr. from the Laboratory of Cellular Physiology (UFRGS) for their technical support.

References

[1] K. B. Smith and M. S. Smith, "Obesity statistics," *Primary Care: Clinics in Office Practice*, vol. 43, no. 1, pp. 121–135, 2016, ix.

[2] C. M. Patterson, A. A. Dunn-Meynell, and B. E. Levin, "Three weeks of early-onset exercise prolongs obesity resistance in DIO rats after exercise cessation," *American Journal of Physiology-Regulatory, Integrative and Comparative Physiology*, vol. 294, no. 2, pp. R290–R301, 2008.

[3] R. Krogh-Madsen, M. Pedersen, T. P. J. Solomon et al., "Normal physical activity obliterates the deleterious effects of a high-caloric intake," *Journal of Applied Physiology*, vol. 116, no. 3, pp. 231–239, 2014.

[4] WHO, "Air quality guidelines – global update 2005," 2016, December 2017, http://www.who.int/phe/health_topics/outdoorair/outdoorair_aqg/en/.

[5] G. S. Hotamisligil, "Inflammation and metabolic disorders," *Nature*, vol. 444, no. 7121, pp. 860–867, 2006.

[6] P. Martín-Gallán, A. Carrascosa, M. Gussinyé, and C. Domínguez, "Biomarkers of diabetes-associated oxidative stress and antioxidant status in young diabetic patients with or without subclinical complications," *Free Radical Biology & Medicine*, vol. 34, no. 12, pp. 1563–1574, 2003.

[7] M. To, Y. Kono, N. Ogura et al., "Obesity-related systemic oxidative stress: an important factor of poor asthma control," *Allergology International*, vol. 67, no. 1, pp. 147–149, 2018.

[8] S. C. Dumith, P. C. Hallal, R. S. Reis, and H. W. Kohl III, "Worldwide prevalence of physical inactivity and its association with human development index in 76 countries," *Preventive Medicine*, vol. 53, no. 1-2, pp. 24–28, 2011.

[9] M. W. Gorr, M. J. Falvo, and L. E. Wold, "Air pollution and other environmental modulators of cardiac function," *Comprehensive Physiology*, vol. 7, no. 4, pp. 1479–1495, 2017.

[10] J. F. Pearson, C. Bachireddy, S. Shyamprasad, A. B. Goldfine, and J. S. Brownstein, "Association between fine particulate matter and diabetes prevalence in the U.S," *Diabetes Care*, vol. 33, no. 10, pp. 2196–2201, 2010.

[11] C. R. Rhoden, E. Ghelfi, and B. González-Flecha, "Pulmonary inflammation by ambient air particles is mediated by superoxide anion," *Inhalation Toxicology*, vol. 20, no. 1, pp. 11–15, 2008.

[12] C. R. Rhoden, G. A. Wellenius, E. Ghelfi, J. Lawrence, and B. González-Flecha, "PM-induced cardiac oxidative stress and dysfunction are mediated by autonomic stimulation," *Biochimica et Biophysica Acta (BBA) - General Subjects*, vol. 1725, no. 3, pp. 305–313, 2005.

[13] Z. Xu, X. Xu, M. Zhong et al., "Ambient particulate air pollution induces oxidative stress and alterations of mitochondria and gene expression in brown and white adipose tissues," *Particle and Fibre Toxicology*, vol. 8, no. 1, p. 20, 2011.

[14] X. D. Qin, Z. Qian, M. G. Vaughn et al., "Gender-specific differences of interaction between obesity and air pollution on stroke and cardiovascular diseases in Chinese adults from a high pollution range area: a large population based cross sectional study," *Science of The Total Environment*, vol. 529, pp. 243–248, 2015.

[15] P. B. Goettems-Fiorin, B. S. Grochanke, F. G. Baldissera et al., "Fine particulate matter potentiates type 2 diabetes development in high-fat diet-treated mice: stress response and extracellular to intracellular HSP70 ratio analysis," *Journal of Physiology and Biochemistry*, vol. 72, no. 4, pp. 643–656, 2016.

[16] J. Chung, A. K. Nguyen, D. C. Henstridge et al., "HSP72 protects against obesity-induced insulin resistance," *Proceedings of the National Academy of Sciences of the United States of America*, vol. 105, no. 5, pp. 1739–1744, 2008.

[17] T. G. Heck, S. P. Scomazzon, P. R. Nunes et al., "Acute exercise boosts cell proliferation and the heat shock response in lymphocytes: correlation with cytokine production and extracellular-to-intracellular HSP70 ratio," *Cell Stress and Chaperones*, vol. 22, no. 2, pp. 271–291, 2017.

[18] M. Krause, K. Keane, J. Rodrigues-Krause et al., "Elevated levels of extracellular heat-shock protein 72 (eHSP72) are positively correlated with insulin resistance in vivo and cause pancreatic β-cell dysfunction and death in vitro," *Clinical Science*, vol. 126, no. 10, pp. 739–752, 2014.

[19] J. Radons, "The human HSP70 family of chaperones: where do we stand?," *Cell Stress and Chaperones*, vol. 21, no. 3, pp. 379–404, 2016.

[20] T. G. Heck, C. M. Schöler, and P. I. H. de Bittencourt, "HSP70 expression: does it a novel fatigue signalling factor from immune system to the brain?," *Cell Biochemistry and Function*, vol. 29, no. 3, pp. 215–226, 2011.

[21] T. Kido, E. Tamagawa, N. Bai et al., "Particulate matter induces translocation of IL-6 from the lung to the systemic circulation," *American Journal of Respiratory Cell and Molecular Biology*, vol. 44, no. 2, pp. 197–204, 2011.

[22] B. Xia, K. Chen, Y. Lv et al., "Increased oxidative stress and plasma Hsp70 levels among gasoline filling station attendants," *Toxicology and Industrial Health*, vol. 33, no. 2, pp. 171–181, 2017.

[23] C. M. Schöler, C. V. Marques, G. S. da Silva, T. G. Heck, L. P. de Oliveira Junior, and P. I. Homem de Bittencourt, "Modulation of rat monocyte/macrophage innate functions by increasing intensities of swimming exercise is associated with heat shock protein status," *Molecular and Cellular Biochemistry*, vol. 421, no. 1-2, pp. 111–125, 2016.

[24] A. S. Mai, A. B. dos Santos, L. C. C. Beber et al., "Exercise training under exposure to low levels of fine particulate matter: effects on heart oxidative stress and extra-to-intracellular HSP70 ratio," *Oxidative Medicine and Cellular Longevity*, vol. 2017, Article ID 9067875, 13 pages, 2017.

[25] L. F. Maatz, G. J. A. Wood, D. H. R. F. Rivero, and P. H. N. Saldiva, "Tracheal instillation of urban $PM_{2.5}$ suspension promotes acute cardiac polarization changes in rats," *Brazilian Journal of Medical and Biological Research*, vol. 42, no. 2, pp. 207–213, 2009.

[26] K. C. Kregel, D. L. Allen, F. W. Booth et al., "Resource book for the design of animal exercise protocols," *American Physiological Society*, 152 pages, 2006.

[27] M. M. Bradford, "A rapid and sensitive method for the quantitation of microgram quantities of protein utilizing the principle of protein-dye binding," *Analytical Biochemistry*, vol. 72, no. 1-2, pp. 248–254, 1976.

[28] S. Marklund and G. Marklund, "Involvement of the superoxide anion radical in the autoxidation of pyrogallol and a convenient assay for superoxide dismutase," *European Journal of Biochemistry*, vol. 47, no. 3, pp. 469–474, 1974.

[29] P. M. Bock, M. Krause, H. T. Schroeder et al., "Oral supplementations with L-glutamine or L-alanyl-L-glutamine do not change metabolic alterations induced by long-term high-fat diet in the B6.129F2/J mouse model of insulin resistance," *Molecular and Cellular Biochemistry*, vol. 411, no. 1-2, pp. 351–362, 2016.

[30] B. Marmett, R. B. Nunes, K. S. de Souza, P. D. Lago, and C. R. Rhoden, "Aerobic training reduces oxidative stress in skeletal muscle of rats exposed to air pollution and supplemented with chromium picolinate," *Redox Report*, vol. 23, no. 1, pp. 146–152, 2018.

[31] T. G. Heck, R. B. Nunes, M. R. Petry et al., "Residual oil fly ash (ROFA) inhalation promotes lung and heart oxidative stress without hemodynamic effects in exercising rats," *Journal of Exercise Physiology Online*, vol. 17, no. 1, 2015.

[32] J. E. Sharman and M. Stowasser, "Australian association for exercise and sports science position statement on exercise and hypertension," *Journal of Science and Medicine in Sport*, vol. 12, no. 2, pp. 252–257, 2009.

[33] M. L. Harbison and J. D. Brain, "Effects of exercise on particle deposition in Syrian golden hamsters," *The American Review of Respiratory Disease*, vol. 128, no. 5, pp. 904–908, 1983.

[34] T. G. Heck, M. R. Petry, A. Maslinkiewicz et al., "Effects of ambient particles inhalation on lung oxidative stress parameters in exercising rats," *Journal of Exercise Physiology Online*, vol. 17, no. 3, pp. 58–69, 2015.

[35] I. M. Kostrycki, M. N. Frizzo, G. Wildner et al., "Hematological response of acute exercise in obese mice: the obesity attenuation effect on leukocytes response," *Journal of Exercise Physiology Online*, vol. 19, no. 6, 2016.

[36] A. Yoshimura, Y. Shimomura, T. Murakami et al., "Glycogen depletion of the intrafusal fibers in a mouse muscle spindle during prolonged swimming," *American Journal of Physiology-Regulatory, Integrative and Comparative Physiology*, vol. 271, no. 2, Part 2, pp. R398–R408, 1996.

[37] J. M. Petrosino, V. J. Heiss, S. K. Maurya et al., "Graded maximal exercise testing to assess mouse cardio-metabolic phenotypes," *PLoS One*, vol. 11, no. 2, article e0148010, 2016.

[38] T. Bruder-Nascimento, O. J. Ekeledo, R. Anderson, H. B. le, and E. J. Belin de Chantemèle, "Long term high fat diet treatment: an appropriate approach to study the sex-specificity of the autonomic and cardiovascular responses to obesity in mice," *Frontiers in Physiology*, vol. 8, p. 32, 2017.

[39] A. Giacca, Y. Groenewoud, E. Tsui, P. McClean, and B. Zinman, "Glucose production, utilization, and cycling in response to moderate exercise in obese subjects with type 2 diabetes and mild hyperglycemia," *Diabetes*, vol. 47, no. 11, pp. 1763–1770, 1998.

[40] F. Kim, M. Pham, E. Maloney et al., "Vascular inflammation, insulin resistance, and reduced nitric oxide production precede the onset of peripheral insulin resistance," *Arteriosclerosis, Thrombosis, and Vascular Biology*, vol. 28, no. 11, pp. 1982–1988, 2008.

[41] Q. Sun, P. Yue, J. A. Deiuliis et al., "Ambient air pollution exaggerates adipose inflammation and insulin resistance in a mouse model of diet-induced obesity," *Circulation*, vol. 119, no. 4, pp. 538–546, 2009.

[42] R. C. Walsh, I. Koukoulas, A. Garnham, P. L. Moseley, M. Hargreaves, and M. A. Febbraio, "Exercise increases serum Hsp72 in humans," *Cell Stress & Chaperones*, vol. 6, no. 4, pp. 386–393, 2001.

[43] D. P. Gelain, M. A. de Bittencourt Pasquali, C. M. Comim et al., "Serum heat shock protein 70 levels, oxidant status, and mortality in sepsis," *Shock*, vol. 35, no. 5, pp. 466–470, 2011.

[44] M. Whitham and M. B. Fortes, "Heat shock protein 72: release and biological significance during exercise," *Frontiers in Bioscience*, vol. 13, no. 13, pp. 1328–1339, 2008.

[45] E. Rubio, A. I. Valenciano, C. Segundo, N. Sánchez, F. de Pablo, and E. J. de la Rosa, "Programmed cell death in the neurulating embryo is prevented by the chaperone heat shock cognate 70," *The European Journal of Neuroscience*, vol. 15, no. 10, pp. 1646–1654, 2002.

[46] H. Adachi, M. Katsuno, M. Waza, M. Minamiyama, F. Tanaka, and G. Sobue, "Heat shock proteins in neurodegenerative diseases: pathogenic roles and therapeutic implications," *International Journal of Hyperthermia*, vol. 25, no. 8, pp. 647–654, 2009.

[47] F. Cangeri di Naso, R. Rosa Porto, H. Sarubbi Fillmann et al., "Obesity depresses the anti-inflammatory HSP70 pathway, contributing to NAFLD progression," *Obesity*, vol. 23, no. 1, pp. 120–129, 2015.

[48] P. Newsholme and P. I. H. de Bittencourt Jr., "The fat cell senescence hypothesis: a mechanism responsible for abrogating the resolution of inflammation in chronic disease," *Current Opinion in Clinical Nutrition and Metabolic Care*, vol. 17, no. 4, pp. 295–305, 2014.

[49] M. Krause, T. G. Heck, A. Bittencourt et al., "The chaperone balance hypothesis: the importance of the extracellular to intracellular HSP70 ratio to inflammation-driven type 2 diabetes, the effect of exercise, and the implications for clinical

management," *Mediators of Inflammation*, vol. 2015, Article ID 249205, 12 pages, 2015.

[50] E. Ten Caten Martins, R. Z. dos Santos, A. B. dos Santos et al., "Detectable levels of eHSP72 in plasma are associated with physical activity and antioxidant enzyme activity levels in hypertensive subjects," *Cell Stress & Chaperones*, vol. 23, no. 6, pp. 1319–1327, 2018.

[51] M. A. Febbraio, J. L. Mesa, J. Chung et al., "Glucose ingestion attenuates the exercise-induced increase in circulating heat shock protein 72 and heat shock protein 60 in humans," *Cell Stress & Chaperones*, vol. 9, no. 4, pp. 390–396, 2004.

[52] S. Laing, G. Wang, T. Briazova et al., "Airborne particulate matter selectively activates endoplasmic reticulum stress response in the lung and liver tissues," *American Journal of Physiology-Cell Physiology*, vol. 299, no. 4, pp. C736–C749, 2010.

[53] S. Bellini, F. Barutta, R. Mastrocola, L. Imperatore, G. Bruno, and G. Gruden, "Heat shock proteins in vascular diabetic complications: review and future perspective," *International Journal of Molecular Sciences*, vol. 18, no. 12, 2017.

[54] B. K. Pedersen, "The anti-inflammatory effect of exercise: its role in diabetes and cardiovascular disease control," *Essays in Biochemistry*, vol. 42, pp. 105–117, 2006.

Hindawi
Journal of Diabetes Research
Volume 2018, Article ID 3274084, 12 pages
https://doi.org/10.1155/2018/3274084

Research Article

Advanced Glycation End Products Increase MDM2 Expression via Transcription Factor KLF5

Pu Wang[1], **Yu Cheng Lu**[1], **Yuan Fei Li**[2], **Lan Wang**[1] and **Shao Chin Lee**[1,3]

[1]*School of Life Sciences, Shanxi University, Taiyuan, Shanxi 030006, China*
[2]*Department of Oncology, The First Clinical Hospital of Shanxi Medical University, Taiyuan, Shanxi 030006, China*
[3]*Department of Bological Science, School of Life Sciences, Jiangsu Normal University, Xuzhou, Jiangsu 221000, China*

Correspondence should be addressed to Shao Chin Lee; lee_shao@hotmail.com

Received 25 March 2018; Revised 23 May 2018; Accepted 20 June 2018; Published 9 September 2018

Academic Editor: Julia M. dos Santos

Type 2 diabetes increases the risk for all-site cancers including colon cancer. Diabetic patients present typical pathophysiological features including an increased level of advanced glycation end products (AGEs), which comes from a series of nonenzymatic reactions between sugars and biological macromolecules, positively associated with the occurrence of diabetic complications. MDM2 is an oncogene implicated in cancer development. The present study investigated whether diabetes promoted MDM2 expression in colon cells and the underlying mechanisms. Our results showed that AGE increased the protein level of MDM2 in a cell model and promoted binding between MDM2 and Rb as well as p53, which led to degradation of Rb and p53. KLF5 was able to bind to the regulatory sequence of the MDM2 gene, and knockdown of the KLF5 protein level inhibited the AGE-triggered MDM2 overexpression, which indicated that KLF5 was the transcription factor for MDM2. In a mouse model of diabetes, we found that AGE level was increased in serum. The protein levels of both KLF5 and MDM2 were increased. KLF5 was able to bind to the regulatory sequence of the MDM2 gene. In conclusion, our results suggest that diabetes increases the level of AGE which enhances the expression of MDM2 via transcription factor KLF5 in colon cells. MDM2 overexpression is a candidate biological link between type 2 diabetes and colon cancer development.

1. Introduction

Type 2 diabetes is a prevalent endocrine disease worldwide, which causes tremendous economic and health burden [1]. Epidemiologic research suggests that people who suffered from this diabetes have a significantly increased risk for many types of cancer such as colon cancer, endometrial cancer, and breast cancer [2]. For colon cancer, in particular, a 1.5- to 3.0-fold increase in cancer risk is observed [3–5]. Nevertheless, the biological links between type 2 diabetes and cancer remain unknown. Common pathophysiological factors in diabetes, hyperinsulinemia, hyperglycemia, increased level of saturated fatty acids, and advanced glycation end-products (AGEs) [2], are associated with increased cancer risk. However, the underlying molecular mechanisms are to be explored.

AGEs are a complex and heterogeneous group of compounds which comes from a series of nonenzymatic reactions between sugars and biological macromolecules (proteins, lipids, and nucleic acid) [6]. AGEs have been shown to accumulate in various tissues under diabetic conditions, and they participate in the development of diabetic vascular complications (nephropathy, retinopathy, and atherosclerosis) and nondiabetic disease such as senescence and tumours [7]. Glycosylated hemoglobin A1 has been used as an important indicator for diabetes diagnosis and treatment outcome. There is evidence of an association between AGEs and cancer development; epidemiological data demonstrate that the serum concentration of glyceraldehyde-derived AGEs in patients with colorectal cancer is increased and is closely related to an increased risk of rectal cancer [8]. Experiments *in vitro* show that AGEs can promote migration and invasion of breast and colon cancers through the ERK-MMP pathway; moreover, AGEs can enhance colon formation, as observed in soft agar colon formation assay [9, 10]. When BSA drove AGEs are administered ip, they are able to promote the liver metastasis of human colorectal cancer [11].

MDM2 is an oncogene, the amplification and overexpression of which are linked to progression and poor prognosis of different cancers. It can bind directly to cancer suppressors p53 and Rb to promote their inactivation and/or degradation [12].

In clinical samples, increase in MDM2 gene amplification and cytoplasmic expression are observed in colon cancer, which is associated with advanced cancer staging [13]. However, many tumours exhibit high MDM2 and MDMX protein levels without increased copy number [14]. Thus, transcriptional regulation of MDM2 expression in different tissues appears to be the mechanism for increased MDM2 expression [14]. Several transcription factors have been found in MDM2 transcriptional regulation, which include SP1, p53, NF-κB, and KLF6 [15–19]. MDM2 is expressed at different levels in different tissues without known reasons and mechanisms; trigger- or tissue-specific transcriptional factors have not been documented [14].

Kruppel-like factor 5 (KLF5) belongs to the family of Kruppel-like transcription factors, of which 17 members have been identified to date. Members of this family have been implicated in an extensive array of biological processes including embryonic development, control of cellular proliferation and differentiation, and stress response [20]. KLF5 is expressed in the reproductive organs, pancreas, prostate, skeletal muscle, and lung [21]. However, the highest level of its expression is found in intestinal epithelial cells [22]. Studies *in vivo* have demonstrated essential roles of this protein in various biological processes. KLF5 can function as a transcriptional activator or repressor, a promoter or inhibitor of cell growth and survival, and either an oncogene or tumor suppressor, depending on the cellular and genetic context in which it operates [23]. More importantly, evidence suggests that KLF5 plays an important role in intestinal tumorigenesis. In $LGR5^+$ stem cells, which contain an oncogenic mutant β-catenin, the production of lethal adenomas and carcinomas is completely inhibited by KLF5 deletion [24].

KLF family members are closely related to Sp1 transcription factors but are distinguished by a unique pattern of three cysteine-2/histidine-2 zinc finger motifs separated by seven conserved amino acids at the carboxy terminal of the proteins [25]. Both KLF5 and SP1 bind to similar elements within GC-rich promoter sequences of target genes. Existing data show that SP1 targets at the MDM2 gene basally or under different stimuli [26]. Differential transcriptional activities between SP1 and KLF5 have not been well documented.

From the above, we have a hypothesis that AGEs could promote colon cancer development through active KLF5.

2. Materials and Methods

2.1. Cell Culture. HCT116 (human colon cancer cell) cells were kindly provided by Dr. B. Vogelstein of the Johns Hopkins University School of Medicine, which were maintained in DMEM (low glucose, 5 mM) supplemented with 50 U/ml penicillin, 50 μg/ml streptomycin, and 10% (v/v) fetal calf serum. The culture medium and reagents for the colon cancer cells were purchased from Gibco (Beijing, China).

2.2. Chemicals and Antibodies. Chemicals were purchased from Sigma (St. Louis, MO, USA). Anti-KLF5 antibody (sc-398470, mice, 1 : 1000) was purchased from Santa Cruz (California, USA). Rabbit antibodies against p53 (D120082, 1 : 500), Rb (D221069, 1 : 500), p-Rb (D151284, 1 : 500), MDM2 (D155246, 1 : 500), SP1 (D161137, 1 : 500), actin (D110001,1 : 1000), anti-histone 2A antibody (D151717, 1 : 1000), and anti-BSA (D120272, 1 : 200) were purchased from Sangon (Shanghai, China). Anti-rabbit fluorescent antibody flux 488 (number 4412, Goat, 1 : 1000) was purchased from Cell Signaling. CHIP Kit (P2078) and Cell Cycle Detection kit (C1052) were purchased from Beyotime (Shanghai, China).

2.3. Preparation of AGEs. 50 mg/ml BSA (Sigma, USA) was incubated with 0.5 mmol/l D-glucose (Sigma, USA) for 8 weeks at 37°C. The unincorporated sugar was removed by dialysis against 0.2 mmol/l PBS (pH 7.4). 50 mg/ml nonglycated BSA was incubated without D-glucose as a negative control. The AGEs preparations were scanned for fluorescent intensity using a fluorospectrophotometer (SpectraMax M5, USA). AGEs had fluorescent peak at excitation wavelength of 370 nm and slit 2 nm. Data were processed using GraphPad Prism 6.

2.4. Flow Cytometric Analysis of AGEs Cell-Binding Assay. HCT116 cells seeded on 6-well plates were treated with 50 μg/ml AGEs at 37°C for 4 hours. Cells were collected by centrifugation at 1000g for 5 min, washed with ice-cold PBS, and then fixed with 70% cold ethanol and stored at 4°C for 24 h. Cells were centrifuged again, washed with cold PBS twice, and incubated with anti-BSA antibody for 1 hour at room temperature, and then cells were washed three times with ice-cold PBS followed by FITC-conjugated secondary antibody in 1x PBS for 1 hour at room temperature in the dark, then cells were washed again and measured by flow cytometry. Data were analyzed by FlowJo 7.6.

2.5. Western Blot Analysis. The cultured HCT116 cells and mouse colon tissues were lysed in RIPA buffer. Proteins were separated by polyacrylamide gel electrophoresis and transferred onto PVDF membrane. After blocking for 1 hour at room temperature with TBST containing 0.05% (v/v), Tween-20, and 5% (w/v) nonfat milk, the membranes were incubated with primary antibodies overnight at 4°C, followed by washes with TBST containing 0.05% Tween-20. The membranes were then incubated with a horseradish peroxidase-conjugated secondary antibody for 1 hour at room temperature. ECL reagents (number 32106, Thermo Biosciences) were used to visualize the protein bands, which were captured on an X-ray film.

2.6. Knockdown of Protein Level. The predesigned siRNA oligonucleotides (Sangon Technology, Shanghai, China) were as follows:

(1) KLF5, 5′-AAAGUAUAGACGAGACAGUGC-3′ (sense) and GCCTGTCTCGTCTTCTTT (antisense)

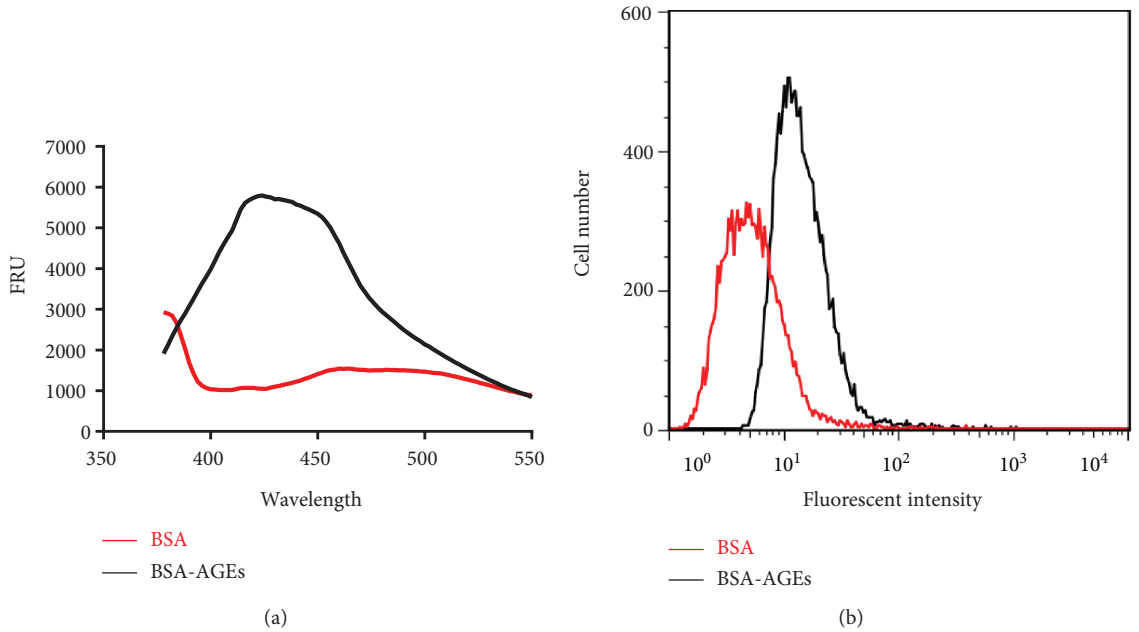

Figure 1: Quanlity assessment of BSA-AGEs and their binding to cells. (a) Full-wavelength scanning was performed to analyze the fluorescent density of quanlity of the prepared AGEs, which indicated the aunlity of the preparation. Excitation wavelength was 370 nm. (b) Cells were treated with AGEs for 4 hours and stained with indirect immunofluorescence staining against BSA and then measured by flow cytometry, which indicated the cell binding of AGE. Every experiment was repeated at least three times.

(2) SP1, 5′AACAGCGTTTCTGCAGCTACC-3′(sense) and GGTAGCTGCAGAAACGCTGTT (antisense)

(3) RAGE, 5′-GCCGGAAAUUGUGAAUCCUTT-3′ (sense) and AAGGTTCCTTTCCGGC (antisense)

HCT116 cells (5×10^4 cells per well) were seeded in 6-well plates and cultured for 24 hours and then were transfected with 200 nM SiRNA oligonucleotides using Lipofectamine 2000 transfection reagent (11668-019, Invitrogen), according to the manufacturer's instructions. Transfection efficiency was evaluated by Western blot analysis 24 hours after transfection.

2.7. Immunoprecipitation. Cultured HCT116 cells were harvested under nondenaturing conditions, washed by ice-cold PBS for 3 times, lysed in 0.5 ml ice-cold cell lysis buffer, and centrifuged. The supernatant was collected to a new tube and incubated with 20 μl Protein G Plus/Protein A agarose (IP05 Millipore) with gentle shaking for 2 hours at 4°C. Protein G Plus/Protein A agarose was then removed by centrifuge for 10 min at 4°C, and the supernatant was incubated with primary antibody overnight at 4°C with gentle shaking. Afterwards, 30 μl Protein G Plus/Protein A agarose were added and incubated under gentle shaking for 4 hours at 4°C. Finally, Protein G Plus/Protein A agarose was collected by centrifuge followed by 2x loading buffer resuspension and heating at 100°C and microcentrifuge for 1 minute at 14000g.

2.8. Chromatin Immunoprecipitation. Cultured HCT116 cells were washed and cross-linked using 1% formaldehyde for 20 min, and mouse colon tissues were cross-linked using 1% formaldehyde for 30 min and homogenized. After stopping cross-linking by addition of 0.1 mol/l glycine, cell lysates were sonicated and centrifuged. Immunoprecipitations were performed using the KLF5 antibody in the presence of BSA/salmon sperm DNA and a 50% slurry of protein A agarose beads. Input and immunoprecipitates were washed and eluted and then incubated for 2 h at 42°C in the presence of proteinase K followed by 6 h at 65°C to reverse the formaldehyde cross-linking. DNA fragments were recovered by phenol/chloroform extraction and ethanol precipitation. The related fragments on promoters of MDM2 were amplified by reverse transcription PCR. DNA bands on agarose gels were detected on a UV transilluminator, and graphs were reverse treated by FluorChem HD2 (Alpha Innotech 1.3.0.7). Primers used were as follows:

(i) Human primer 1 GGAGTGTCACAGCGCCAAA (forward) and CAATTGGGTCCGGGGCTC (reverse)

(ii) Human primer 2 TAAAAGCGCAGAGTAACCG CT (forward) and CGCTGGAGTTGTACCCAAA TG (reverse)

(iii) Human primer 3 GTGGACACTGAGTCATACT GCT (forward) and AAAAGAAGGGTCAGAA ATGAAGGC (reverse)

(iv) Mouse primer 1 ATTGCGGTTTCGAGCGGTAA (forward) and GCCGCCTCCTGGACCAATA (reverse)

(v) Mouse primer 2 TGTGGCGTGAGTGACTGAAA (forward) and AAGACTTTAAAAATAGGCAAG GTGA (reverse)

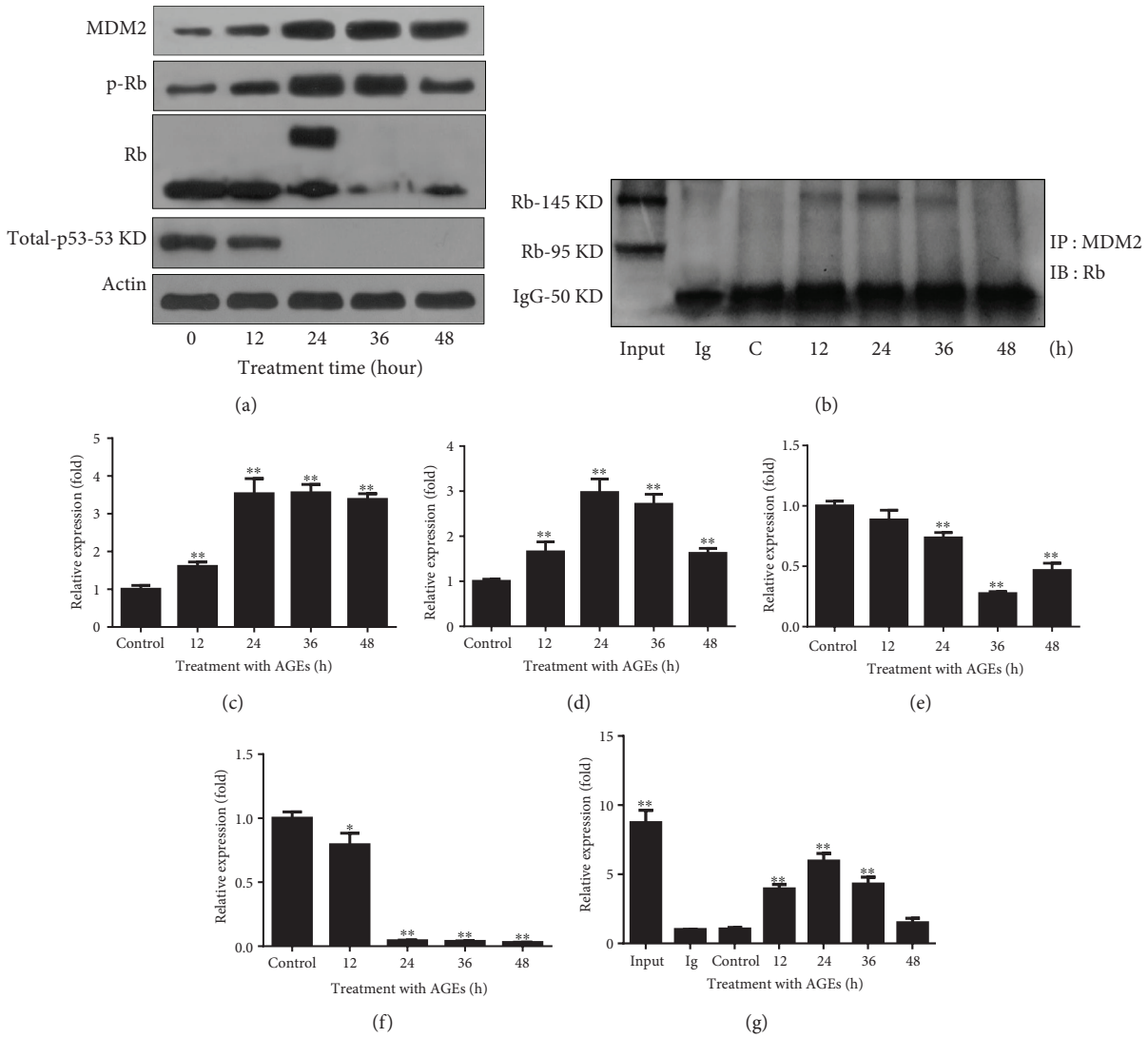

Figure 2: AGEs promote expression of MDM2, degradation of p53 and Rb degradation, and phosphorylation of Rb. (a) Cells were treated with AGEs (50 μg/ml) for indicated times; MDM2, p-Rb, Rb, and p53 were quantified by Western blot analysis, which showed that the expression level of MDM2 was increased and the level of RB as well as p53 was decreased. Phosphorylation of Rb was increased. (b) Cells were treated with BSA-AGEs (50 μg/ml) for indicated times, anti-MDM2 antibody was used for immunoprecipitation, and anti-Rb antibody was used for Western blot analysis, which showed the binding between MDM2 and Rb. Every experiment was repeated at least three times. (c–f) The bands of MDM2 (c), pRb (d), Rb (e), and total p53 (f) in Figure 2(a) were quantified using ImageJ. (g) The band of Rb in Figure 2(b) was quantified using ImageJ. Every experiment was repeated at least three times. Asterisks denote significant difference amongst experimental groups. $^{*}p < 0.05$ and $^{**}p < 0.01$.

2.9. Diabetic Mouse Model. Diabetes was induced in ICR mice by consecutive injection of 50 mg/kg streptozotocin (STZ) (0.05 mol/l sodium citrate, pH 5.5) for 5 days after an 8 h fast. Animals with fasting blood glucose >14 mg/dl were considered to be diabetic. After 8 weeks of injections, blood samples were collected by removing the eyeball; latter, mice were killed by dislocation of the cervical spine. Blood routine examinations were analyzed at the Hospital of Shanxi University by flow cytometry. All *in vivo* procedures were performed according to the National Institutes of Health Guide for the Care and Use of Laboratory animals. Animals were maintained at a barrier area of the laboratory animal center, and padding was changed every day. Blood AGEs were detected by fluorescence quantification at excitation wavelength 370 nm and emission wavelength was 440 nm. The fluorescent intensity was aligned by serum protein concentration.

2.10. Statistical Analysis. All of the experiments were performed in triplicate. The data in figures were expressed as mean ± SD, the data of quantified blot bands were expressed as mean (fold) ± SD, and nonparametric test was performed to compare the difference between two groups. One-way ANOVA was performed to show the time-dependent effects observed in the study. The statistical analysis software package SPSS21 was employed for statistical comparisons. A p value < 0.05 was considered as statistically significant.

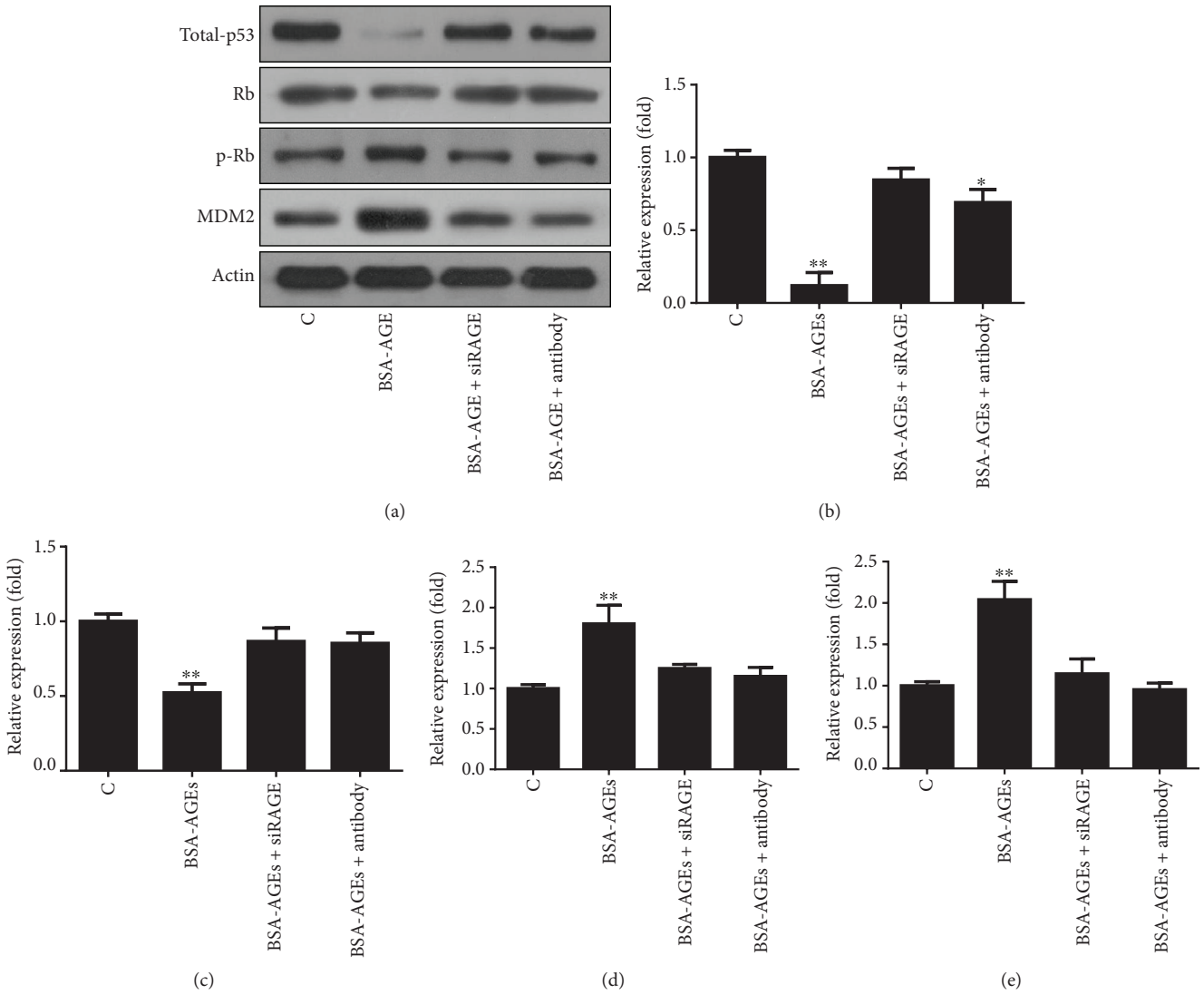

Figure 3: AGEs trigger signaling via their receptor RAGE. Cells were pretreated with RAGE siRNA or anti-RAGE antibody followed by treatment with BSA-AGEs (50 μg/ml) for 24 hours. Both siRNA and anti-RAGE inhibited the effects of AGEs on the levels of MDM2, Rb, and p53. (b–e) The bands of p53 (b), Rb (c), p-Rb (d), and MDM2 (e) in Figure 3(a) were quantified using ImageJ. Every experiment was repeated at least three times. Asterisks denote significant difference amongst experimental groups. $^{*}p < 0.05$ and $^{**}p < 0.01$.

2.11. Experimental Design. Firstly, we prepared the AGEs using the BSA-glucose incubation method. Flow cytometry was performed to verify its ability of binding the HCT116 cancer cell line. Then, we analyzed the protein levels of p53, Rb, p-Rb, and MDM2 by Western blot. Finally, we examined whether KLF5 was the transcription for MDM2. Candidate sequences of KLF5 binding to the human MDM2 gene regulatory sequence were predicted in the JASPAR database. Its binding ability was also verified by chromatin immunoprecipitation in the HCT116 cell line. We also quantified the protein level of klf5 and MDM2 and their binding in the colon tissues of healthy and diabetic mice, to show that their expressions and binding were also elevated in colon tissues in diabetes.

3. Results

3.1. BSA-AGEs Quality and Its Cell Binding. Wavelength spectrum scanning showed that the prepared BSA-AGEs had an obvious absorption peak at the wavelength between 400 and 450 nm (Figure 1(a)). There was a significant increase (6.1 ± 0.8, $p < 0.01$) in the area under the curve. Next, we investigated the cell-binding ability of the prepared BAS-AGEs using flow cytometry analysis. The results showed that after treatment with BSA-AGEs, cell fluorescence intensity was significantly increased, compared with that in the cells treated with BSA alone (23.1 ± 3.1 versus 7.81 ± 0.65; $p < 0.01$) (Figure 1(b)). Results from MTT assay showed that AGEs did not inhibit cell viability from the concentrations from 50 to 300 μg/ml (figure not shown). We used the concentration of 50 μg/ml in all the experimental treatments, since the cell appeared to psroliferate well at this concentration of BSA-AGEs.

3.2. BSA-AGEs Enhances the Expression of MDM2 and Phosphorylation of Rb and Decreases the Protein Levels of Rb and p53. Results from the Western blot analyses showed

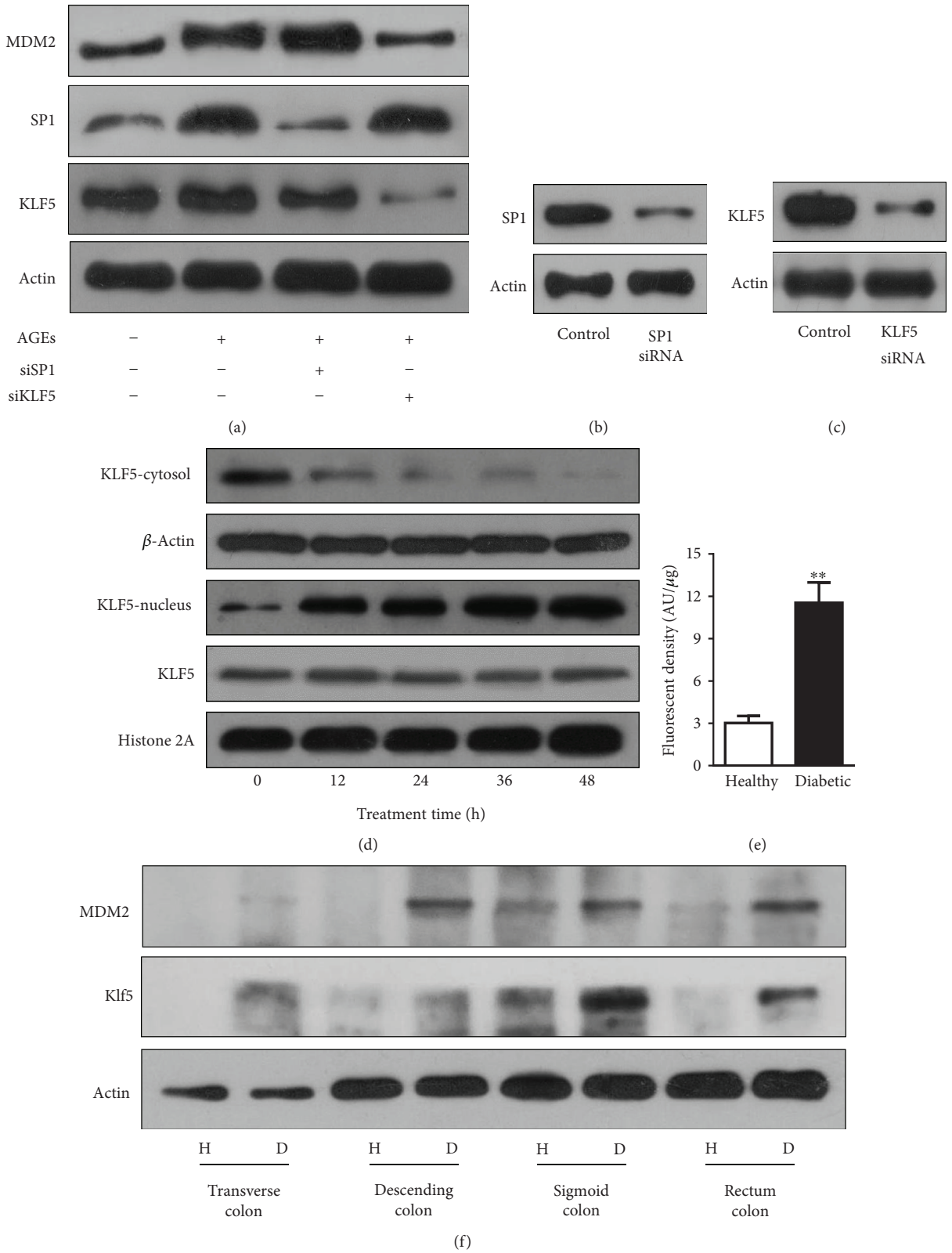

Figure 4: Continued.

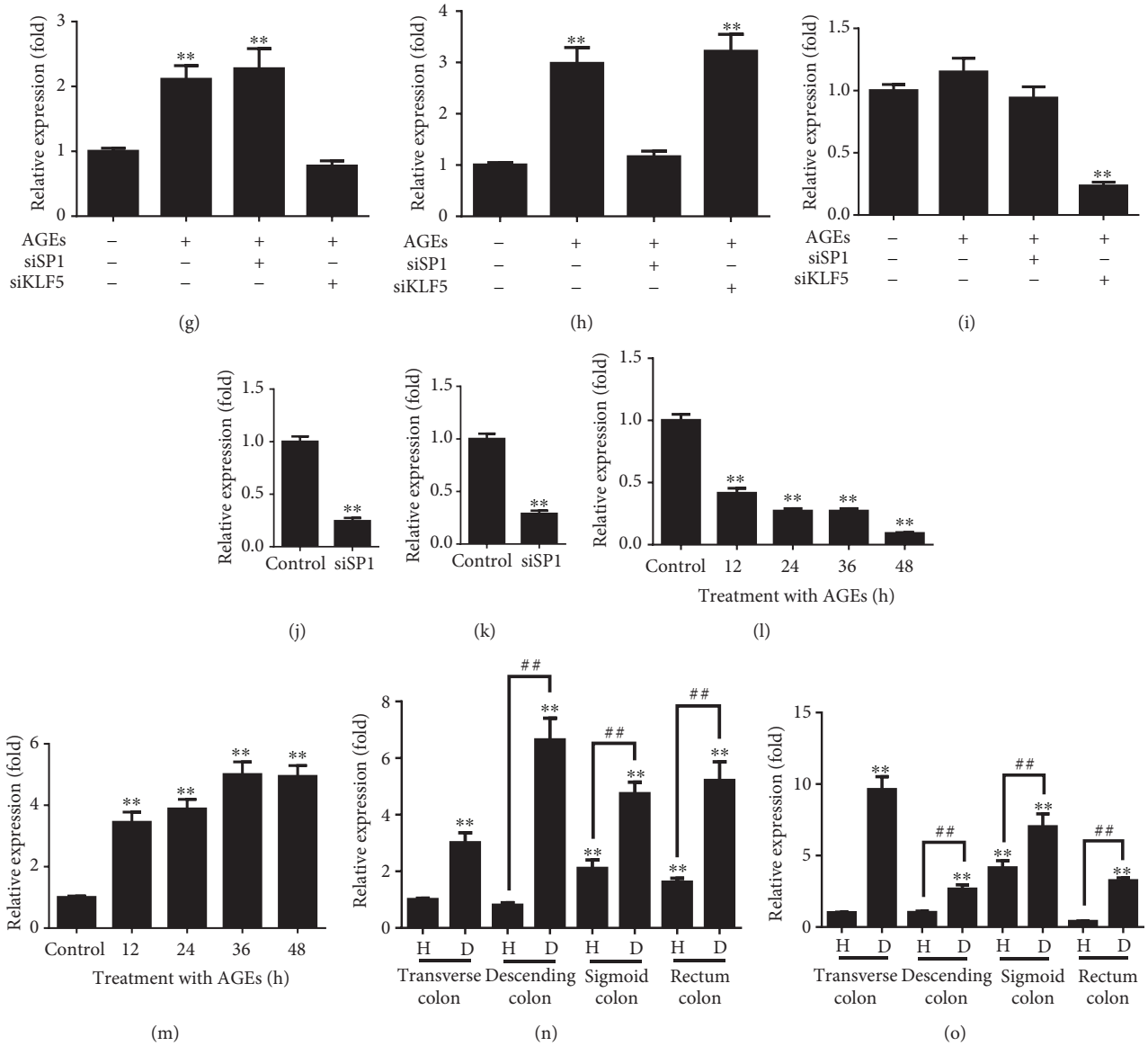

Figure 4: Transcription factor KLF5 regulates MDM2 gene expression. (a) Cells were treated with siRNA target of SP1 or KLF5 to test their effects on the levels of proteins. KLF5 siRNA rather than SP1 siRNA inhibited the AGE-caused changes in the protein levels. (b) SP1 siRNA knocked down the SP1 protein level; (c) KLF5 siRNA knocked down the KLF5 protein level; (d) AGEs triggered the nuclear translocation of KLF5; (e) the level of AGEs in serum of diabetic mice was increased. Serum fluorescent intensity represented the AGE level. (f) The protein levels of both KLF5 and MDM2 were increased in the colon of diabetic mice; (g–i) The bands of MDM2 (g), SP1 (h), and KLF5 (i) in Figure 4(a) were quantified using ImageJ. (j–k) The bands of SP1 (j) and KLF5 (k) in Figures 4(b) and 4(c) were quantified using ImageJ. (l–m) The bands of KLF5 in the cytosol (l) and nucleus (m) in Figure 4(d) were quantified using ImageJ. (n–o) The bands of MDM2 (n) and KLF5 (o) in Figure 4(f) were quantified using ImageJ. Every experiment was repeated at least three times. Asterisks denote significant difference compared to the control group; well number denotes significant difference compared to the healthy group within the same section of colons. $^{\#\#}p < 0.01$ and $^{**}p < 0.01$.

that AGEs upregulated the expression of MDM2 (control (1 ± 0.10): 12 h (1.6 ± 0.12): 24 h (3.5 ± 0.41): 36 h (3.6 ± 0.22): 48 h (3.4 ± 0.15), $p < 0.01$) and downregulated the protein levels of Rb (control (1 ± 0.04): 12 h (0.88 ± 0.08): 24 h (0.74 ± 0.04): 36 h (0.27 ± 0.016): 48 h (0.46 ± 0.06), $p < 0.01$) and p53 (control (1 ± 0.05): 12 h (0.79 ± 0.09): 24 h (0.04 ± 0.004): 36 h (0.038 ± 0.006): 48 h (0.029 ± 0.002), $p < 0.01$) as well as phosphorylation of Rb (control (1 ± 0.05): 12 h (1.6 ± 0.22): 24 h (2.9 ± 0.35): 36 h (2.7 ± 0.22): 48 h (1.6 ± 0.11), $p < 0.01$), which leads to its inactivation, in a time-dependent manner (Figure 2(a)). Moreover, MDM2 directly bound to Rb after 12 (3.9 ± 0.33), 24 (5.9 ± 0.55), and 36 (4.3 ± 0.51) hours of treatment ($p < 0.01$); the maximum binding occurred at 24 hours (Figure 2(b)).

3.3. AGE Signals through Its Receptor. To investigate whether the AGEs bound to its receptor (receptor of advanced glycation end product (RAGE)) to regulate the levels of Rb and

Table 1: Demographic data of experimental animals.

	Healthy subjects	Diabetic subjects
n	6	6
Weight (g)	29.4 ± 2.57	$20.8 \pm 1.48^{**}$
Blood glucose (mmol/l)	8.04 ± 1.34	$28.7 \pm 1.99^{**}$
HbA1c (mmol/l)	6.55 ± 1.04	$17.38 \pm 4.64^{**}$
LDL (mmol/l)	0.12 ± 0.05	$0.44 \pm 0.27^{*}$
HDL (mmol/l)	2.59 ± 0.64	$3.536 \pm 0.76^{*}$
TC (mmol/l)	3.1 ± 1.2	$5.12 \pm 1.08^{*}$
TG (mmol/l)	0.33 ± 0.25	$4.58 \pm 1.39^{**}$

Data are means ± SD or medians (range). $^{*}p < 0.05$ and $^{**}p < 0.01$.

p53, we treated the cells with RAGE siRNA that knocked down the RAGE level (Figure 3(a)) or RAGE antibody, which is aimed at inhibiting RAGE signaling, and found that both treatments were able to inhibit the AGEs-caused decrease in protein levels of p53 (control (1.0 ± 0.05): BSA-AGEs (0.12 ± 0.09): BSA-AGEs + siRAGE (0.85 ± 0.08): BSA-AGEs + antibody (0.69 ± 0.09), $p < 0.01$) and Rb (control (1.0 ± 0.05): BSA-AGEs (0.52 ± 0.06): BSA-AGEs + siRAGE (0.87 ± 0.09): BSA-AGEs + antibody (0.85 ± 0.07), $p < 0.01$) as well as the AGE-caused increase in Rb phosphorylation (control (1.0 ± 0.05): BSA-AGEs (1.80 ± 0.23): BSA-AGEs + siRAGE (1.25 ± 0.05): BSA-AGEs + antibody (1.15 ± 0.11), $p < 0.01$) (Figure 3(a)).

3.4. KLF5 Transcribes MDM2 in the Cell Model. We next examined the responsible transcription factor that enhanced the MDM2 expression by targeting at SP1 and KLF5. We found that the treatment increased the protein level of SP1 (1.0 ± 0.05 versus 2.98 ± 0.31, $p < 0.01$) (Figure 4(a)). However, knockdown of SP1 (1.0 ± 0.05 versus 0.28 ± 0.03, $p < 0.01$) (Figure 4(b)) had no effect on the AGEs-enhanced MDM2 expression (Figure 4(a)). Although the protein level of KLF5 was not significantly increased in the AGEs-treated cells (Figure 4(a)), KLF5 siRNA which decreased its protein level (1.0 ± 0.05 versus 0.24 ± 0.03, $p < 0.01$) (Figure 4(c)) was able to abolish the upregulation of MDM2 expression by AGEs (Figure 4(a)). Since the activity of transcription factors is often dependent on subcellular localizations, we investigated the level of KLF5 in the cytosol and nucleus fractions to test whether AGEs increased the nuclear translocation. The results showed that the concentration of KLF5 started to decrease in the cytosol fraction and to translocate to the nucleus from 12 hours (1.0 ± 0.05 versus 0.41 ± 0.04, $p < 0.01$) of the AGEs treatment, which continued to 48 hours (1.0 ± 0.05 versus 0.09 ± 0.007, $p < 0.01$) (Figure 4(d)). We investigated whether KLF5 transcribed the MDM2 animal model of diabetes. Mice were treated with STZ to induce diabetes. Table 1 shows that the mice became diabetic after 8 weeks of STZ treatment, in particular the AGEs level, as indicated by the increase in fluorescent intensity of serum from diabetic mice (3.0 ± 0.2 versus 11.5 ± 0.7; $p < 0.01$) (Figure 4(e)). The fluorescent intensity was measured at a wavelength of 350 nm which indicated the level of AGEs. The protein level of KLF5 was both increased in the transverse colon (1.0 ± 0.05 versus 3.0 ± 0.35, $p < 0.01$), descending colon (0.8 ± 0.09 versus 6.6 ± 0.77, $p < 0.01$), sigmoid colon (2.1 ± 0.3 versus 4.7 ± 0.41, $p < 0.01$), and rectum colon (1.6 ± 0.14 versus 5.2 ± 0.66, $p < 0.01$) of diabetic mice (Figure 4(f)) as well as the protein level of MDM2 in the transverse colon (1.0 ± 0.05 versus 9.6 ± 0.9, $p < 0.01$), descending colon (1.0 ± 0.1 versus 2.6 ± 0.3, $p < 0.01$), sigmoid colon (4.1 ± 0.5 versus 7.0 ± 0.6, $p < 0.01$), and rectum colon (0.39 ± 0.04 versus 3.2 ± 0.2, $p < 0.01$) of diabetic mice.

3.5. Evidence that KLF5 Transcribes MDM2 in an Animal Model of Diabetes. To obtain further evidence that KLF5 transcribed MDM2, we performed chromatin immunoprecipitation to pull down the transcriptional regulatory sequence of MDM2 using the KLF5 antibody. A total of 4 pieces of human MDM2 gene-binding candidate sequences were obtained after binding site prediction using the JASPAR database (Figure S1). In particular, we designed primers to cover the binding sequences, and the predicted first and third candidate binding sequences were 138 bp and 166 bp in length, respectively. Indeed, we were able to show that the KLF5 antibody pulled down two pieces of sequences which had the calibrated length close to those of the first and third KLF5-binding sequences (138 and 166 bp, respectively; Figure S1) in the transcription regulatory region of MDM2 (Figures 5(a) and 5(b)).

Finally, four pieces of mouse MDM2 gene candidate binding sequences for KLF5 were identified in the JASPAR database (Figure S2). We designed two sets of primers to amplify the binding sequences. Primer 1 amplified the first two binding sequences, and primer 2 amplified the third and fourth binding sequences. Using the KLF5 antibody, we were able to pull down the third and fourth KLF5 binding sequences from the MDM2 gene in chromatin immunoprecipitation assay, which was about the predicted size of 190 bp (Figure 5(c)).

4. Discussion

In this study, for the first time, we showed that AGEs *in vitro* could trigger the overexpression of MDM2 (Figure 2(a)) which directly bond to p53 and Rb, which led to Rb and p53 degradation (Figures 2(a) and 2(b)). Increase in MDM2 expression was also seen in a diabetic mouse model (Figure 4(b)). Furthermore, transcription factor KLF5 was found to directly transcribe MDM2 *in vitro* and *in vivo*, which was responsible for the increased MDM2 expression (Figures 4(e), 4(f), and 5(c)).

In diabetes, raised insulin and insulin-like growth factors stimulate cancer cell proliferation and metastasis. Increases in inflammatory cytokines in diabetes promote tumour development, which include interleukin-6 (IL-6), monocyte chemoattractant protein, plasminogen activator inhibitor-1 (PAI-1), adiponectin, leptin, and tumor necrosis factor-alpha [27]. Due to the increase in cytokines, several prooncogenes are hyperactivated in diabetes. Akt/mTOR is positively associated with diabetes cancer initiation and progression [28]. SIRT1 deacetylates and inactivates p53 and HIF1A,

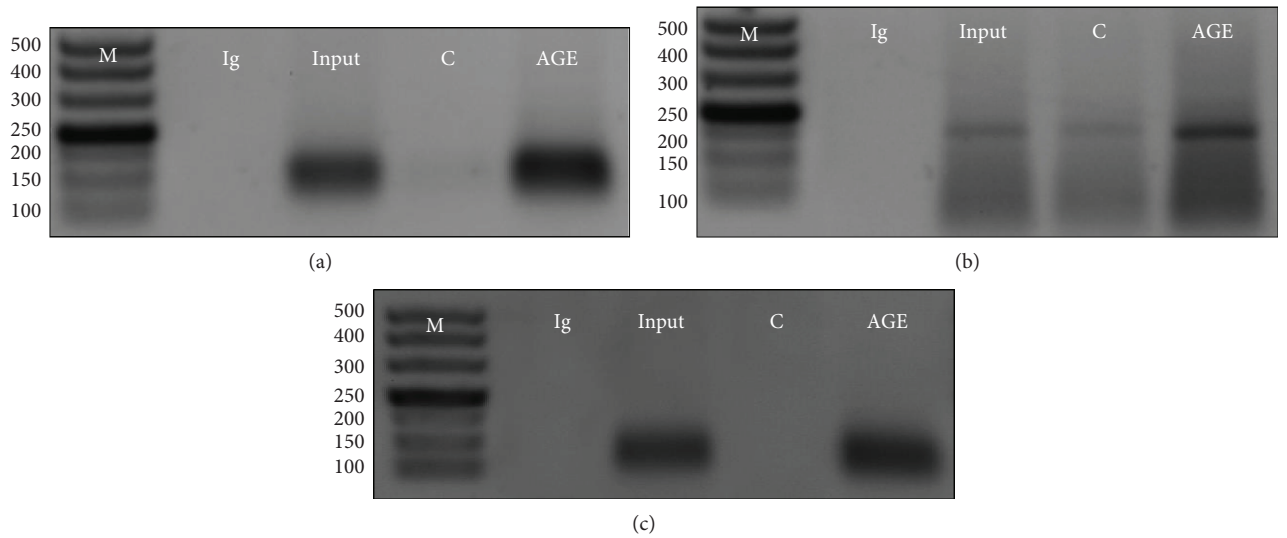

Figure 5: Evidence that KLF5 transcribed MDM2 *in vitro* and *in vivo* in a diabetic animal model. (a) Chromatin immunoprecipitation pulled down the first piece of KLF5-binding sequence (predicted 138 bp) in the human MDM2 gene. (b) Chromatin immunoprecipitation pulled down the third piece of the KLF5-binding sequence (predicted 166 bp) in the human MDM2 gene. (c) Chromatin immunoprecipitation pulled down the third and fourth KLF5-binding sequences in the mouse MDM2 gene, which was predicted to be 190 bp in size; H: healthy; D: diabetic. M: DNA size marker. Every experiment was repeated at least three times.

active liver X receptor proteins, peroxisome proliferator-activated receptor γ, and NFKB1 to promote cell proliferation [29]; RAS signaling, the excessive activation of which is associated with colon cancer initiation, is reported to promote cancer development in diabetes [30].

In normal cells, p53 are carefully controlled at a low concentration by MDM2 and MDMX, presented MDM2 are required for development and protect cells from cellular stress [31]. However, continued presence of MDM2 is required for cancer initiation [32] and results in sustained regression of tumors [33]. MDM2 is known as the main regulator of Rb and p53 in many human cancers [34]. MDM2 is able to mediate Rb degradation directly [35] or in an ubiquitin-independent manner [36]. MDM2 can directly interact with p53 through the N-terminal regions and promote p53 proteasomal degradation in the cytoplasm [37, 38]. Specifically in colon cancer, increases in MDM2 protein expression and gene amplification are observed [12, 39], which is associated with increased colorectal cancer risk and can be used as a prognostic marker [33]. Knockdown of MDM2 enhances the efficacy of cisplatin-based chemotherapy *in vitro* and *in vivo* [40] as well as radiotherapy [41]. In the present study, AGEs promote MDM2 expression which triggers Rb and p53 inactivation/degradation (Figures 2(a) and 2(b)). p53 function is impaired in 69.4% of colon cancer [42, 43]. Knockout or mutation of p53 *in vitro* or *in vivo* can cause tumorigenesis. Mutation of Rb is involved in cancer initiation in many types of human cancer [44]. Conditional depletion of Rb can disrupt the coordination between DNA replication and mitosis [45], induce missed regulation of pluripotency networks [46], and cause early-stage cancer [47]. In embryo cells with mutant p53, knockout of Rb is sufficient to initiate tumorigenesis [48]. Thus, dysregulation of oncogenes and tumor suppressors is implicated in cancer development, including cancer development in diabetes. Our results, more specifically, support a view that AGEs-caused MDM2 overexpression as well as inactivation of p53 and Rb contribute to the development of colon cancer in type 2 diabetes.

Cell stimulation with lysophosphatidic acid can increase the expression of MDM2; under experimental conditions, knockdown of SP1 but not KLF5 blocks the MDM2 overexpression [49]. This shows that, under experimental conditions, SP1 rather than KLF5 serves as the transcription factor for MDM2, which is different from our results that AGEs increased the MDM2 expression via KLF5 (Figure 4(d)). The difference is likely to be due to that different triggers activate different signaling pathways and/or transcription factors. AGEs is found to activate RAS and ERK1/2 in PC12 and colon cancer cells *in vitro* [50, 51]. In IEC6 cells, overexpression of KRAS upregulates KLF5 [52]. Sphingosine-1-phosphate enhances KLF5 expression through the G(i)-protein-Ras-ERK/p38 pathway in neointimal cells and vascular smooth muscle cells [53], indicating that the KLF5 transcriptional activity is closely related to MAPK signaling.

In HCT116 cells, AGEs did not increase the protein level of KLF5, but promoted the nuclear translocation (Figure 4(d)), whereas, in our diabetic mouse model, KLF5 protein level was increased (Figure 5(b)). This might be due to the different behaviors of KLF5 between nontransformed and cancerous cells. Indeed, in nontumorous cells (i.e., IEC8 and IMCE), overexpression of KLF5 enhances cyclin D expression, cell proliferation, and colony formation. In contrast, overexpression of KLF5 in colon cancer cell shows the opposite effects [54]. In cancer cells, microRNA mir-143 and mir-153 directly inhibit the expression of KLF5 [55, 56].

In conclusion, our results showed that KLF5 directly transcribed MDM2 *in vitro* in a cell model and *in vivo* in

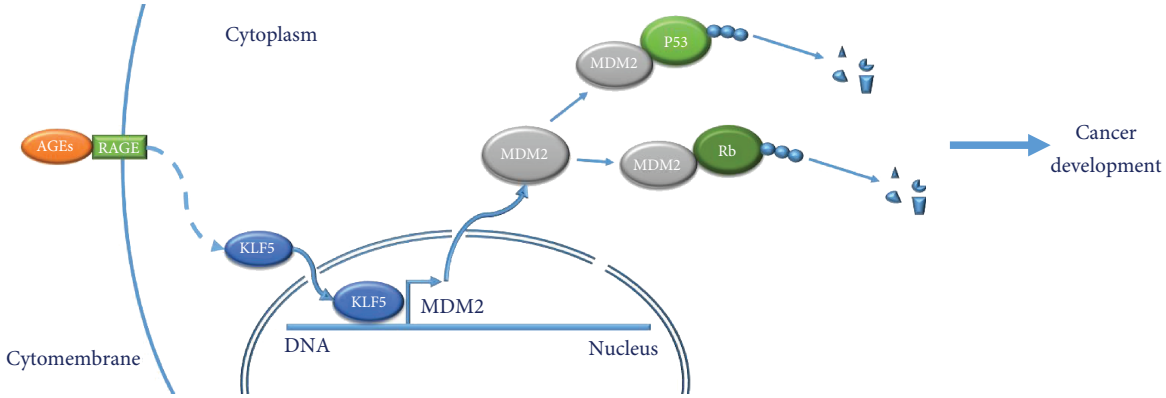

Figure 6: Conclusion figure of our research in this paper. Advanced glycation end products promote the nucleus translocation of transcription factor KLF5, which directly bind to the transcriptional regulatory region of MDM2 and promote its expression. Overexpressed MDM2 directly binds and promotes cancer suppressor Rb and p53 degradation via the ubiquitination pathway.

diabetes mouse colon, which was responsible for AGEs-increased expression of MDM2 (Figure 6). Overexpression of oncogene (i.e., MDM2) and inactivation of tumor suppressor (i.e., p53 and Rb) are a candidate biological link between type 2 diabetes and colon cancer development.

Data Availability

The data used to support the findings of this study are available from the corresponding author upon request.

Conflicts of Interest

The authors declare no conflicts of interest.

Acknowledgments

The authors thank Dr. ZY Li for her help in establishing our cell culture facility. This work was supported by Shanxi University (nos. 113533901005 and 113545017; Talent Recruitment Fund) and the Department of Science and Technology of Shanxi Province (2015081034 and 201601D11066).

Supplementary Materials

Figure S1: predicted binding sequences of transcription factor KLF5 in the transcriptional regulatory region of human MDM2 gene and primer design. Figure S2: predicted binding sequences of transcription factor KLF5 in the transcriptional regulatory region of mouse MDM2 gene and primer design. *(Supplementary Materials)*

References

[1] NCD Risk Factor Collaboration (NCD-RisC), "Worldwide trends in diabetes since 1980: a pooled analysis of 751 population-based studies with 4.4 million participants," *The Lancet*, vol. 387, no. 10027, pp. 1513–1530, 2016.

[2] E. Giovannucci, D. M. Harlan, M. C. Archer et al., "Diabetes and cancer: a consensus report," *CA: A Cancer Journal for Clinicians*, vol. 60, no. 4, pp. 207–221, 2010.

[3] T. I. L. Nilsen and L. J. Vatten, "Prospective study of colorectal cancer risk and physical activity, diabetes, blood glucose and BMI: exploring the hyperinsulinaemia hypothesis," *British Journal of Cancer*, vol. 84, no. 3, pp. 417–422, 2001.

[4] F. B. Hu, J. E. Manson, S. Liu et al., "Prospective study of adult onset diabetes mellitus (type 2) and risk of colorectal cancer in women," *Journal of the National Cancer Institute*, vol. 91, no. 6, pp. 542–547, 1999.

[5] E. Weiderpass, G. Gridley, O. Nyrén, A. Ekbom, I. Persson, and H. O. Adami, "Diabetes mellitus and risk of large bowel cancer," *Journal of the National Cancer Institute*, vol. 89, no. 9, pp. 660-661, 1997.

[6] R. Singh, A. Barden, T. Mori, and L. Beilin, "Advanced glycation end-products: a review," *Diabetologia*, vol. 44, no. 2, pp. 129–146, 2001.

[7] V. P. Singh, A. Bali, N. Singh, and A. S. Jaggi, "Advanced glycation end products and diabetic complications," *The Korean Journal of Physiology & Pharmacology*, vol. 18, no. 1, pp. 1–14, 2014.

[8] S. Y. Kong, M. Takeuchi, H. Hyogo et al., "The association between glyceraldehyde-derived advanced glycation end-products and colorectal cancer risk," *Cancer Epidemiology, Biomarkers & Prevention*, vol. 24, no. 12, pp. 1855–1863, 2015.

[9] K. J. Lee, J. W. Yoo, Y. K. Kim, J. H. Choi, T. Y. Ha, and M. Gil, "Advanced glycation end products promote triple negative breast cancer cells via ERK and NF-κB pathway," *Biochemical and Biophysical Research Communications*, vol. 495, no. 3, pp. 2195–2201, 2018.

[10] H. Kuniyasu, Y. Chihara, and H. Kondo, "Differential effects between amphoterin and advanced glycation end products on colon cancer cells," *International Journal of Cancer*, vol. 104, no. 6, pp. 722–727, 2003.

[11] R. Deng, H. Wu, H. Ran et al., "Glucose-derived AGEs promote migration and invasion of colorectal cancer by up-regulating Sp1 expression," *Biochimica et Biophysica Acta*, vol. 1861, no. 5, pp. 1065–1074, 2017.

[12] J. Hernández-Monge, A. B. Rousset-Roman, I. Medina-Medina, and V. Olivares-Illana, "Dual function of MDM2 and MDMX toward the tumor suppressors p53 and RB," *Genes & Cancer*, vol. 7, no. 9-10, pp. 278–287, 2016.

[13] M. Hav, L. Libbrecht, L. Ferdinande et al., "MDM2 gene amplification and protein expressions in colon carcinoma: is

targeting MDM2 a new therapeutic option?," *Virchows Archiv*, vol. 458, no. 2, pp. 197–203, 2011.

[14] M. Wade, Y. C. Li, and G. M. Wahl, "MDM2, MDMX and p53 in oncogenesis and cancer therapy," *Nature Reviews. Cancer*, vol. 13, no. 2, pp. 83–96, 2013.

[15] D. M. Gilkes, Y. Pan, D. Coppola, T. Yeatman, G. W. Reuther, and J. Chen, "Regulation of MDMX expression by mitogenic signaling," *Molecular and Cellular Biology*, vol. 28, no. 6, pp. 1999–2010, 2008.

[16] A. Gembarska, F. Luciani, C. Fedele et al., "MDM4 is a key therapeutic target in cutaneous melanoma," *Nature Medicine*, vol. 18, no. 8, pp. 1239–1247, 2012.

[17] N. A. Laurie, S. L. Donovan, C. S. Shih et al., "Inactivation of the p53 pathway in retinoblastoma," *Nature*, vol. 444, no. 7115, pp. 61–66, 2006.

[18] K. I. Pishas, F. Al-Ejeh, I. Zinonos et al., "Nutlin-3a is a potential therapeutic for Ewing sarcoma," *Clinical Cancer Research*, vol. 17, no. 3, pp. 494–504, 2011.

[19] J. McEvoy, A. Ulyanov, R. Brennan et al., "Analysis of MDM2 and MDM4 single nucleotide polymorphisms, mRNA splicing and protein expression in retinoblastoma," *PLoS One*, vol. 7, no. 8, article e42739, 2012.

[20] B. B. McConnell and V. W. Yang, "Mammalian Krüppel-like factors in health and diseases," *Physiological Reviews*, vol. 90, no. 4, pp. 1337–1381, 2010.

[21] J. T. Dong and C. Chen, "Essential role of KLF5 transcription factor in cell proliferation and differentiation and its implications for human diseases," *Cellular and Molecular Life Sciences*, vol. 66, no. 16, pp. 2691–2706, 2009.

[22] M. D. Conkright, M. A. Wani, K. P. Anderson, and J. B. Lingrel, "A gene encoding an intestinal-enriched member of the Krüppel-like factor family expressed in intestinal epithelial cells," *Nucleic Acids Research*, vol. 27, no. 5, pp. 1263–1270, 1999.

[23] S. M. Diakiw, R. J. D'Andrea, and A. L. Brown, "The double life of KLF5: Opposing roles in regulation of gene-expression, cellular function, and transformation," *IUBMB Life*, vol. 65, no. 12, pp. 999–1011, 2013.

[24] T. Nakaya, S. Ogawa, I. Manabe et al., "KLF5 regulates the integrity and oncogenicity of intestinal stem cells," *Cancer Research*, vol. 74, no. 10, pp. 2882–2891, 2014.

[25] J. Kaczynski, T. Cook, and R. Urrutia, "Sp1- and Krüppel-like transcription factors," *Genome Biology*, vol. 4, no. 2, p. 206, 2003.

[26] L. Duan, R. E. Perez, L. Chen, L. A. Blatter, and C. G. Maki, "p53 promotes AKT and SP1-dependent metabolism through the pentose phosphate pathway that inhibits apoptosis in response to Nutlin-3a," *Journal of Molecular Cell Biology*, 2017.

[27] R. C. M. van Kruijsdijk, E. van der Wall, and F. L. J. Visseren, "Obesity and cancer: the role of dysfunctional adipose tissue," *Cancer Epidemiology, Biomarkers & Prevention*, vol. 18, no. 10, pp. 2569–2578, 2009.

[28] S. L. Habib and S. Liang, "Hyperactivation of Akt/mTOR and deficiency in tuberin increased the oxidative DNA damage in kidney cancer patients with diabetes," *Oncotarget*, vol. 5, no. 9, pp. 2542–2550, 2014.

[29] J. Yang, R. Nishihara, X. Zhang, S. Ogino, and Z. R. Qian, "Energy sensing pathways: bridging type 2 diabetes and colorectal cancer?," *Journal of Diabetes and its Complications*, vol. 31, no. 7, pp. 1228–1236, 2017.

[30] J. K. Brewer, "Behavioral genetics of the depression/cancer correlation: a look at the Ras oncogene family and the 'cerebral diabetes paradigm'," *Journal of Molecular Neuroscience*, vol. 35, no. 3, pp. 307–322, 2008.

[31] J. K. Buolamwini, J. Addo, S. Kamath, S. Patil, D. Mason, and M. Ores, "Small molecule antagonists of the MDM2 oncoprotein as anticancer agents," *Current Cancer Drug Targets*, vol. 5, no. 1, pp. 57–68, 2005.

[32] A. Meye, P. Würl, M. Bache et al., "Colony formation of soft tissue sarcoma cells is inhibited by lipid-mediated antisense oligodeoxynucleotides targeting the human mdm2 oncogene," *Cancer Letters*, vol. 149, no. 1-2, pp. 181–188, 2000.

[33] I. Chaar, T. A. Arfaoui, E. H. O. el Amine et al., "Impact of MDM2 polymorphism: increased risk of developing colorectal cancer and a poor prognosis in the Tunisian population," *European Journal of Gastroenterology & Hepatology*, vol. 24, no. 3, pp. 320–327, 2012.

[34] D. B. S. Yap, J.-K. Hsieh, F. S. G. Chan, and X. Lu, "mdm2: a bridge over the two tumour suppressors, p53 and Rb," *Oncogene*, vol. 18, no. 53, pp. 7681–7689, 1999.

[35] C. Uchida, S. Miwa, K. Kitagawa et al., "Enhanced Mdm2 activity inhibits pRB function via ubiquitin-dependent degradation," *The EMBO Journal*, vol. 24, no. 1, pp. 160–169, 2005.

[36] P. Sdek, H. Ying, D. L. F. Chang et al., "MDM2 promotes proteasome-dependent ubiquitin-independent degradation of retinoblastoma protein," *Molecular Cell*, vol. 20, no. 5, pp. 699–708, 2005.

[37] S. M. Picksley, B. Vojtesek, A. Sparks, and D. P. Lane, "Immunochemical analysis of the interaction of p53 with MDM2;–fine mapping of the MDM2 binding site on p53 using synthetic peptides," *Oncogene*, vol. 9, no. 9, pp. 2523–2529, 1994.

[38] G. W. Yu, S. Rudiger, D. Veprintsev, S. Freund, M. R. Fernandez-Fernandez, and A. R. Fersht, "The central region of HDM2 provides a second binding site for p53," *Proceedings of the National Academy of Sciences of the United States of America*, vol. 103, no. 5, pp. 1227–1232, 2006.

[39] A. Forslund, Z. Zeng, L. X. Qin et al., "MDM2 gene amplification is correlated to tumor progression but not to the presence of SNP309 or TP53 mutational status in primary colorectal cancers," *Molecular Cancer Research*, vol. 6, no. 2, pp. 205–211, 2008.

[40] Y. Yu, P. Sun, L. C. Sun et al., "Downregulation of MDM2 expression by RNAi inhibits LoVo human colorectal adenocarcinoma cells growth and the treatment of LoVo cells with *mdm2*siRNA3 enhances the sensitivity to cisplatin," *Biochemical and Biophysical Research Communications*, vol. 339, no. 1, pp. 71–78, 2006.

[41] H. Wang, P. Oliver, Z. Zhang, S. Agrawal, and R. Zhang, "Chemosensitization and radiosensitization of human cancer by antisense anti-MDM2 oligonucleotides: *in vitro* and *in vivo* activities and mechanisms," *Annals of the New York Academy of Sciences*, vol. 1002, no. 1, pp. 217–235, 2003.

[42] J. Gao, B. A. Aksoy, U. Dogrusoz et al., "Integrative analysis of complex cancer genomics and clinical profiles using the cBioPortal," *Science Signaling*, vol. 6, no. 269, article pl1, 2013.

[43] E. Cerami, J. Gao, U. Dogrusoz et al., "The cBio cancer genomics portal: an open platform for exploring multidimensional cancer genomics data," *Cancer Discovery*, vol. 2, no. 5, pp. 401–404, 2012.

[44] Y. Song, D. Gilbert, T. N. O'Sullivan et al., "Carcinoma initiation via RB tumor suppressor inactivation: a versatile approach to epithelial subtype-dependent cancer initiation in diverse tissues," *PLoS One*, vol. 8, no. 12, article e80459, 2013.

[45] R. J. Bourgo, U. Ehmer, J. Sage, and E. S. Knudsen, "RB deletion disrupts coordination between DNA replication licensing and mitotic entry in vivo," *Molecular Biology of the Cell*, vol. 22, no. 7, pp. 931–939, 2011.

[46] M. S. Kareta, L. L. Gorges, S. Hafeez et al., "Inhibition of pluripotency networks by the Rb tumor suppressor restricts reprogramming and tumorigenesis," *Cell Stem Cell*, vol. 16, no. 1, pp. 39–50, 2015.

[47] L. A. Maddison, B. W. Sutherland, R. J. Barrios, and N. M. Greenberg, "Conditional deletion of Rb causes early stage prostate cancer," *Cancer Research*, vol. 64, no. 17, pp. 6018–6025, 2004.

[48] S. Kitajima, S. Kohno, A. Kondoh et al., "Undifferentiated state induced by Rb-p53 double inactivation in mouse thyroid neuroendocrine cells and embryonic fibroblasts," *Stem Cells*, vol. 33, no. 5, pp. 1657–1669, 2015.

[49] S. J. Lee, Y. R. No, D. T. Dang et al., "Regulation of hypoxia-inducible factor 1α (HIF-1α) by lysophosphatidic acid is dependent on interplay between p53 and Krüppel-like factor 5," *Journal of Biological Chemistry*, vol. 288, no. 35, pp. 25244–25253, 2013.

[50] H. M. Lander, J. M. Tauras, J. S. Ogiste, O. Hori, R. A. Moss, and A. M. Schmidt, "Activation of the receptor for advanced glycation end products triggers a $p21^{ras}$-dependent mitogen-activated protein kinase pathway regulated by oxidant stress," *Journal of Biological Chemistry*, vol. 272, no. 28, pp. 17810–17814, 1997.

[51] K. Fukami, S. Yamagishi, M. T. Coughlan et al., "Ramipril inhibits AGE-RAGE-induced matrix metalloproteinase-2 activation in experimental diabetic nephropathy," *Diabetology and Metabolic Syndrome*, vol. 6, no. 1, p. 86, 2014.

[52] M. O. Nandan, B. B. McConnell, A. M. Ghaleb et al., "Krüppel-like factor 5 mediates cellular transformation during oncogenic KRAS-induced intestinal tumorigenesis," *Gastroenterology*, vol. 134, no. 1, pp. 120–130, 2008.

[53] S. Usui, N. Sugimoto, N. Takuwa et al., "Blood lipid mediator sphingosine 1-phosphate potently stimulates platelet-derived growth factor-A and -B chain expression through $S1P_1$-G_i-Ras-MAPK-dependent induction of Kruppel-like factor 5," *Journal of Biological Chemistry*, vol. 279, no. 13, pp. 12300–12311, 2004.

[54] N. W. Bateman, D. Tan, R. G. Pestell, J. D. Black, and A. R. Black, "Intestinal tumor progression is associated with altered function of KLF5," *Journal of Biological Chemistry*, vol. 279, no. 13, pp. 12093–12101, 2004.

[55] A. Pagliuca, C. Valvo, E. Fabrizi et al., "Analysis of the combined action of miR-143 and miR-145 on oncogenic pathways in colorectal cancer cells reveals a coordinate program of gene repression," *Oncogene*, vol. 32, no. 40, pp. 4806–4813, 2013.

[56] J. Y. Liu, J. B. Lu, and Y. Xu, "MicroRNA-153 inhibits the proliferation and invasion of human laryngeal squamous cell carcinoma by targeting KLF5," *Experimental and Therapeutic Medicine*, vol. 11, no. 6, pp. 2503–2508, 2016.